

**CONDUCTION MECHANISM IN POLYMER
NANO-COMPOSITE ELECTROLYTE SYSTEM**

**THESIS
SUBMITTED TO**



**THE MAHARAJA SAYAJIRAO UNIVERSITY OF
BARODA**

FOR THE AWARD OF DEGREE OF
DOCTOR OF PHILOSOPHY
IN
PHYSICS

SUBMITTED BY

NIRALI H. GONDALIYA

RESEARCH GUIDE

Prof. D.K. KANCHAN

SOLID STATE IONICS & GLASS RESEARCH LABORATORY

Department of Physics, Faculty of Science
The M.S. University of Baroda
Vadodara – 390002 (GUJ)

AUGUST- 2013

DECLARATION BY THE CANDIDATE

I hereby declare that the contents of the thesis, in full or in parts, entitled “**CONDUCTION MECHANISM IN POLYMER NANO-COMPOSITE ELECTROLYTE SYSTEM**” submitted for the award of “*Doctor of Philosophy*” in the Physics Department, Faculty of Science, The M.S. University of Baroda, India, have not been submitted to any other Institute or University for the award of any other degree.

Nirali H. Gondaliya

Dr. Dinesh K. Kanchan
Professor in Physics
email : d_k_kanchan@yahoo.com
Ph : +91 9426765292



PHYSICS DEPARTMENT
Faculty of Science
The M.S. University of Baroda
Vadodara - 390 002 (Guj.) INDIA
Ph. : 91-265-2795339 (ext. 24)

CERTIFICATE

This is to certify that the work, carried out by Ms. Nirali H. Gondaliya, Research Scholar in the thesis entitled “**CONDUCTION MECHANISM IN POLYMER NANO-COMPOSITE ELECTROLYTE SYSTEM**” for the award of “*Doctor of Philosophy*” in the Physics Department, Faculty of Science, The M.S. University of Baroda, India, is original in its contents and has not been submitted for the award of any other degree to any other University or Institute in India or abroad. She has spent the required period of time i.e., more than 200 days of attendance in the Department during her course and Ph.D. work. The contents of the research work carried out in the thesis embodies a bonafide piece of the work done by her under my guidance.

Prof. Dinesh. K. Kanchan
Research Supervisor
&
Director, Research and Consultancy Cell
(MSU)

DEDICATION

I dedicate this work to my family,
to my husband *Himanshu Gondaliya*, for his support and giving me strength to carry on this journey. He has been strength of pillar to me. He stood by me during thick and thin days for the past years and his never ending love towards me. And to My Dearest daughter, *Sanskriti*, who means world to me. Her smile makes me to forget all my worries.

ACKNOWLEDGEMENTS

“Life is a journey not a destination”

As adventure seekers go on expedition, the journey to carry out research gives me the same pleasure and I am delighted to submit this thesis. I thank God for giving me strength and courage to complete this work.

The first person who has been the guiding force and pillar in this voyage is **Prof. Dinesh K. Kanchan** who guided me and along with it, he encouraged & motivated me for moving ahead towards my goal. His expertise in subject helped me to overcome challenges encountered in this research work. Words are not enough to express my gratitude towards him and his wife Prof. Rolee Kanchan for providing such supportive environment for student like me who is oscillated between family and job.

I am also grateful to former Head, Prof. C.F. Desai for his support and providing laboratory facilities. I thank all staff members of Physics Department of The M.S. University of Baroda, India, for their help and cooperation.

I specially thank Poonam Sharma for sharing both formal and informal discussion and standing unconditional with me in all my rise and fall. I thank my seniors Dr. Meenakshi Pant and Manish Jayswal for their continuous support and advice. I am also thankful to my present colleagues Prajakta Joge and Dharmesh Kothari for their love and friendly environment.

I am very grateful to Mr. R.C. Joshi and Mr. J.M. Patel of *Shri S'ad Vidhya Mandal Institute of Technology (SVMIT)*, Bharuch, India for providing me sponsorship to do this work.

I am thankful to my parents, my in-laws and Mr. & Mrs. Desai for helping me to complete this journey.

It would not have been possible to write this Ph. D thesis without the help and support of my friends Vaisali, Nital, Payal, Ganshyam and entire CSE/IT Department of SVMIT, Bharuch, and my dearest friend Jemini for taking care of my daughter when I was busy with my research work.

Thank you all for helping me in my endeavor.

Nirali H. Gondaliya

Preface

Man-made polymers have been associated since the age of industrialization and have found applications in all aspects of human life. These materials found their usefulness in all leading industrial and non-industrial applications. The general belief was that polymers are insulating and have been utilized mainly for insulation purposes. However, since the demonstration of ion conducting properties of PEO polymer in 1973 by P.V. Wright, a new class of ion conducting materials has been explored. The low ionic conductivity of solid polymer electrolytes limits their application at ambient temperature. Thus, considerable efforts have been devoted to improve their ionic conductivity. The polymer electrolytes field is fascinating, and although it is not completely understood, it still holds the key to the development of new energy sources. Therefore, the present thesis deals with the preparation, characterization and conductivity studies on the PEO based polymer nano-composite electrolyte systems with and without plasticizer. The thesis has been divided into the following seven chapters.

Chapter one gives general introduction of solid electrolytes including polymer electrolytes. A brief discussion of the material such as host polymer PEO, salt complexation, nano-fillers, and plasticizer is also included in this chapter. *Chapter two* presents the theoretical background of various characterization studies done on prepared samples. It also presents a detailed discussion of various models of dc and ac conductivity which includes, free volume theory, Configurational Entropy model, Space charge model, Amorphous phase model, dynamic percolation theory. *Chapter three* deals with the experimental details of all studies used to pursue the present work. *Chapter four* discusses the results of various characterization studies carried out on all prepared samples. *Chapter five* contains the results of impedance spectroscopy i.e.; dc conductivity and ac conductivity of the all prepared polymer electrolyte samples. The conductivity plots of all the prepared samples are thermally activated and follow Arrhenius behavior. Effect of salt, nanofiller and plasticizer concentrations on conductivity in five different series is discussed in detail. In *Chapter six*, Dielectric and Modulus formalisms obtained from impedance are studied to understand the relaxation mechanism. In *Chapter seven*, the con-

clusion from the characterization results, ac and dc conductivity, dielectric and modulus studies and their dependence on the temperature and composition of the present system have been summarized. The publications emerged out of the present work are also included at the end of Chapter seven.

Vadodara

12th Aug, 2013

Nirali H. Gondaliya

Table of Contents

Contents	Page No.
Chapter-1 Introduction	1-36
1.1 Introduction	2
1.2 Solid state electrolyte	2
1.2.1 Classification of Solid electrolyte	2
1.2.2 Comparison between NIC and FIC	4
1.3 Timeline of Solid State Electrolytes	4
1.4 Anionic conductors	5
1.4.1 Oxide ion conductors	6
1.4.2 Fluoride ion conductors	6
1.5 Cationic conductors	6
1.5.1 Silver ion conductors	7
1.5.2 Copper ion conductors	7
1.5.3 Lithium ion conductors	7
1.5.4 Sodium ion conductors	8
1.6 Classification of Solid electrolytes	8
1.6.1 Glasses	8
1.6.2 Gels	9
1.6.3 Polymers	9
1.7 Solid polymer electrolytes (SPEs)	9
1.7.1 Properties of host Polymer	9
1.7.2 Complex Formation	11
1.7.3 Fillers	14
1.7.4 Plasticizer	17
1.8 Different Polymer electrolytes	19
1.8.1 Polymer-salt electrolytes /Solid Polymer electrolytes (SPE)	19
1.8.2 Nano Composite Polymer Electrolytes (NCPE)	20
1.8.3 Plasticized Polymer Electrolytes	22
1.8.4 Plasticized Nano Composite Polymer Electrolytes (PNCPE)	23
1.9 Application	24
1.9.1 Battery applications	24
1.9.2 Non-battery application	27
1.9.3 Electrochromic Devices	28
1.10 Present Investigation	28
References	32

Chapter- 2 Theoretical Details	37-72
2.1 Introduction	38
2.2 Description of characterization techniques	38
2.2.1 Fourier Transform Infrared Spectroscopy (FTIR)	38
2.2.2 Differential Scanning Calorimetry (DSC)	39
2.2.3 X- ray Diffraction (XRD)	42
2.2.4 Scanning Electron Microscope (SEM)	44
2.2.5 Transport number measurement	47
2.3 Complex Impedance Spectroscopy	48
2.3.1 Dielectric Analysis	50
2.3.2 Modulus Analysis	57
2.4 Theoretical models of Conductivity	59
2.5 Temperature dependence of conductivity	60
2.5.1 Arrhenius Theory	60
2.5.2 Vogel–Tammann–Fulcher (VTF) theory	61
2.6 Models for DC Conductivity	62
2.6.1 Free Volume Theory	62
2.6.2 Configurational Entropy Model	63
2.6.3 Space charge models	64
2.6.4 Amorphous phase model	65
2.6.5 Dynamic Bond Percolation theory	65
2.7 Frequency dependence of conductivity	66
2.7.1 Jonscher’s Power law	67
2.7.2 Jump relaxation model	67
2.8 Various other models	68
References	69

Chapter- 3 Experimental Techniques	73-84
3.1 Introduction	74
3.2 Material used in preparing polymer electrolytes	74
3.3 Methods and sample preparation	75
3.4 Characterization Technique	77
3.4.1 Fourier Transform Infrared Spectroscopy (FTIR)	78
3.4.2 Differential Scanning Calorimetry (DSC)	78
3.4.3 X-ray Diffraction (XRD)	79
3.4.4 Scanning Electron Microscopy (SEM)	80
3.4.5 Transport Number Measurements	81
3.4.6 Conductivity Measurement	82
References	84

Chapter- 4 Characterization Studies	85-109
4.1 Fourier Transform Infrared Spectroscopy (FTIR)	86
4.2 Differential Scanning Calorimetry (DSC)	93
4.3 X-ray Diffraction studies (XRD)	97
4.4 Scanning Electron Microscopy (SEM)	102
4.5 Transport Number	105
References	108
Chapter- 5 Conductivity Studies	110-137
5.1 Introduction	111
5.2 Complex Impedance Analysis	111
5.3 DC Conductivity	120
5.4 AC Conductivity	124
References	135
Chapter- 6 Modulus and Dielectric Analysis	138-176
6.1 Introduction	139
6.2 Dielectric Analysis	139
6.3 Modulus Analysis	152
6.4 Scaling of Modulus	170
References	175
Chapter- 7 Conclusion	177-180
List of Publication	181-185

CHAPTER 1

INTRODUCTION

***T**his chapter covers an outline of solid polymer electrolytes followed by its classification & development. Different types of Polymer electrolytes are discussed in later part of this chapter along with its complexation with salt, nanofiller and plasticizer. The concluding part of this chapter consists of various applications of these solid polymer electrolytes.*

1.1 Introduction

The solids which possess very high conductivity have been identified since the end of the last century [1-5]. Later, in particular a variety of solids exhibiting appreciably high ionic conductivity at their operating temperature has been identified by various scientists [6] and named them as “*SUPERIONIC MATERIALS*”. They are otherwise called as Fast Ionic Conductors or *Solid electrolytes*. The arena of studying such materials is named as “*SOLID STATE IONICS*” by Prof. T. Takahshi after which, the field gained momentum and attracted many scientists from various sectors of physics Electrochemistry, Material Science, Metallurgy and Energy. The study of the ionic conduction in various super ionic conductors in the forms of single crystals, amorphous materials, composites, polymeric solids and thin films are widely carried out by the characterization of their physio-chemical properties.

After, the observation of ionic conduction in solid material by Michael Faraday about one and half century ago [7], Nernst added its flavor by the development of the stabilized zirconia. This stabilized zirconia is one of the most widely used oxide- solid electrolyte in oxygen sensors which served as a resistance in the heating type light source and was known as *Nernst Glower*. Since then, a remarkable observation was made Tubant *et. al.*[8]and Ketellar [9] that AgI and Ag₂HgI₄ material respectively shows that there conductivity increases remarkably when heated to a temperature well below their melting point. All this triggered the area of research with an optimum approach in developing solid electrolyte material with operating temperature below its melting point electrolyte such as leakage, low energy density, limited operating temperature range etc. By the entry of this solid electrolyte material the disadvantages faced by liquids are over come.

1.2 Solid state electrolyte

Unlike conventional electrolyte material i.e. liquid electrolyte, solid state electrolytes are used. This Solid state materials exhibit high ionic conductivity at ambient temperature and hence are termed as *solid electrolytes*.

1.2.1 Classification of Solid electrolyte

Solid electrolyte i.e., ionic conductors can be broadly classified into two:

- i) Normal Ionic Conductors (NIC's)
- ii) Fast Ionic Conductors (FIC's)

Normal Ionic Conductors (NICs)

The more commonly known ionic solids like NaCl, KCl, etc. have a room temperature conductivity of 10^{-12} to 10^{-16} S/cm. In these materials, thermally generated imperfections in the periodic arrangement of the lattice structure lead to the migration of the ions [10] as shown in Fig. 1.1. Beside this, other metal halides like silver and copper etc. have been found to exhibit low ionic conductivity [5]. Therefore, these materials are termed as *normal ionic conductors* (NICs).

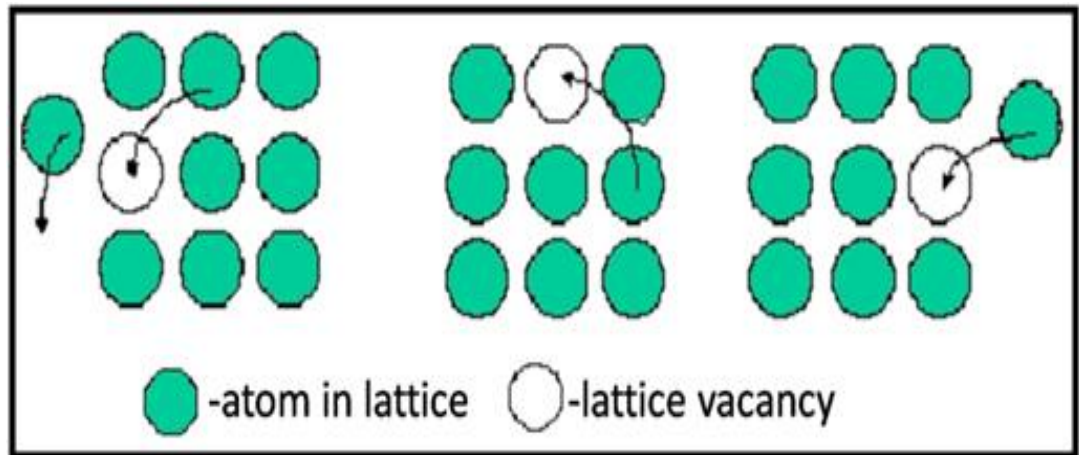


Fig. 1.1 Schematic diagram of normal ion conduction

Fast Ionic Conductors (FICs)

Solid materials that exhibit high ionic conductivity at ambient temperature are termed as Fast ionic conductors (FICs), usually of the order of those found in molten salts



Fig. 1.2 Schematic diagram of fast ion conduction [12]

(10^{-6} to 10^{-1} S/cm) at ambient temperature [8]. Due to high ionic conductivity of this solid material compared to liquid electrolytes, they were termed '*solid electrolytes*' [11]. In these solid electrolyte materials, the principal charge carriers are ions they can be both cation and/or anion. Fig. 1.2 depicts Schematic diagram of ion conduction in polymer electrolyte system.

1.2.2 Comparison between NIC and FIC

- i) The FICs are characterized by high electrical conductivity $\sim 10^{-2}$ S/cm at room temperature. The NICs have low electrical conductivity of the order of 10^{-12} S/cm.
- ii) Either cations or the anions are the only mobile charge carriers in FICs with a transport number 1.0, whereas in NICs both the ions (anion and cation) are mobile.
- iii) The number of mobile charge carriers is approximately 10^{22} cm^{-3} (temperature independent) for FICs, whereas it is only 10^{16} cm^{-3} (temperature dependent) for NICs.
- iv) The activation energy for ion migration in FICs is very low, whereas in NICs the activation energy for ion migration is high.
- v) In NICs, the conduction process is highly temperature dependent and is essentially a thermally activated process.

1.3 Timeline of Solid State Electrolytes

In 1833, Faraday discovered the first silver ion conductor in silver sulfide, Ag₂S [13, 14]. The oxygen ion conductivity at high temperature was found in yttria stabilized zirconia in 1899 by Nernst [15]. Tubant and Lorentz have reported the superionic phase in α -AgI in 1913 [8]. This discovery stimulated a great interest in the ion conducting properties of solids. Later in 1932, Tubant reported high ionic conduction at high temperature in Ag₂Se [16.]. Until 1960, only stabilized zirconia and silver iodide (above 147 °C) were known to have very high ionic conductivities. In the year 1966, Ag₃SI was found to exhibit high silver ion conductivity at room temperature [17]. In 1967, sodium β -alumina was found to have a high sodium ion conductor [18]. Very high ionic conductivity, to the order of 0.3 S/cm at room temperature was obtained in Rb.Ag₄I₅ by Bradley

and Greene [19] and by Owens & Argue [20] independently. Since then, various kinds of cation and anion conductors exhibiting high ionic conductivity at ambient conditions and at high temperatures have been synthesized. Numerous cationic (Ag^+ , Cu^+ , Li^+ , Na^+ , K^+ etc.), anionic (O^{2-} , F^-) and proton conductors have been reported. An excellent history of the development and a list of these materials are available in the text by Chandra [10]. Since then high ionic conductors have been found in glassy or amorphous and polymeric forms [10, 21-24]. High ionic transport is also obtained by dispersing insulating particles in ionic solids. Such materials are called dispersed solid electrolytes or composite solid electrolytes [25]. A wide variety of fast ion conducting materials is available today. Depending on the type of mobile ions, they are classified into two categories: (a) anionic and (b) cationic.

1.4 Anionic conductors

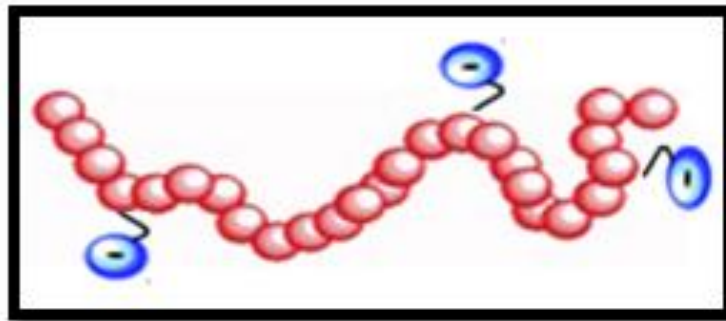


Fig. 1.3 Schematic diagram of Anion conduction.

The high conductivity in anionic conductors is due to the presence of negative ions, which are the mobile carriers (Fig. 1.3). There are two types of anionic conducting species:

- i) Oxygen ion conductors (O^{2-}) and
- ii) Halide ion conductors (e.g. F^-).

The ionic conductivity of these conductors is generally temperature dependent as well as depends on type impurities with which it is doped. As both these factor control the number of point defects and their mobility [26, 27]. Most of the O^{2-} ion conducting materials is used for the fuel cells and F^- conducting compounds are used for the optical fibers [26-28].

1.4.1 Oxide ion conductors

Generally, oxides conductors like CeO_2 and ThO_2 have fluorite structure between the room temperature and melting points. These oxides are distinctive in the way that they form solid solutions in an unusually wide composition range with alkaline earth oxides such as CaO and Y_2O_3 . Enhancement in ionic conductivity of about two orders of magnitude is generally observed. Later, other compounds like yttria stabilized Thoria and calcia stabilized Zirconia with distorted fluorite structure have been found to have good oxygen ion conduction. In general, under this classification, a homogenous solid solution phase is easily formed when the cation size of a host (such as CeO_2) and a guest (such as Gd_3O_3) are almost equal. These oxygen ion conductors are found to have a wide range of application in solid state ionic devices like sensors, partial pressure gauges and fuel cells. [29]

1.4.2 Fluoride ion conductors

According to Gellings et.al. [30] fluoride ion, generally is thought to be more mobile in the solid state compared to oxide ion. However, the ionic radii of both these ions are almost same $\sim 1.4 \text{ \AA}$, but its mono-valence results in higher mobility. Also, Fluorine ion being the smallest among the halogen series provides good anionic conduction, as in $\beta\text{-PbF}_2$ the first known *fast ionic conductor* which exhibits an ionic conductivity of 10^{-6} S/Cm at ambient temperature. The solid solution of PbF_2 with SnF_2 i.e. PbSnF_4 , and CaF_2 with rare earth fluoride such as LaF_3 has exhibited conductivity of the order of 10^{-3} Scm^{-1} at ambient temperature [31, 32]. The fluoride ion conductivity of PbF_2 has also been enhanced by three orders of magnitude by the dispersion of submicron size particles of insulating oxides like Al_2O_3 and SiO_2 [33]. F^- ion conduction has also been realized in glassy electrolytes [34] and nanometer size multilayer structures of $\text{BaF}_2/\text{CaF}_2$ by molecular beam epitaxy on alumina substrates at 770 K in which Fluoride ion exhibits space charge layer conduction [35]. Fluoride ion conducting materials have also been introduced as electrode materials for rechargeable lithium batteries due to the high electro negativity value of fluorine and high free energy of formation [36].

1.5 Cationic conductors

The conductivity in cationic conductors is due to the presence of positive ions, which are the mobile carriers in these materials. Cationic conducting fast ionic conductors are further classified on the basis of different mobile ions such as silver ion, copper ion, lithium ion and sodium ion.

1.5.1 Silver ion conductors

This category of ion conductors are widely studied and used since many decades due to their high ionic conductivity at ambient temperature. In few polycrystalline Compounds such as RbAg_4I_5 , Ag_3SI and $\text{Ag}_6\text{I}_4\text{WO}_4$ high ionic conducting is observed [37, 38]. The unique example of superionic conductor is α -AgI which undergoes a phase transition at 147°C and exhibiting exceptionally high ionic conductivity due to structural disorder originating in its crystallographic nature. Fast silver ion conduction has also been reported on glassy [39] as well as polymer electrolyte systems [40]. However, solid electrolytes with Ag^+ as mobile ion have low decomposition potentials and low energy densities when used in solid state batteries.

1.5.2 Copper ion conductors

These classes of ion conductors is similar to that of silver ion conductors in size and co-ordination number but the number of copper ion conductors is very small. In 1973, Takahashi et al. [41] and Sammells et al. [42] have independently prepared large number of copper compounds with large organic cations. Generally, most of the copper ion conducting materials are obtained by stabilizing the high conducting α -phase of CuI, at ambient temperatures similar to silver ion conductors. The replacement, of silver ion by copper ion is scientifically as well as practically beneficial due to its low cost compared to silver. Copper ion conducting amorphous electrolytes, such as, $\text{CuI-Cu}_2\text{O.MoO}_3$ and $\text{CuI-Cu}_2\text{O-P}_2\text{O}_5$ have also been reported to have high conductivity of the order of 10^{-2} S/cm at ambient temperatures [43, 44]. However, there is a possibility of electronic conductivity in Cu^+ based glasses since copper has two oxidation states.

1.5.3 Lithium ion conductors

A wide variety Lithium ion conducting solid electrolytes has been developed since past many years. Such rapid development of this class of electrolytes is due to its wide range of application in high energy density batteries due to their light weight, ease

of handling and high electrochemical potential [45, 46]. The small cationic size as well as high polarizing power of lithium ion makes this class of solid electrolyte as a best choice for various applications as compared to other ions. Numerous lithium ion conducting systems such as $\text{Li}_2\text{O-LiX-M}_x\text{O}_y$ ($X = \text{I, Br, Cl}$; $\text{M}_x\text{O}_y = \text{P}_2\text{O}_5, \text{B}_2\text{O}_3$) [47, 48], $\text{Li}_2\text{S-GeS}_2$, $\text{Li-Na-}\beta\text{-alumina}$ [49], LiAlSiO_4 [50] etc. and polymer electrolytes: $\text{PEO-LiCF}_3\text{SO}_3$, PEO-LiBF_6 , PEO-LiClO_4 , etc have also been reported to possess high ionic conductivity enabling these electrolytes for their practical application in solid state ionic devices.

1.5.4 Sodium ion conductors

Sodium ion conductors or β -Alumina family of compounds having the general formula $\text{M}_2\text{O.nX}_2\text{O}_3$, where M is a monovalent cation ($\text{M} = \text{Cu}^+, \text{Ag}^+, \text{Na}^+, \text{K}^+$), X is a trivalent cation ($\text{X} = \text{Al}^{3+}, \text{Ga}^{3+}, \text{Fe}^{3+}$) and n can have values in the range of 5 to 11, are most important member of this family due to their two-dimensional ionic structure for which various kinds of solid electrolyte materials can be derived. Among these, sodium β -alumina exhibits an ionic conductivity of the order of 10^{-2} S/cm at ambient temperature and it is the well known sodium ion conductor [51]. A large number of sodium ion conducting systems analogous to the lithium ion conducting counterparts e.g.; $\text{Na}_7\text{M}_3(\text{X}_2\text{O}_7)_4$ ($\text{M} = \text{Al; Ga; Cr; Fe, X D P; As}$) [52], $\text{Na}_2\text{O-NaCl-Na}_2\text{O-B}_2\text{O}_3$, PEO-NaI-SiO_2 , ranging from composites[53], polymer electrolytes[54] and glasses [55] have been investigated for device applications.

1.6 Classification of Solid electrolytes

1.6.1 Glasses

Glasses are prepared by quenching a molten mixture of network or glass formers ($\text{SiO}_2, \text{Al}_2\text{O}_3$ and B_2O_3 etc) and network modifiers ($\text{Ag}_2\text{O}, \text{Na}_2\text{O}$ and BaO etc). Addition of metallic salts ($\text{LiI}, \text{AgI}, \text{NaI}$ and CuI etc) enhances the ionic conductivity. All glasses are characterized by their glass transition temperatures (T_g). They can be used to stabilize a high temperature phase at room temperature, such as the conducting glass $82\text{AgI-13.5Ag}_2\text{O} - 4.5 \text{ B}_2\text{O}_3$, which shows conductivity of the order of 10^{-2} S/cm at room temperature.

1.6.2 Gels

Gel electrolytes are macroscopically solid but show liquid like behavior microscopically, due to the presence of a large number of micropores filled with liquid. Aerogels are an interesting class of gels. They have very high porosity (~ 90%) and large surface area per unit mass. The structure of aerogels can be modeled in terms of fractals and the extremely high specific surface area can lead to interesting properties. Gels in the form of thin films are usually prepared by the sol-gel technique and are increasingly replacing materials prepared by other popular methods of depositing films like vapor deposition and electro-deposition. Many materials of the above discussed categories, especially polymers and glasses can be fabricated in the form of gels.

1.6.3 Polymers

Polymers are substances containing a large number of structural units joined by the same type of linkage. These substances often form into a chain-like structure. Polymer electrolytes are obtained by complexation of such chain like structure polymer with certain salts. This is a comparatively new class of fast ion conductors and a lot of new work is still being done on in this field. There may be both solid and gel polymer electrolytes depending on the host polymer used. Detail discussion of this class of electrolytes is done in later part of this chapter.

1.7 Solid polymer electrolytes (SPEs)

The class of ionically conducting solid material based on host polymer with a variety of guest salt species form *Solid Polymer Electrolytes* (SPEs).

1.7.1 Properties of host Polymer

To act as a successful polymer host, a polymer should generally have a minimum of three essential characteristics [56]:

- i) A polymer repeat unit should have a donor group (an atom with at least one lone pair of electron) to form coordinate bond with cations.
- ii) Low barriers to bond rotation so that segmental motion of the polymer chain can take place readily.

iii) A suitable distance between coordinating centers because the formation of multiple intra-polymer ion bonds appears to be important.

Numerous potential polymer hosts for solid polymer electrolyte have been tried. These include both polyethers as well as nonpolyether classes [57]. Fig. 1.4 represents

Polymer host	Repeating unit	T _g /°C	T _m /°C	Mol. wt.
Poly(ethylene oxide), PEO	-(CH ₂ CH ₂ O) _n -	-64	65	100,000
Poly(propylene oxide), PPO	-(CH(-CH ₃)CH ₂ O) _n -	-60	-	220,000
Poly(acrylonitrile), PAN	-(CH ₂ CH(-CN)) _n -	85	317	150,000
Poly(methyl methacrylate), PMMA	-(CH ₂ C(-CH ₃)COOCH ₃) _n -	105	-	996,000
Poly(vinyl chloride), PVC	-(CH ₂ CHCl) _n -	82	-	220,000
Poly(vinylidene fluoride), PVDF	-(CH ₂ CF ₂) _n -	-62	171	275,000
PVDF-HFP	-(CH ₂ CF ₂) _x (CF ₂ CF-CF ₃) _y -	-62	140	400,000

Fig. 1.4 Some polymers used in solid polymer electrolytes

few such polymers which can be used as host for polymer electrolytes. Among the polyethers besides PEO, propylene oxide (PPO), PEO-PPO, PEO-PPO-PEO etc. have been successfully tried for reasonable conductivities. But PEO proves to be ideal candidate among all available electrolyte materials.

Poly (ethylene oxide) (PEO) polymer

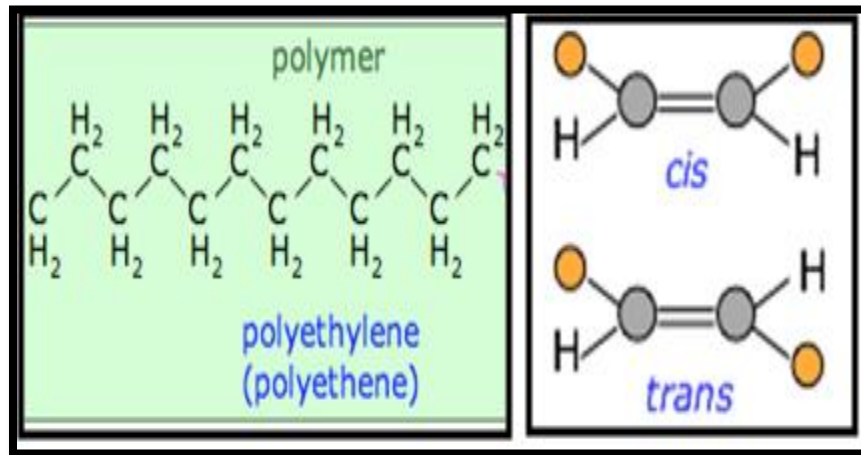


Fig. 1.5 crystal structure of poly (ethylene oxide) [23].

For an ideal electrolyte material the common donor groups must be oxygen atom as in case of polyethers (e.g. PEO, PEG and PPO), sulphur atoms for polysulphide or ni-

trogen atom for polyimine (e.g. PEI). Considering, simple electrostatic law, the order of stability for coordination of alkali metals or alkali earth ions to sites with different heteroatom would be expected to follow the relative values of the negative charge on the latter: $O > NR > NH > S$, where R is $n\text{-C}_8\text{H}_{17}$ [58, 59]. Out of many macromolecules which satisfy the above mentioned criteria, none have shown any advantage over poly (ethylene oxide) PEO. The property to forms an extremely large range of metal salt complexes has made PEO the most widely studied host polymer till to date. Its commercial interest is high from the point of view of cost, as it is easy to prepare, it has both the liquid and the solid types, and it has high chain flexibility and easy solubility in a number of common organic solvents such as methanol and acetonitrile.

Another point to be mentioned is that the polymer backbone also should be flexible to curl around the cation and the length of monomeric unit must be such that the donor groups are neither too far from, nor too near to each other. This can be observed from the fact that although PEO ($-\text{CH}_2\text{-CH}_2\text{-O-}$) coordinates a number of cations, $-\text{CH}_2\text{-O}$ and $-\text{CH}_2\text{-CH}_2\text{-CH}_2\text{-O-}$ are not good host polymers. PEO is a semi-crystalline polymer consisting of crystalline and amorphous regions which was confirmed from X-ray, DSC and IR studies. The $-\text{CH}_2\text{-CH}_2\text{-O-}$ repeat unit of PEO makes its most stable configuration to adopt a helical conformation. The crystal structure of PEO has been determined by Takahashi and Todokoro [60]. The ability of the PEO polymer chains to orient of on application of stress high degree of flexibility. From the IR and Raman studies [61, 62], it was the confirmed that the rotation of chain for crystalline PEO have been obtained. A schematic diagram of it is shown in Fig. 1.5. But, in the amorphous and molten state, the conformation of such rotation is more disordered.

During the transient stages of crystallization, majority of the crystallisable polymers form spherulites as the dominant morphological entity [63]. As their name suggests, these are spherically symmetric arrays of lamellar crystals immersed in the amorphous materials as seen from the schematics Fig. 1.6. The structures in polymer spherulites are in fact due to highly elongated chain-folded lamellae, radiating from a central point.

1.7.2 Complex Formation

Complexation is the process by which the parent polymer and the salt interact to

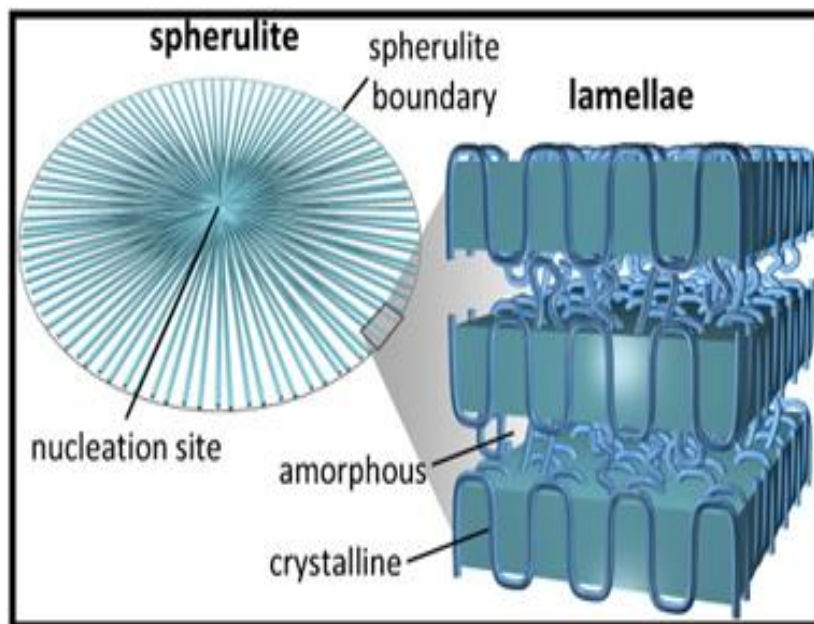


Fig. 1.6 Structure of a spherulites and helical chains stacked together in a well-ordered lattice of crystalline lamellae and amorphous inter-lamellar links [64].

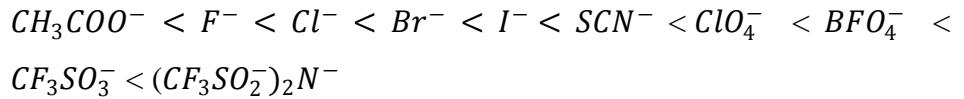
form a polymer-salt complex [65] as shown in Fig. 1.7. Generally, the method adopted for the preparation of many polymer electrolytes till date is complexation only. Most of these complexes are prepared by solution cast method. In this method, a salt and a polymer is dissolved in a common solvent such as methanol or acetonitrile. The solution is stirred for a few hours for complete dissolution of salt and polymer and a viscous solution is obtained. This viscous solution is then cast on a Teflon or polytetrafluoroethylene surface and kept in an inert atmosphere for slow evaporation of the solvent. Vacuum drying and heating processes are also used to make sure that all the remaining solvents are removed from the solution.

Consistency in the casting process is a very important requirement. The temperature at which the films undergo drying is also important as higher temperatures usually induce the formation of high-melting spherulites as the sample cools [56]. Moreover, crystal formations may be effected by the nature of the solvent, its rate of removal and the traces of the solvent left which may act as nucleation site or plasticizer [56].

Characteristics of salts favorable for complexation

The characteristics for a salt to be suitable for polymer-salt complex formation are [56]:

- i) Low lattice energy or high solvation energy,
- ii) Smaller cationic radii and bigger anionic size,
- iii) The charge density of the anion should be low to reduce the number of ion-pairs with cations. Among the most frequently used anions, the ionic conductivity for a given cation (e.g. Li^+) increases in the sequence given below:



The large 'soft' anions towards the right such as ClO_4^- or CF_3SO_3^- which have low ion-dipole stabilization energies, but relatively large energies of solvation due to mutual polarizability, are therefore likely to be the most suitable choice for polymer electrolytes. But different kinds of salts have been used for forming the salt-polymer complexes. Most common are the monovalent cations: Li^+ , Na^+ , K^+ , Cs^+ and NH_4^+ . Some divalent cations: Mg^{2+} , Zn^{2+} , Ni^{2+} , Co^{2+} and some trivalent cations like La^{3+} , Nd^{3+} and Eu^{3+} have also been used [60]

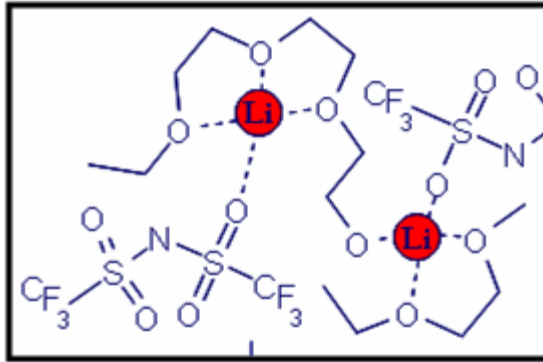


Fig. 1.7 A schematic diagram of interaction of parent polymer and salt.

AgCF₃SO₃ and LiCF₃SO₃ Salts

Silver trifluoromethane sulphonate (AgCF_3SO_3) and lithium trifluoromethane sulphonate (LiCF_3SO_3) are constructed of silver (Ag^+) and lithium (Li^+) cation respectively and trifluoromethane sulphonate (CF_3SO_3^-) as anion. Structure of AgCF_3SO_3 is shown in Fig. 1.8. Both these salts i.e.; AgCF_3SO_3 and LiCF_3SO_3 possess almost all the characteristics mentioned in the previous sub-section. The Li-salt has low ion-dipole stabilization energy and also large solvation energy. Due to small cationic size and high polarizing

power of Li^+ -ions as compared to other ions it is widely used as dopant salt. Many research groups have pursued research on a viable solid-state inorganic Li^+ - ion conducting solid electrolyte since the 1970s for solid-state lithium batteries application.

Literature survey reflects that LiCF_3SO_3 as dopant salt is extensively studied dopant salt [66-70], but major drawback of lithium dopant salt is its toxic nature which motivated research workers to explore few other salts too. In this race of searching an alternative of lithium salt Silver based salt have merged to be an appropriate choice [71, 72].

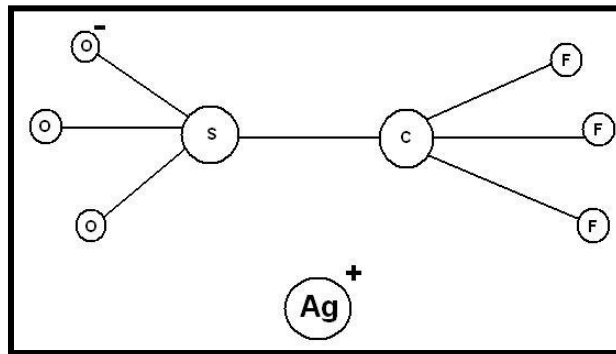


Fig. 1.8 Schematic structure of AgCF_3SO_3 .

1.7.3 Fillers

Fillers are particles added to material to modify the structure of existing product or to make better properties of the mixture material. *Nano fillers* are those materials which have the structural features in between of those of atoms and the bulk materials while most micro-structured fillers have similar properties to the corresponding bulk materials. The properties of materials with nanometer dimensions are significantly different from those of atoms and bulks materials. This is mainly due to the nanometer size of the materials which render them:

- ❖ large fraction of surface atoms;
- ❖ high surface energy;
- ❖ spatial confinement;
- ❖ reduced imperfections,
- ❖ chemically and electrically inert.

The main purpose of dispersion of inorganic filler is to improve the mechanical stability in the polymer electrolyte system. Dispersion of inorganic fillers can also improve the ionic conductivity in a polymer electrolyte. Besides improving the transport

properties, the addition of ceramic filler has been found to enhance the interfacial stability of polymer electrolytes. Addition of nanofiller increases the free volume of the polymer electrolyte as shown in Fig. 1.9.

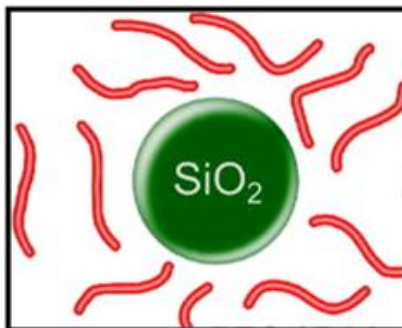


Fig. 1.9 A schematic diagram indicating increase in free volume on addition of nanofiller into the polymer electrolyte.

Silicon dioxide (SiO_2)

Silicon dioxide, also known as silica (from the Latin *silex*), is a chemical compound that is an oxide of silicon with the chemical formula SiO_2 . It has been known since ancient times. In the majority of silicates, the Si atom shows tetrahedral coordination, with 4 oxygen atoms surrounding a central Si atom. The most common example is seen in the quartz crystalline form of silica SiO_2 . In each of the most thermodynamically stable crystalline forms of silica, on average, all 4 of the vertices (or oxygen atoms) of the SiO_4 tetrahedra are shared with others, yielding the net chemical formula: SiO_2 . The two-dimensional amorphous structure of glassy silica (SiO_2) is shown in Fig. 1.10. No long-range order is present; however there is local ordering with respect to the tetrahedral arrangement of oxygen (O) atoms around the silicon (Si) atoms. Note that a fourth oxygen atom is bonded to each silicon atom, either behind the plane of the screen or in front of it; these atoms are omitted for clarity.

Aluminum Oxide (Al_2O_3)

Fig. 1.11 shows a unit cell of Aluminum Oxide (Al_2O_3). Aluminum Oxide, Al_2O_3 , commonly referred to as alumina, is the most cost effective and widely used material in the family of material science. The raw materials from which this high performance technical grade ceramic is made are readily available and reasonably priced, re-

sulting in good value for the cost in fabricated alumina shapes. With an excellent combination of properties and an attractive price, it is no surprise that fine grain technical grade alumina has a very wide range of applications. Excellent size and shape capability, high strength and stiffness, available in purity ranges from 94%, an easily metallizable composition, to 99.5% for the most demanding high temperature applications.

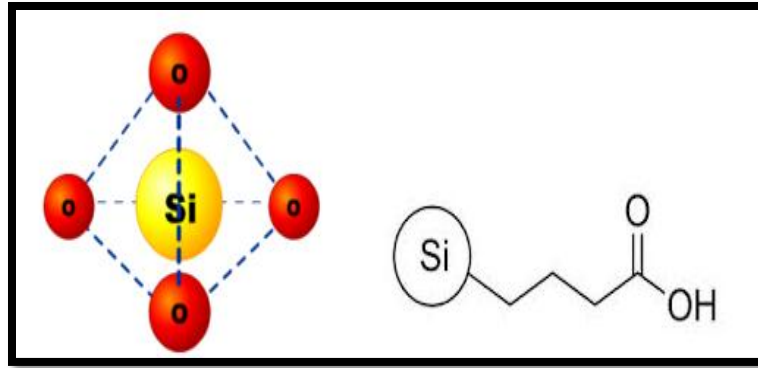


Fig. 1.10 Structure of SiO_2 .

Aluminum oxide possesses strong ionic interatomic bonding giving rise to its desirable material characteristics. It can exist in several crystalline phases which all revert to the most stable hexagonal alpha phase at elevated temperatures. The composition of the ceramic body can be changed to enhance particular desirable material characteristics. An example would be additions of chrome oxide or manganese oxide to improve hardness and change color. Other additions can be made to improve the ease and consistency of metal films fired to the ceramic for subsequent brazed and soldered assembly.

These inorganic nano fillers (Al_2O_3 and SiO_2) are hydrophilic compounds due to the presence of hydroxyl groups on the surface. These nano-filler are a superior candidate as inorganic inert filler because it provides large surface contact area with its branched primary structure. It thus enhances the volume fraction of amorphous proportion of polymer systems and thereby increases the ionic conductivity. A part from that, the incorporation of nano-filler improves interfacial stability. Moreover, these nano-fillers have high ability to tailor the surface functionalities by forming the native surface and also by giving rise to flaw by reducing the fracture strength in the polymer chains.

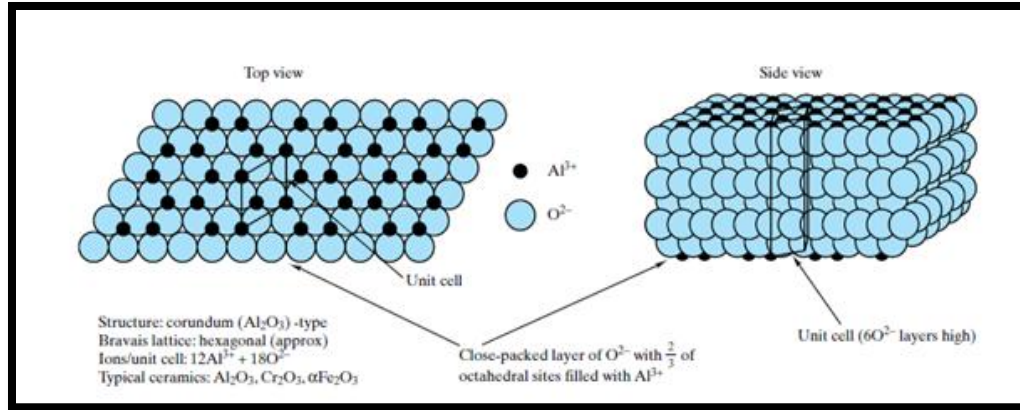


Fig. 1.11 Al_2O_3 unit cell is shown superimposed on the repeated stacking of layers of close-packed O^{2-} ions. The Al^{3+} ions fill two-thirds of the small (octahedral) interstices between adjacent layers.

Advantages of nano fillers

- ❖ It enhances the mechanical properties such as modulus, tensile or tears strength etc.
- ❖ It serves as abrasion resistance.
- ❖ It increases the ionic conductivity
- ❖ It enhances the volume fraction of amorphous proportion of polymer systems.
- ❖ It improves interfacial stability of the polymer systems.

1.7.4 Plasticizer

Plasticizers are low molecular weight material. Plasticizers work by embedding themselves between the chains of polymers, spacing them apart (increasing the "free volume"), and thus significantly lowering the glass transition temperature for the plastic and making it softer. A wide variety of plasticizers are available few of them are depicted as follows: Polyethylene glycol (PEG), Ethylene carbonate (EC), propylene Carbonate (PC), diethyl formamide (DMF) [73] etc.

Characteristics of plasticizer

The main features of the plasticizer are [74-76];

- ❖ Specific nature of the plasticizer
- ❖ Low viscosity
- ❖ High dielectric constant,

- ❖ High salt solvating power
- ❖ Polymer-plasticizer interaction,
- ❖ Ion-plasticizer coordination
- ❖ Increases mobility of ionic conduction
- ❖ Reduction in crystalline nature.

Poly (ethylene glycol) PEG Plasticizer

Polyethylene glycols (PEGs) are prepared by polymerization of ethylene oxide and are commercially available over a wide range of molecular weights from 300 g/mol to 10,000,000 g/mol. PEG is also known as the low molecular weight waxy or soft solid PEO which has the end product of the polymerization of ethylene oxide (oxyalkylation)

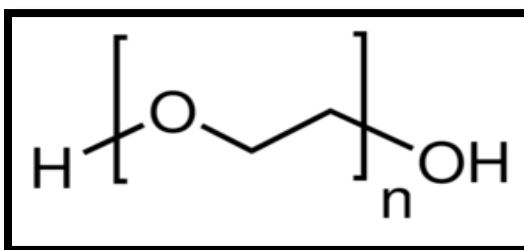


Fig. 1.12 Chemical structure of Polyethylene glycol (PEG).

in the presence of Lewis acid or base catalysts. PEG is similar to PEO i.e., semicrystalline and water-soluble polymers that are commercially available in a wide range of molecular weights depending on the number of monomers. While PEG and PEO with different molecular weights find use in different applications and have different physical properties (e.g., viscosity) due to chain length effects, their chemical properties are nearly identical. Polyethylene glycol is produced by the interaction of ethylene oxide with water, ethylene glycol, or ethylene glycol oligomers. The reaction is catalyzed by acidic or basic catalysts. The chemical formula is $\text{H}(\text{OCH}_2\text{CH}_2)_n \text{OH}$.

The chains can adopt either a helical or extended structure depending upon the electrostatic interaction of the oxygen units with either ions or charged surfaces. Lower molecular weight ($M_w < 1000$) PEGs are viscous and colorless liquids, while PEGs with the molecular weight of 800 to 2000 is pasty or flaky materials with a low melting range, while above a molecular weight of 3000, PEGs are available in solid form with the melting point to a upper limit of about 65°C. Fig. 1.12 depicts the Chemical structure of Po-

lyethylene glycol (PEG).

1.8 Different Polymer electrolytes

Polymer electrolytes are generally classified into:

- ❖ Polymer-salt electrolytes/ Solid Polymer electrolytes (SPE)
- ❖ Nano Composite Polymer Electrolytes (NCPE)
- ❖ Plasticized Composite Polymer Electrolytes
- ❖ Plasticized Nano Composite Polymer Electrolytes (PNCPE)

1.8.1 Polymer-salt electrolytes /Solid Polymer electrolytes (SPE)

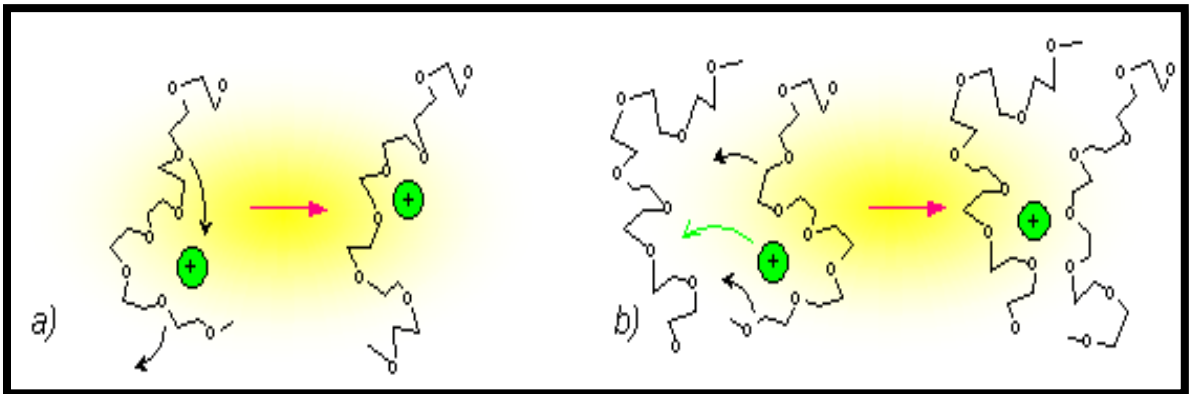


Fig. 1.13 Different mechanisms of cation motion inside polymer electrolyte: assisted by polymer chain motion : a) intra-chain hopping ; b) inter-chain hopping [77].

Polymer electrolytes (PEs) or solid polymer electrolytes (SPEs) are basically made up of a polymer and a salt that can form a complex with the polymer. The main advantage of polymeric electrolytes is their favorable electrical, optical, and mechanical properties; ease of fabrication in thin-film form; and ability to form effective electrode–electrolyte contacts. To achieve a well-complexed polymer electrolyte system, the choice of polymer, as well as that of the metal salt, plays the key role. The choice of the polymer host depends mainly on the characteristics of (1) the presence of a sequential polar group with large sufficient electron donor power to form coordination with cations; (2) a low hindrance to bond rotations, thereby favoring easier segmental motion; and (3) a suitable distance between coordinating centers, to form multiple intra-polymer ion bonds. Hence, such characteristic polymers, like polyethylene oxide (PEO), polypropylene oxide, polyethylenimine, and polyethylene succinate, have been examined as host polymers [78-81].

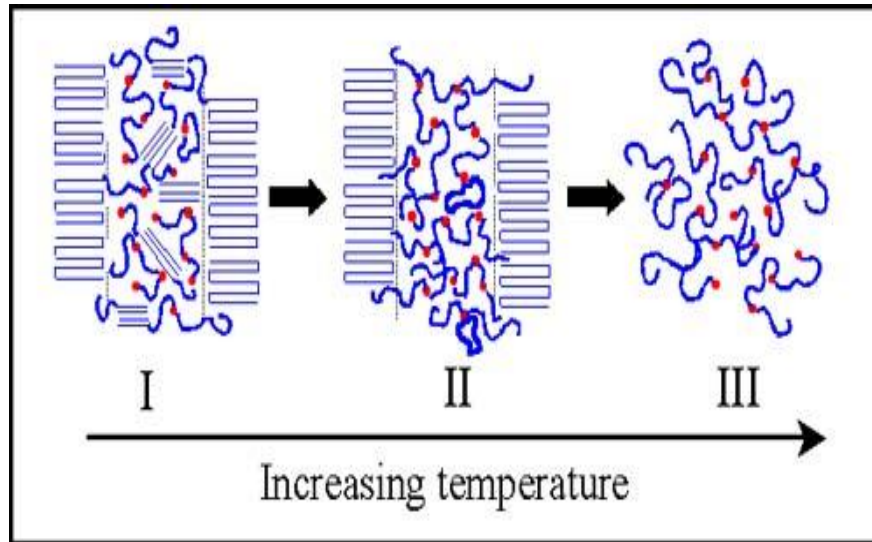


Fig. 1.14 A cartoon of thermally activated process

Various alkali metal-ion-conducting polymer electrolytes were reported in the literature. Few such PEO-based systems complexed with NaI [82], NaClO₄ [83], NaSCN [84], and NaCF₃SO₃ [85] and lithium salts such as LiBF₄, LiF₆ and LiB(C₆H₅)₄ [86], LiSCN [87], and LiCF₃SO₃ and LiClO₄ [88] have been studied. As stated by most experimental work, cation mobility occurs in the amorphous phase and its diffusion occurs through a complex mechanism involving the PEO segmental mobility. For that, crystallization has to be avoided by modifying the polymer structure or by adding salts to inhibit regular packing. A schematic diagram is shown in Fig. 1.13 indicating inter-chain and intra-chain hopping mechanism as part of their conduction process. But, on increasing the salt content further cluster formation starts which hinders the conduction process. This leads to decrease in ionic conductivity. Ionic conductivity of Solid polymer electrolyte is also a thermally activated process, as on heating the polymer chain expands and become more flexible. Generally, in SPE conduction takes place in amorphous region, therefore on increasing in flexibility enhancement in conductivity is observed. A cartoon of such thermally activated process is shown in Fig. 1.14. The main limitation of these solid polymer electrolytes is its low ionic conductivity at ambient temperature.

1.8.2 Nano Composite Polymer Electrolytes

Solid polymer electrolytes (SPEs) suffer from many technical limitations which includes low ionic conductivity, low transference number, poor mechanical stability and

poor electrolyte-electrode contact. These limitations are removed to a great extent by the introduction of nanofillers in the SPEs.

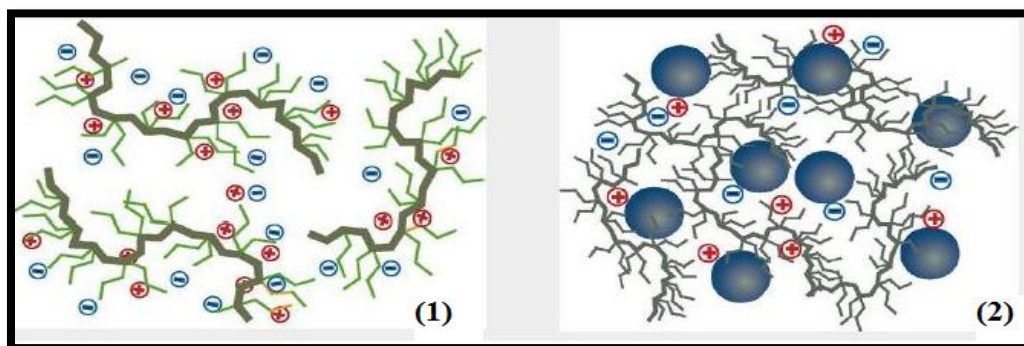


Fig. 1.15 Schematic diagram of polymer electrolyte system (1) without nanofiller and (2) with nanofiller

The composite formed by dispersing the fillers in the polymer electrolytes are known as “*composite polymer electrolytes*” (CPE’s) [89]. Addition of chemically inert and electrically insulating nano-filler such as SiO_2 , Al_2O_3 , TiO_2 , ZnO , etc [90] to SPE’S enhances their conductivity by a few orders of magnitude [91-93]. Conductors thus formed are known as “*Nano Composite Polymer Electrolytes (NCPE)*”. These NCPE’s offer’s some attractive advantages such as superior interfacial contacts, highly flexible, improve ionic transportation, high ionic conductivity and better thermodynamic stability. Fig. 1.15 depicts the polymer systems without (1) and with (2) nano-filler. Addition of nano-filler increases the free volume in the material by generating new conducting pathways. Ion prefers to travel through this pathway which results in enhancement of conductivity as shown in Fig. 1.16.

Various research workers’ had different perspectives regarding the mechanism of nano-filler. Weston and Steele [92] were the first to report the improvement of mechanical properties of (PEO) 8LiClO_4 on doping with β -alumina powder of $40\ \mu\text{m}$ size. Since then there have been a lot of interest in CPE's and most of these studies have been carried out with high molecular weight PEO. It has been found that in addition to the mechanical properties, the doping of inorganic fillers lead to improvements in ionic conductivity, transference number and interfacial behavior with lithium metal electrodes. Croce et.al. [94] used Lewis-acid base type model to explain enhancement in conductivity. According to which nano-filler inhibits recrystallization of host chains and providing new conduct-

ing path ways at the filler surface through Lewis- acid base interaction among different species in SPE.

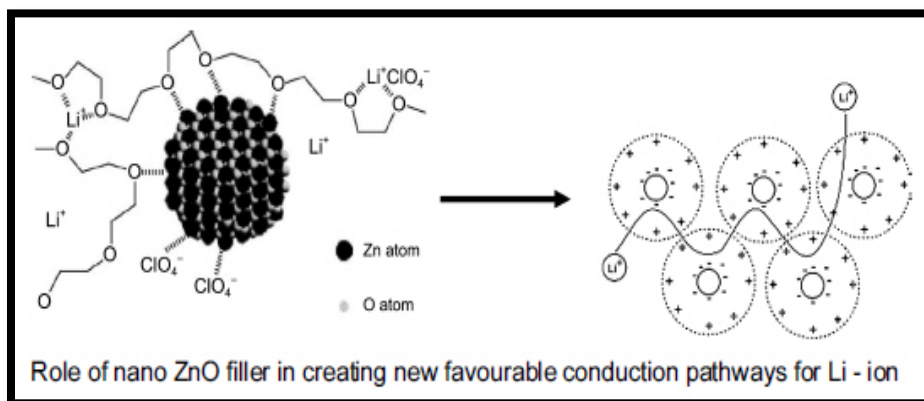


Fig. 1.16 *Li ion prefers to conduct through new conducting pathways.*

Jow and Wagner [95] suggested that the enhancement might arise from formation of a space-charge layer along the interface between the two phases, thus giving rise to increased charge density and conductivity along the interface. Roman et al. [96] have used a three-component percolation type model to explain the increased conductivity. They included three regions; a conductive phase corresponding to the bulk electrolyte, a highly conductive phase at the interface and the insulating phase itself. They found two thresholds and their model can fit the observed behavior for LiI/Al₂O₃ nearly quantitatively with the percolation model. Wang and Dudney [97] have presented a calculation based on a representation of the composite material as an arrangement of cubic particles, with the center of each cube constituting the insulating phase, and the concentric cubic layers about this insulating cube representing areas of enhanced conductivity. Outside of these layers, the conductivity is uniform, fixed at the value of the pure electrolytes. To fit the experimental concentration dependence, they have considered the conductivity in the cubical sheath region that exhibits a relatively sharp maximum at a distance roughly 600Å from the cube center. They suggested that this behavior is a combined result of carrier concentration and mobility.

1.8.3 Plasticized Polymer Electrolytes

Another alternative method to enhance the ionic conductivity of SPEs is addition of Nonvolatile monomeric liquid or low molecular weight polymer additives [98-100].

These additives are known as plasticizers.

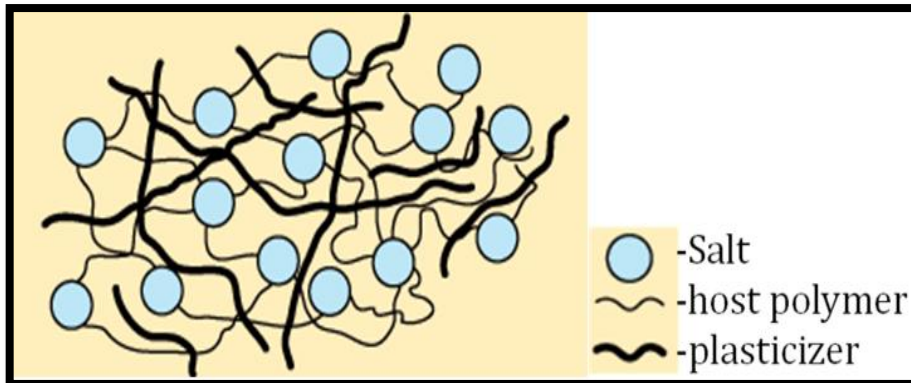


Fig. 1.17 A schematic diagram of plasticized polymer electrolytes.

A schematic diagram of such plasticized polymer electrolytes is shown in Fig. 1.17. Wide variety of plasticizers is used few of them are ethylene carbonate (EC), propylene Carbonate (PC), diethyl formamide (DMF) and very low molecular weight polyethylene glycol. Addition of plasticizers tends to decrease the ion association by increasing the relative permittivity of the system. It also lowers the glass transition temperature and the crystallinity of the semi-crystalline polymers. Moreover, plasticizers often provide an alternate conduction path such that the ion motions may be decoupled from the local motions of the polymers.

The increase in concentration of plasticizer causes the transition from the glassy state to rubbery region at progressively lower temperature. Eventually, it results in a maximum segmental motion of ions [101]. However, upon addition of plasticizer, some limitations are obtained such as low flash point, slow evaporation, and decreases in thermal and mechanical properties, electrical and electrochemical stabilities.

1.8.4 Plasticized Nano Composite Polymer Electrolytes (PNCPE)

There are many reports on ionic conductivity enhancement in SPEs by incorporation of plasticizers. Also, many studies have been focused on enhancement of ionic conductivity by addition of nano sized filler. However, very few reports are available in the Literature dealing “Combined effect” [102] of plasticizer and nanofiller on electrical and thermal properties of SPE’S. Hence, the recent trends are incorporating plasticizer into nanocomposite polymer electrolytes (NCPE’s). Such studies are particularly

important as the loss of mechanical strength of the electrolyte membranes due to plasticization could be re-gained by the incorporation of the nano-filler and vice versa. Plasticization of nanocomposite polymer electrolytes helps in improving the ionic conductivity of polymer electrolytes. To increase amorphous nature of the system, low molecular weight plasticizers are added to the conventional PEO-Salt-nano-filler (NCPE) matrix [103-105]. The low viscosity of the plasticizer decreases glass transition T_g value and increases the amorphous content, whereas high dielectric constant of plasticizer helps to get better ionic dissociation. The decrease in glass transition T_g values results, in an increase in the local chain flexibility which is coupled to the ion mobility.

Some possible explanations for the above observation are

- i) Decrease in the degree of crystallinity.
- ii) Increase in disorder.
- iii) Changes in the glass transition temperature.
- iv) Lewis acid-base interactions at the surface of the nano-filler.
- v) Decrease in ion-association and ion-polymer interaction.
- vi) Increase in ion-mobility.
- vii) Space-charge formation and improved conduction pathways.
- viii) Electrostatic interactions between the ionic species and the fillers.

1.9 Application

Solid state electrolytes have a wide spectrum of industrial applications such as Battery and Non-battery application.

1.9.1 Battery applications

In 1748 Benjamin Franklin first coined the term *battery*. A brief history of battery is mentioned in Fig. 1.18. A battery or cell is a device that produces electric energy from a chemical reaction.

A cell/battery consists of a negative electrode, an electrolyte, which conducts ions; a separator; also an ion conductor and a positive electrode. Battery or cell is further classified into Conventional cells, Solid state battery and Fuel cells.

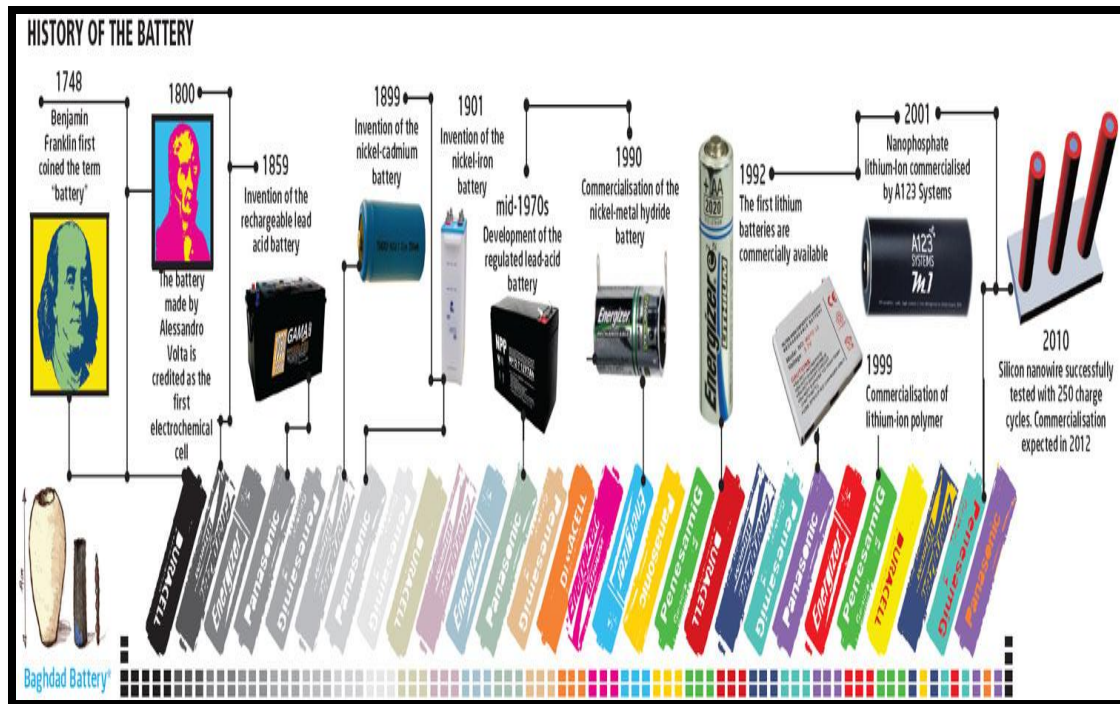


Fig. 1.18 A brief history of batteries

Conventional cells

The nickel –cadmium cells are the commercial batteries available for long since after the dry cells. These batteries have the mechanism almost similar to the zinc anode and manganese di-oxide cathode with KOH or $\text{NH}_4\text{Cl} + \text{ZnCl}_2$ dry cell with the proton and electron diffusion. The proton diffusion enables a reversible reaction at the nickel electrode and hence the cells could be recharged. Similarly, lithium cells have been commercialized from mid 1970, as a power sources for calculators, watches and semiconductors devices. These batteries could not recharge. They are divided into two major types of cathode materials, graphite fluoride and MnO_2 type. LiClO_4 and LiBF_4 / propylene carbonate are often used.

Among various solid electrolytes, stabilized zirconia and β -alumina are widely used in sodium –sulfur batteries. The principle, of sodium-sulfur batteries was established in 1967 by Kummer and his co-workers [106]. These batteries generates as emf of about 2.17V. Sodium-sulfur batteries are high density batteries compared with the conventional batteries. The theoretical energy density by weight is 790 Wh / kg is 4.7 times greater than the lead acid battery. They possess high operating temperature range and the actual

energy density is 200 to 300 Wh /kg. These features are favorable to use them as power sources for electric vehicle and power storage systems.

Solid state batteries with copper and silver as active materials have also been brought into the scientific picture but they exhibit only 0.067-0.69V, which is less than half the value of the manganese dry cells. Generally, the electrolytes used are RbI_3 with $(\text{CH}_3)_4\text{NI}_9$ as cathodes. A five layer battery composed of RbAg_4I_5 as the electrolytes exhibits 3.3V. The energy density is not so high but the shelf life has been observed to be 10years. A battery with $\text{RbCu}_1\text{I}_7\text{Cl}_{13}$ (electrolyte), $\text{Cu-Cu}_x\text{TiS}_2$ (cathode) and $\text{Cu}_x\text{Mo}_6\text{S}_{8-y}$ (anode) has been reported.

Solid State Batteries

In the early stages, batteries used to have liquid electrolytes and many of these batteries had a lot of disadvantages. Liquid electrolyte batteries have a limited working temperature range and are less rugged. These batteries did not have design flexibility and usually have a much shorter shelf life compared to solid electrolyte batteries. Leakage was another problem related to liquid electrolyte batteries. With the advent of solid electrolyte batteries, most of these limitations are overcome, not only as electrolyte materials, but solid electrodes are also used as electrode materials for battery applications. Li^+ based batteries are the most widely used solid state batteries, because of the high energy density and high current capability. Due to the advantage of design flexibility, these batteries are being used in quite a lot of electronic gadgets of varied sizes and shapes.

Fuel Cells

High temperature solid oxide fuel cells (SOFCs) have become of great interest as a potentially economical, environment friendly and energy efficient means of producing electricity [107, 108]. SOFCs are but only one type of fuel cell. Fuel cells are devices capable of giving continuous electrical voltage and current by electrochemically combining fuel and air across an ion conducting material. They work almost on the same principle as the batteries, but need to be supplied with fuel and air continuously. In SOFCs, the ion conduction takes place via vacancy mechanism. Ceramic materials like zirconia (ZrO_2) [109] or ceria (CeO_2) can be prepared with oxygen ion vacancies; sometimes this is achieved by doping. These materials start conducting through oxygen ion vacancies at

high temperatures, when air is used as one electrode. Some of the fuel cells like direct methanol fuel cells (DMFCs) use polymer electrolytes and work at a much lower temperature compared to SOFCs. They are eco friendly, cost effective, light and compact, easy to fabricate and highly energy efficient devices which have considerable potential for small and large scale applications.

1.9.2 Non-battery application

Beside, battery application solid polymer electrolytes have been widely used in sensing devices. As sensors are key elements in the fast developing industrial field. In generally, sensors are devices, which convert physical or chemical quantities into electrical signals, which can be processed and counted. The sensors are employer to carries out a quantitative analysis of a certain property of the substance depending upon the requirement. Few such sensors are discussed below:

Sensors

Most of the sensors are based on fast ionic conductors. They basically use these two principles: 1) the chemical potential difference across the electrolyte material (potentiometric sensor) and 2) the charge passed through the electrolyte (amperometric sensor). Many of these sensors are used in gas and humidity sensing. When the electrolyte is kept at two different pressures (e.g. exposed to two different gases at different pressures, one as reference gas), a low e.m.f. is produced due to the flow of ions. Sensors based on FIC materials are classified into three major types. In type I sensors, the gas to be detected coupled directly with the mobile ions of the solid electrolytes through an electrochemical reaction: $O_2 + 4e^- \rightarrow 2O^{2-}$. In type II sensors, the oxygenic gases like CO_2 are converted into the immobile ions (CO_3^{2-} of the solid electrolyte). In type II sensors, the cell is attached with a porous layer of Na_2SO_4 or Na_2CO_3 (auxiliary phase) respectively to detect some of the gases like SO_2 or CO_2 with an electrochemical cell using NASICON [110]. The base electrolyte itself has nothing to do with the oxygenic gases. This type of sensors has an advantage that it does not need a reference gas for operation.

Mostly all the sensing devices measures chemical or physical quantities. But for making the device to be handy, speedy-and easy, the quantity measured is made to be electrical signal. Determination of the concentration of ions (Chemical Sensing) is more

probable for making this a successful one. Sensors have been widely used throughout the world as hazard alarms for homes use to control units for automated production lines. Automated oxygen sensors based on zirconia are used in the combustion control and for preventing air-pollution. Chemical sensors are of four types namely:

- i) EMF type: transducing the difference of chemical potential into (yttria-stabilized zirconia (YSZ) and calcia stabilized zirconia (CSZ) are widely used for this types of sensors) (used in nuclear power plants)
- ii) Limiting current types: transducing the concentration of the species concerned into the limited current of an electrolyte cell (A system of air –H₂ is used for this type)
- iii) Semiconductor types: utilizing the conductivity changes of semiconductor on adsorption or partial reducing of semiconductors.
- iv) FET type: utilizing changes of source –drain current of a FET on absorption of chemical species onto its gate electrode.

Sensors made of β -alumina, LaSrCoO₃, AgCl (+Ag₂S), AgI (+Ag₂S), CdS (+Ag₂S) and LaF₂ (+EuF₂) have been used for various purpose like alcohol sensors, co sensors, H₂ sensors, humidity sensors, ion sensors, ion sensors, and chemical species like SO_x and NO_x sensors.

1.9.3 Electrochromic Devices

Electrochromism can be defined as a color change induced in a material by an applied electric field or current [111]. Some ions in solid compounds can be reduced or oxidized electrochemically with a consequent change in color. Electrochromism occurs due to one of the processes like the production of color centers due to trapping of the injected electrons, the transferring of charge from one type of impurity center to another by the electric field which causes the growing of an adsorption band associated with one type of impurity center at the expense of the other, the induction of a shift in absorption band (and hence color) due to a tunneling process or the electrochemical reduction and oxidation of certain ions or molecules accompanied by a change in color.

1.10 Present Investigation

In the present research work, the main objective is to investigate the effect of var-

ious PEO-based solid polymer electrolytes with silver and lithium dopant salt upon addition of nano-sized inorganic filler and/or plasticizer on electrical properties. The aspire of this work is also to study the temperature dependence of the solid composite polymer electrolytes and examine the mechanisms pertaining to transport of conducting ions of these solid composite polymer electrolytes Besides, it is aimed to study the dielectric behaviour of the solid composite polymer electrolytes and characterize these by morphological, structural and thermal properties of these solid composite polymer electrolytes. The morphology of polymer electrolytes were scrutinized by scanning electron microscopy (SEM), whereas the structural behaviour of these solid composite polymer electrolytes are characterized by means of X-ray diffraction (XRD) and fourier transform infrared (FTIR). Thermal properties of polymer electrolytes are studied by differential scanning calorimetry (DSC) studies.

A large number of lithium ion conductors have been developed by different worker worldwide because of the availability of insertion materials to realize high energy density solid state batteries. The present work is directed towards investigation of analogues or similar silver systems as well as lithium nano systems. Since, much work has already been reported on PEO-LiCF₃SO₃ polymer electrolytes [112], further study to modify the system with incorporation of nano-filler. From earlier investigations, it appears that, the improvements in conductivity of silver salt (AgI, AgNO₃ etc) with additives was not that much successful. In this context, investigation of some AgCF₃SO₃ based silver and LiCF₃SO₃ based lithium ion conducting systems has been undertaken to improve the cationic conductivity through different routes on (i) polymer-salt complexation PEO:AgCF₃SO₃, (ii) effect of nano-filler SiO₂ on Polymer-salt complexation (PEO:AgCF₃SO₃), (iii) effect of plasticizer PEG on nano composite polymer electrolyte PEO:AgCF₃SO₃:SiO₂, as well as effect of (iv) nano particle Al₂O₃ on PEO: LiCF₃SO₃:PEG, and (v) finally effect of plasticizer PEG on PEO:LiCF₃SO₃: Al₂O₃ composite polymer electrolytes. In the present work, a PEO-based composite polymer electrolyte system has been prepared and several experiment techniques such as XRD, DSC, FTIR, Impedance spectroscopy and transference number measurement have been employed to characterize the polymer electrolyte system.

Earlier attempts have been made to enhance the conductivity of pure PEO by add-

ing various salt like LiBF_4 , LiPF_6 and $\text{LiB}(\text{C}_6\text{H}_5)_4$, LiSCN , LiSO_3CF_3 and LiClO_4 , NaSCN , NaI , NaClO_4 , NaSCN , NaCF_3SO_3 , NaPF_6 , NH_4I , NH_4ClO_4 , LiClO_4 , AgI , AgNO_3 [113-120]etc. In present case, AgCF_3SO_3 and LiCF_3SO_3 salts are used. But the low ionic conductivity of polymer salt complex limits their application at ambient temperature [121]. To further improve the ion conductivity nano-filler SiO_2 is added to the PEO: AgCF_3SO_3 and Al_2O_3 to PEO: LiCF_3SO_3 solid polymer electrolyte system. The fillers affect the PEO dipole orientation by their ability to align dipole moments while the thermal history determines the flexibility of the polymer chains for ion migration. It generally improves the transport properties, the resistance to crystallization, and the stability of the electrode/electrolyte interface. Another alternative approach is the addition of low molecular weight plasticizers like PC, EC, PEG etc. to the nano composite polymer electrolyte system. Plasticizers are small molecules that are chemically similar to polymer. They create gaps between the polymer chains for greater mobility and reduce the inter-chain interactions. It is the material not only enhances the deformability of a polymeric compound but also reduces glass transition temperature value. It is observed that plasticization is the conventional way to reduce the crystallinity and increases the amorphous phase content of the polymer electrolytes. Usually both crystalline and amorphous phase are present in polymer electrolytes but conductivity mainly occurs in amorphous phase. Hence, to further increase the amorphous phase of PEO: AgCF_3SO_3 : SiO_2 and PEO: LiCF_3SO_3 : Al_2O_3 nano composite polymer electrolytes plasticizer PEG is also added, to study its effect on the conduction and its electrolyte properties.

Thus, in present work, following different series of solid polymer electrolytes are investigated.

i) PEO- AgCF_3SO_3 (x wt %)

In this series, the amount of PEO is fixed and salt AgCF_3SO_3 is varied from 2 to 11 wt% of PEO to observe its effect in PEO system.

ii) PEO- $[\text{AgCF}_3\text{SO}_3]_{7\text{wt}\%}$ - SiO_2 (x wt %) ,with x = 5, 10, 15 and 20 wt%

In the second series, the amount of PEO- AgCF_3SO_3 (7 wt %) is fixed and nano filler SiO_2 is varied to observe the effect of nano filler on PEO- AgCF_3SO_3 system.

iii) PEO-[AgCF₃SO₃]_{7wt%} -[SiO₂]_{20wt%}-PEG (x wt %),

with x = 5, 10, 15, 20 and 25 wt%

In this series, the amount of plasticizer PEG is varied to observe the effect of plasticizer on PEO-AgCF₃SO₃-SiO₂ system.

iv) PEO-[LiCF₃SO₃]_{5wt%} -[PEG]_{10wt%}- Al₂O₃ (x wt %)

with x = 1, 2,3,4 and5 wt%

In the fourth series, the amount of nano filler Al₂O₃ is varied to observe the effect of nano filler on PEO-LiCF₃SO₃-PEG system

v) PEO-[LiCF₃SO₃]_{5wt%} -[Al₂O₃]_{1wt%} -PEG (x wt %)

with x = 5, 10, 15, 20, 25 and 30 wt%

In the fifth series, the amount of plasticizer PEG is varied to observe the effect of plasticizer on PEO-LiCF₃SO₃- Al₂O₃ system.

References:

- [1] E. Warburg, Widemann, *Ann. Physik*, 21 (1884) 622.
- [2] E. Warbug, F. Tegetmeier, Wiedemann, *Ann. Physik*, 32 (1888) 455.
- [3] A.R. West, *Solid State Chemistry and its applications*, John Wiley & Sons Pvt. Ltd., Singapore 2003.
- [4] M. Armand, J.M. Tarascon, *Nature* 10(1998) 439-448.
- [5] C. Tubandt, H. Reinhold, *Electrochem*, 29 (1923) 313.
- [6] T. Takahashi (eds.), *High conductivity solid Ionic Conductors-Recent Trends and Applications*, World Scientific, Singapore (1989).
- [7] M. Faraday, *Experimental Researches in Electricity*, Taylor and Francis, London, I (1839) 1339
- [8] C. Tubandt, E. Lorentz, *Z. Physik. Chem.*, 86 (1913) 513.
- [9] J.A.A. Ketelaar, *Trans Faraday Soc.* 34 (1938) 874.
- [10] S. Chandra, *Superionic Solids: Principles and Applications*, North Holland Publishing Company (1981).
- [11] B. John, Goodenough, *J. Pure and Appl. Chem.*, 67 (1995) 931.
- [12] M. Wakihara, *Materials Science and Engineering: R: Reports*, 33(4) (2001) 109.
- [13] W. Van Gool (Ed.) *Fast Ion Transport in Solids*, North Holland Publishing Company (1973).
- [14] T. Minami, *J. Non-Cryst. Solids* 95-96 (1987) 107.
- [15] W. Nernst, *Z. Electrochem.* 6 (1899) 41.
- [16] C. Tubandt, in: *Handbuch der Experimental Physik* XII part I, W. Wien, F. Harms (Eds.), Akadem. Verlag (1932).
- [17] B. Reuter, K. Hardel, *Ber. Bunsenges. Phys. Chem.* 70 (1966) 82.
- [18] Y.F.Y. Yao, J.T. Kummer, *J. Inorg. Nucl. Chem.* 29 (1967) 2453.
- [19] J.N. Bradley, P.D. Greene, *Trans. Faraday. Soc.* 62 (1966) 2069.
- [20] B.B. Owens, G.R. Argue, *Science* 157 (1967) 308.
- [21] B.V.R. Chowdari, S. Chandra, S. Singh, P.C. Srivastava (Eds.). *Solid State Ionics -Materials and Applications*, World Scientific. Singapore (1992).
- [22] B.V.R. Chowdari, K. Lal. S.A. Agnihotry, N. Khare, S.S. Sekhon, P.C. Srivastava, S. Chandra (Eds.), *Solid State Ionics - Science and Technology*, World Scientific, Singapore (1998).
- [23] B.V.R. Chowdari, S.R.S. Prabaharan, M. Yahaya, I.A. Talib (Eds.), *Solid State Ionics -Trends in the New Millennium*, World Scientific, Singapore (2002).
- [24] *Proceeding of the International Conferences on Solid State Ionics*, *Solid State Ionics*, 9-10 (1983), 18-19 (1986), 28-30 (1988), 40-41 (1990), 53-56 (1992), 86-88 (1996), North Holland Publishing Company, Amsterdam.
- [25] R.C. Agrawal, R.K. Gupta, *J. Mater. Sci.* 34(1999) 1131-1162.
- [26] C. Wagner, *Naturwiss*, 31 (1943) 365.
- [27] C. Lucat, P. Sorbe. J. Portier, J.M. Reau, P. Hagenmuller. J. Granec, *Mater. Res. Bull.* 12 (1977) 145.

- [28] T. Jensen, A. Dening, G. Huber, B.H.T. Chai, *Opt. Lett.* 21 (1996) 585.
- [29] R. Ramamoorthy, P. K. Dutta, S.A. Akbar, *J. Mater. Sci.* 38 (2003) 4271 – 4282.
- [30] P.J. Gellings, H. J. M. Bouwmeester, *The CRC Handbook of Solid State Electrochemistry*, CRC Press, Inc. 1997.
- [31] J.M Reau, , C. Lucat, J. Portier, P. Hagenmuller, L. Cot, S. Vilminot, *Mater. Res. Bull.*, 13 (1978) 877.
- [32] P.S. Anantha, K. Hariharan, In B.V.R. Chowdari, H.-L. Yoo, G.M. Choi and J.-H. Lee (Eds.) *Solid State Ionics: The Science and Technology of Ions in Motion*, World Scientific, Singapore, (2004) 955-962.
- [33] K. Hariharan, J. Maier, *J. Electrochem. Soc.*, 142 (1995) 3469.
- [34] L.A. Bueno, J.P. Donoso, C.J. Magon, I. Kosacki, F.A. Dias Filho, C.C. Tambelli, Y. Messaddeq, S.J.L. Ribeiro, *J. Non-Cryst. Solids*, 351 (2005) 766.
- [35] N. Sata, K. Eberman, K. Eberl, J. Maier, *Nature*, 408 (2000) 946.
- [36] L. Patro, K. Hariharan, *Solid State Ionics* 239 (2013) 41.
- [37] L.W. Strock, *Z. Phys. Chem. B*, 25 (1934) 41 1.
- [38] S. Hoshino, *J. Phys. Soc. Japan*, 10 (1955) 197.
- [39] Y. Oyama, J. Kawamura, *Solid State Ionics*, 53-56 (1992) 1221.
- [40] H. Eliasson, I. Albinsson, B.E. Mellander, *Electrochim. Acta*, 43 (1998) 1459.
- [41] T. Takahashi, *J. Appl. Electrochem.*, 3 (1973) 79.
- [42] A. F. Sammells, J. Z. Cougoutas, B.B. Owens, *J. Electrochem. Soc.*, 122 (1975) 1291.
- [43] N. Machida, M. Chusho, T. Minami, *J. Non-Cryst. Solids*, 101 (1988) 70-74.
- [44] M. Sukeshini, K. Hariharan, *J. Mater. Sci. Lett.*, 9 (1990) 544-546.
- [45] P. Knauth, *Solid State Ionics*, 180 (2009) 911–916.
- [46] G. Nazri, G. Pistoia (Eds), *Lithium batteries-Science and Technology*, Kluwer Academic Publishers, London (2004).
- [47] R. Mercier, J.P. Malugani, B. Fahys, G. Robert, *Solid State Ionics* 5(1981)663.
- [48] J. P. Malugani, , G. Robert, *Solid State Ionics* 1 (1980) 519.
- [49] W. L. Roth, G. C. Farrington, *Science* 196 (1977) 1332.
- [50] I. D. Raistrick, C. Ho, R. A. Huggins, *Mater. Res. Bull.* 11 (1976) 953.
- [51] Y. Yao, J.T. Kummer, *J. Inorg. Nucl. Chem.*, 29, (1967) 2453.
- [52] R. C. Agrawal, R. K. Gupta, *J Mater. Sci.* 34 (1999) 1131.
- [53] P. S Anantha, K. Hariharan, *J. Phys. Chem. Solids*, 64 (2003) 1131.
- [54] Y. Chatani, S. Okamura, *Polymer*, 28 (1987) 1815.
- [55] C. C. Hunter, M.D. Ingram, *Solid State Ionics*, 14 (1984) 31.
- [56] F. M. Gray. *Solid Polymer Electrolytes*. VCH Publishers, 1991.
- [57] P. Bahadur, N V Sastry, *Principles of Polymer Science*, 2nd Edition, Narosa Publishing House Ltd.2009.

- [58] H. K. Frensdor, *J. Amer. Chem. Soc.*, 93(1971) 600.
- [59] C. A. Vincent, Polymer electrolytes, *Progress in Solid State Chemistry*, 17 (1987) 145.
- [60] Y. Takahashi, H. Tadokoro, *Macromolecules*, 6 (1973) 672.
- [61] J. Maxfield, I.W. Shepherd, *Polymer*, 16 (1975) 505.
- [62] K. J. Liu, J. L. Parsons. *Macromolecules*, 2 (1969) 529.
- [63] J. D. Hoffman, G. T. Davis, J. I. Lauritzen, *Treatise on solid-state chemistry, Crystalline and non-crystalline solids* - edited by N. B. Hannay, Plenum Press, New York, 3 (1976) 497.
- [64] M. Ramanathan, B. Seth, Darling, *Progress in Polymer Science*, 36 (2011) 793.
- [65] S.H. Kim, M.J. Misner, L.Yang, O. Gang, B.M. Ocko, T.P. Russell, *Macromolecules* 39.24 (2006): 8473-8479.
- [66] R. Frech, S. Chintapalli, P. G. Bruce, C. A. Vincent, *Chem. Commun.* (1997)157.
- [67] M. Forsyth, J. Sun, D. R. Macfarlane, A. J. Hill, *J. Polymer Science Part B: Polymer Physics*, 38 (2000) 341.
- [68] N. Ataollahi, A.Ahmad, H. H. Hamzah, M.Y. Rahman, N.S. Mohamed, *Appl. Mech. and Mater*, 117 (2013) 313.
- [69] S. Ramesh, T. F. Yuen, C. J. Shen, *Spectrochimica Acta Part A*, 69 (2008) 670.
- [70] J. H. Kim, B.R. Min, C.K. Kim, J. Won, Y. S. Kang, *J Phys Chem. B*, 106 (2002)2786.
- [71] S. A. Suthanthiraraj, D.J. Sheeba, *Indian J. Phys.* 79(2005) 807.
- [72] S. U. Hong, C. K. Kim, Y. S. Kang, *Macromolecules*, 33 (2000) 7918.
- [73] B. Scrosati, C. A. Vincent, *M.R.S. Bulletin*, 25 (2000) 28.
- [74] C. Labreche, J. Prud'home, *J. Power sources*, 81/82 (1999)130.
- [75] C.Berthier, W.Grorecki, M.Minier, M.B.Armand, J.M.Labagno, P.Rigand, *Solid State Ionics* 11 (1988) 91.
- [76] M. Kumar, S.S. Sekhon, *Ionics* 8 (2002) 223.
- [77] A. Bhide, K. Hariharan, *J Power Sources*, 43(10) (2007) 4253.
- [78] M. B. Armand, *Ann. Rev. Mater. Sci.* 16 (1986) 245.
- [79] J. R. MacCallum, C.A.Vincent, (eds), *Polymer electrolyte reviews*. Elsevier, London (1987).
- [80] P.G. Bruce, *Solid-state electrochemistry*. Cambridge University press, Cambridge, (1995).
- [81] D. Fauteux, M.D. Lupien, C.D. Robitaille, *J. Electrochem. Soc.* 134 (1987) 2761.
- [82] U. Sasikala, P. Naveen Kumar, V.V.R.N.Rao, A. K. Sharma, *Inter. J. Engg. Sci. & Adv. Technology*, 2 (2012) 722.
- [83] S. G. Greenbaum, Y. S. Pak, M. C. Wintersgill, J. J. Fontanella, J. W. Schultz, *J Electrochem Soc* 135 (1988) 235.
- [84] S. G. Greenbaum, K.J. Ademic, Y.S. Pak, M.C. Wintersgill, J.J. Fontanella, *Solid State Ionics*, 1042 (1988) 28.
- [85] S. A. Hashmi, A. Chandra, S. Chandra, In: Chowdari BVR et al. (eds) *Solid-State Ionics. Materials and Applications* World Scientific, Singapore, (1992) 567.

- [86] E. A. Retman, M.L. Kaplan, R.J. Cava, *Solid State Ionics* 17 (1985) 67.
- [87] P. R. Sorenson, T. Jacobson, *Electrochim Acta*, 27 (1982)1675.
- [88] S. A. Hashmi, H.M. Upadhyaya, A.K. Thakur, A.L. Verma, *Ionics* 6 (2000) 248.
- [89] A. Turkovic, P. Dubcek, K. Juraic, S. Bernstorff, M. Buljan, *American Journal of Nanoscience and Nanotechnology*, 1 (2013) 6.
- [90] J. B. Phipps, D. H. Whitmore, *Solid State Ionics*, 9-10 (1983)123-130.
- [91] M. Kbalá, M. Makyta, A. Levasseur, and P. Hagenmuller, *Solid State Ionics*, 15 (1985)163.
- [92] J. E. Weston, B.C.H. Steele, *Solid State Ionics*, 7 (1982) 75.
- [93] S. K. Tripathi, A. Gupta, A. Jain, M. Kumari, *Indian J. Pure Applied Physics*, 51(2013) 358.
- [94] F. Croce, L. Persi, B. Scrosati, F. Serriano, E. Plichta, M.A. Hendrickson, *Electrochim Acta* 46 (2001) 2457.
- [95] T. Jow, J. Bruce Wagner, Jr. *J. Electrochem. Soc.*, 126 (1979) 1963.
- [96] H. E. Roman, A. Bunde, W. Dieterich, *Phys. Rev. B* 34 (1983) 3439.
- [97] J. C. Wang, N. Dudney. *Solid State Ionics*, 18-19 (1986)112.
- [98] C. W. Kuo, W.B. Li, P.R.Chen, J.W.Liao, C.G. Tseng, T.Y. Wu, *Int. J. Electrochem. Sci.*,8 (2013) 5007.
- [99] C. W. Kuo, C.W. Huang, B.K. Chen, W.B. Li, P.R. Chen, T.H. Ho, C.G. Tseng, T.Y. Wu, *Int. J. Electrochem. Sci.*, 8 (2013) 3834.
- [100] K. Mishra , D.K. Rai, *Appl. Mech. Mater.*, 110-116 (2012) 278.
- [101] Z. Osman, Z.A Ibrahim, A.K Arof, *Carbohydrate Polymers*, 44 (2001) 167.
- [102] M. R. John, L. B. Fen, *Ionics*, 16 (2010) 335.
- [103] H.M.J.C. Pitawala, M A K L. Dissanayake, V.A. Seneviratne, B.E. Mellander, I. Albinson, *J. Solid State Electrochem*, 12 (2008) 783.
- [104] H.M.J.C. Pitawala, M A K L. Dissanayake, V.A. Seneviratne *Solid State Ionics*, 178(13/14) (2007) 885.
- [105] J.T. Kummer, N. Weber, *Battery Having a Molten Alkali Metal Anode and a Molten Sulfur Cathode*. U.S. Patent 3, 413,150,(1968).
- [106] A. B. Stambouli, E. Traversa, *Renewable and Sustainable Energy Reviews* 6 (2002) 433.
- [107] A. Atkinson, S. Barnett, R. J. Gorte, J. T. S. Irvine, A. J. McEvoy, M. Mogensen, S. C. Singhal & J. Vohs, Research Article abstract *Nature Materials* 3(2004) 17.
- [108] V. Vladislav, K. N. Evgeny, Navmovich Alim, A. Vecher, *J Solid state Electrochem*, 3 (1999) 61.
- [109] N. Yamazoe, N. Miurs, *J. Electroceramic*, 2(1998) 243.
- [110] I. F. Chang, B. L. Gilbert, T. I. Sun, *J. Electrochem. Soc.*, 122 (1975) 955.
- [111] C.A. Vincent, Polymer electrolytes. *Prog. Solid State Chem.*, 17(1987) 145.
- [112] E.A. Reitman, M.L. Kaplan, R.J. Cava, *Solid State Ionics* 17 (1985) 67.
- [113] P.R. Sorensen, T. Jacobson, *Electrochim. Acta* 27 (1982) 1675.
- [114] Y.L. Lee, B. Crist, *J. Appl. Phys.* 60 (1986) 2683.

- [115] D. Fauteux, M.D. Lupien and C.D. Robitaille, *J. Electrochem. Soc.* 134 (1987) 2761.
- [116] S.G. Greenbaum, K.J. Adami⁶, Y.S. Pak, M.C. Wintersgill, J.J. Fontanella, *Solid State Ionics*, 28-30 (1988) 1042.
- [117] S.A. Hashmi, A. Chandra and S. Chandra, *Solid State Ionics: Materials and Applications*, ed. B.V.R. Chowdari (World Scientific, Singapore, (1992) 567.
- [118] A. Chandra. P.C. Srivastava and S. Chandra, *Solid State Ionics: Materials and Applications*, ed. B.V.R. Chowdari (World Scientific, Singapore, (1992) 397.
- [119] N. Srivastava, S.A. Hashmi and S. Chandra, *Solid State Ionics: Materials and Applications*, ed. B.V.R. Chowdari (World Scientific, Singapore, 1992) pp. 561.
- [120] G. MacGlashan, Y.G. Andreev, P.G. Bruce. *Nature*, 398(1999) 792.
- [121] H.J. Walls, J.U. Zhou, J.A. Yerian. *J. Power Sources* 89(2000)156.
-

CHAPTER 2

THEORETICAL DETAILS

***I**n this chapter theoretical details of various techniques used for characterization is discussed. Later part of chapter consists of discussion of different models used in understanding the conduction mechanism in polymer electrolytes.*

2.1 Introduction

Scientific breakthroughs are often a result of the innovative invention, development and implementation of new scientific instruments and techniques has been revealed from the past. The development of instrumentation and associated techniques are important for scientific progress. Materials characterization is one of key components of materials science which investigates the relationship between the structure of materials at atomic or molecular scales and their macroscopic properties. Hence, it has become of utmost importance to have a basic idea of fundamental of instruments used for characterization. Fundamentals of few commonly used characterization techniques are discussed below.

2.2 Description of characterization techniques

In the field of polymers, various types of evaluative and analytical methods are available. These instruments include Fourier Transform Infrared (FTIR) spectrometer, Differential Scanning Calorimeter (DSC), X-ray Diffractometer (XRD), Scanning Electron Microscope (SEM) and Impedance Spectrometer (IS). As the structural and thermal analyses are of great interest, investigation of solid polymer electrolytes were generally carried out by X-ray diffraction (XRD), scanning electron microscopy (SEM) and FTIR spectroscopy. Complex impedance spectroscopy is commonly employed to study the ionic conductivity, electrical as well as dielectric properties and modulus formalism of the solid electrolytes.

2.2.1 Fourier Transform Infrared Spectroscopy (FTIR)

Fourier transform infrared spectroscopy (FTIR) is a prime and versatile analytical technique used to examine polymeric materials. The main fundamental of FTIR is to determine structural information about a molecule. It facilitates the study such as polymer reactions, degradation, cross-linking etc. because the spectra can be scanned and recorded in a matter of seconds. It is a qualitative analysis to identify unknown material accomplished by the comparison. In addition, it allows the spectra to generate the hidden spectra via digital subtraction. A very small size is sufficient to undergo the analysis for highly localized sections of the sample by coupling the FTIR instrument with a microscope. FTIR is also used to study the all types of polymer composites. The incorporation of do-

part salt, nanofiller or plasticizer in to the host polymers is confirmed by absorption, shifting, broadening etc. of the characteristic peak. Additionally, if any interaction arises from chemical or physical interaction between them is also exhibited.

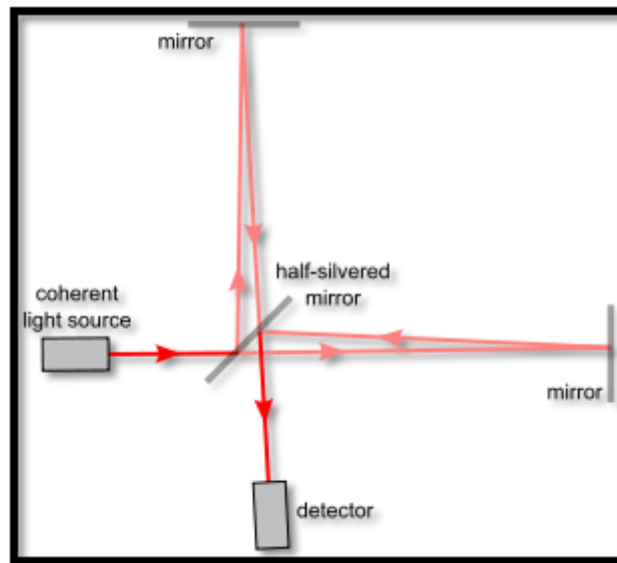


Fig. 2.1 *The optical diagram of a Fourier Transform Infrared Spectrometer.*

The main principle of FTIR is based on interferometry which is an optic study. It separates infrared beam of light serving as a light source radiation into two ray beam as shown in Fig. 2.1. Once the beam of infrared is passed through the sample, the molecules absorbed by the infrared radiation and then excited to a higher energy state. Thus, the energies associated with these vibrations are quantized; within a molecule and only specific Vibrational energy levels are allowed. The amount of energy absorbed at each wavelength is recorded. The frequencies which have been absorbed by the sample are determined by detector and the signal is amplified. Hence, IR spectrum is obtained. FTIR spectroscopy is not only applied in the crystalline region of complexation, but it is also used to study the complexation in amorphous phase [1].

2.2.2 Differential Scanning Calorimetry (DSC)

E.S. Watson and M.J. O'Neill in 1962 developed a technique in order to carry out thermal analysis and to investigate physical and chemical properties of various materials. Since then, various techniques are employed for thermal analysis the specimen such as:

Thermo gravimetric analysis (TGA), Differential thermal analysis (DTA), Differential scanning calorimetry (DSC), Dynamic mechanical thermal analysis (DMTA) etc. Out of all these techniques Differential scanning calorimetry (DSC) is the most widely used technique [2, 3]. DSC is used to analyze the specimen like polymer, glasses, organic materials, inorganic materials etc.

The schematic diagram is shown in the Fig. 2.2. As shown in figure, it consist of two pans i.e.; one reference pan which is either an empty pan or filled with inert material, like anhydrous alumina and another pan in which the investigated sample is encapsulated. An individual heater is provided to the both sample as well as reference and both of them are maintained at almost the equal temperature throughout the experiment. Generally, the temperature program for a DSC analysis is designed such that the sample holder temperature increases linearly as a function of time. The reference sample should have a well defined heat capacity over the range of temperatures to be scanned. In the cell, a metallic disc (made of constantan alloy) is the primary means of heat transfer to and from the sample and the reference. The sample contained in a metal pan and the reference (an empty pan) pan is placed on raised platforms formed in the constantan disc. When the heat is supplied through the disc, the differential heat flowing to the sample and reference is been measured. The basic principle in this technique is that the specimen undergoes a physical transformation such as phase transitions; more or less heat will need to flow to it than the reference to maintain both at the same temperature. The amount of heat flowing through the specimen depends on whether the process is exothermic or endothermic. If a solid specimen melts to a liquid it will require more heat flowing through the specimen to increase its temperature at the same rate as the reference. This is due to the absorption of heat by the specimen as it undergoes the endothermic phase transition from solid to liquid. In same manner when the specimen undergoes exothermic processes (such as crystallization) less heat is required to raise the specimen temperature. By observing the difference in heat flow between the specimen and reference, differential scanning calorimeters are able to measure the amount of heat absorbed or released during such transitions. These exothermic or endothermic heat flows are graphically analyzed as a function of time or temperature as shown in Fig. 2.3. This curve can be used to calculate enthalpies of transitions. This is done by integrating the peak corresponding to a giv-

en transition. It can be shown that the enthalpy of transition can be expressed using the following equation:

$$\Delta T = q Cp/ K \dots\dots\dots (2.28)$$

Where, ΔT is the difference in the temperature between the reference and the sample material, q is the heating rate, Cp is heat capacity (at constant pressure) and K is the calibration for the particular instrument being used. Fig 2.3 shows that a shift in the base line is resulted, from the change in the heat capacity of the sample. These curves are used to analyze the phase transitions, such as melting, glass transitions and crystallization. These transitions involve energy changes or heat capacity changes that can be detected by DSC technique with great sensitivity.

Differential scanning calorimetry (DSC) technique is employed to measure a various characteristic properties of a sample such as glass transition temperature T_g , crystallization temperature (T_c) and crystalline melting point (T_m) [4, 5].

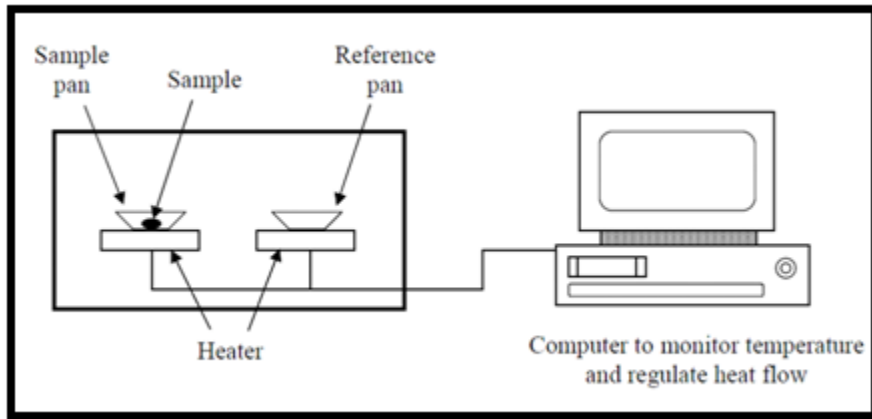


Fig. 2.2 Schematic representation of the DSC unit

The glass transitions temperature T_g is an important parameter of a polymeric material which is used as a measure for evaluating the flexibility of a polymer molecule and to investigate the type of response when the polymeric material would exhibit to mechanical stress. At the glass transition temperature T_g , the phase transformation takes place wherein, solid converts to liquid (or melt) state. When the amorphous polymer is heated, kinetic energy of the molecule increases. As the polymer retains its rubbery properties, the mobility of molecules is still restricted even if there is a presence of short-range vi-

brations and rotations. Polymer above T_g will be soft and flexible and exhibits delayed elastic response. Hence they will arrange themselves continuously into a crystalline form. At this stage, heat is given out from the system and it is known as crystallization temperature (T_c). At temperature above T_c the polymer loses its elastometric behavior and it termed as crystalline melting temperature (T_m). All this phases are shown in DSC curve. Hence DSC plays a vital role in determining the glass transition temperature (T_g), crystallization temperature (T_c) and crystalline melting point (T_m) of polymer materials.

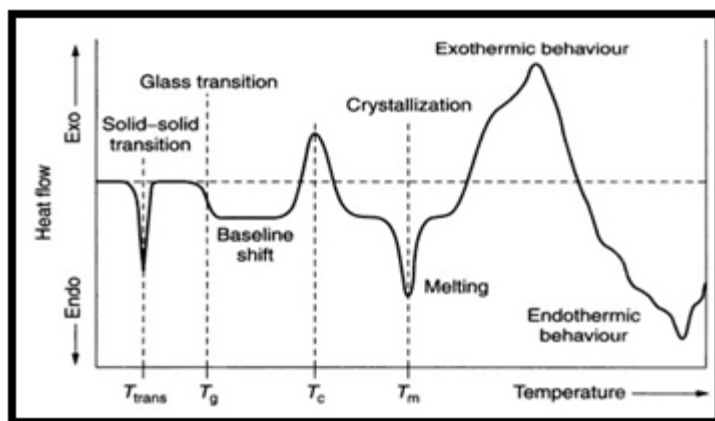


Fig. 2.3 A typical DSC plot obtained for polymer sample [6].

2.2.3 X- ray Diffraction (XRD)

The presence of a known compound or phase in a specimen can be detected by X-ray diffraction technique (XRD). The identification of compounds for qualitative analysis can be carried out using this technique. According to Smart and Moore [6], XRD data also provides a rough idea of the purity of sample. It is an identification of unknown crystalline materials, characterization of crystalline or amorphous materials. X-ray, in general is an electromagnetic radiation ranging from 10^{-10} m of wavelength i.e $\sim 1 \text{ \AA}$ and lies between γ -ray and the ultraviolet in the electromagnetic spectrum. Usually a tungsten filament is electrically heated and a beam of electrons are thus emitted. These electrons are accelerated by a high potential difference (20–50kV) and allowed to strike a metal target, copper (Cu). The incident electrons have sufficient energy to knock out (or ionize) electrons from the innermost K shell ($n = 1$) as shown in Fig 2.4 (a) and this in turn creates vacancies. An electron in an outer orbital ($2p$ or $3p$) immediately drops down to occupy

the vacant and the energy released appears as radiation, as shown in Fig. 2.4(b).

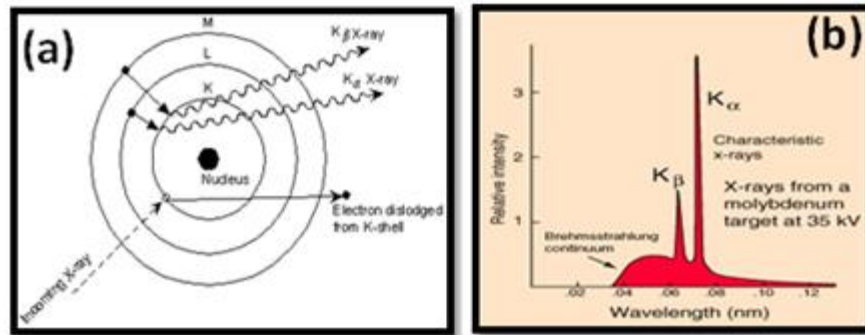


Fig. 2.4 Generation of K_{α} and K_{β} transitions.

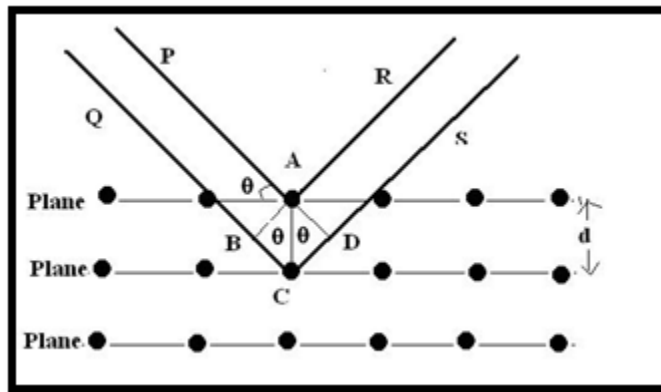


Fig. 2.5 Derivation of Bragg's law.

Bragg's law is used to analyze X-ray diffraction technique. As X-rays are electromagnetic waves of shorter wavelength they are emitted when fast moving electrons i.e. cathode rays, strike a target of high atomic weight. Only 2% energy of cathode rays appears as X-rays, the remaining energy appears as heat. This method provides valuable information on many aspects of structural studies including crystal imperfection, such as grain boundaries and dislocation, preferred orientation in polycrystalline materials and the network of atoms in solids.

Consider a plane lattice crystal with interplanar distance d . Suppose a beam of X-rays of wavelength λ is incident on the crystal at an angle θ , the beam will be reflected in all possible atomic planes. The path difference between any two reflected waves is equal to the integral multiple of wavelength (Fig. 2.5). The ray P gets reflected from the surface while the ray Q has to undergo some path difference. The extra distance traveled by the

ray Q from the figure is (BC +CD). From the diagram either BC or CD is equal to $d \sin \theta$. So the path difference is

$$d \sin \theta + d \sin \theta = n \lambda$$

$$2 d \sin \theta = n \lambda$$

Here n is the order = 1, 2, 3 ... n .

This is Bragg's law. When these X -ray of wavelength λ is incident on atoms, each atoms acts as a source of secondary radiation. The crystal behaves as a series of parallel reflecting planes. Hence, the X -rays are reflected according to ordinary laws of reflection. The reflected X -ray, due to their relative path differences, interfere either destructively or constructively. The beam of reflected X -rays will reinforce each other if the path difference between the two beams of X -ray from different parallel planes is equal to some integral multiple of wavelength of X -rays. This is the condition for constructive interference between two rays. Reflected X -rays produces the X -ray spectrum with maximum and minimum intensity. When the reflected X -rays are in phase with each other (constructive interference) maxima are obtained and when they are out of phase with each other (destructive interference) minima are obtained.

2.2.4 Scanning Electron Microscope (SEM)

The first Scanning Electron Microscope (SEM) was made in 1942; then later in 1965's it was first commercialized by Cambridge Scientific Instruments. Its late development was due to the electronics involved in "scanning" the beam of electrons across the sample. In the characterization of solid-state materials, scanning electron microscopy (SEM) is widely used to investigate the structure, morphology and crystallite size, to examine the surface defects of crystal, and to determine the distribution of elements [7].

Fig. 2.6 shows a basic construction of the Scanning Electron Microscope (SEM) instrument. It consist of electron optical system to produce electron beam, a specimen stage to place the sample, a secondary-electron detector (SED) to collect secondary electrons a visual display unit (VDU) .

The electron optical system consists of electron gun, a condenser lens and objective lenses to produce an electron beam, a scanning coil to scan the electron beam and a

visual display unit to visualize the image so formed.

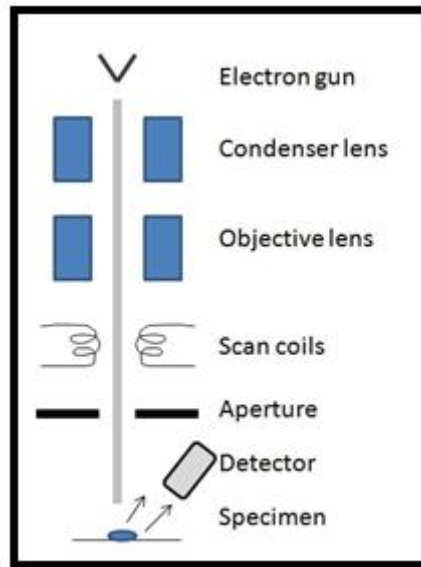


Fig. 2.6 *Basic construction of SEM*

- i) *Electron gun*: A schematic diagram of basic construction of SEM is shown in Fig. 2.6. An electron beam is produced by heating the tungsten filament and then focused by magnetic beam with extraneous particles in the atmosphere. The electrons thus emitted as a beam flows into the metal plate i.e. anode by maintaining it at positive potential. The electron beam passes through a hole made at the centre of the anode. The current of the electron beam can be adjusted by placing an electrode between anode and cathode and maintaining at negative potential. The electrons from this finely focused beam are scanned across the surface of a sample in a series of lines and frames called a raster.
- ii) *Lens*: (1) *Magnetic lens*- This type of lens are specially fabricate by passing a direct current through the coil wound electric wire forming rotational- symmetric magnetic field. Thus, the lens action is produced on the electron beam. The main feature of this lens is that one can change the current passing through the coil and vary the strength of the lens. This is not achieved by an optical lens. (2) *Condenser & Objective lens*- Condenser lens is placed below the electron gun so that the diameter of the electron beam can be adjusted. Along with condenser lens an objective lens is also placed below the condenser lens, so as to produce a fine elec-

tron beam.

- iii) *Specimen stage*: A specimen stage which moves smoothly in horizontally (x, y) as well as vertically (z) and supports the specimen i.e specimen should not fall on tilting or rotating the specimen stage. As shown in Fig. 2.7, the x and y movements are used for the selection of the field view, while z movement is used to vary image resolution. Generally the specimen is observed at high magnification.
- iv) *Secondary-electron detector (SED)*: Depending upon the energy of the emitted electron, secondary (less than 50eV) and backscattered electrons (greater than 50eV) are separated [8]. Detectors of each type of electrons are placed in the microscope in proper positions to collect them.

A florescent substance is coated on the tip of the SED and a voltage of about 10- 20kV is applied depending upon the material analyzed. The secondary electron from the specimen which is generated attracted towards this applied voltage and generates light. The light thus, is then amplified and converted into the electron signal. By changing the voltage the number of secondary electron can be easily controlled.

- v) *Visual display Unit (VDU)*: The amplified output signals from the secondary electron detector strikes on the screen of VDU (CRT-Cathode ray tube, LCD- liquid crystal display, LED etc) which forms the SEM images [8]. For backscattered electrons, the atomic number of the elements in the sample is used to determine the contrast in the produced image. The distribution of different chemical phases in the sample can also be known through these images. The resolution in the image is not as good as for secondary electrons because of the emission of these electrons from a depth in the sample. The brightness of the image formed by backscattered electron increases with the atomic number of the elements. This means that regions of the sample consisting of light elements (low atomic numbers) appear dark on the screen and heavy elements appear bright. Hence, to describe the crystallographic structure of the specimen backscattered are used. The topography of the chemical composition of the specimen can be carried out by X-rays in SEM which contributes in Energy Dispersive X-Ray Analysis (EDX or EDS)

vi) *Magnification*: On changing the width of the electron beam when the SEM image appears on VDU the magnification of the image will simultaneously change. As the size of the monitor remains unchanged, by varying the scan width the magnification can be increased or decreased accordingly.

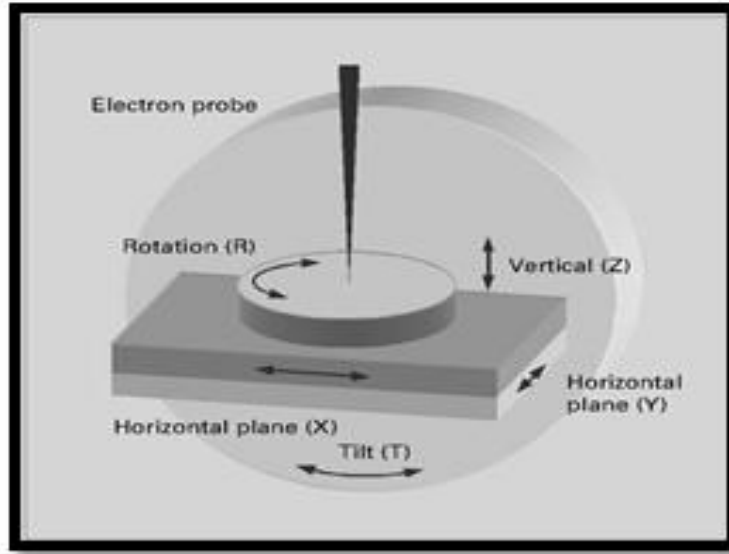


Fig. 2.7 Schematic diagram of Specimen stage.

The analysis of SEM is confined only for surface images but the resolution and crystallographic information are limited as they refer to the surface only. Other limitation is that the specimen should be conducting, so non-conducting materials are carbon or gold-palladium coated and the materials with atomic number smaller than the carbon are not detected with SEM. Thus for the purpose of detailed material characterization Scanning Electron Microscope (SEM) is used.

2.2.5 Transport number measurement

The transport number of a polymer system signifies the contribution of ionic conductivity to the total conductivity. Therefore, it is one of the key factors to be considered while choosing the system as an electrolyte or to be used as a cathode material for battery and electrochromic application. The ionic transport number of various electrolyte materials has been measured using different techniques which include PEFM-NMR measurements, tracer diffusion experiments, complex impedance measurements, limiting current measurements, Tubandt method, EMF measurements, potentiostatic polarization and

transient ionic current measurements. The data obtained are somewhat scattered [9].

Hence, it is one of the key factors to be considered while analyzing the system for electrolyte materials or to be used as a cathode material (in mixed conducting system) for battery application. Generally, the transport number measurement can be carried out through different methods namely, Tubandt's method [9], Hebb-Wagner's polarization method [10] and electrochemical (EMF) method [11, 12]. The electronic contribution to the total conductivity can be obtained from Wagner polarization technique, whereas the other techniques give about ionic nature of the conducting species. There are many methods to ensure the transference number.

2.3 Complex Impedance Spectroscopy

According to J. R. Macdonald *et. al.* [13] complex impedance spectroscopy is a modern name for the small-signal ac measurement and analysis of electrical response data over an appreciable span of frequency. In last many years Impedance spectroscopy has been widely employed owing to the following factors: firstly, because of the development and availability of computer-based automatic measuring equipment; secondly, because of an increasing number of demonstrations of its usefulness in analyzing data for a wide variety of materials; and finally, because of the development of powerful and time-saving methods of data presentation and analysis. Although IS measurements are simple in principle, they are often complicated in practice. Impedance spectroscopy is generally, employed to characterize the electrical properties of materials. It is extensively used to for to see the dynamics of bound or mobile charge in the bulk or interfacial regions of any kind of solid or liquid material, glasses, polymeric materials, semiconducting materials, electronic as well as ionic and mixed electronic–ionic materials and even insulator too.

Impedance spectroscopy is considered to be a basic and ideal tool to characterize the solid electrolyte material [14] where the frequency dependent impedance data give the information about the bulk conductivity and the overall transport process of the solid electrolytes. The applied AC voltage and the resulting current across a cell have the form

$$V = V_{Max} \text{Sin} (\omega t) \quad \dots\dots\dots (2.1)$$

$$I = I_{Max} \text{Sin} (\omega t + \phi) \quad \dots\dots\dots (2.2)$$

Where, ϕ is the phase angle and $\omega = 2\pi f$, f is the frequency of measurement. The phase angle ϕ corresponds to the phase difference between the applied voltage and current. Thus, magnitude of impedance is given by

$$|Z| = V_{Max} / I_{Max}$$

The impedance is composed of a frequency independent resistive term R and a capacitive term $1/j\omega C$, where $j = \sqrt{-1}$. The absolute value $|Z|$ and the phase angle ϕ are related to real and imaginary parts of the impedance (Z' and Z'') as follows:

$$Z' = |Z| \cos \phi \quad \dots\dots\dots (2.3)$$

$$Z'' = |Z| \sin \phi \quad \dots\dots\dots (2.4)$$

The projection of real and imaginary parts of impedance on x and y axis is known as *complex impedance plane* (Fig. 2.8) which is an implicit function of frequency. In ac, the resistance, R , is replaced by the impedance, Z and can be written as

$$Z^* = Z' - jZ'' \quad \dots\dots\dots (2.5)$$

where, Z' is the real part and Z'' the imaginary part of Z^* .

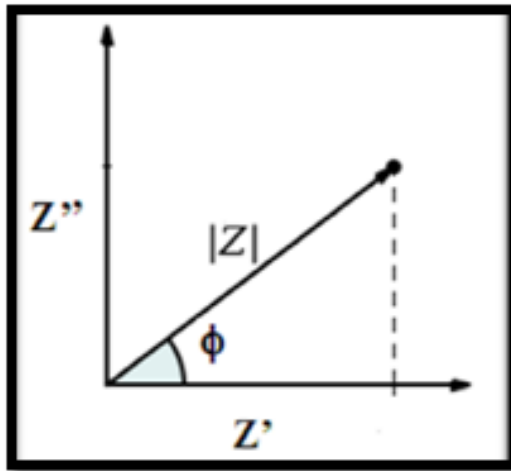


Fig. 2.8 Impedance plot in complex plane

The impedance $Z(\omega)$ has both magnitude $|Z|$ and phase angle ϕ and can be expressed in both polar as well as Cartesian forms.

In Polar form, Impedance $Z(\omega)$ may be written as

$$Z(\omega) = |Z| \exp(-j\phi), \dots \dots \dots (2.6)$$

where, phase angle (ϕ) is expressed as,

$$\phi = \tan^{-1} \left(\frac{Z''}{Z'} \right),$$

magnitude $|Z| = [(Z')^2 + (Z'')^2]^{1/2}$ and

$$\exp(-j\phi) = \cos(\phi) - j \sin(\phi).$$

In Cartesian form,

$$Z(\omega) = Z [\cos(\phi) - j \sin(\phi)] = Z' - jZ'' \dots \dots \dots (2.7)$$

The calculated data are displayed in the complex plane in the form of real and imaginary component as an implicit function of frequency and is called the complex impedance plot. Fig. 2.9 shows complex impedance plots corresponding to the basis for the conductivity measurements in the electrochemical cells. Several other measurements along with ionic conductivity [14] such as dielectric permittivity and modulus are carried out using the data obtain from IS.

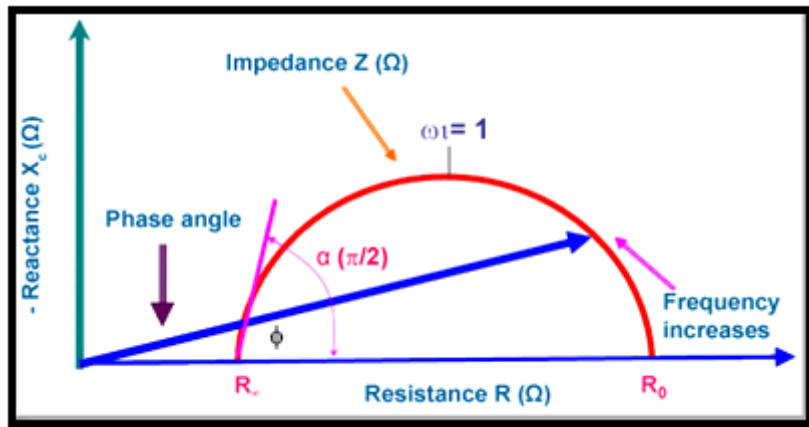


Fig. 2.9 Cole plot in the impedance plane, derivation of the phase angle, resistance (R), reactance (X_c), impedance (Z) and the frequency of the applied current [15].

2.3.1 Dielectric Analysis

The concept of electrical impedance was first introduced by Oliver Heaviside in the 1880's and was soon developed in terms of vector diagrams and complex representation by A. E. Kennelly and C. P. Steinmetz [14].

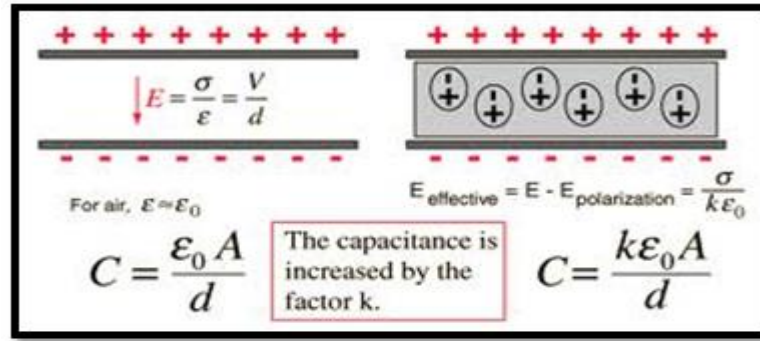


Fig. 2.10 Polarization of dielectric material placed between parallel plate capacitor.

Since past few decades, after the classic paper of Bauerle's [17] on the application of ac methods to stabilized zirconia, impedance spectroscopy has found a great thrust as a tool for investigating solid electrolytes, electrode materials and the interfacial regions between them [18].

The existence of atomic and molecular forces results to Dielectric polarization. Dielectric polarization is developed whenever charges in a material are somewhat displaced with respect to one another. But, this displacement is observed only under the influence of an electric field. In a capacitor, the charges i.e. negative (-ve) and positive (+ve) charge within the dielectric are displaced towards positive electrode and negative electrode respectively as shown in Fig. 2.10. Restoring force acts on the charges which are confined in a dielectric and hence, either work is done on the system or by the system, resulting in the transfer of energy. During charging of a capacitor, the polarization effect opposes the applied electric field and draws charges onto the electrodes which leads to storing of energy. And during discharging process of a capacitor the energy stored during charging process is been released. Hence, the materials which possess easily polarizable charges will result in generating high degree of charges which can be stored in a capacitor. The proportional increase in storage ability of a dielectric with respect to vacuum is defined as the *dielectric constant* of the material [19, 20]. The degree of polarization ‘P’ is related to the dielectric constant K and the electric field strength \vec{E} as follows

$$P = \epsilon_0(K - 1)\vec{E} \dots\dots\dots(2.8)$$

Polarization is generally classified into various modes [10] such as:

- i) Electronic polarization
- ii) Ionic polarization
- iii) Dipole Orientation polarization and
- iv) Space charge polarization.

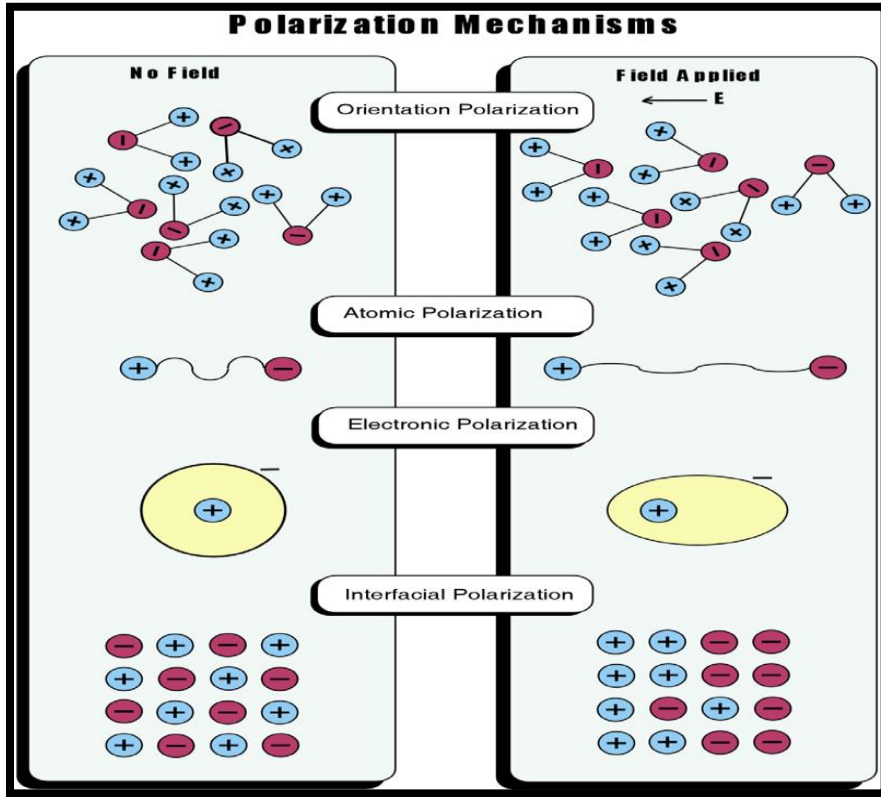


Fig. 2.11 Schematic representation of Electronic, Atomic or ionic, Dipolar and Space charge polarization mechanism in dielectric materials

i) Electronic Polarization

This effect is common in almost all the materials, as it involves distortion of the center of charge symmetry of the basic atom. A small dipole is created when the nucleus of an atom and the negative charge centre of the electrons shift on application of a field as shown in Fig. 2.11. This polarization effect is small, despite of the vast number of atoms within the material, because the moment arm of the dipoles is very short, perhaps only a small fraction of an Angstrom $\approx 1 \text{ \AA}$.

ii) Ionic Polarization

This effect is common in certain materials, which consists of crystal lattices occupied by cations and anions. Under the influence of an electric field, dipole moments are created by the shifting of these ions towards their respective (opposite) polarity of the field. The displacement, of the dipoles can be relatively large in comparison to the electronic displacement, (although still much less than one Angstrom unit), and therefore can give rise to high dielectric constants in some ceramics (Fig. 2.11).

iii) Dipole Orientation polarization

Under the influence of applied electric field permanent dipoles of the material involves themselves in the phenomenon of rotation. Although, these permanent dipoles generally exist in ceramic compounds, such as in SiO_2 , these compounds have no center of symmetry for positive and negative charges. Therefore, dipole orientation is not found to occur, as the dipole is restricted from shifting by the rigid crystal lattice, reorientation of the dipole is not allowed due to the distortion of the lattice. In polymeric materials such dipole orientation is observed more often due to their ability of atomic reorientation. It is important to note that this mechanism of permanent dipoles is not the same as that of induced dipoles of ionic polarization (Fig. 2.4).

iv) Space Charge Polarization.

This effect is common in many crystal lattices such as polycrystalline ceramics. The space charge polarization generally, occurs due to the diffusion of ions along the direction of applied electric field, which results, in redistribution of charges in dielectric materials as shown in Fig. 2.4.

Effect of Frequency on Polarization

In this frequency dependent mechanism the polarization effect is observed to vary with time along with variation in frequency of applied field. Therefore, it can be said that the effective contribution of polarization to the dielectric constant is frequency dependent. In this mechanism the response of electronic displacement to the field reversals is rapid compared to that of ionic displacement. In ionic displacement, ions are larger and are less mobile because they shift within the crystal structure. Therefore in electronic dis-

placement no lag of the polarization occurs up to 10^{16} Hz whereas the ionic displacement decreases at 10^{13} Hz. At this frequency, the ionic displacement begins to lag the field reversals, resulting in increasing the loss factor and much smaller contribution to the dielectric constant. But, at higher frequency, the rotation of ionic molecules cannot respond to the field reversal and hence results in loss factor. Dipole orientation and space charge polarization have slower frequency responses [19]. The resultant effect is illustrated in Fig. 2.12.

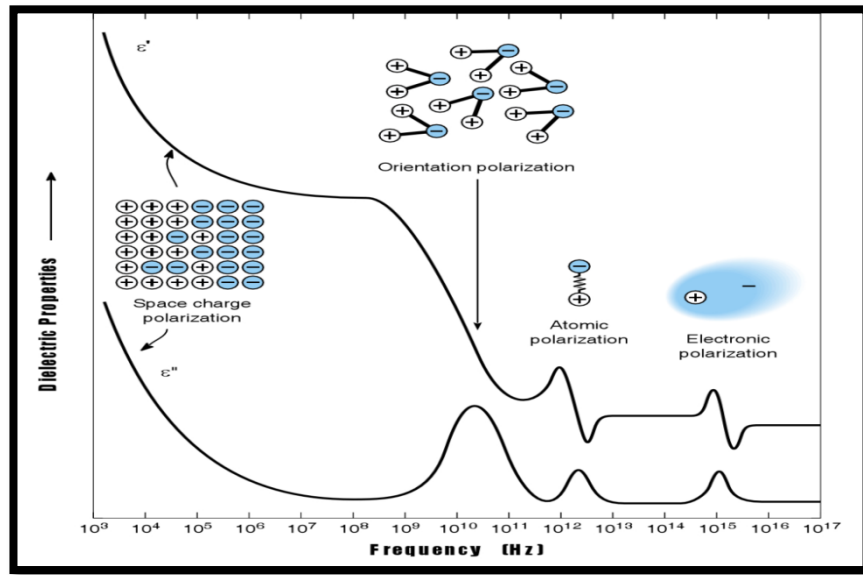


Fig. 2.12 Polarization mechanisms.

It can be seen from the figure that a point when the applied frequency equals the natural frequency of the material a peak is observed near the limiting frequency for ionic and electronic polarization are due to the resonance. When dielectric constant of a capacitor is measured, the variation of the polarization mechanism with frequency is reflected. As expected, capacitance value, i.e., dielectric constant, always decreases with increased frequency, for all ceramic materials, although with varying degrees depending upon which type of polarization mechanism is dominant in any particular dielectric type. The dielectric relaxation as well as conductivity relaxation can be explained and understood easily through ionic conduction studies in solids. All materials are liable to show increasing movements of ions at sufficiently higher temperature, either intrinsic to their lattice as in the case of ionic solids, or extrinsic due to impurity in purely covalent lattice

including many polymers [21, 22]. This is normally expected to lead to dc conduction, although in many cases there is evidence of low frequency dispersion in data which on superficial analysis may be considered to represent dc conduction [19, 23]. There are numerous materials which conduction is due to motion of ions.

Generally, ionic conduction relies on the random migration of ions stimulated by thermal energy as long as the applied electric field is small enough. Migration mechanism is created by the hopping of ions from its normal position on the lattice to an adjacent equivalent but empty site. Hence, to understand the properties of solids including polymers, information regarding the motion of the mobile ions is necessary. This is obtained by analyzing the dielectric spectra in the wide frequency range, for which relaxation of the ion motion and network motion contribute. Relaxation is a process which generally, occurs in dielectric materials having low electrical conductivity. Such processes are mainly observed in linear systems where a response and stimulus are proportional to one another in equilibrium [24, 25]. The details of formulations for measuring the dielectric parameters are discussed below in brief. According to Maxwell equation the permittivity of a medium is defined as: $\vec{D} = \epsilon \vec{E}$, where \vec{D} is the displacement vector and \vec{E} is applied electric field. The displace vector is also equal to the surface charge per unit area. Consider a parallel plate capacitor of area A , separated by a distance ‘ t ’ (in vacuum). If a potential ‘ V ’ be applied to it and the charge carried by ‘ Q ’ then the electric field strength is V/t in *Volt/m* units.

Hence, permittivity can be written as :

$$\epsilon = \vec{D} / \vec{E} \dots\dots\dots(2.9)$$

Relative permittivity or dielectric constant is one of the most important parameter which is widely used, Relative permittivity, is defined as $\epsilon' = \epsilon/\epsilon_0$ and using eq.2.9 we get,

$$\epsilon = \frac{\vec{D}}{\vec{E}} = \left(\frac{Q}{A}\right) \left(\frac{V}{t}\right) = \left(\frac{Qt}{A}\right)\dots\dots\dots (2.10)$$

Therefore,

$$\epsilon' = \left(\frac{Qt}{A\epsilon_0}\right)\dots\dots\dots (2.11)$$

From eq. 2.11 the value of capacitance and dielectric constant can be determined. The relative permittivity is usually known as permittivity and is always greater than unity. Suppose a parallel plate is filled by a medium of permittivity ϵ' is given by

$$\epsilon' = C/C_0 \dots\dots\dots (2.12)$$

Assume that a dielectric material is subjected to an alternative electric field as given below:

$$\vec{E} = \vec{E}_0 \cos \omega t \dots\dots\dots (2.13)$$

The induced current in the dielectric does not change exactly at the same time i.e., the current and voltage are maximum and minimum at different times. The current is found to lead the potential in phase. In a similar way the electrical displacement is also not in same phase with applied electric field (\vec{E}).

The expression for displacement vector \vec{D} is

$$\vec{D} = D_0 \cos (\omega t - \delta) \dots\dots\dots (2.14)$$

$$\begin{aligned} &= D_0 \cos \omega t \cos \delta + D_0 \sin \omega t \sin \delta \\ &= D_1 \cos \omega t + D_2 \sin \omega t \dots\dots\dots (2.15) \end{aligned}$$

Where $D_1 = D_0 \cos \delta$, $D_2 = D_0 \sin \delta$ and δ are phase angle. It is clear from the equation that D_0 is proportional to E_0 and the ratio D_0/E_0 is generally Frequency dependent. So dielectric permittivity (ϵ') and dielectric loss (ϵ'') can be written as

$$(\epsilon') = (D_0/E_0) \cos \delta \dots\dots\dots (2.16)$$

$$(\epsilon'') = (D_0/E_0) \sin \delta \dots\dots\dots (2.17)$$

The energy absorbed by the dielectric material can be measured using factor $\sin \delta$. It is well known that, in a capacitor the dielectric medium usually has a resistance (R) and impedance (Z), which are related to the phase angle. It is considered that for (R) to be very large than loss factor, it can be written as:

$$\sin \delta \approx \tan \delta = [(\frac{1}{\omega})RC]$$

$\tan \delta$ is known as tangent loss. The complex permittivity is given by

$$\varepsilon^* = \varepsilon' - j\varepsilon'' \dots\dots\dots (2.18)$$

Where ε' and ε'' are real and imaginary parts of complex permittivity can be measured using impedance data by the following Equation:

$$\varepsilon^* = \left(\frac{1}{j\omega Z^* C_0}\right) \dots\dots\dots (2.19)$$

Where Z^* is complex impedance, $C_0 = \varepsilon_0(A/t)$, where A is the area of the sample, t is the thickness of the sample and ε_0 is permittivity of vacuum.

2.3.2 Modulus Analysis

Using the electrical modulus $M^* = \frac{1}{\varepsilon^*}$ representation [25, 26], dispersion of the conductivity in the frequency domain is more conveniently interpreted in terms of conductivity relaxation time, τ . Complex electric modulus M^* formalism is used very frequently when the relaxation is presumed to be due to the motion of ions or electrons [27]. Although, originally conceived as a formalism to separate space-charge effects from the bulk conductivity, the M^* representation is now widely used to analyze ionic conductivities by associating a conductivity relaxation time (τ) with the ionic process [27, 28]. The use of modulus formalism in presenting frequency dependent dielectric or conductivity data has the advantage of eliminating any spurious effect due to contacts or interfaces (Maxwell-Wagner effects) [29, 30]

The electric modulus according to Macedo et.al [25] is defined as the electric analog of the dynamical mechanical modulus and was related to the complex permittivity $\varepsilon^*(\omega)$ by

$$\begin{aligned} M^*(\omega) &= \left(\frac{1}{\varepsilon^*(\omega)}\right) \\ &= \{ \varepsilon'(\omega) - j\varepsilon''(\omega) \} / |\varepsilon^*(\omega)|^2 \dots\dots\dots(2.20) \end{aligned}$$

$$= M'(\omega) + jM''(\omega)$$

$$= M_\infty \left[1 - \int_0^\infty \exp(-j\omega t) \left(\frac{-d\phi(t)}{dt}\right) dt \dots\dots\dots(2.21) \right]$$

where, M' and M'' are the real and imaginary part of the complex modulus M^*

and $M_\infty = \frac{1}{\epsilon^*}$ is the inverse of high frequency dielectric constant ϵ_∞ [26, 31]. The function $\phi(t)$ gives the time evolution of the electric field within the materials and $\omega = 2\pi f$ is the angular frequency.

Analysis of electric relaxation in terms of complex permittivity $\epsilon^*(\omega)$ gives relaxation parameters, characteristics of the decay of the displacement vector \vec{D} , under the constraint of constant electric field, \vec{E} [32]. It has been suggested [26, 27, 31, 33-36] that for electrical relaxation in dielectric relaxation in dielectrics containing a substantial concentration of mobile charges, it is generally more fruitful to focus attention on the decay of electric field \vec{E} at constant \vec{D} (displacement vector). If surface charges of an opposite sign are instantaneously placed on opposite faces of an ionic conductor at time zero and then maintained at a constant value, an electric field will arise inside the material which with time will decay to zero due to migration of the mobile ions. The expression for the decay of electric field in time domain can be written as

$$\vec{E}(t) = \vec{E}(0) \phi(t) \quad \dots\dots\dots (2.22)$$

Where $\vec{E}(0)$ denotes the electric field at time $t = 0$ and $\phi(t)$ is a macroscopic decay function of the general form

$$\phi(t) = \int_0^\infty g(\tau_\sigma) \exp[-(t/\tau_\sigma)^\beta] d\tau_\sigma \quad \dots\dots\dots (2.23)$$

Thus,

$$E(t) = E(0) \int_0^\infty g(\tau_\sigma) \exp[-(t/\tau_\sigma)^\beta] d\tau_\sigma \quad \dots\dots\dots (2.24)$$

Where τ_σ an electric field or conductivity relaxation is time, and $g(\tau_\sigma)$ is a normalized density function for relaxation times.

Thus, using Eqs. 2.21 and 2.23, it become

$$M^*(\omega) = M_\infty \int_0^\infty g(\tau_\sigma) \left[\frac{j\omega \tau_\sigma}{1+j\omega \tau_\sigma} \right] d\tau_\sigma \quad \dots\dots\dots(2.25)$$

In glassy material, the decay function $\phi(t)$ is found to exhibit non exponential (i.e. if there is a distribution of relaxation times and $g(\tau_\sigma)$ is not a delta function) nature. The decay of the electric field due to the migration of mobile ions will then give rise to a

non zero frequency dispersion ($\epsilon_0 - \epsilon_\infty$) in the dielectric constant ϵ' . In time domain, a good description for the decay function is the so called stretched exponential introduced by *Kohlrausch-Williams – Watts* (KWW) [37-39] and is given as,

$$\phi(t) = \exp \left\{ - \left(\frac{t}{\tau_\sigma} \right)^\beta \right\} \quad \text{where } 0 < \beta < 1 \dots\dots(2.26)$$

Where τ_σ and β are the parameter of stretched exponential function and are respectively the conductivity relaxation time and the Kohlrausch exponent. The value β varies from 1 (Debye process) to 0. The smaller is the value of β , the larger is the deviation of relaxation with respect to a Debye type relaxation. The β parameter has been interpreted either as representative of a distribution of relaxation times [32] or as 59ignify59rristic of cooperative motions between charge carriers [37, 40]. Analysis of the impedance data on the modulus formalism assumes importance, as it suppresses the electrode effects occurring at low frequencies [41-43] and the modulus can also be used for studying conductivity relaxation times [44, 45]. The electric modulus data can be obtained from the complex impedance data according to the relation

$$M^* = M' + j M'' = j\omega Z^* C_o \dots\dots\dots(2.27)$$

Such that $C_o = \epsilon_o (A/t)$ is the vacuum capacitance, Z^* is the complex impedance, $\epsilon_o = 8.854 \times 10^{-14} \text{ F/cm}$ is the permittivity of free space, A and t are the cross section and thickness of the sample respectively. In the present work impedance data were converted into electric modulus using the relationship $M' = \omega Z' C_o$ and $M'' = j\omega Z'' C_o$ respectively [46, 47] where Z' and Z'' are the real and imaginary part of the complex impedance respectively. Many workers have discussed the advantage of adopting electrical modulus to analysis the dielectric response of materials [48-53].

2.4 Theoretical models of Conductivity

Armand *et. al.* [54] was the first one to suggest the ion transport mechanism in polymer electrolytes. For a long time the proper mechanism of ion transport was not very clear. Primarily it was believed that the ion conduction take place in the crystalline phase [55, 56] inside the PEO helices. Later it was realized that the amorphous phase was the main contributor in ion conduction [56] and the crystalline phases are basically insula-

tors. However, it is difficult to explain ion-transport in a macromolecular system. Some of the theories, proposed to explain the conduction mechanism in these systems are briefly described below.

2.5 Temperature dependence of conductivity

In order to explain the ion transport phenomena in the polymer electrolytes number of empirical relationships have been developed. Generally, in polymer electrolytes, the crystalline phase exhibits Arrhenius conductivity, whereas the amorphous phase exhibits the VTF conductivity [57]. Thus, polymer electrolytes may be considered as a two component system. At temperature below the melting point, the fraction of the crystalline phase is prevail. Hence, the overall conductivity behavior of polymer electrolytes is dominated by Arrhenius behavior. When the temperature is increased, the fraction of the amorphous phase regions increases such that at a certain temperature, T_c ; the fraction of the amorphous phase is large enough to create a continuous connection between the amorphous cubes. At this temperature the electrical conductivity changes from Arrhenius-like to VTF-like behavior. This temperature T_c is called critical temperature or a percolation temperature. At temperatures above the melting point, all parts of polymer electrolytes are amorphous and the conductivity is absolutely VTF-like. Some of temperature dependent ion- conducting theories are discussed below:

2.5.1 Arrhenius Theory

This theory gives a fundamental association which describes the liner relationship of $\ln \sigma$ with inverse of temperature. A Swedish chemist Svante Arrhenius developed this theory in 1889 [58]. Initially this theory was developed for liquid electrolytes but later on it is also used for the solid ones. In solids the ions hop from one vacant site to another by overcoming the energy barrier i.e., activation energy E_a that exists between these. Under the applied electric field E , the potential energies in the direction of the field and that opposite to it get altered. Then the ions start hopping along the direction of field giving rise to an ion current density j (assuming only one direction):

$$j = (na^2 e^2 v E) / kT = \sigma E \quad \dots\dots\dots (2.28)$$

where k is the Boltzmann constant, n is the number of defects per unit volume

[59] ($n \propto \exp(-G/2kT)$ G is the Gibbs free energy for the creation of defects), a is the inter-ionic distance, e is the charge of the ion and σ is the ionic conductivity and ν is the jump frequency or the probability of a jump from one site to another, in the absence of any external electric field and is given by:

$$\nu = \nu_0 \exp(-\Delta G/kT) \dots\dots\dots (2.29)$$

where ν_0 is the attempt frequency and $\Delta G = \Delta H - T\Delta S$, ΔH and ΔS are the enthalpy and entropy of diffusion respectively. ΔG is the energy of migration and it is the difference between the free energy of the ion at the normal lattice point and that atop the barrier.

Therefore, we get,

$$\sigma = A/T \exp(-E_a/kT) \dots\dots\dots (2.30)$$

Where, $A = ba^2e^2k$ is the pre exponential factor (b is the constant of proportionality) and $E_a = \Delta G + G/2$ is the activation energy for migration and creation of defects. This equation is known as Arrhenius equation [60, 61] and it implies that $\ln(\sigma T)$ vs. $1/T$ fits a straight line (a linear relationship) and the slope gives the activation energy.

2.5.2 Vogel–Tammann–Fulcher (VTF) theory

The temperature dependence of the ionic conductivity measured from polymer electrolytes obeys non-Arrhenius behavior which is the characteristic of ionic motion being coupled with the host matrix. The temperature dependence of the conductivity exhibits an apparent activation energy that increases as temperature decreases. This behavior is most commonly described by the empirical Vogel–Tammann–Fulcher (VTF) equation, which was first developed to describe the viscosity of supercooled liquids [62- 64].

According to Vogel-Tammann-Fulcher (VTF) [64], the migration of metal ion mostly depends on the segmental motion of polymer chain in the amorphous phase and the temperature dependent conductivity of polymer films which is given as:

$$\sigma = AT^{-1/2} \exp\left[-\frac{B}{k_B(T-T_0)}\right] \dots\dots\dots (2.31)$$

where T_0 is the reference temperature corresponding to an ideal glass transition tempera-

ture at the thermodynamic equilibrium; A is a pre-exponential factor, which is determined by the transport coefficient and proportional to the number of carrier ions, B is a constant with the dimensions of energy and k_B is Boltzmann constant.

2.6 Models for DC Conductivity

2.6.1 Free Volume Theory

It is a macroscopic approach which explains the interdependence of ionic conductivity of polymer electrolytes with temperature and pressure. According to Cohen and Turnbull [65, 66] this theory is applied to supercooled liquids and glasses but later on it was applied to amorphous systems and glass transitions [67]. The basic assumption of the free volume theory is that the diffusion of ions is not an activated process but rather a result of redistribution of free volume within the material. The molecules are considered as hard spheres confined to their cages. Once a hole (free volume) is opened the molecule moves in it with a thermal velocity u . Using this, diffusion coefficient can be given by:

$$D = ga^*u \exp \left[\frac{-\gamma v^*}{\alpha v_M (T - T_0)} \right] \dots\dots\dots(2.32)$$

where γ is a geometric factor, a^* is roughly molecular diameter, γv^* is molecular volume, v_M is mean molecular volume of the species whose motions create free volume, α is the difference in thermal expansion coefficient between liquid and glass over the same range and T_0 is the temperature at which the free volume disappears (close to the equilibrium glass transition temperature). The above equation is derived by explicitly on maximizing the number of ways of distributing the free volume, by not including all such distributions. It is the matter of accessibility which limits the validity of VTF in situations involving ionic transport in polymeric electrolytes.

Using the Nernst – Einstein [68] equation $\sigma = nq^2D/kT$ where n and q are the number and the charge of the conducting species respectively, with the assumption that $u \sim T^{1/2}$ the equation can be transformed to:

$$\sigma = \sigma_0 \exp \left[\frac{-B}{k(T - T_0)} \right] \dots\dots\dots(2.33)$$

The above mentioned equation is identical to the empirical VTF equation [63] which has been fitted to the thermal dependence of many polymer electrolytes exceeding-

ly well. Even though this equation is widely used to fit a large number of experimental data, it is worth noticing that it has been derived by considering the motion of the polymer host alone. But, the free volume theory portrays very lucrative, and can be used to derive the VTF equation, some disadvantages are associated with it [69, 70].

Firstly, it is a quasi-thermodynamic theory, and therefore not based on microscopic description of the materials. This is a major drawback to its used as a vehicle to interpret and predict variations in conductivity such as concentration, ion size, and ion charge or coordination environment. Secondly, no dynamics or kinetics is included in the simple free volume model; in particular, the free volume is assumed to move instantaneously with no constraints [71], and no effects of ion-ion correlation or ion-polymer complexation are included. Finally, there are some quite straight forward experimental results, such as a maximum in conductivity as the ion concentration is varied [72, 73] that cannot be explained using VTF conductivity curves always.

Therefore, to describe the results in cases where the ionic motions are high or ion pair formation is large, such equation may not be useful. Also, it does not account for the variation due to change in the percentage of amorphous regions in a semi-crystalline polymer. According to Bruce [74] free volume models can describe the conductivity behavior up to some extent only, but the kinetic effects associated with macromolecules were neglected and hence a clear picture related to the model is not obtained.

2.6.2 Configurational Entropy Model

Like the free volume theory, the configurational entropy model too describes the motion of host polymer. The configurational entropy theory was originally developed by Gibbs and DiMarzio [75] who replaced the single parameter of free volume theory with two parameters. First parameter is counting the number of lattice sites and second one is the number of distorted bonds. This is another quasi-thermodynamic representation based on entropy rather than volume as the important parameter. A fascinating feature of this model is the existence of a second order phase transition at a temperature T_2 where the configurational entropy vanishes. On cooling the number of configurations that the system can have decrease and at a particular temperature, this tends to zero.

According to the model proposed by Adam and Gibbs [76] two parameters ((i) the

number of lattice site and (ii) number of distorted bonds) are introduced into the free volume theory. The mass transportation mechanism in this model is assumed to be a group cooperative rearrangement of the chain. The probability W , of a mass- transporting rearrangement in the polymer electrolytes can be expressed as:

$$W = A \exp(-\Delta\mu S_c^*/kTS_c) \dots\dots\dots(2.34)$$

where A is a coefficient, S_c^* is the minimum configuration entropy required for rearrangement, S_c is the configurational entropy at temperature T , and Δ is the free energy barrier per mole which impedes the rearrangement. Bruce [74] mentioned that both VTF and WLF equation can be derived from the configurational entropy model. This theory has broadly been applied to the problems in glasses, polymers and molten salts [77] but it has not been applied extensively to polymer electrolytes.

2.6.3 Space charge models

This model discussed the physical approaches to explain conductivity enhancements in some two-phase composite electrolyte systems and referred to as the space charge model. In case of liquid systems, a composite can be formed but only with high inorganic particle content [78]. In these circumstances, the conductivity is observed to enhance as compared to the pure solutions. This type of materials can be described as a viscous grain ensemble wetted by the liquid or ‘soggy sand’ – like system. Because of interfacial interactions, a synergetic effect is observed yielding one order of rise in magnitude of the conductivity value. Some similarity in the properties between the ‘soggy sand’ systems and solid composite polymeric electrolytes can be observed. In both these cases, a covalent organic matrix produces a ground state for the charge carriers present in the form of undissociated salt particles (contact ion pairs). Thus, the conductivity effect would consist of absorption of one of the pair’s constituents, resulting in a break-up of the ion pair and generating a mobile counter ion. In all these cases, a percolation type of behavior is observed, which is typical for the enhancement of the interfacial conductivity. Additionally, the increment is higher for the acidic filler (SiO_2) as compared to analogous system with the basic oxide (Al_2O_3). This suggests the existence of a mechanism related to anion absorption on the grain surfaces. This, in turn, leads to an increase of the number of the cations in the space charge layer surrounding the filler particle. The relative enhancement of the conductivity value is higher for low polar solvent such as (tetrahydrofu-

ran THF, $\epsilon = 7.4$) than with the high polar solvent (like methanol $\epsilon = 32.6$). This observation confirms the absorption mechanism because the salt dissociation constant is significantly lower for the less polar system.

2.6.4 Amorphous phase model

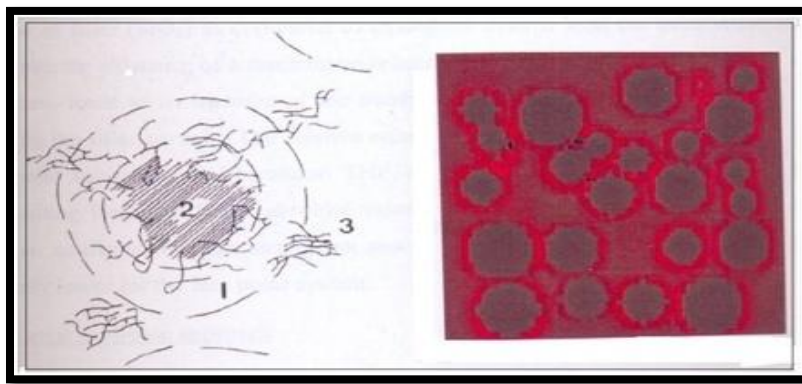


Fig. 2.1 (a) Schematic drawing of morphology of composite polyether non-conductive-filler electrolytes: (1) Highly conductive interface layers coating the surfaces of grains, (2) dispersed insulating grains, (3) polymer ionic conductor matrix; (b) Formation of conducting pathways [79].

In a variety of composite polymer electrolytes, based on high molecular weight PEO matrix, a decrease in the degree of crystallinity has been identified (resulting an increase in the ionic conductivity) as compared to undispersed PEO-salt complexes. On the basis of the results obtained, an ‘amorphous phase’ model was developed which is shown in Fig. 2.13. This explains the increase in the conductivity in composite polymer electrolytes [80].

In the crystalline PEO-salt complex systems, filler particles (e.g. $\alpha\text{-Al}_2\text{O}_3$) act as nucleation centers and probably attached to PEO segments via acid Al surface centers. Since, there are a large number of these nucleation centers, crystallization process becomes faster due to higher nucleation rate and, in consequence, a bigger level of disorder, typically, like the liquid state, is frozen during solidification of the polymeric matrix as observed in the cooling process or solvent evaporation.

2.6.5 Dynamic Bond Percolation theory

Druger, Nitzan and Ratner proposed the dynamic bond percolation theory [81, 82] in 1983 which describes diffusion of small particles (ions, electrons) in a medium which in addition to being statistically disordered is also undergoing dynamic rearrangement

processes on a shorter time scale compared to the observation time. This model is natural extension of the static bond percolation model, which describes transport in systems in which hops between sites are either forbidden or allowed with specific fixed probabilities to systems in which the host structure is evolving. This model is the only microscopic model developed so far that takes into account the actual situation in the polymer electrolytes i.e. ionic motion combining the ionic transitional motion/hopping and dynamic segmental (chain) motion of the polymer host above the glass transition temperature ($T > T_g$). Actually, DBP model, an extension of SBP model, deals with the hopping/diffusion of small particles through a dynamically disordered medium. It is based on the idea that the lattice in polymer electrolytes is no longer static but undergoes rearrangements that re-assign the open and closed bonds. Physically, these rearrangements correspond to orientational motions of the host polymer lattice. In case of polymer electrolytes, the motion of polymer segments (chains) is expected above glass transition temperature (T_g). So, for ($T > T_g$), various stable sites with ion will move with respect to one another and thereby changing the complexation of open or close bonds. Such a dynamic motion of the polymeric host is then modeled by allowing the hopping probabilities to readjust or renew their values on a time scale corresponding to polymer motion. Details of dynamic bond percolation model along with its limitations are thoroughly reviewed in the literature. For application to polymer electrolytes, the sites are localization positions for mobile ions, while the bonds are pathways for motion between sites.

2.7 Frequency dependence of conductivity

In general, electrical characterization of the materials can be done by dc and ac measurement technique. Though the dc measurement technique is straight forward, it cannot be implemented for ionic or mixed electronic-ionic systems because on application of dc field, the ionic material gets polarized. Due to which the ionic conductivity gradually ceases, giving only electronic conductivity. To overcome the above problem, ac technique is preferred over dc technique. Frequency dependent conductivity behavior of ionically conducting solid electrolytes has been the focus of a large number of studies [83, 84] although very limited understanding of this multi-faceted problem has been achieved so far.

2.7.1 Jonscher's Power law

There are large numbers of theories, to explain the dispersion behavior of solid polymer electrolytes, amongst which the universal model for ac transport seems to have been successful. The frequency dependence of conductivity is a sum of dc conductivity due to the movement of free charges and polarization conductivity due to the movement of bound charges. With decreasing frequency, the conductivity $\sigma(\omega, T)$ decreases and approaches the direct current conductivity σ_{dc} . The low conductivity value at low frequencies is related to the accumulation of ions due to the slow periodic reversal of the electric field. In the high frequency region, the power law nature $\sigma(\omega) \propto \omega^n$ is observed and the conductivity sharply increases with frequency. This universal behavior in conductivity is given by Jonscher [85] which describes the dispersion behavior observed in ac conductivity. The variation of conductivity with frequency may be expressed to the well known power law of ac behavior which indicates a non-random process wherein the ion motion is correlated [86,87] and given by the following equation,

$$\sigma(\omega) = \sigma_{dc} + A\omega^n \quad \dots\dots\dots(2.35)$$

where $\sigma(\omega)$ is the conductivity at a particular frequency, σ_{dc} is the dc conductivity at zero frequency, A is a constant and n is the frequency exponent lies in the range of $0 < n < 1$. The above expression is known as the *power law of ac behavior*. Because the power law of ac behavior is observed in wide range of materials, Jonscher called it “*Universal Behavior*” [85, 88-90]. The Eq. 6.37 is accepted universally for considering the sample conductivity, hopping charges, frequency dependence of conductivity etc. The frequency exponent n was calculated from the slope of the plot $\log(\sigma' - \sigma_{dc})$ versus $\log \omega$, which is a straight line. If exponent n values lie in the range 0.6-0.9 then it is said that the correlation motion is sub-diffusive and indicates a preference on the part of ions that has hopped away to return to the position/site from where it started. The exponent is a measure of degree of interaction with the environment. Jonscher [84] had shown that a non zero n in the dispersive region of conductivity is due to the energy stored in the short range collective motion of ions. A higher n implies that large energy is stored in such collective motions.

2.7.2 Jump relaxation model

In *jump relaxation model*, Funke [91] has proposed that the dc plateau and the power law region should be considered as a single entity. Both these regions together represent ‘*successful*’ and ‘*unsuccessful*’ hopping of the mobile ions. According to this model, at very low frequencies ($\omega \rightarrow 0$), an ion can jump from one site to its neighboring vacant site successfully contributing to dc conductivity. At high frequency, the probability for the ion to go back again to its initial site increases due to the short time periods available. This high probability for the correlated forward backward hopping at high frequencies together with the relaxation of the dynamic cage potential is responsible for the high frequency dispersion. This theory is generally applicable in glassy electrolytes.

2.8 Various other models

Various other theories [92-93] have been proposed to understand the conduction mechanism in the amorphous materials. Two distinct models: quantum mechanical tunneling (QMT) and correlated hopping over a barrier (CBH), or their combination are proposed to explain the relaxation of dipoles. In order to predict the interdependence of temperature and frequency the experimental data of the ac conductivity is needed to be examined precisely. According to the quantum mechanical tunneling (QMT) model [92-93], the exponent n is almost equal to 0.8 and increases slightly with increasing temperature or is temperature independent. In case of correlated barrier – hopping (CBH) model [94], the exponent n decreases with increasing temperature. Long [92] proposed that if the spatial extent of the polaron radius is large when compared with the interatomic spacing, an appreciable overlap of the polaron distortion cloud occurs because of the long-range of dominant coulomb interaction, with a result of reduced polaron-hopping energy [95]. While according to overlapping large polaron tunneling (OLPT) model [94] exponent n decreases from unity with the rise in temperature and exhibits a minimum at a certain temperature and subsequently increases with further increment in temperature.

References:

- [1] M. Watanabe, S. Nagano, K. Sanui, N. Ogata, *Solid State Ionics*, 28-30 (1988) 911-917.
- [2] W. Pascheto, M.G. Parthun, A. Hallbrucker and G.P. Johari, *J. Non-Cryst. Solids*, 171 (1994) 182-190.
- [3] W.V. Johnston, H. Wiedersich, G.W. Linderberg, *J. Chemical Phys.* 51(1969) 3739-3747.
- [4] M.H. Bhat, F.J. Berry, J. Jiang, K.J. Rao, *J. Non-Cryst. Solids* 291(2001) 93-106.
- [5] H.S. Barbara, *Polymer analysis*, University of Technology, Sydney, Australia, John Wiley & Sons Ltd, (2004) 56.
- [6] L. Smart, E. A. Moore, *Physical Methods for Characterizing Solids*, *Solid State Chemistry: An introduction*. New York: Taylor & Francis, (2005) 175–238.
- [7] C. R. Brundle, C. A. Evans Jr, S. Wilson, *Encyclopedia of materials characterization*, Butterworth-Heinemann publications, 1992.
- [8] R.F. Egerton, *Electron Energy-Loss Spectroscopy in the Electron Microscope*, A Division of Plenum Publishing Corporation, New York, (2nd. Ed.) 1996.
- [9] C. Tubandt, *Z. Anorg. Allg. Chem.* 115 (1921) 105-126.
- [10] J. B. Wagner, C. Wagner, *J. Chem. Phys.* 26 (1957) 1597-1601.
- [11] K. Kiukkola, C. Wagner, *J. Electrochem. Soc.* 104 (1957) 379-387.
- [12] L. Smart, E. A. Moore, *Physical Methods for Characterizing Solids*, *Solid State Chemistry: An introduction*, New York: Taylor & Francis (2005) 175–238.
- [13] J. R. Macdonald, L. D. Potter, *Solid State Ionics* 23 (1987) 61-79.
- [14] J. R. Macdonald (ed.), *Impedance spectroscopy emphasizing solid state materials and systems* (New York Wiley) (1987).
- [15] M. J. Tuorkey, T. J. Biosens, *Bioelectron*, 3(2012)4.
- [16] E. Barsoukov, J.R. Macdonald, *Fundamentals of Impedance Spectroscopy. Impedance Spectroscopy Theory, Experiment, and Applications*. 2nd Edition (pp. 1–26). New Jersey: John Wiley and Sons (2005).
- [17] J.E. Bauerle, *J. Phys. Chem. Solids* 30 (1960) 2657.
- [18] W.I. Archer and R.D. Armstrong, *Specialist Periodical Reports, Electrochemistry*, The Chemical Society. (London), 7 (1980) 157.
- [19] T. Meisel, K. Seybold, *Crit. Rev. and Chem.* 12 (1981) 267.
- [20] D. A. John “*The analytical chemistry Handbook*”, New York, Mc Graw Hill, Inc. (1995) 15.1 -15.5.
- [21] T. Blythe, D. Bloor, *Electrical Properties of Polymers*, 2nd Ed., Cambridge University Press (2005).
- [22] J. A. Varela, O. J. Whittemore, *J. Am. Ceram. Soc.*, 66(1) (1983) 77-82.
- [23] E. Pungor, *A Practical guide to Instrumental analysis*, Boca Ranton, Florida, (1995) 181-191.
- [24] H. H. Wilard, L. L. Merritt, Jr. J. A. Dean, ‘*Instrumental methods of analysis*’, *Affiliated East West Press Pvt. Ltd., New Delhi, Fourth Edition*, (1965) 124.
- [25] P. B. Macedo, C. T. Moynihan, R. Bose, *J. Phys. Chem. Glasses* 13 (1972) 171-179.

- [26] C. T. Moynihan, L. P. Boesch, N. L. Laberge, *Phys. Chem. Glasses*, 14 (1973) 122-125.
- [27] C. A. Angell, *Chem. Rev.* 90 (1990) 523.
- [28] S. R. Elliott, *Physics of Amorphous Materials*, Longman, London (1984).
- [29] S. R. Elliott, *J. Non-Cryst. Solids*, 170 (1994) 97.
- [30] V. Provenzano, L. P. Boesch, V. Volterra, C. T. Moynihan, P. B. Macedo, *J. Am. Ceram. Soc.* 55 (1972) 492.
- [31] N. G. Mc Crum, B. E. Read, G. Williams, "Anelastic and Dielectric effects in Polymeric Solids", Wiley London (1967).
- [32] C. T. Moynihan, L. P. Boesch, N. L. Laberge, *Phys. Chem. Glasses*, 14(6) (1974) 639.
- [33] F. S. Howell, R. A. Bose, P. B. Macedo, C. T. Moynihan, *J. Phys. Chem.* 78,6 (1974) 639-648.
- [34] J. H. Ambrus, C. T. Moynihan, P. B. Macedo, *J. Phys. Chem.* 76(22) (1972) 3287.
- [35] K. L. Ngai, S.W. Martin., *Phys. Rev. B* 40 (1989) 10550.
- [36] K. L. Ngai, J. N Mundy, H. Jain, G. Balzer-Jollenbeck, O. Kanert, *Phys.Rev. B* 39 (1989) 6169.
- [37] R. Kohlraush, *Prog. Ann. (Leipzig)* 12 (1847) 393.
- [38] G. Williams, D. C. Watts, *Trans. Faraday Soc.* 66 (1970) 80.
- [39] K. L. Ngai, H. Jain, *Solid State Ionics* 18-19 (1986) 362.
- [40] M. Hodge, M. D. Ingram, A. R. West, *J. Electroanal Chem.* 74 (1976) 125-143.
- [41] K. C. Shobha, K. J. Rao, *Solid State Ionics*, 81 (1995) 145-156.
- [42] M. Ganguli, K. J. Rao, *J. Non-Cryst. Solids*, 243 (1999) 251-267.
- [43] J. M. Reau, X. Y. Jun, J. Senegas, *Solid State Ionics*, 95 (1997) 191-199.
- [44] S. Ghosh, A. Ghosh, *Solid State Ionics*, 149 (2002) 67-72
- [45] A. S. Nowick, B. S. Lim, *J. Non-Cryst. Solids* 172-174 (1994) 1389-1394
- [46] R. S. Kumar, K. Hariharan, *Mat. Chem. & Phys.* 60 (1999) 28-38
- [47] K. Prabakar, S. K. Narayandass, and D. Managalaraj, *Mater. Sci. Engg. B.* 98 (2003) 225.
- [48] P. Dutta, S. Biswas, and S. K. De, *Mater. Res. Bull.* 37 (2002) 193.
- [49] G. C. Psarras, E. Manolakaki, and G. M. Tsangaris, *Composites A.* 34, (2003) 1187.
- [50] R. Mishra and K. J. Rao, *Solid State Ionics.* 106 (1998) 113.
- [51] M. A. L. Nobre and S. Lanfredi, *J. Phys. Chem. Solids.* 64 (2003) 2457.
- [52] S. Ramesh, M.F. Chai, *Materials Science and Engineering B*, 139 (2007) 240-245.
- [53] Robitaille, C.D. and D. Fauteux, *J. Electrochem. Soc.*, 133 (1986) 315-325.
- [54] M. B. Armand, J. M. Chabango, M. J. Duclot, *Fast Ion Transport in Solids*, Elsevier North Holland, (1979) 131.
- [55] J.M. Parker, P.V. Wright, C.C. Lee, *Polymer*, 22(10) (1981) 1305-1307.
- [56] C. Berthier, W. Gorecki, M. Minier, M.B. Armand, J.M. Chabagno, and P. Rigaud, *Solid State Ionics*, 11(1) (1983) 91-95.
- [57] N.K. Karan, D.K. Pradhan, R. Thomas, B. Natesan, R.S. Katiyar, *Solid State Ionics* 179 (2008) 689-696.

- [58] Crawford, E. T. Arrhenius: *From Ionic Theory to the Greenhouse Effect. Uppsala Studies in History of Science, Canton, MA: Science History Publications, (1996) 23.*
- [59] A. G. Guy, *Introduction to Materials Science, McGraw Hill, Kogakusha Ltd., (1972).*
- [60] P. Colomban, editor. *Proton Conductors: Solids, membranes and gels-materials and devices. Cambridge University Press, 1992.*
- [61] H. Yugami, M. Ishigame, *Fundamental physics and promising applications of superionic conductors. Japanese J. Appl. Phys., 32(1993)853-859.*
- [62] H. Vogel, *Phys. Z. 22 (1921) 645.*
- [63] G. Tammann, W. Hesse, *Z. Anorg, Allg. Chem. 156 (1926) 245.*
- [64] T. Uma, T. Mahalingam, U. Stimming, *Mater Chem Phys 85 (2004)131.*
- [65] H. M. Cohen, D. Turnbull, *J. Chemical Physics, 31(1959) 1164-1169.*
- [66] D. Turnbull, H. M. Cohen, *The Journal of Chemical Physics, 34(1)(1961) 120-125.*
- [67] G.U. Losi, W. G. Knauss, "Free Volume Theory and Nonlinear Thermoviscoelasticity," *Polymer Science and Engineering, 32(1992)542-557.*
- [68] R. J. D. Tilley, *Understanding solids: The science of materials, John Wiley & Sons, Ltd. (2004).*
- [69] M. Goldstein, *J. Physical Chemistry, 77 (1973)667-673.*
- [70] C. A. Angell, W. Sichina. *Thermodynamics of the glass transition: empirical aspects. Annals of the New York Academy of Sciences, 279(1976) 53-67.*
- [71] H. M. Cohen, G. S. Grest, *Phys. Rev. B 20(1979) 1077 – 1098.*
- [72] P. M. Blonsky, D. F. Shriver, Paul Austin, H. R. Allcock, *J. Amer. Chemical Soc. 106 (1984) 6854-6855.*
- [73] N. Kobayashi, M. Uchiyama, K. Shigehara, E. Tsuchida. *J. Physical Chemi. 89 (1985) 987-991.*
- [74] P. G. Bruce, *Solid State Electrochemistry, New York (1995).*
- [75] H. J. Gibbs, E. A. DiMarzio, *The Journal of Chemical Physics, 28 (1958) 373-383.*
- [76] G. Adam, J. H. Gibbs, *The Journal of Chemical Physics, 43 (1965) 139-146.*
- [77] E. Williams, C. A. Angell, *Polym. Sci., Polym. Lett., 11 (1973) 383-387.*
- [78] A. J. Bhattacharyya, J. Maier, *Advanced Materials, 16 (2004) 811–814.*
- [79] J. Przulski, W. Wiczorek, *Solid State Ionics 53-56 (1992)1071-1076.*
- [80] Y.K. Mahipal, *Ph.D. Thesis, Submitted to Pt. R.S. University, Raipur, 2011.*
- [81] S. D. Druger, A. Nitzan, M. A. Ratner, *Journal of Chemical Physics, 79(1983) 313-3142.*
- [82] S. D. Druger, M. A. Ratner, A. Nitzan, *Solid State Ionics, 9-10 (1983) 1115-1120.*
- [83] A. K. Jonscher, *J. Phys. C: Solid State Phys. 6 (1973) 1235.*
- [84] A. K. Jonscher, *J. Mat. Sci. 16 (1981) 2037.*
- [85] K. Funke, *Z. Phys. Chem. (NF) 154 (1987) 251.*
- [86] P. Sharma, *Ph.D. Thesis, Submitted to M.S. University of Baroda, 2013.*
- [87] G. P. Triberis, *J. Non-Cryst. Solids 74 (1985) 1.*
- [88] H. R. Killias, *Phys. Rev. Lett. 20 (1966) 5*

- [89] C. Cramer, K. Funke, B. Roling, T. Saatkamp, D. Wilmer, M. D. M.D. Ingram, A. Pradel, M. Ribes, G. Taillades, *Solid State Ionics* 86-88 (1996) 481.
- [90] K. Funke, *Solid State Ionics* 18-19 (1986) 183.
- [91] K. Funke, *Prog. Solid State Chem.* 22 (1992) 111.
- [92] A. R. Long, *Adv. Phys.* 31 (1982) 533.
- [93] S.R. Elliott, *Philos. Mag. B*, 37 (1978) 553.
- [94] I.G. Austin and N. F. Mott, *Adv. Phys.* 18 (1969) 41.
- [95] M. Pollok, *Phys. Rev.* 138 (1965) A1822.
-

CHAPTER 3

EXPERIMENTAL TECHNIQUES

A *description of method used for sample preparation and the experimental techniques like FTIR, DSC, XRD, SEM ,transport number & conductivity measurements used for characterization of solid polymer electrolytes are discussed in this chapter.*

3.1 Introduction

This chapter describes the preparation method and theories of characterization (experimental techniques). The experimental technique includes X-ray diffraction (XRD), Differential Scanning Calorimetry (DSC), Fourier transform infra red spectroscopy (FT-IR), Scanning electron microscope (SEM) and Wagner's polarization technique.

3.2 Material used in preparing Polymer Electrolytes

Present Solid polymer electrolytes are prepared using high purity chemicals, such as:

1. Host Polymer :

Polyethylene oxide (PEO)

Structure : - (CH₂ - CH₂ - O)-_n, Molecular weight (M.W): 1 x 10⁶, Glass transition temperature : -60° C, Melting point: 66 °C, State: White Powder, Company: Sigma-Aldrich

2. Dopant salt :

(a) Silver trifluoromethane sulphonate (AgCF₃SO₃)

(b) Lithium trifluoromethane sulphonate (LiCF₃SO₃)

Company: Sigma-Aldrich

3. Nanofillers :

(a) Silicon dioxide (SiO₂), Particle size= < 50nm, 101,96 g/mol,

Company: Sigma-Aldrich chemical

(b) Aluminum dioxide (Al₂O₃), Particle size= < 50nm, 101, 96 g/mol,

Company: Sigma-Aldrich chemical

4. Plasticizer :

Poly (ethylene glycol) (PEG)

Structure: [H(- O - CH₂ - CH₂-)_n- OH] H (OCH₂CH₂)_nOH,

Molecular weight (M.W): 4000, Glass transition temperature: -60° C,

Melting point: 55° C, Company: Loba Media.

5. Solvent :

Acetonitrile

State: Polar aprotic solvent (liquid). Permittivity: high static permittivity of 36.6 at 30 °C. Acetonitrile promotes the dissociation of alkali metal salt in the solution. It is

used for the synthesis of polymer electrolytes by solution cast technique.

6. Storage : **Desiccators**

In laboratory use, the most common desiccators are circular and made of heavy glass. The substance is put in the upper compartment (on the porcelain plate). The lower compartment of the desiccators contains lumps of freshly calcined quicklime or calcined calcium chloride to absorb water vapors. The round-glass rim of the desiccator lid must be thoroughly greased with a thin layer of petroleum jelly melted together with beeswax or paraffin wax. A common use for desiccators is to moisture-sensitive or hygroscopic samples. In order to open the desiccators without damage, remove the lid sideways horizontally not to upwards. Cover the desiccators in the same way [1] therefore, prepared polymer electrolyte samples were stored in desiccators to prevent them any contamination from moisture.

3.3 Methods and Sample preparation

Commercially available analytical reagent (AR) grade materials have been used in all the preparation. Samples are prepared by solution cast technique [2-4]. In this technique, at first stage the protic solvent helps the salt to dissociate into ions (cations and anions), dissolves into solvent and thereafter it interact with polymer chains. As the solvent is gradually evaporated, polymer/ions complexing is favored if there is a strong interaction between polymers and ions.

Using above mentioned chemicals, the following five series of polymer electrolytes are prepared. The starting materials were weighed in the desired proportion using micro analytical balance. The amount of material used to prepare sample is denoted in wt%.

1. First series: Silver based Solid Polymer Electrolyte System :

PEO-AgCF₃SO₃ (PA-series)

In the first series, the amount of Poly (ethylene oxide) PEO is fixed and salt AgCF₃SO₃ is varied i.e. PA- 2 (wt %), PA- 3.5 (wt %), PA-5 (wt %), PA-7(wt %) & PA-11(wt %) to observe the effect of salt on PEO system. The solution was prepared by dissolving fixed amount of Poly (ethylene oxide) PEO and different

concentration of Silver trifluoromethane sulphonate (AgCF_3SO_3) in acetonitrile solution.

2. Second series: Silver based Solid nano Composite Polymer Electrolyte System:

PEO- AgCF_3SO_3 – SiO_2 (PAS- series)

In the second series, the amount of PEO- AgCF_3SO_3 (7 wt %) is fixed and nano filler SiO_2 is varied i.e. PAS-5 (wt %), PAS-10 (wt %), PAS-15 (wt %), PAS-20 (wt %) & PAS-25 (wt %) to observe the effect of nano filler in PEO- AgCF_3SO_3 system. In the second Series, the solution was prepared by dissolving weighed amount of Poly (ethylene oxide) PEO, 5 wt% of Silver trifluoromethane sulphonate (AgCF_3SO_3) 5wt% and different concentration of nano-particle SiO_2 in acetonitrile solution.

3. Third series: Silver based Solid Plasticized nano Composite Polymer Electrolyte System :

PEO- AgCF_3SO_3 – SiO_2 -PEG (PASP- series)

In the third series, the amount of PEO- AgCF_3SO_3 (7 wt %) – SiO_2 (20 wt %) is fixed and plasticizer PEG is varied i.e. PASP-5(wt %), PASP-10(wt %), PASP-15(wt %), PASP-20(wt %) & PASP-25 (wt %) to observe the effect of plasticizer on PEO- AgCF_3SO_3 - SiO_2 system. In the third Series the solution was prepared by dissolving weighed amount of Poly (ethylene oxide) PEO, 5wt% of Silver trifluoromethane sulphonate (AgCF_3SO_3), 20wt% of nano-particle SiO_2 and various proportion of Poly (ethylene glycol) PEG in acetonitrile solution.

4. Fourth series : Lithium based Solid nano Composite Polymer Electrolyte System :

PEO- LiCF_3SO_3 –PEG- Al_2O_3 (PLA-series)

In the fourth series, the amount of PEO- LiCF_3SO_3 (5 wt %)-PEG (10 wt %) is fixed and nano filler Al_2O_3 is varied i.e. PLA-1 (wt %), PLA -2 (wt %), PLA -3 (wt %), PLA-4 (wt %) & PLA-5 (wt %) to observe the effect of nano filler on PEO- LiCF_3SO_3 -PEG system. In the fourth series the solution was prepared by dissolving weighted amount of Poly (ethylene oxide) PEO, 5wt% of Lithium trif-

lithium trifluoromethane sulphonate (LiCF_3SO_3), 10wt% of Poly (ethylene glycol) PEG and various proportion of nanofiller Al_2O_3 in acetonitrile solution.

5. Fifth series: Lithium based Solid plasticized nano composite polymer electrolyte system :

PEO- LiCF_3SO_3 - Al_2O_3 -PEG (PLP-series)

In the fifth series, the amount of PEO- LiCF_3SO_3 (5 wt %) - Al_2O_3 (1 wt %) is fixed and plasticizer PEG is varied i.e. PLP-5(wt %), PLP -10(wt %), PLP -15(wt %), PLP-20(wt %) & PLP -25 (wt %) to observe the effect of plasticizer on PEO- LiCF_3SO_3 - Al_2O_3 system. In the fifth series the solution was prepared by dissolving weighed amount of Poly (ethylene oxide) PEO, 5wt% of Lithium trifluoromethane sulphonate (LiCF_3SO_3), 1wt% of nano-particle Al_2O_3 and various proportion of Poly (ethylene glycol) PEG in acetonitrile solution

The mixture, thus, formed was constantly allowed to stir for 48 hrs at ambient temperature. The homogenous and viscous solution thus obtained in each steps (series) was cast in PTFE plates. Solvent evaporation was carried out in closed apparatus for 24 to 30 hrs at ambient temperature. Semi-transparent homogenous membranes having thickness ranging from 10-30 μm and good mechanical strength were obtained. Any contamination with the external environment was carefully avoided by performing the entire procedure in closed apparatus. The obtained solid homogenous films were cut into pieces of required dimension for studies like FTIR, DSC, XRD, SEM and transport number measurement, while for conductivity measurements samples were cut into pieces of about 1mm diameter.

3.4 Characterization Techniques

The various characterization techniques employed to study the prepared polymer samples are mentioned below:

- ❖ *Fourier Transform Infrared Spectroscopy (FTIR)*
- ❖ *Diffraction Scanning Calorimetry (DSC)*
- ❖ *X-ray Diffraction (XRD)*
- ❖ *Scanning Electron Microscopy (SEM)*
- ❖ *Transport number measurements*
- ❖ *Conductivity measurements*

3.4.1 Fourier Transform Infrared Spectroscopy (FTIR)



Fig. 3.1 Image of FTIR instrument.

FTIR is a powerful and useful characterization method for polymers, and materials in general [6]. This is an economic, short time characterization that allows to establish the chemical composition, microstructure, chemical interactions and even to follow variation of specific functional groups with time, during reactions. All this features makes the FTIR an essential characterization technique for analyzing polymeric material [7, 8].

FTIR spectroscopy of the prepared polymer electrolyte samples was carried out using JASCO 4100 series in the wave number ranging from 400 to 4000 cm^{-1} as shown in Fig. 3.1. FTIR is an upgraded technique of conventional IR spectroscopy. In this technique the optical pathway is used to detect radiation coming from the sample and the reference source is designed to produce an interferogram, a plot of intensity versus time. This signal is converted into frequency domain, using Fourier transformation. The data thus obtained is plotted and analyzed.

3.4.2 Diffraction Scanning Calorimetry (DSC)

Thermal analyses of the prepared samples are carried out using NETZSCH 200 F3. Before starting the measurements, the base line corrections have been made in order to compensate the difference in the signal, which may account for the possible non identical nature of pans or heating elements. Calibration of empty pan should provide flat baseline. Polymeric materials generally have an endothermic slope due to increasing heat capacity with increasing temperature. Normally curvature in the graph is not part of cali-

bration procedure but causes errors in analyses. Hence, it can be eliminated if necessary with baseline subtraction.



Fig. 3.2 Image of DSC apparatus.

The baselines are obtained under the required experimental conditions for the system under study. The investigation on polymer electrolytes has been aimed at determining the glass transition temperature (T_g) of the polymer samples. For this, thin pieces of polymer film weighing about 2-3 mg were encapsulated in aluminum pans for DSC measurements. The measurements were carried out from -100°C to 100°C at heating rates of $10^{\circ}\text{C}/\text{min}$, under nitrogen atmosphere. In the case of polymer electrolytes, DSC measurements have been carried out in order to determine the glass transition temperature (T_g) and the crystallization melting temperature T_m of the polymer samples. Fig. 3.2 shows the picture of DSC apparatus employed for thermal analysis of the prepared polymer electrolyte samples. The result of the DSC experiment is a graphical representation with endothermic and exothermic peak corresponding to the glass transition temperature (T_g) and crystallization temperature (T_m).

3.4.3 X-ray Diffraction (XRD)

X-ray diffraction is a phase selective method and can be used favorably for investigating phase transition phenomena [5]. In the present investigation, for structural characterization of the prepared polymer samples room temperature X-ray diffraction patterns of the prepared films have been recorded using a Bruker NSZ, model D8, U.S.A,

X-ray diffract meter employing a Cu-K α radiation. The measurements were recorded for 2θ values from 10° - 80° at a scanning rate of 2° per minute. Fig. 3.3 shows the diagram of the XRD instrument.

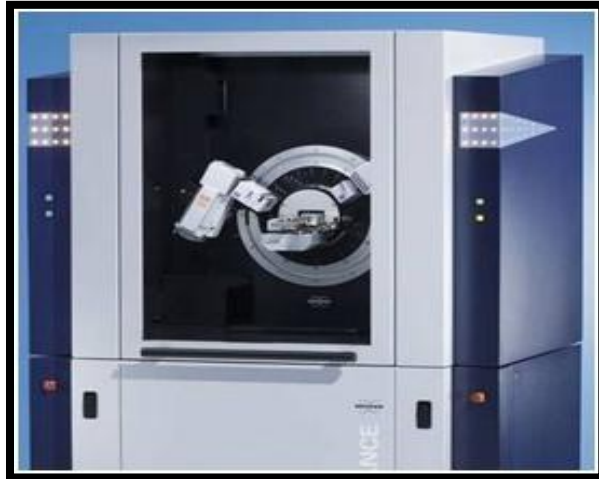


Fig. 3.3 *Image of XRD Instrument.*

3.4.5 Scanning Electron Microscopy (SEM)



Fig. 3.4 *Image of SEM instrument.*

Scanning Electron Microscopy (SEM) technique is used to observe the surface morphology of prepared polymer sample. Characterization of the sample was carried out using JOEL JSM – 6380LV instrument at 15-20 kV. Fig. 3.4 shows the image of SEM instrument used during the surface analysis of the prepared polymer electrolyte samples. The piece of prepared samples was sticky to the surface made by adhering conductive carbon cement on a SEM sample holder. The images so formed are observed on the computer attached to the SEM instrument.

3.4.6 Transport number measurements

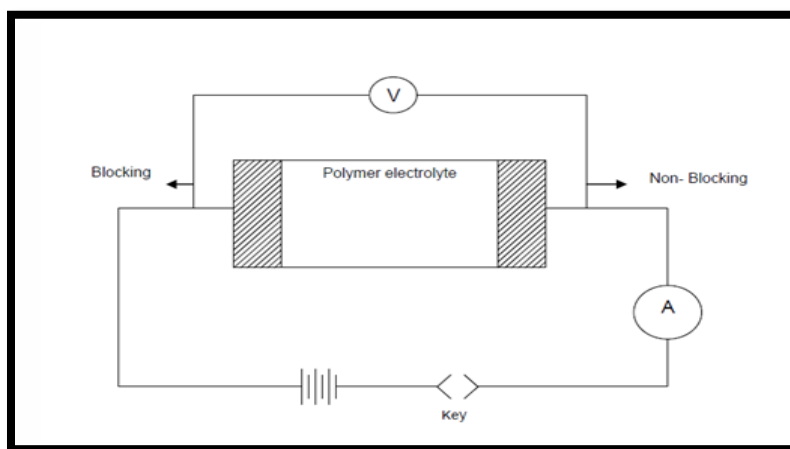


Fig. 3.5 Experimental setup of Wagner technique.

The ionic transport number is measured by means of Wagner's Polarization technique. The schematic diagram of the experimental set up is shown in Fig. 3.5. The sample is polarized under dc bias of constant voltage. In this method, a constant voltage less than decomposition potential (i.e. less than 1) is applied across the sample, which is placed between a pair of blocking electrodes. The current flowing through the circuit is monitored as function of time using a current source measuring unit. In order to confirm that the conduction mechanism of the prepared polymer electrolyte sample, the ionic transport number is measured. The sample is placed between a pair of silver electrodes [9]. An appreciable amount of current, I_0 , is resulted in the output by the application of a dc voltage to the above configuration. After a long interval of time, i.e., around 48 hours, the cell is completely polarized and delivers steady currents, I_s which shows no change is the steady current with time. Decrease in polarization current can be attributed to the migration of

ions due to applied field and is balanced by diffusion due to the concentration gradient. Thus, the resulting steady-state current is only due to electrons or holes. The ionic contribution is evaluated through the equation [10]:

$$t_i = I - \frac{I_s}{I_0}$$

where, t_i is the ionic transport number and is found to be nearly equal to unity for most of the materials investigated in the present study.

3.5 Conductivity measurement

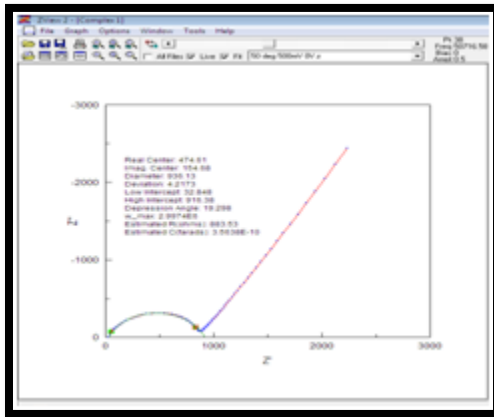


Fig. 3.6 Z-view plot.



Fig. 3.7 Sample holder for the conductivity measurements.



Fig. 3.8 AC Conductivity measurement setup

In Solid state electrolytes, the conductivity measurements are of prime importance. Impedance spectroscopy is a powerful ac technique, which has received the wide spread acceptance today for the determination of true bulk conductivity of ionic/super ionic/mixed electronic-ionic systems [11-16]. In this method, the real and imaginary values of the sample impedance are recorded as a function of frequency of the applied voltage. The impedance values are plotted on the complex impedance (Argand) diagram as shown in the screen shot (Fig 3.6) and the d.c. conductivity is calculated from the analysis of these plots. For the impedance measurements, all the polymer samples were cut into small pieces of about 1mm thickness to serve as electrolytes. The measurements were made with two probe method. The sample inside the sample holder (as shown in Fig. 3.7) is kept in contact with two polished, properly cleaned and spring loaded copper electrodes of a cell and the cell was kept in a furnace controlled by mercury contact thermometer and relay. Fig. 3.8 shows the conductivity measurement setup for impedance analysis. The impedance measurements were made using Solartron 1260 in the frequency range from 1 Hz to 32 MHz at different temperatures and the sample was heated at the interval of 5°C.

References:

- [1] V. Alexeyev, *Quantitative Analysis*. Lightning source Inc. ISBN 0-89875- 034-2
- [2] A. Karmakar and A. Ghosh, *Phys. Rev. E* 84 (2011) 051802-1-9.
- [3] Ce-Wen Nan, L. Fan, Y. Lin, Q. Cai, *Phys. Rev. Lett.* 19 (2003) 266104-1-4.
- [4] A. J. Bhattacharyya, T. R. Middya, and S. Tarafdar, *Phys. Rev B*, 60 (1999) 909-915.
- [5] R. Androsch, M. Stolp, H. J. Radosch, *Thermochimica Acta* 271 (1996) 1-8
- [6] Lee, L.H., Ed. (1977). *Characterization of Metal and Polymer Surfaces: Polymer Surfaces* Academic Press, ISBN-10: 0124421016, New York, USA (Lee, 1977)
- [7] J. Schoonman, F.G. Dijkman, *J. Solid State Chem.* 5 (1972) 111.
- [8] N. Srivastava, A Chandra, S., *Phys. Rev. B* 52 (1995) 225.
- [9] J. E. B. Randles, *Trans. Farad. Soc.* 1 (1947) 11.
- [10] J. E. Bauerle, *J. Phys. Chem. Solids* 30 (1969) 2657.
- [11] J. R. Macdonald, in: “*Superionic Conductors*” (eds.) G. D. Mahan and W. L. Roth (Plenum Press, New York) 1976, 81.
- [12] J. R. Macdonald, (eds.) “*Impedance Spectroscopy*” (John Wiley & Sons, New York) 1987.
- [13] C. G. Gabrieli, “*Identification of Electrical Processes by Frequency Response Analysis*”, Technical Report No. 4183, Issue-2, 1984 (Solartron Instruments, UK).
- [14] B. E. Mellander, A. Lunhden, in: “*Materials for Solid State Batteries*” (eds.) B. V. R. Chowdari, S. Radhakrishnana (World Scientific Singapore) (1986), 161.
- [15] S. P. S. Badwal, in: “*Solid State Ionic Devices*” (eds.) B. V. R. Chowdari, S. Radhakrishna (World Scientific, Singapore) (1988), 165.
- [16] M. Pant, *Ph.D. Thesis*, Department of Physics, The M.S. University of Baroda, 2010.

CHAPTER 4

CHARACTERIZATION STUDIES

In this chapter, the results of characterization studies viz., Fourier Transform Infrared Spectroscopy (FTIR), Differential scanning Calorimetry (DSC), X-ray diffraction (XRD), Scanning Electron Micrographs(SEM) & transport number of all samples of solid polymer electrolytes are discussed.

4.1 Fourier Transform Infrared Spectroscopy (FTIR)

Fourier transform infrared spectroscopy (FTIR) is an exquisite tool for probing into the structural and functional features of macromolecular system and aggregates [1-10]. FTIR brings greater versatility to polymer structural studies. It facilitates the study as the spectra can be scanned, recorded and transformed into a matter of seconds. Besides, it is a qualitative identification of unknown sample which can accomplish by the comparison. Additionally, the interaction which arises from chemical or physical interaction between the polymer, salt, nano-filler and or plasticizer can also be exhibited.

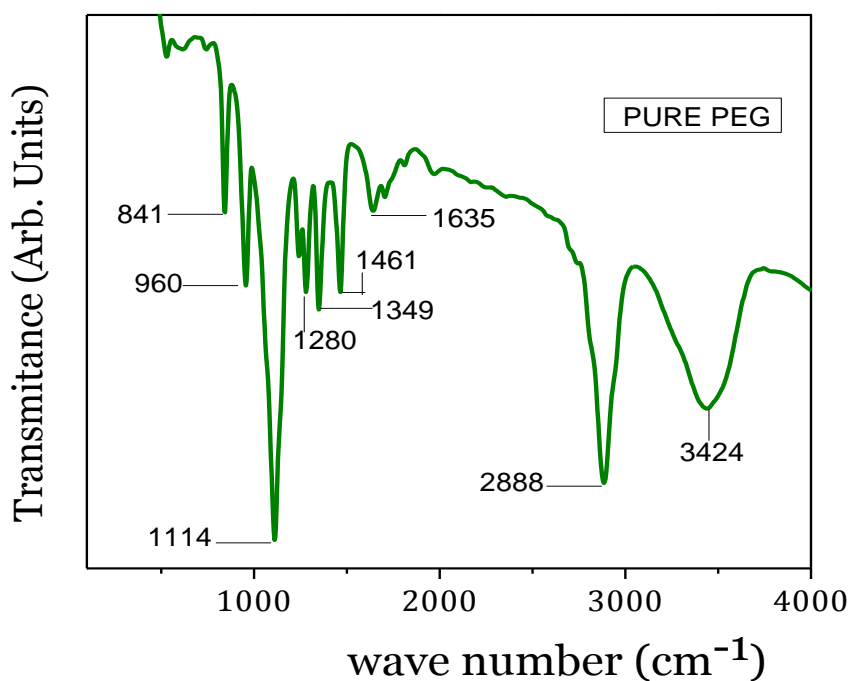


Fig. 4.1 FTIR of Pure PEG.

As mentioned in chapter 1, poly ethylene glycol (PEG) belongs to ether group with similar structure and property like PEO but PEG is low molecular weight material and hence it is widely used as plasticizer. For reference purpose the FTIR spectrum of Pure PEG is shown in Fig. 4.1. The characteristic groups present in plasticizer PEG are: C-O-C (ether) stretching vibration at 1050-1150 cm⁻¹, C-O (alcohols) stretching vibration at 1000-1260 cm⁻¹, C-H (alkanes) stretching vibration at 2850-2960 cm⁻¹, C-H (alkanes) stretching vibration at 1300-1450 cm⁻¹ and O-H (hydroxyl) at 3200-3600 cm⁻¹[11-13].

The FTIR spectra of pure polyethylene oxide PEO is shown in Fig. 4.2 which

shows the presence of aliphatic C-H stretching mode can be observed at 2876 cm^{-1} , CH_2 scissoring mode at 1466 cm^{-1} , CH_2 wagging mode at 1360 and 1341 cm^{-1} , CH_2 twisting mode at 1279 cm^{-1} , 1240 cm^{-1} of C-O stretching vibration, a band of C-O-C stretching at $1,100\text{ cm}^{-1}$, CH_2 rocking and C-O-C vibration mode at 960 cm^{-1} , CH_2 rocking at 841 cm^{-1} while C-O-C bending at 528 cm^{-1} . The semi-crystalline phase of PEO is confirmed by the presence of triplet peak of C-O-C stretching at 1100 cm^{-1} band [14, 15]. C-O-C stretching vibrations are observed at 1145 , 1095 and 1059 cm^{-1} with maximum intensity at 1095 cm^{-1} [16, 17].

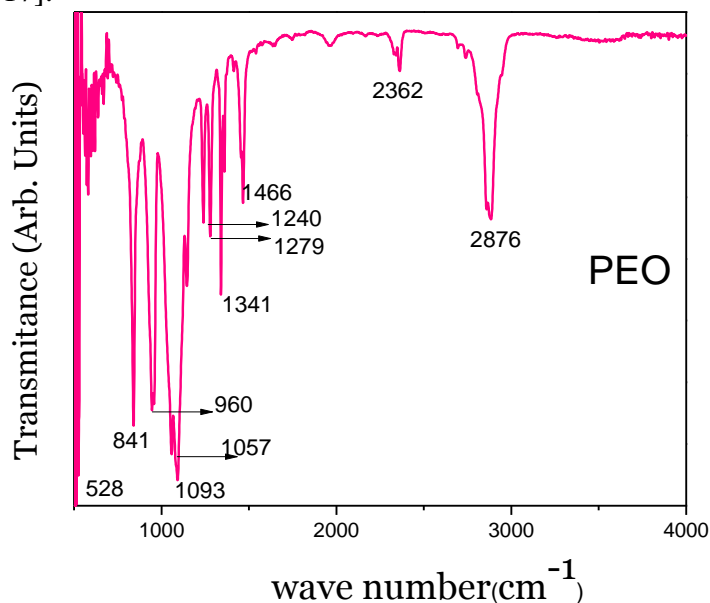


Fig. 4.2 FTIR spectra of Pure PEO.

At the initial stage the content of PEO is kept constant and amount of AgCF_3SO_3 salt is varied. Some changes as shown in Fig. 4.3 in the intensity of peaks in the IR spectra of these PEO: AgCF_3SO_3 (PA) series has been observed on addition of AgCF_3SO_3 . The presences of two new peaks; one at 636 cm^{-1} which is assigned to the $\delta_s(\text{SO}_3)$ mode of free triflate ion and another at 1028 cm^{-1} corresponding to the SO_3 symmetric mode [18] has been observed. Both these characteristic peaks become prominent on increasing AgCF_3SO_3 content. If the cations of AgCF_3SO_3 become co-ordinated with the ether oxygen of PEO, the spectral changes are expected to be in the C-O-C stretching band at 1057 and 1093 cm^{-1} . According to Huang *et.al.* and D.R. MacFarlane *et. al.*[19, 20] effect of ion pairing is observed at 1200 cm^{-1} band due to anti-symmetric stretching mode of SO_3 . In present case the variation in this band is observed and intensity of peak at 1240 cm^{-1} is

observed to increase at PA-11. This implies that ion association must have started.

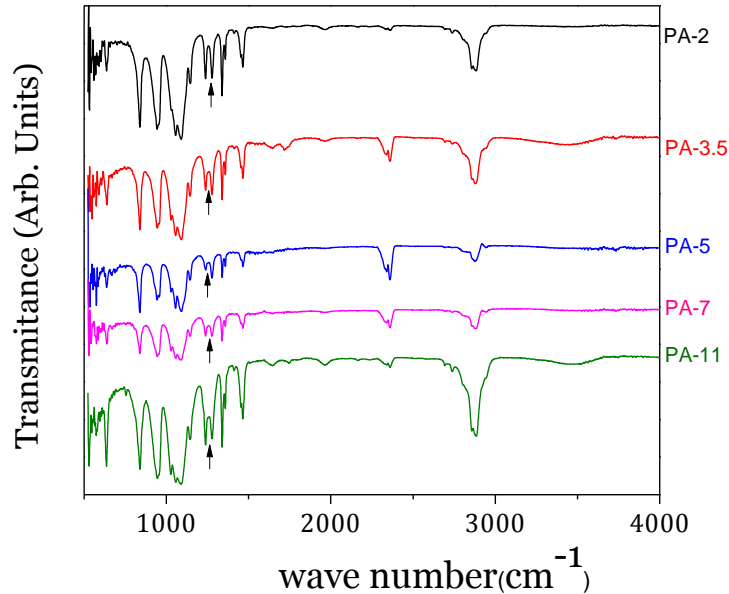


Fig. 4.3 FTIR spectra of PA series.

No change has been observed in the spectral range of 945 - 836 cm⁻¹ for all samples of PA series; suggest that the symmetrical rocking mode of CH₂ group has not been affected by complexation with AgCF₃SO₃. But, the CH₂ twisting mode at 1279 cm⁻¹ and the band at 2876 cm⁻¹ of CH₂ stretching are observed to vary with the salt variation.

Thus, it can be concluded from the emergence of new peaks at 636 and 1028 cm⁻¹ and change in the intensity of 1057 and 1093 cm⁻¹ peaks of C-O-C that the complexation of salt in host polymer PEO has been taken place. Also, the enhancement in peaks intensity at 1240 cm⁻¹ for higher amount of salt AgCF₃SO₃ implies that ion association has occurred.

Addition of nano-filler to solid polymer electrolytes, facilitate the increase of the free volume and consequently the amorphous phase of the system. The FTIR spectra of the series where various amount of nano-fillers SiO₂ is added to PEO: AgCF₃SO₃ (5wt %) sample of PA series is shown in Fig. 4.4. According to Saikia and Kumar [21] addition of SiO₂ increases the defects concentration along the SiO₂ particles interface, this is mainly attributed to higher degree of amorphousity in the polymer system.

The C-H stretching band at 2876 cm⁻¹ is broadens whereas, the intensity of peaks

around 2300 cm^{-1} reduces and the width of the C-O-C stretching band observed around $1000\text{-}1150\text{ cm}^{-1}$ decreases. On addition of SiO_2 nano-filler the well defined peak at 841 and 960 cm^{-1} in PA system blends with other surrounding peaks. Further a new peak around 1736 cm^{-1} has been observed at higher nano-filler composition. Also, a broadened peak at 3437 cm^{-1} which is characteristics of O-H stretching mode of surface hydroxyl group of SiO_2 is observed only in PAS-25 [22].

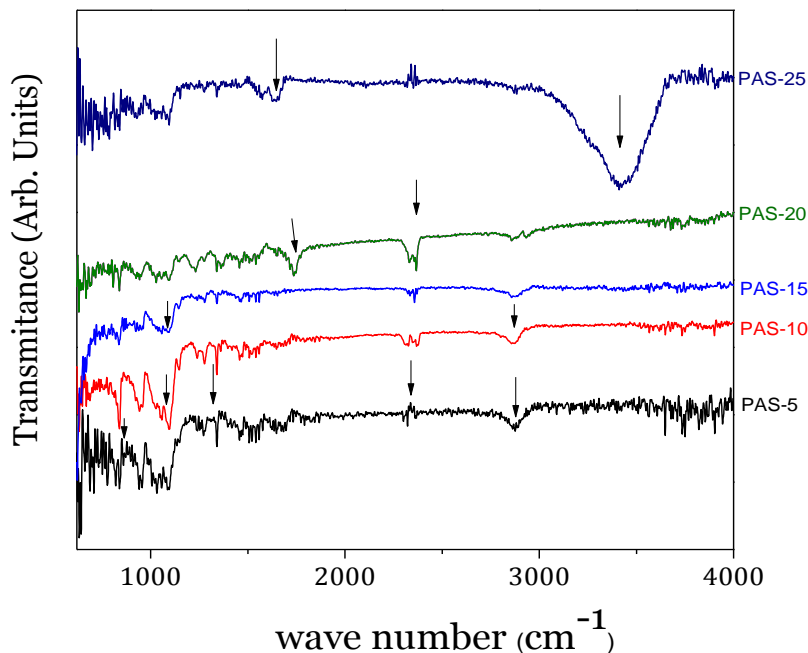


Fig. 4.4 FTIR spectra of PAS series.

As silica is a hydrophilic compound and prefers to form silanol (Si-OH) bonding on the surface of silicon atom of silica. Formation of hydrogen bonding between SiO_2 grains is favorable with the presence of Si-OH bond, leading to the formation of three-dimensional network when sufficient amount of SiO_2 is embedded into the polymer salt matrix. Therefore, it imparts high viscosity of polymer electrolytes with addition of SiO_2 [23], resulting in increase in amorphous phase of the system. Hence, the broadening of the IR bands with the addition of SiO_2 in polymer electrolyte increases, indicating the amorphous nature of the samples.

Now, in above mentioned PAS system, plasticizer PEG is varied. The FTIR spectra of so formed PASP i.e. PEO-AgCF₃SO₃-SiO₂-PEG is shown in Fig. 4.5. As mentioned earlier that the FTIR spectra of PEO and PEG are similar, hence no new peak are

expected. But, the intensity of existing peaks are reduced or broadened on addition of plasticizer PEG to polymer nano composite electrolyte system (PAS). The intensity of the peaks in the entire range from 500-3000 cm^{-1} gradually decreases with the addition of PEG.

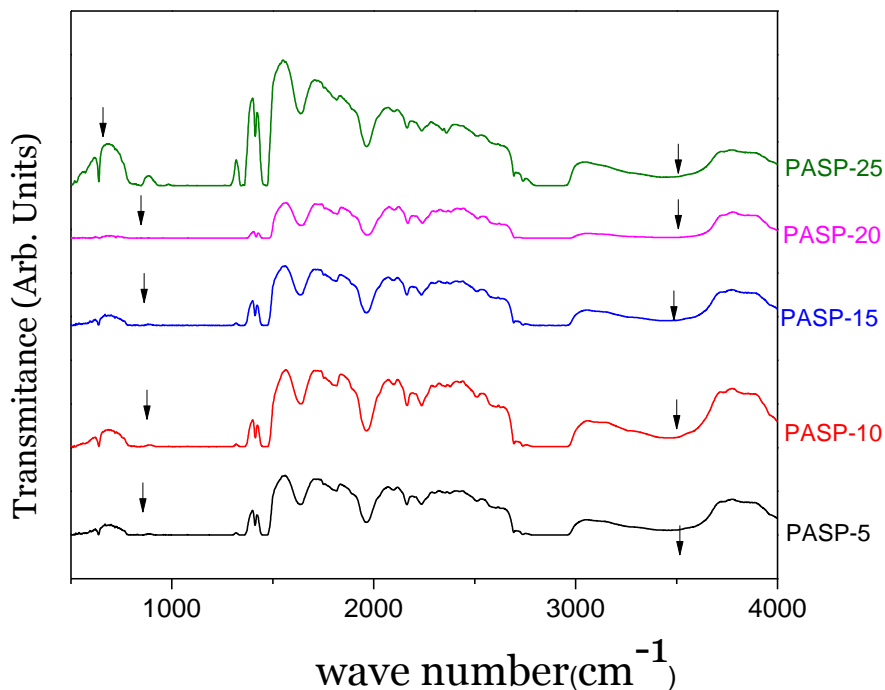


Fig. 4.5 FTIR spectra of PASP for series

A broadened aliphatic C-H stretching vibrational bond around 2700 to 3000 cm^{-1} and Vibrational band of OH-stretching group at 3300 cm^{-1} are clearly seen, indicating increase of amorphous phase of system. The lowest intensity of peaks and broadening is found in a sample of PASP-20 which is concluded as the highest amorphous sample.

Thus, it can be ascribed that with the addition of PEG, the increase in amorphousity is the main feature of the IR spectra. The physical strength of the films reduces and such sample are decayed or broken into pieces with passage of time within few months due to the presence of sulphate group in the silver salt.

Therefore, in the next system the silver salt is been replaced by LiCF_3SO_3 and nano-filler SiO_2 by Al_2O_3 . The FTIR spectra of so formed, system: PEO: LiCF_3SO_3 : PEG: Al_2O_3 (PLPA) is shown in the Fig 4.6. The presences of characteristic peak of LiCF_3SO_3 salt with the host polymer PEO can be confirmed by appearance of signature peak of 526

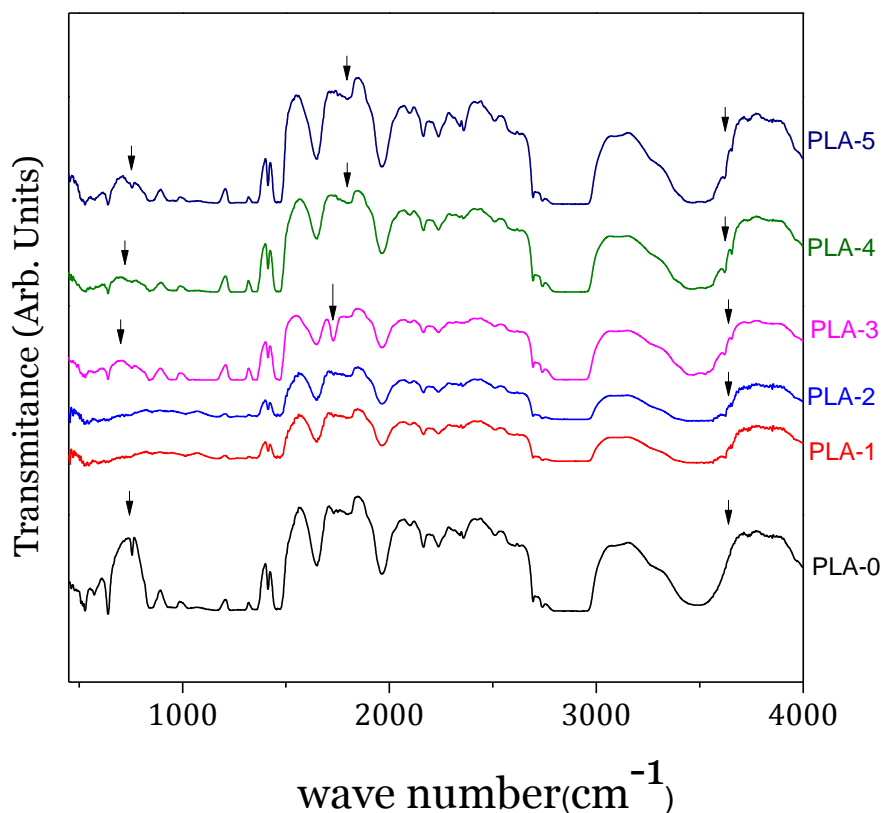


Fig. 4.6 FTIR spectra of PLA series

cm^{-1} consistent with $\delta_{\text{as}}(\text{CF}_3)$ [24-26], $\delta_{\text{s}}(\text{SO}_3)$ mode of free triflate ion assigned to 636 cm^{-1} and symmetric stretching mode SO_3 at 1033 cm^{-1} . Also, the unique weak absorption band at 757 cm^{-1} corresponding to ion triplet ($\text{Li}^+ - \text{CF}_3\text{SO}_3^- - \text{Li}^+$) [26] is observed in the filler free sample and slight kink at higher values of nano-filler i.e. 5wt% Al_2O_3 . While, the presences of new peaks at 1732 and 3615 cm^{-1} are also observed indicating complexation of nano-filler Al_2O_3 with the plasticized polymer electrolyte. The peak at 1732 cm^{-1} is observed to shift towards the higher wave number side, indicating the decrease in the band length of this Vibrational band. Wang *et.al.*, [27] too observed the shifting of peaks at 1409 and 634 cm^{-1} on addition of Al_2O_3 to PAN- LiClO_4 system, while Suthanthiraraj *et.al.* [28] has discussed the suppression of association of Ag^+ and CF_3SO_3^- on addition of Al_2O_3 nano-filler to PVDF- AgCF_3SO_3 system. In our case the peak intensity of IR spectra for 1wt% of nano-filler Al_2O_3 to be minimum when compared with the sample without Al_2O_3 . However, beyond 1 wt% of Al_2O_3 , the IR peaks are observed to gradually increase. The overall intensity of the band ranging from 3000 and 4000 cm^{-1}

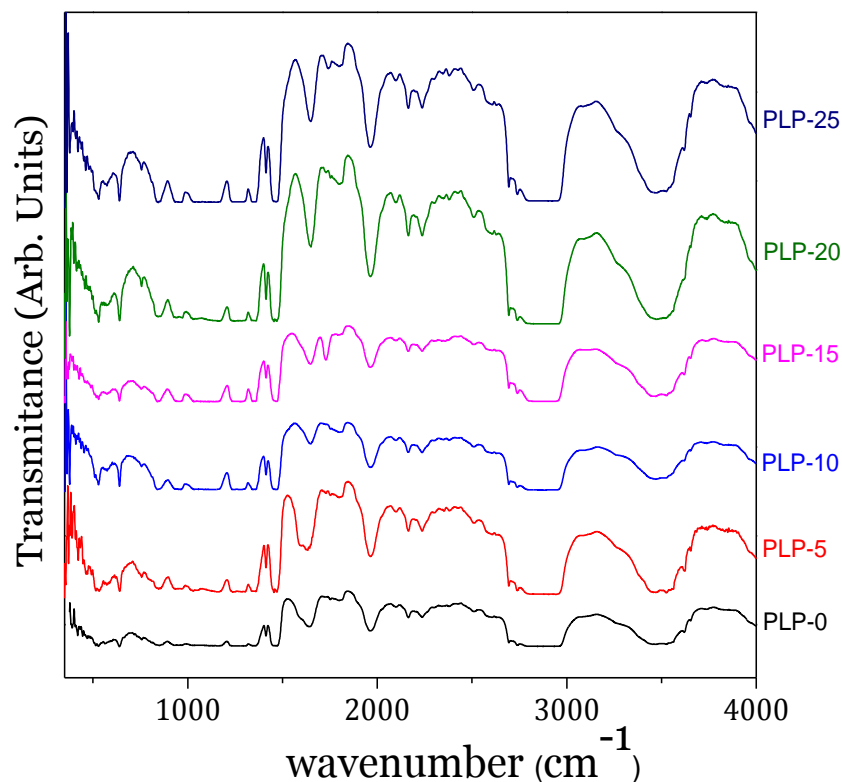


Fig. 4.7 FTIR spectra of PLP series

also gradually increase after 1wt% of Al₂O₃ nano-filler content, which favors the enhancement of crystalline phase. Hence, the inclusion of Al₂O₃ increases the crystallinity in all the samples expect PLA-1.

Now, to understand the effect of plasticizer PEG on the above polymer electrolyte system PLPA the amount of 1wt% Al₂O₃ is kept constant and the amount of plasticizer PEG has been varied. In the IR spectra of this series, beside the overall variation in intensity of IR spectra, the increase in the peak intensity of peaks at 526 cm⁻¹ of δ_{as} (CF₃) and δ_s (SO₃) mode of free triflate ion assigned to 636 cm⁻¹ increases on addition of plasticizer PEG. Peak due to ion triplet (Li⁺ - CF₃SO₃⁻ - Li⁺) at 757 cm⁻¹ starts developing after 10wt% PEG, this increase in intensity indicates that the addition of plasticizer does not substantially dissociates ion. Hence, from above mentioned discussion it can be concluded that the interaction between nanocomposite polymer system and plasticizer has taken place.

Finally, it is worth noticing that the systems with plasticizer are observed to be

more crystalline than compared to that without it. However, with the addition of plasticizer (PEG) in the nanocomposite system, the peaks that were shouldered due to incorporation of nano-filler reappeared; this indicated the degeneration of the amorphous phase in the system. This must be due to the short branching or side-chain group of PEG, which produced a regular helical coil, which favors crystallization. This crystallization results, in hindering the mobility as well as an increase in the rigidity and stiffness modulus (supported by DSC values).

4.2 Differential Scanning Calorimetry (DSC)

Differential Scanning Calorimetry (DSC) technique is used to measure the temperature and heat flow associated with the transition in the prepared sample as a function of time and temperature. The DSC measurement is used to determine the glass transition (T_g) in order to establish an upper limit of temperature to perform the conductivity measurements and to avoid any structural relaxation. Whereas, the melting temperature (T_m) represents the phase transformation of the system, beyond which the system becomes more amorphous due to melting. Kumar *et.al.* [29] has suggested that backbone flexibility is the controlling factor in determining the T_g of a material.

As mentioned in chapter 1, cationic mobility occurs in the amorphous phase and its diffusion occurs through a complex mechanism involving the PEO segmental mobility. But pure PEO is crystalline in nature with low flexibility and cationic mobility. Therefore the need arise to increase the flexibility a PEO-matrix by addition of alkali salt of it. Addition of salt modifies the polymer PEO structure by inhibiting regular packing. Beside this, the dissociation of salt also plays a vital role in increase in flexibility of the polymer-salt system.

The glass transition temperature T_g and melting temperature T_m values for PA series where salt AgCF_3SO_3 is varied is shown in Fig 4.8 (a) and (b). Addition of AgCF_3SO_3 to PEO decreases the T_g values of as compared to pure PEO. On increasing the salt (AgCF_3SO_3) composition the T_g value gradually decreases up to 7wt% of AgCF_3SO_3 . This shows that incorporation of salt AgCF_3SO_3 has increase the flexibility. But after 7wt% AgCF_3SO_3 , increase in T_g indicates reduction in flexibility of PEO-chain in the system. The association of ions gradually results into the increase in glass transi-

tion temperature T_g .

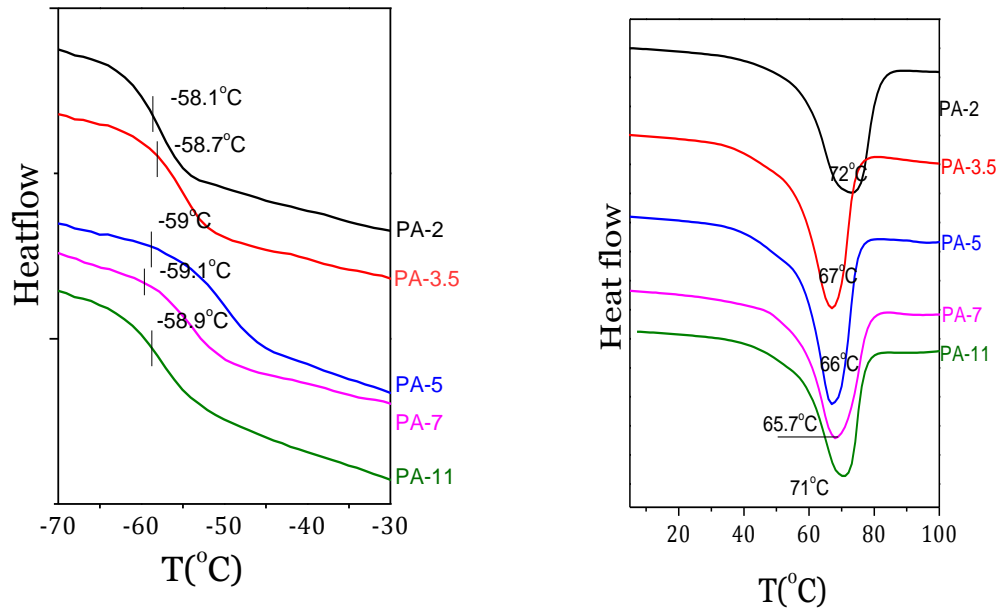


Fig. 4.8 DSC plots of PA-series

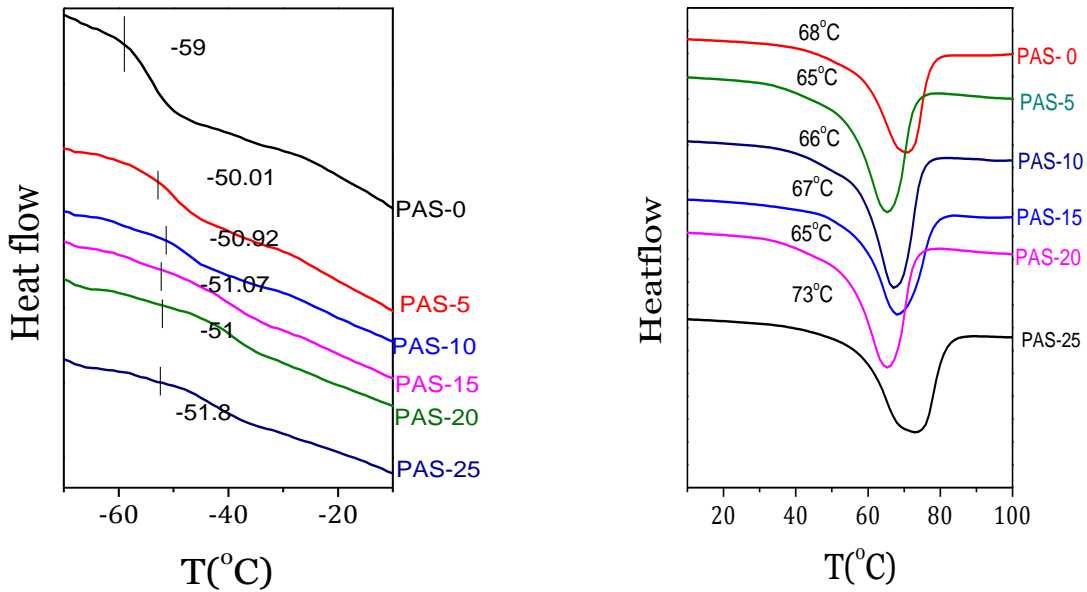


Fig. 4.9 DSC plots of PAS series

Lizhen *et. al.* [30] mentioned in his work that addition of nano-filler SiO_2 to PEO- LiClO_4 the glass transition temperature decreases and as T_g lowers, the amorphous phase becomes more flexible and the ionic conductivity should be enhanced. To examine the

effect of nano-filler SiO₂ in the above system PEO: AgCF₃SO₃ nano-filler SiO₂ has been added. The T_g value on addition of nano-filler SiO₂ has greatly affected the polymer-salt matrix (Fig. 4.9). The glass transition T_g has been reduced by about 9°C for all the sample show the T_g in the range of -50 to -51°C to -58 °C in PAS system. This major change in the T_g value suggests the increase in the formation of an amorphous phase [31-33] on addition of nano-filler SiO₂. T_m value of highest conducting sample i.e. PAS-20 is observed to lowest (Fig. 4.9). Generally, plasticization increases viscosity by interrupting polymer-polymer interaction and results in lowering of T_g values [34-37]. Plasticization of above

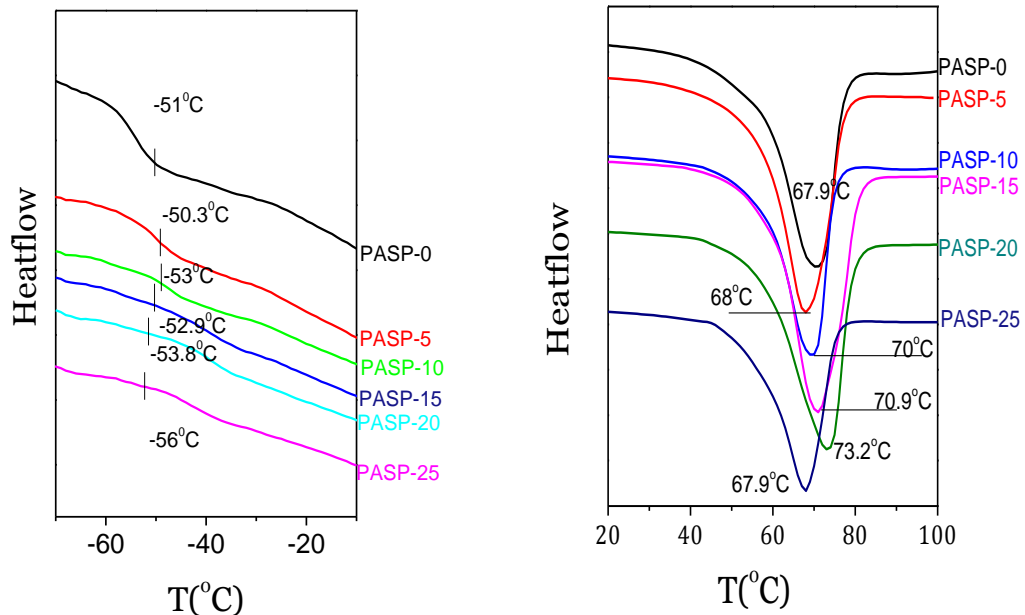


Fig. 4.10 DSC plots of PASP series

mentioned nano composite polymer electrolyte system (PAS). Instead of further decreasing the glass transition temperature, it is observed to increase by about 6°C. On analyzing the glass transition value within the (PASP) system only, a continuous decrease in T_g value is observed as seen from Fig. 4.10, while the T_m values linearly increases up to 20wt% of PEG and there after decreases. This decrease at 25wt% of PEG must be due to dilution effect at higher concentration of PEG.

In next series PLA both the glass transition temperature (T_g) and melting temperature (T_m) decreases as compared to the samples without nano filler Al₂O₃ on addition of

nano-filler Al_2O_3 as shown in Fig 4.11. Both this value obtains minimum value of -61.99°C and 66.98°C respectively for 1wt% of Al_2O_3 . It is reasonable to assume that nano sized Al_2O_3 filler contributes to enhances the flexibility of the polymer chain. But, 1 wt% of Al_2O_3 , with the further incorporation of nano-filler led to an increase in both T_g and T_m values.

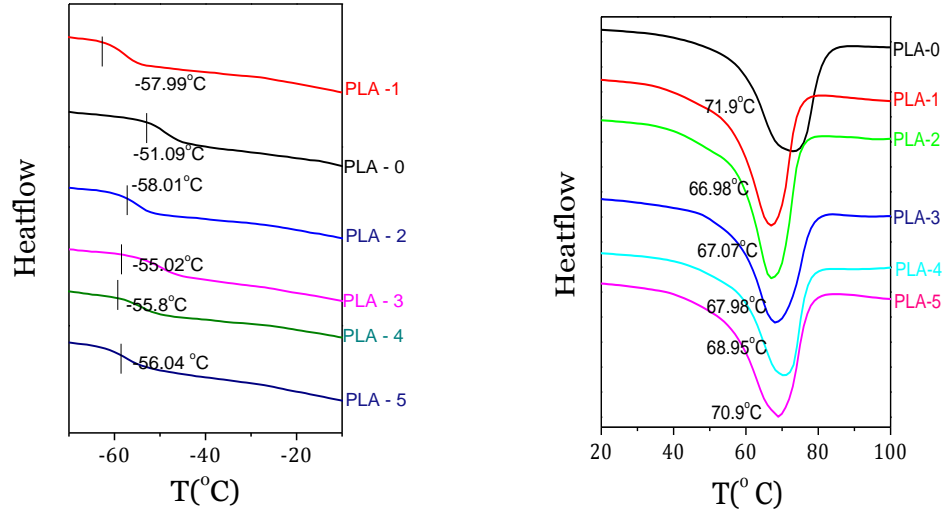


Fig. 4.11 DSC plots of PEO: LiCF_3SO_3 : PEG: Al_2O_3 series

The increase in T_g value reveals an increase in the rigidity of the polymer system and also reduction in amorphous phase which is evident from (XRD) of XRD data. Rahman *et. al.* [38] and others [39] observed that the T_g value is not influenced by the addition of nano-filler to polymer electrolytes. Whereas, in the PLP series to the glass transition temperature T_g and melting temperature T_m decrease (Fig. 4.12) and attain a minimum at PLP-10 and thereafter increase. After PLP-10 further addition of PEG attributed to the dilution effect which increases the cohesive energy of the polymer matrix and hinders the flexibility which results in increasing of T_g values and shifting of T_m values towards higher temperature side.

On analyzing all this five series it could be said that the T_g values of low molecular weight plasticizer PEG are observed to be higher than the systems with nano-filler indicates more flexibility. As the flexibility of polymer system mirrors the glass transition temperature it plays an important role in studying the structural changes of the polymer

electrolytes with heat treatment.

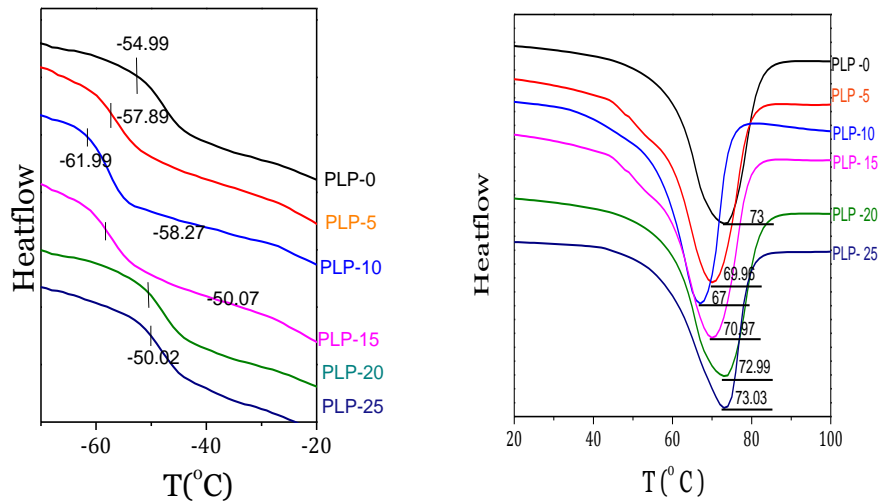


Fig. 4.12 DSC plots of PLP series

4.3 X-Ray Diffraction Studies

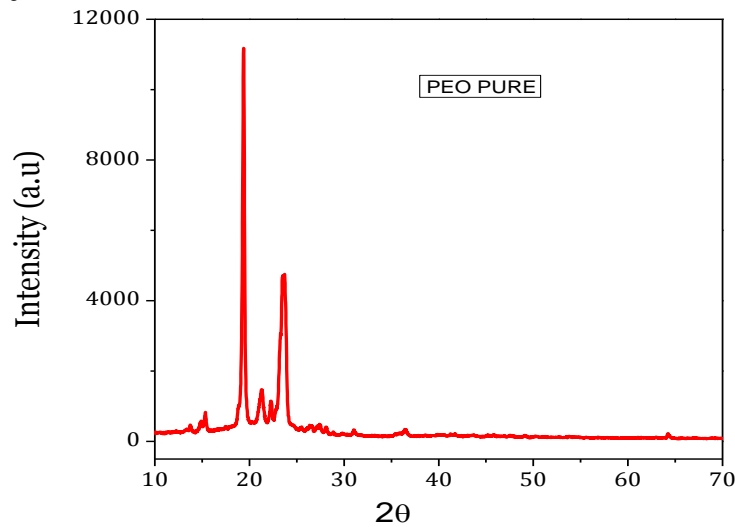


Fig. 4.13 X-ray diffraction patterns of: pure PEO.

The structure of the materials is, generally determined by XRD analysis. X-ray diffraction analysis helps in determining the amorphous / crystalline nature of the prepared samples. The X-ray spectra were measured in the range from 10° to 80° range for all the polymer samples. Fig. 4.13 shows the characteristic X-ray diffraction spectra of the pure PEO [40, 41] which reveals the characteristic peaks at 19° and 23° . Fig. 4.14 shows the X-ray diffraction patterns of PA series. Few differences in diffraction patterns are identified between the complexed and pure PEO films. A decrease in the intensity of

diffractions peaks with increasing salt concentration is observed to decrease up to PA-7 and then increases. Presence of peak corresponding to the pure PEO shows the simultaneous presence of both crystalline complexed and uncomplexed PEO.

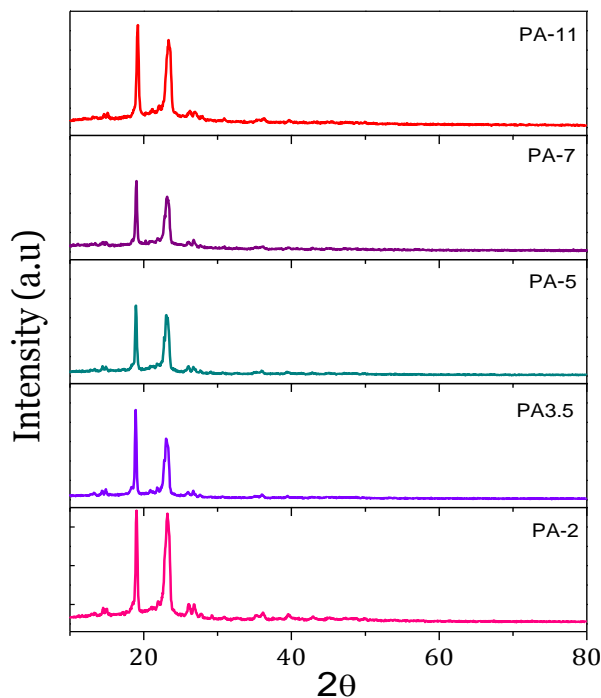


Fig. 4.14 X-ray diffraction patterns of PEO: AgCF_3SO_3 series.

But, no sharp peak is observed for higher concentration of AgCF_3SO_3 indicating the dominant presence of amorphous phase [42]. Hodge *et.al.* [43] Established a correlation between the intensity of the peak and the degree of crystallinity. They observed that the intensity of XRD pattern decrease as the amorphous nature increase with the addition of salt.

Further, in the second step i.e. PAS series the XRD patterns at ambient temperature of all entire polymer samples in which the content of nano-filler SiO_2 is varied is shown in Fig. 4.11. The diffraction patterns are observed to shift towards lower angle side with small broadening with decreased intensity, expect $x= 25$ wt% of SiO_2 . The intensity of $x= 20$ wt% of SiO_2 is found to be lowest. This decrease in the intensity of peaks suggests the increase in the amorphous phase of the samples and indicates that addition of nano-filler SiO_2 has disturbed the crystalline region. Hence, these amorphous nature leads to higher ionic conductivity which is generally observed in amorphous polymer electro-

lytes with flexible backbone.

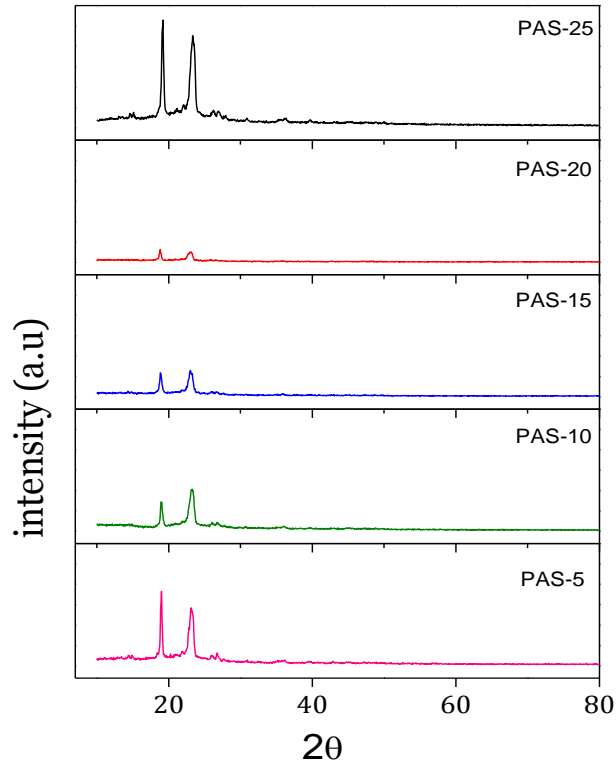


Fig. 4.15 X-ray diffraction patterns of PAS series

In the PASP series (Fig. 4.16) where, PEO, AgCF_3SO_3 , SiO_2 are kept constant and plasticizer PEG is varied. A slight shift from 19.20° to 18.95° for 5wt% and 10wt% sample of PEG is being observed, which indicates that addition of PEG plasticizer have disturb the polymer-salt matrix. The characteristic peak of PEO is observed to decrease with increasing plasticizer PEG content up till 20wt%. This indicates the reduction of crystalline phase, but at 25% PEG peak intensity instead of further decreasing, it increases. The polymer electrolyte system must have under-gone significant structural reorganization when plasticizer PEG is added and an increase in the amorphous phase is observed to be dominant. This suggest that sample with 20wt% PEG is more amorphous compared to other samples; also it is the highest conducting sample. It is also observed that the peak intensity of these series is more compared to the second series indicating that these samples are less amorphous than the PAS series.

In the next system i.e. PLPA series as shown in Fig. 4.16, the peak intensity of filler free sample (0wt% of Al_2O_3) is observed reduce considerably on addition of 1wt%

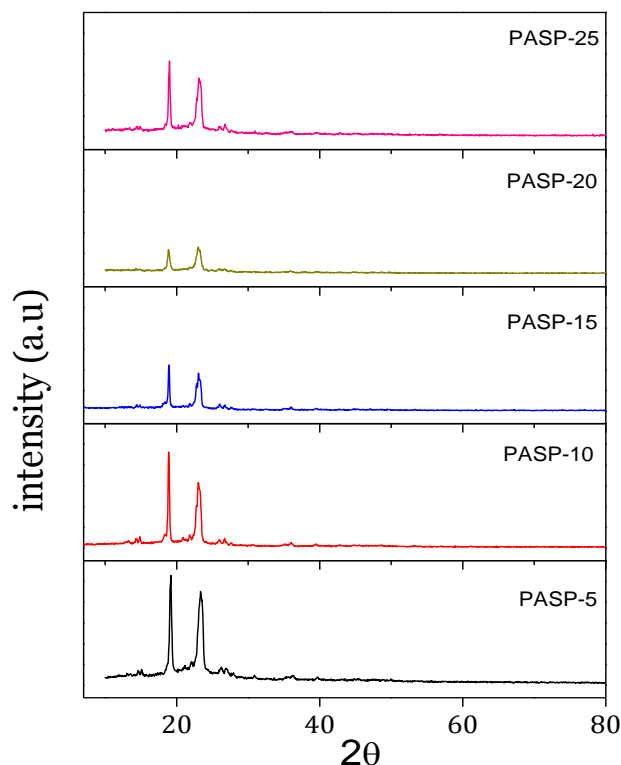


Fig. 4.16 X-ray diffraction patterns of PASP series.

nano-filler Al_2O_3 . But on further increasing the nano-filler Al_2O_3 content (i.e. 2, 3, 4, & 5 wt %) the peak intensity continuously increases. These increases in peak intensity indicate an enhancement in crystalline phase of the polymer systems. At higher concentration of Al_2O_3 , the amorphousness decreases because of desegregation or due to formation of cluster. Suthanthiraraj *et. al.* [45] mentioned that the addition of Al_2O_3 into the polymer-salt complex clearly showed that the intensity of the diffraction peaks of complexed polymer electrolyte system was significantly less than that of the pure PVDF indicating an effective decrease in the crystallinity.

For the PLAP series (PEO: LiCF_3SO_3 : Al_2O_3 : PEG) as shown in Fig. 4.17, the sample show a decrease in the characteristic peaks of PEO peaks after the addition of PEG to system were nano-filler Al_2O_3 is varied. This decrease is observed up to indicates that the polymer complexation has taken place between PEO, LiCF_3SO_3 , Al_2O_3 and PEG and also promotes amorphous region to the polymer structure.

From the above observation, it is clear that these polymer samples are amorphous

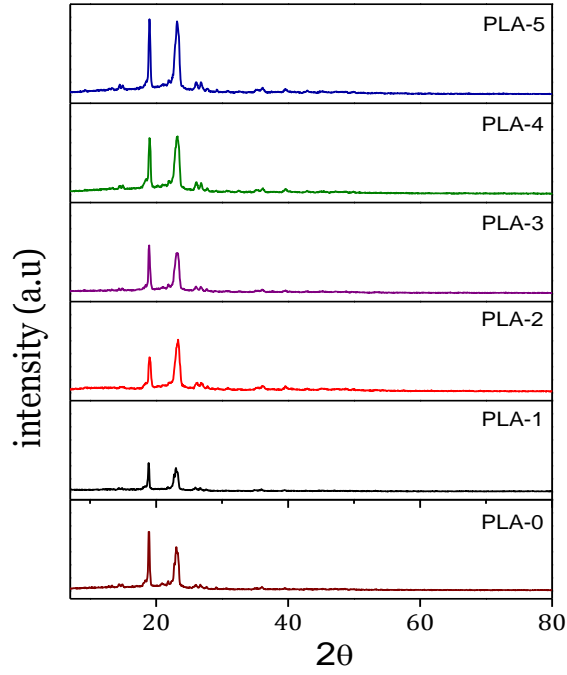


Fig. 4.17 X-ray diffraction patterns of PLA series

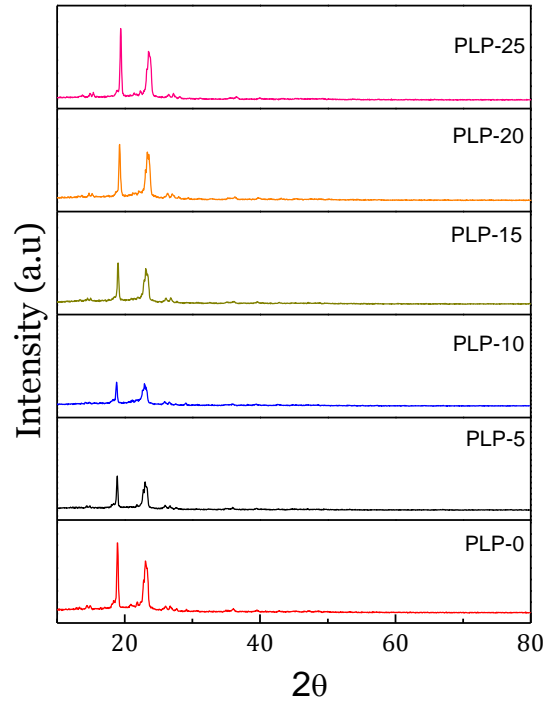


Fig. 4.18 X-ray diffraction patterns of PLP series

in nature as confirmed by their XRD spectrum which reveals the reduction in intensity of

peak compared to that of pure PEO. On comparing the systems with and without plasticizer PEG it is observed that systems with nano-filler are more amorphous compared to that with the plasticizer.

4.4 Scanning electron micrographs (SEM)

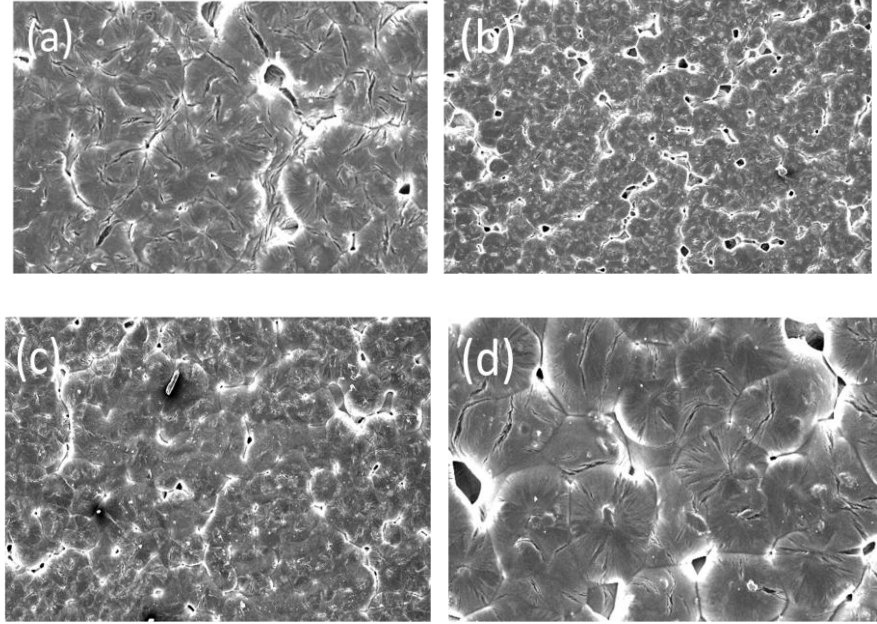


Fig. 4.19 SEM images of (a) PA-2, (b) PA-5, (c) PA-7 and (d) PA-11 samples of PA series

Scanning electron micrographs (SEM) is often used to study the compatibility between various components of the polymer electrolytes through the detection of phase separation and interface [46]. The compatibility between the polymer matrix and the inorganic dopant has great influence on the properties such as, mechanical, thermal ionic conductivity of the polymer electrolytes

Fig. 4.20 shows the SEM micrographs of 2, 5, 7 & 11 wt% of AgCF_3SO_3 for PA series. On addition of AgCF_3SO_3 salt to pure PEO host matrix the amorphous phase increases which can be said from the decrease in the size of spherulites up to 7wt% of AgCF_3SO_3 salt and thereafter at 11wt% of AgCF_3SO_3 it becomes prominent. The SEM micrographs of the system for 10, 15, 20 & 25 wt% of SiO_2 for PAS series is shown in Fig. 4.21. The features of surface smoothening are observed for 10, 15 and 20 wt% of SiO_2 but, for 25wt% of SiO_2 white crystalline patches have developed. All this provides the evidence of change in the microstructure of the samples. Pandey *et.al.* [47] mentioned

that the partial crystalline structure observed in pure PEO, loses its original character on addition of ceramic filler SiO_2 and disturbs the crystalline nature of the system and at higher SiO_2 , dispersion in PEO becomes homogenous followed by the cluster formation.

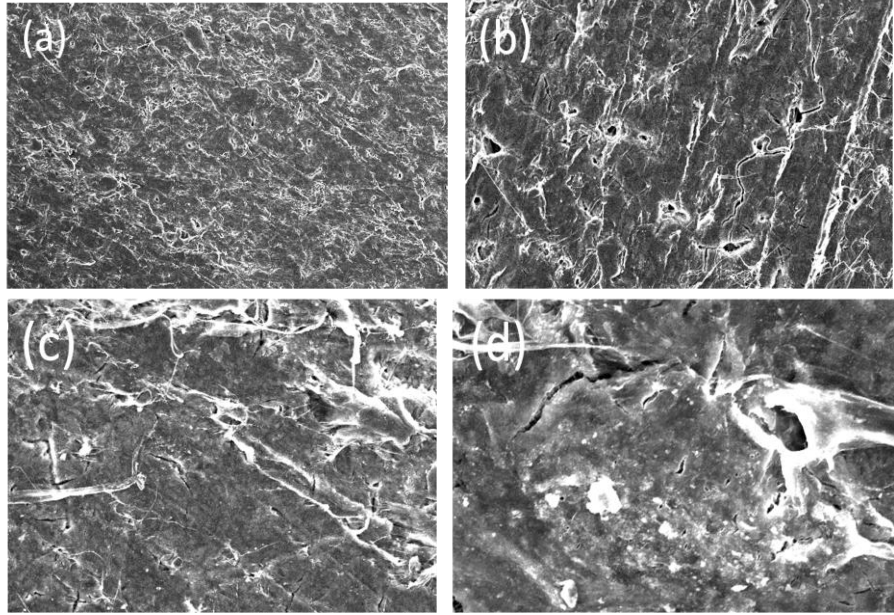


Fig. 4.20 SEM images of (a) PAS- 10, (b) PAS-15, (c) PAS- 20 and (d) PAS 25 samples for PAS series.

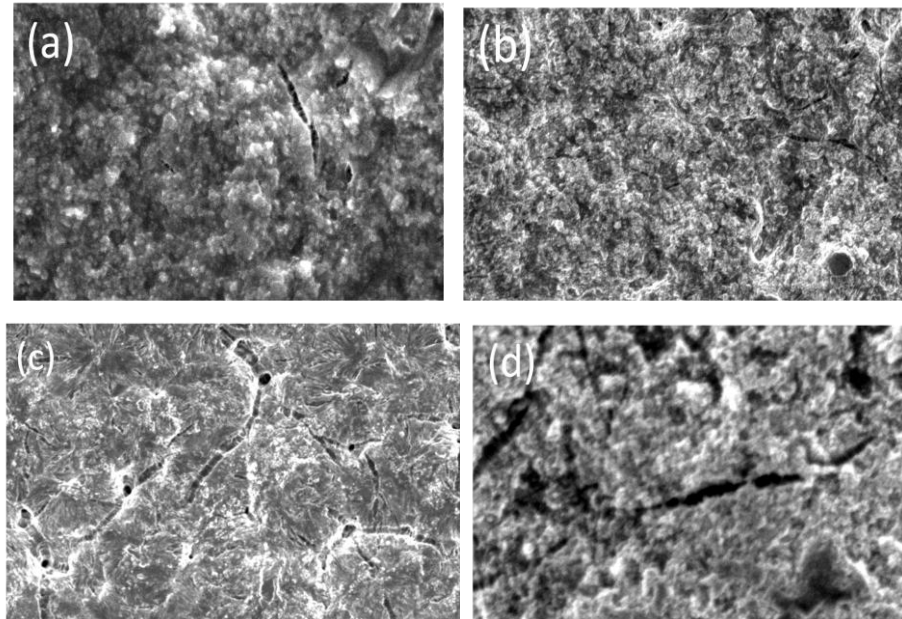


Fig. 4.21 SEM images of (a) PASP-5, (b) PASP-15, (c) PASP-20 and (d) PASP-25 samples of PASP series.

Addition of plasticizer PEG to nanocomposite polymer system changes the Morphology of the prepared samples of the PASP series changes substantially. The overall smoothness of all the samples has been observed in Fig. 4.22 shows considerable de

crease in smoothness compared to that of PAS series. The morphology of the sample with 20wt% of PEG is observed to be more amorphous and smoother.

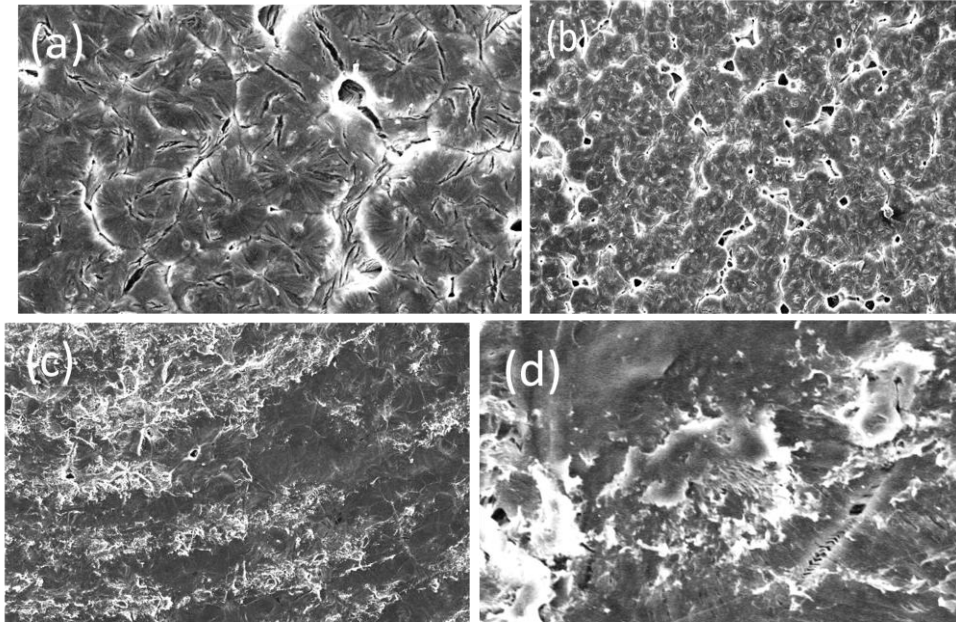


Fig. 4.22 SEM images of (a) PLA-1, (b) PLA-2, (c) PLA-4 and (d) PLA-5 samples of PLA series.

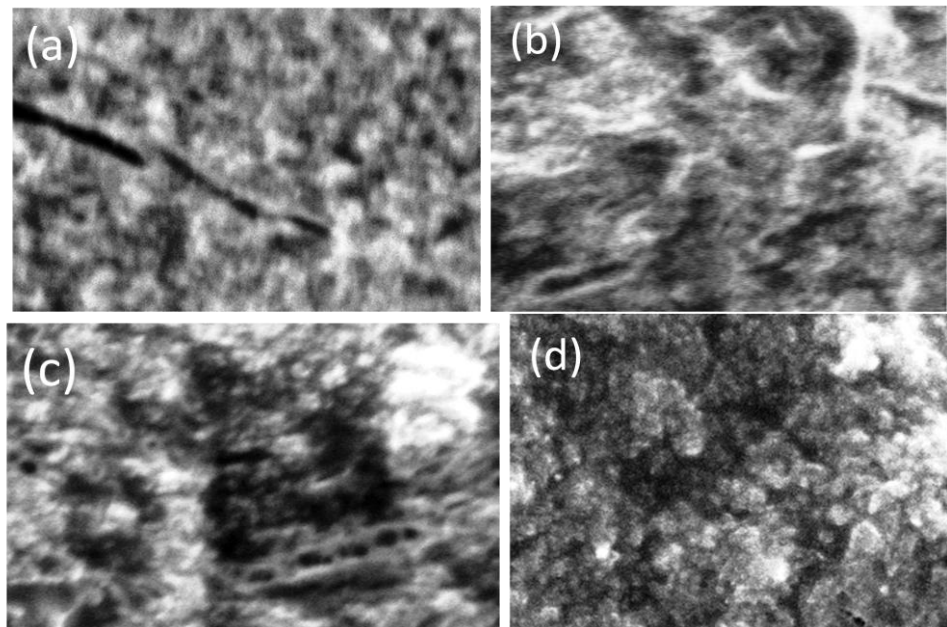


Fig. 4.23 SEM images of (a) PLP-5, (b) PLP-15, (c) PLP-20 and (d) PLP-25 samples of PLP series

Fig. 4.23 shows the SEM images of PLA series. It is observed that PLA-1 sample shows partial formation of spherulites but, on increasing the filler content further it vanishes and white crystalline patches at PLA-5 is observed to develop along with the fea-

ture of surface smoothing. The XRD measurements also suggest the increase in crystallinity hence, are in good agreement with SEM results.

SEM micrographs of PEO: LiCF₃SO₃: Al₂O₃ systems, with variation amounts of PEG are shown in Fig. 4.24. Addition of plasticizer PEG to nanocomposite polymer system shows the roughness in the films. The addition of plasticizer increases the brittleness in the films which is seen as the increased roughness in SEM micrographs and deteriorates the mechanical strength of the film.

On summarizing above systems, it can be concluded that the systems with plasticizer PEG irrespective of the addition of type of salt and nano-filler, the surface of the film become rough on plasticization, while nano-filler enhances the amorphous structure.

4.5 Transport number

The transport measurements are inadequate if performed without the information on the possible type of charge carriers. In solid, the electric charge can be transported by the net macroscopic motion of either electronic or ionic species. It is important that the charge transport in solid polymer electrolyte material be predominantly have ionic motion. Minority electric conduction is generally considered to be deleterious. Method introduced by Wagner [48] which can be especially useful for the evaluation of low levels of electronics conductivity in materials that are primarily ionic conductors.

The transport number of the prepared polymer samples is measured by Wagner's polarization technique. The transference numbers, both ionic (t_{ion}) and electronic (t_{ele}) of various polymer systems complexed with salt, nano filler and plasticizer are evaluated using the Wagner's polarization technique. In this technique, the dc current was monitored as a function of time on application of fixed dc voltage 500 mV across the Ag (+) / electrolyte / Ag (+) cell.

In Wagner's polarization technique, the initial current is the total current (i_T), which is due to the ions (i_{ion}) and the electrons (i_{ele}). As polarization builds up the i_{ion} is blocked and the final current is only the electronic current.

$$i_T = i_{ion} + i_{ele}$$

Therefore,

$$t_{ion} = \frac{\sigma_{ion}}{\sigma_T}$$

and also

$$t_{ion} = \frac{i_{ion}}{i_T}$$

$$= \frac{(i_T - i_{ele})}{i_T}$$

and

$$t_{ele} = \frac{\sigma_{ele}}{\sigma_T}$$

$$= \frac{i_{ele}}{i_T}$$

On observing the Fig. 4.25(a) and (b), it can be said that with the increase in the concentration of salt AgCF_3SO_3 , the ionic transference number increases and attains the maximum value at PA-7 of 0.81. But, at PA-11, the reduction in t_{ion} value results due to ion re-association. Other workers reported the ionic transference number in the range of 0.7-0.9 [49, 50] for PEO-based systems. However, ionic transport number increases and reaches a maximum of 0.9 for PAS-20 polymer electrolyte film where nano-filler SiO_2 is added to the PA system. Y.K Mahipal [51] argued the increase in transport number with the addition of nano-filler SiO_2 to PEO- NaNO_3 polymer electrolyte. The observed variation in ionic transference numbers are in agreement with conductivity behavior of PAS-system (chapter 5).

Generally, addition of plasticizer to the nanocomposite electrolyte results into further improvement of transport property of the polymer electrolyte system due to the characteristic property of plasticizer i.e. dissociating more ions into the system. But, on examining the data presented in the Fig. 4.26 for PASP- series its can be seen that the numerical value of this series is much lower than that of PAS series. This adverse effect is the result of almost similar dielectric value of PEO and PEG due to which the addition of plasticizer PEG may not able to dissociate more salt into the system. Hence, a bit decrease in the ionic transport value is observed as compared to PAS system.

Being smaller in size, lithium ions possess larger mobility as compared to silver ions which make Li-ion conducting salts more appropriate and suitable for battery fabrication. Hence as expected, replacement of silver salt with lithium ion-conducting salt, the ionic transport number show a sudden rise in its transport property.

The ionic transference number of highest conducting samples of both PLA and PLP systems reaches unity as shown in Fig. 4.26 (a) and (b). Therefore, it can be said io-

nic conductivity results in high ~ unity transference number [52].

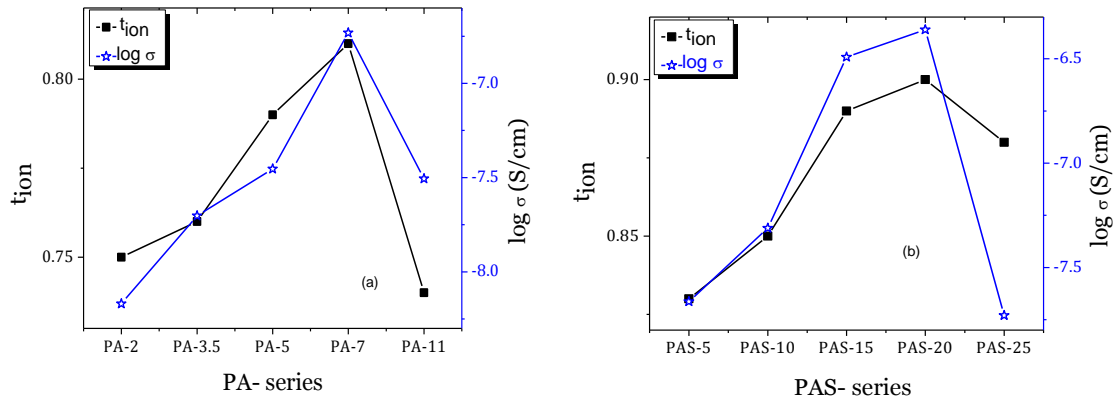


Fig. 4.24 Variation of ionic transport number in (a) PA-series and (b) PAS-series

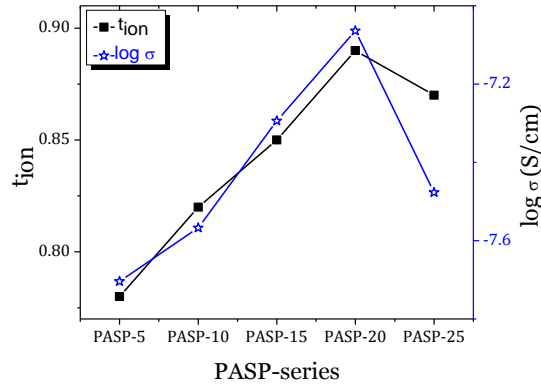


Fig. 4.25 Variation of ionic transport number in PASP-series.

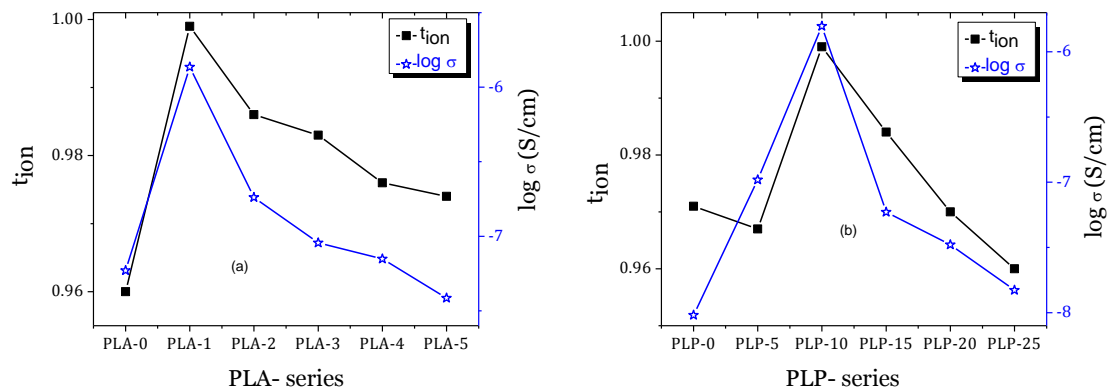


Fig. 4.26 Variation of ionic transport number in (a) PLA-series and (b) PLP-series

Generally, for battery application the value of ionic transference number of polymeric material should practically be greater than 0.9. Hence, it can be concluded from above results that Li-ion conducting polymeric electrolytes with can serve as better electrolyte material.

References:

- [1] C. M. Burba, R. Frech, B. Grady, *Electrochim Acta*, 53 (2007)1548.
- [2] R. Kumar, S. S. Sekhon, *Ionics*, 14(2008) 509.
- [3] C. G. Tan, W. O. Siew, W. L. Pang, Z. Osman, K. W. Chew, *Ionics*, 13 (2007) 361.
- [4] S. Rajendran, M. Sivakumar, R. Subadevi, *Solid State Ionics*, 167(2004) 335.
- [5] R. H. Y. Subban, A. H. Ahmad, N. Kamarulzaman, A.M.M. Ali, *Ionics*, 11(2005) 442.
- [6] S. Rajendran, R. Kannan, O. Mahendran O, *Ionics*, 7(2001)126 .
- [7] A. G. Bishop, D. R. MacFarlane, D. McNaughton, M. Forsyth, *Solid State Ionics*, 85(1996)129.
- [8] J. H. Kim, B. R. Min, C. K. Kim, J. Won, Y. S. Kang, *J. Phys. Chem. B*, 106(2002)2786.
- [9] A. Ferry, P. Jacobsson, L. M. Torell, *Electrochim Acta*, 40 (1995) 2369.
- [10] A. M. Rocco, C. P. Fonseca, R. B. Pereira, *Polymer*, 43 (2002)_3601- 3609.
- [11] D. Snaveley, J. Dubskey, *J. Poly. Sci. A*, 34 (1996) 2575-2579.
- [12] M.A.A. Mendez, E.S.M. Martinez, L.O. Arroyo, G.C. Portillo, E.S. Espindola, *J. Nanopart. Res.* 13 (2011) 2525 – 2532.
- [13] T. Kumar, *Analyst* 15 (1990) 1597.
- [14] Z. Tang, J. Wang, Q. Chen, W. He, C. Shen, X. X. Mao, J. Q. Zhang, *Electrochimica Acta*, 52 (24) (2007) 6638-6643.
- [15] Z. Osman, A.K. Arof, *Electrochimica Acta*, 48 (2003) 993.
- [16] P.Sharma, D.K.Kanchan, N. Gondaliya, *Ionics* 19(2013)777–785.
- [17] M. Sunder, S. Selladurai, *Ionics*, 12 (2006) 281-286.
- [18] S. A. Suthanthiraraj, R. J Kumar, B. Paul, *Ionics*, 16(2009) 145- 151.
- [19] W. Huang, R. Frech, *Polymer* 35(1994) 235-242.
- [20] D. R. MacFarlane, P. Meakin, A. Bishop, D. McNaughton, J. M. Rosalie, M. Forsyth, *Electrochim. Acta* 40(1992) 2333-2337.
- [21] D. Saikia, A. Kumar, *European Polymer Journal*, 41 (2005), 563-568.
- [22] J. Jiang, D. Gao, Z. Li, G. Su, *Reactive and Functional Polymers*, 66 (2006) 1141-1148.
- [23] S. Ahmad, S. A. Agnihotry, *J. Power Sources*, 140 (2005) 151-156.
- [24] R. Frech, G. A. Giffin, F. Y. Castillo, D. T. Glatzhofer, J Eisenblatter, *Electrochim Acta*, 50(2005) 3963.
- [25] C. P. Rhodes, R. Frech, *Solid State Ionics*, 136–137 (2000) 1131.
- [26] M. Deepa, N. Sharma, S. A. Agnihotry, R. Chandra, *J. Mater Sci*, 37(2002) 1759.
- [27] Z. Wang, X. Huang, L. Chen, *Electrochem. Solid State Lett*, 6 (2003)-E40,.
- [28] S. A. Suthanthiraraj, B. Joseph Paul, *Ionics* , 13 (2007) 365-368.
- [29] Kunal Kumar, G. Christopher, Robertson, Sebastian Pawlus, F. H. Steven, Alexei P. Sokolov, *Macromolecules*, 41(2008) 7232-7238.
- [30] B. L. Fana, B. Ce-Wen Nana, S. Zhao *Solid State Ionics*, 164 (2003) 81- 86.
- [31] F. Croce, G. B. Appetecchi, L. Persi, B. Scrosati, *Nature*, 394 (1998) 456.

- [32] B. Scrosati, F. Croce, L. Persi, *J. Electrochem. Soc.*, 5 (2000) 1718.
- [33] W. Wiczczyk, J. R. Stevens, Z. Florjanczyk, *Solid State Ionics*, 85 (1996) 76.
- [34] L. R. A. K. Bandara, M. A. K. L. Dissanayake, B. E. Mellander, *Electrochim. Acta*, 43 (1998) 1447.
- [35] I. E. Kelly, J. R. Owen, B. C. H. Steele, *Electronal. Chem.*, 168 (1984) 467.
- [36] M. Gorecki, R. Andreani, C. Berthier, M. B. Amand, M. Mail, J. Roos, D. Brikmann, *Solid State Ionics.*, 18 (1986) 295.
- [37] D. R. Macfarlane, J. Sun, P. Meakin, P. Fasouloupoulos, J. Hey, M. Forsyth, *Electrochim. Acta*, 40 (1995) 2131.
- [38] M.Y. A Rahman, A. Ahamnd, S. A. Wahab, *Ionics*, 15 (2009) 221-225.
- [39] T. J. Singh, S.V. Bhat, *J Power Sources*, 129 (2004)280.
- [40] T. Janaki Rami Reddy, V. B. S. Achari, A. K. Sharma, V. V. R. Narasihma Rao, *Ionics* 13(2007)55.
- [41] T. Sreekanth, M. Jaipal Reddy, S. Ramalingaiah, U.V. Subba Rao, *J. Power Sources*, 79 (1999) 105.
- [42] V. M. Mohan, V. Raja, A. K. Sharma, V.V.R Narasimha Rao, *Ionics* , 12 (2006) 219-226.
- [43] R.M. Hodge, G.H. Edward, G. P. Simon, *J. Polymer*, 37 (1996) 1371.
- [44] P. Sharma, D. Kanchan, N. Gondaliya, *Open Journal of Organic Polymer Materials*, 2(2012) 38-44.
- [45] S. Austin Suthanthiraraj, B. Joseph Paul, *Ionics*, 13(2007) 365–368.
- [46] S. Zhang, J. Y. Lee, L. Hong, *J. Power Sources*, 126(2004)125.
- [47] K. Pandey, M. M. Dwivedi , M. Tripathi, M. Singh , S. L. Agrawal, *Ionics*, 14 (2008), 515- 523.
- [48] W. Wagner and J. B. Wagner, *J. Chemical Phys.*, 26 (6) (1957) 1597.
- [49] S. Chandra, S. A. Hashmi, M. Saleem, R.C. Agrawal, *Solid State Ionics*, 67 (1993) 1-7.
- [50] V. Kambila, G. Sunita Sundari, M. Chandra Sekhar, A. Srinivasa Rao, *International Journal of Chemical and Biochemical Sciences*, 1(2012) 59-64.
- [51] Y. K. Mahipal, *Ph. D. Thesis*, Pt. R. SS University, Raipur, India 2011.
- [52] M. Doyle, T. F. Fuller, J. Newman, *Electrochim. Acta*, 39 (1994) 2073.

CHAPTER 5

CONDUCTIVITY STUDIES

This chapter deals with the conductivity results of prepared solid polymer samples. The details of temperature and composition dependence of conductivity along with its conduction mechanism are discussed in later part of this chapter.

5.1 Introduction

A conductivity study is one of the important studies that is carried out on solid materials in order to characterize the bulk resistance; grain boundary resistance, polarization etc. of the prepared samples. Conductivity measurement can be carried out using various techniques. The technique used in the present study is the complex impedance spectroscopy which provides the information on electrical properties of materials and their interface with electronically conducting electrodes. It may be used to investigate the dynamics of bound or mobile charge in the bulk or interfacial regions of any kind of solid or liquid material such as ionic, semiconducting, and mixed electronic-ionic as well as insulators (dielectrics) too. Complex impedance spectroscopy is used to measure dc as well as ac conductivity, these measurements are based on the studies made on the measurement of cell impedance/admittance over a range of temperatures and frequencies and analyzing them in complex impedance plane [1, 2]. This is particularly characterized by the measurement and analysis of Z^* (impedance) or Y^* (admittance) and plotting of these functions in the complex plane, known as Nyquist diagrams.

Sluyter et. al. in 1960 [3] used complex impedance spectroscopy technique to study the polarization phenomenon of aqueous electrochemical cells. Since then, it has been considered to be one of the most powerful tool to analyze electrochemical processes in the field of aqueous electrochemistry [4-7]. Bauerle [1] was the first to use this technique to study the basic polarization process in the cell of yttria stabilized zirconia (YSZ). Thereafter, complex impedance spectroscopy had been in use for characterizing a wide range of electrolyte and electrode materials, which include polymers, oxides, glasses, polycrystalline and composites.

5.2 Complex Impedance Analysis

Complex impedance spectroscopy is the most elegant and powerful technique for electrical characterization of solids, in general and electrochemical devices including electrodes as well as electrolytes in particular. This technique is often used to obtain bulk conductivity of the material. Complex impedance spectroscopy had attracted attention due to its one of the important feature of dispersion of semicircle. Jonscher *et.al.* [8] have

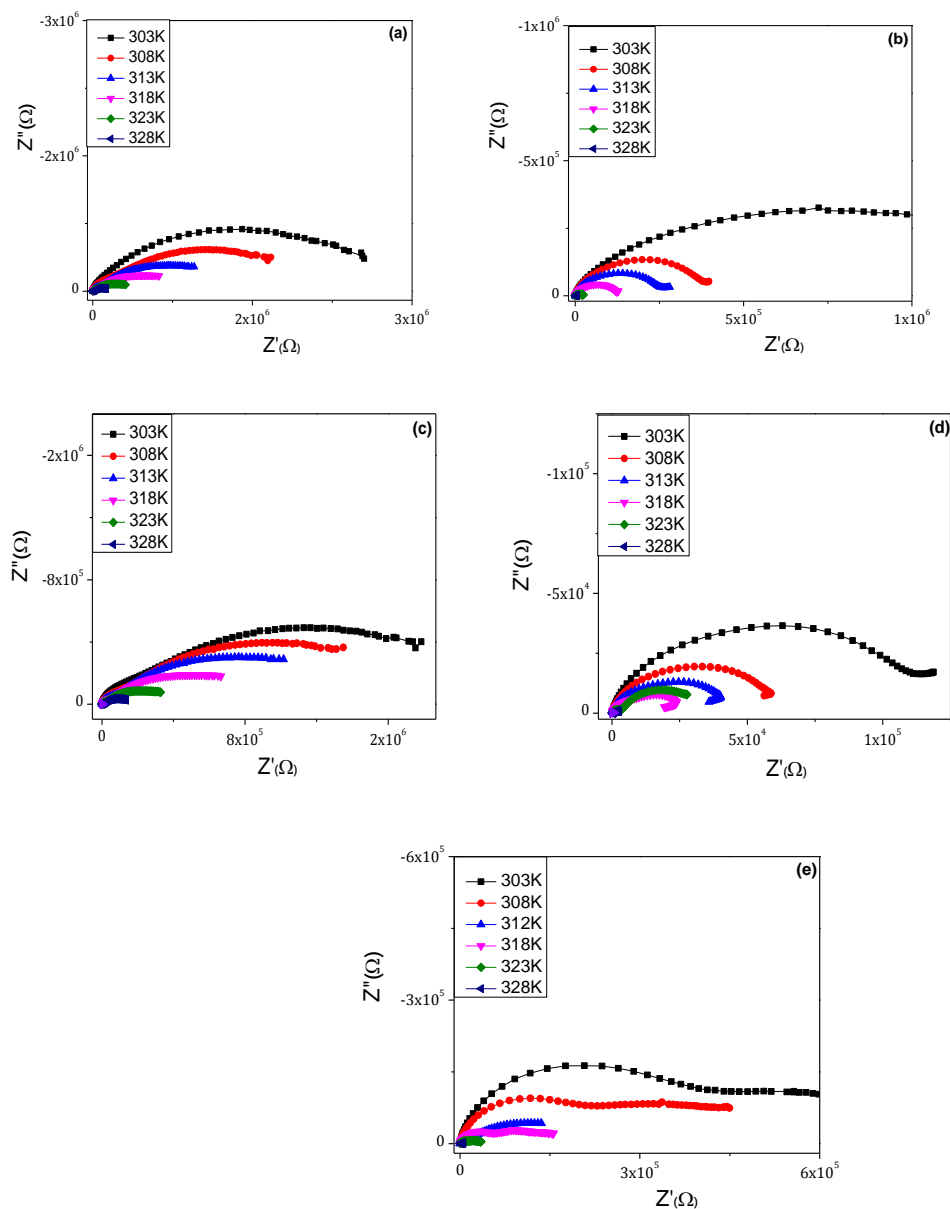


Fig. 5.1 Impedance plots of PA series (a) PA -2, (b) PA -3.5, (c) PA -5, (d) PA -7 and (e) PAS -11 at different temperatures.

considered the semicircle depression as an essential property of dielectric and ionic conductors where they have viewed this phenomenon as an inherent property of elementary jump of an ion due to local energy stored [9].

To determine the electrical conductivity and the ac behavior of the prepared polymer electrolyte system complex impedance measurements were carried out over a range of temperature and frequencies.

At first stage to see the effect of variation of silver salt concentration in PEO polymer, the impedance spectra of PEO-AgCF₃SO₃ (PA-series) system at different temperature are

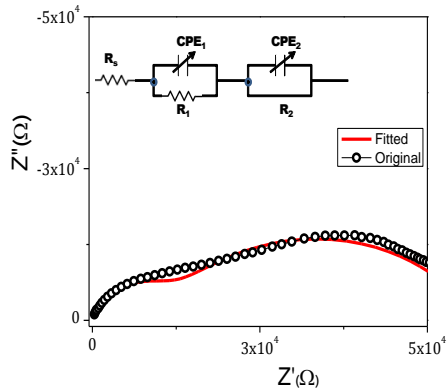


Fig.5.2 Equivalent-circuit fitting for PA-11 at 313K

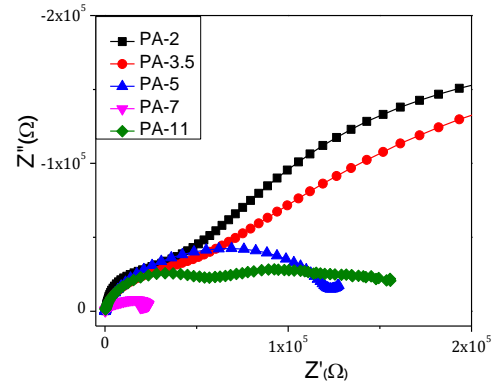


Fig.5.3 Impedance plot of PA series at 313K.

recorded. Figs. 5.1 (a)-(e) show impedance plot of PEO: AgCF₃SO₃ samples at different temperatures for PA-series. The complex impedance plots show depressed semicircle at the high frequency arises from the bulk relaxation [10, 11]. The intercept of axis shifts towards origin i.e. the bulk resistance of the sample decreases with increase of temperature in all the samples. The size of the depressed semicircle decreases with the increase of temperature as expected in solid electrolytes and the real axis intercept of the plot shifts towards the origin. The high frequency semicircle in the impedance plot is a characteristic of the parallel combination of a capacitor and a resistor, respectively which are the bulk capacitance and the bulk resistance of the material [12]. The equivalent-circuit fitted curve is obtained from Z-view2 program. The intercept of the fitted semicircle the real axis (Z' axis) is used to obtain the bulk resistance (R_b) of the electrolyte.

Fig. 5.2 shows the fitted curve for PA-11 polymer film and its inset shows its equivalent-fitted circuit. The fitted plots represent a series combination of two parallel lumped RC circuits. The first semi circle arises due to the bulk resistance of the sample while the other semicircle ($R_2 C_2$ couple) arises due to polarization of mobile Ag⁺ ions at the electrode-electrolyte interface [12]. An equivalent circuit is generally used to analyze impedance spectroscopy because it is simpler and can provide the complete picture of the prepared polymer electrolyte systems.

The impedance plot for PA-11, shown in Fig. 5.1 (e), can be divided into two well defined regions: a slanted spike at low frequency and a semicircle portion which reveals the characteristic of a parallel combination of bulk resistance and bulk capacitance of the polymer matrix at high frequency [13]. However, the spike is slanted at an angle less than

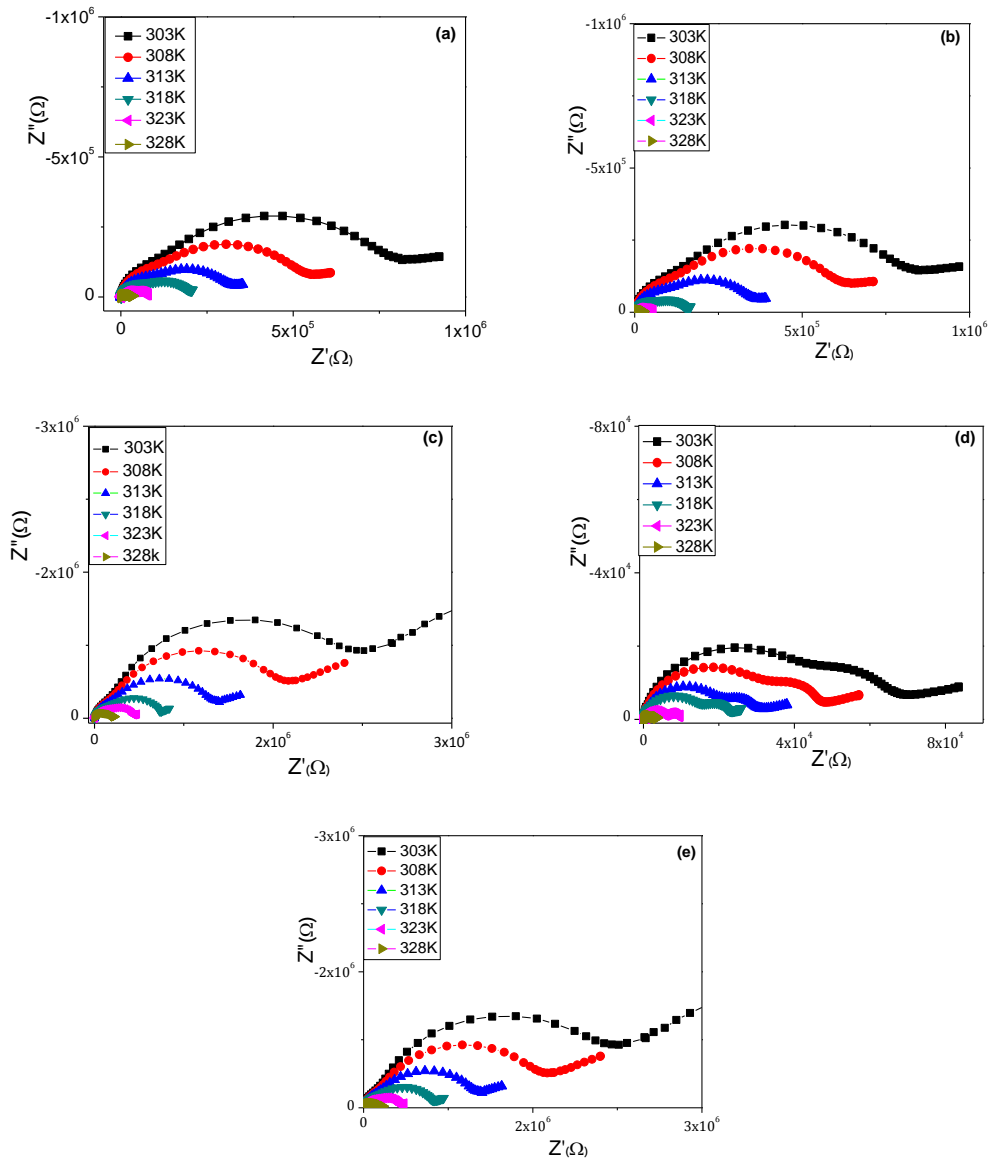


Fig. 5.4 Impedance plot of PAS series (a) PAS -5, (b) PAS -10, (c) PAS -15, (d) PAS -20 and (e) PAS -25 at different temperatures.

90° . This phenomenon indicates the non-Debye nature. In addition, the angle and the amount of inclination is attributed to the distribution of conductivity relaxation time which defined as the time required to build up charges at the electrode and electrolyte interface before the electric field changes the direction[14].

Impedance plot for all samples of PA series at 313K is shown in Fig.5.3. It is clear from the figure that the resistance of the samples decreases with the increasing salt content up to 7wt% (PA-7) and thereafter its value increases at 11wt% of AgCF_3SO_3 . The decrease in the resistance value indicates that ion dissociation has taken place but after 7wt% of AgCF_3SO_3 salt, more ions are produced that might cause the blocking of con-

ducting pathways and increases the resistance values.

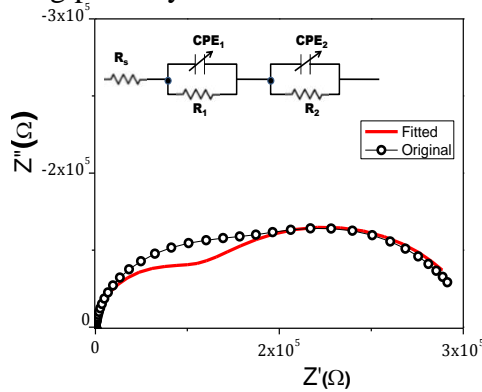


Fig.5.5 Equivalent-circuit fitting for PAS-15 at 313K.

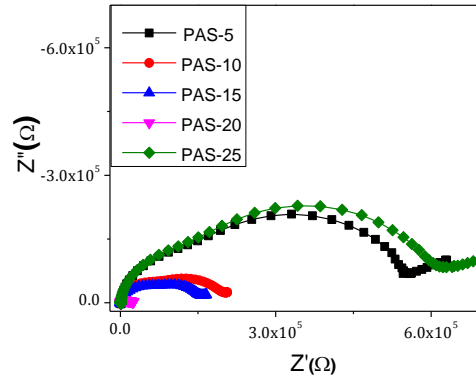


Fig. 5.6 Impedance plot of PAS series at 313K.

To further enhance the properties of polymer salt system, dispersion of nano-filler in polymer film with lowest resistance value is done. For this, the nano-filler concentration ranging from 5 to 25 wt% in steps of 5 is added in PA-7 polymer sample to obtain PAS-series. The impedance spectra of different samples of PAS series at different temperatures are presented in Figs. 5.4 (a) to (e) and Fig. 5.5 depicts the equivalent-circuit fitted graph for PAS-15 sample. In PAS system, bulk resistance values decrease with increase in temperature. At the same time, the frequency of the maximum of the semicircle for the interface shifts towards a higher frequency as the temperature increases.

Fig.5.6 shows impedance plot of PAS series PEO: AgCF₃SO₃: SiO₂ at 313K. As seen from the Figure the resistance of the samples decreases continuously with increasing nano-filler SiO₂ content expect for PAS-25 polymer film where the resistance increases. Addition of nano-filler in polymer salt complex must have increases the matrix amorphousity and providing new conducting pathways resulting into decrease in resistance up to 20 wt% of SiO₂.

Next to PAS system, plasticization of highest conducting nano-composite (PAS-20 sample) as PASP series (PEO-AgCF₃SO₃-SiO₂-PEG) where, plasticizer (PEG) is varied in the 5, 10, 15, 20 & 25 wt% has been made. The complex impedance measurements of the samples of PASP series over a range of temperature and frequency are carried out. A reduction in bulk resistance values with the increase in temperature is the main feature in this system too. Figs. 5.7 (a) to (e) show the impedance plot of all the samples of PASP series at 303K. Fig. 5.8 depicts equivalent –circuit (inset of figure) fitted impedance curve for PASP-20 polymer film. The impedance curves show depressed

semicircular arc. The lowest bulk resistance value in PASP-20 polymer electrolyte is observed. Beyond that concentration the observed increase in bulk resistance is due to dilution effect of plasticizer [15].

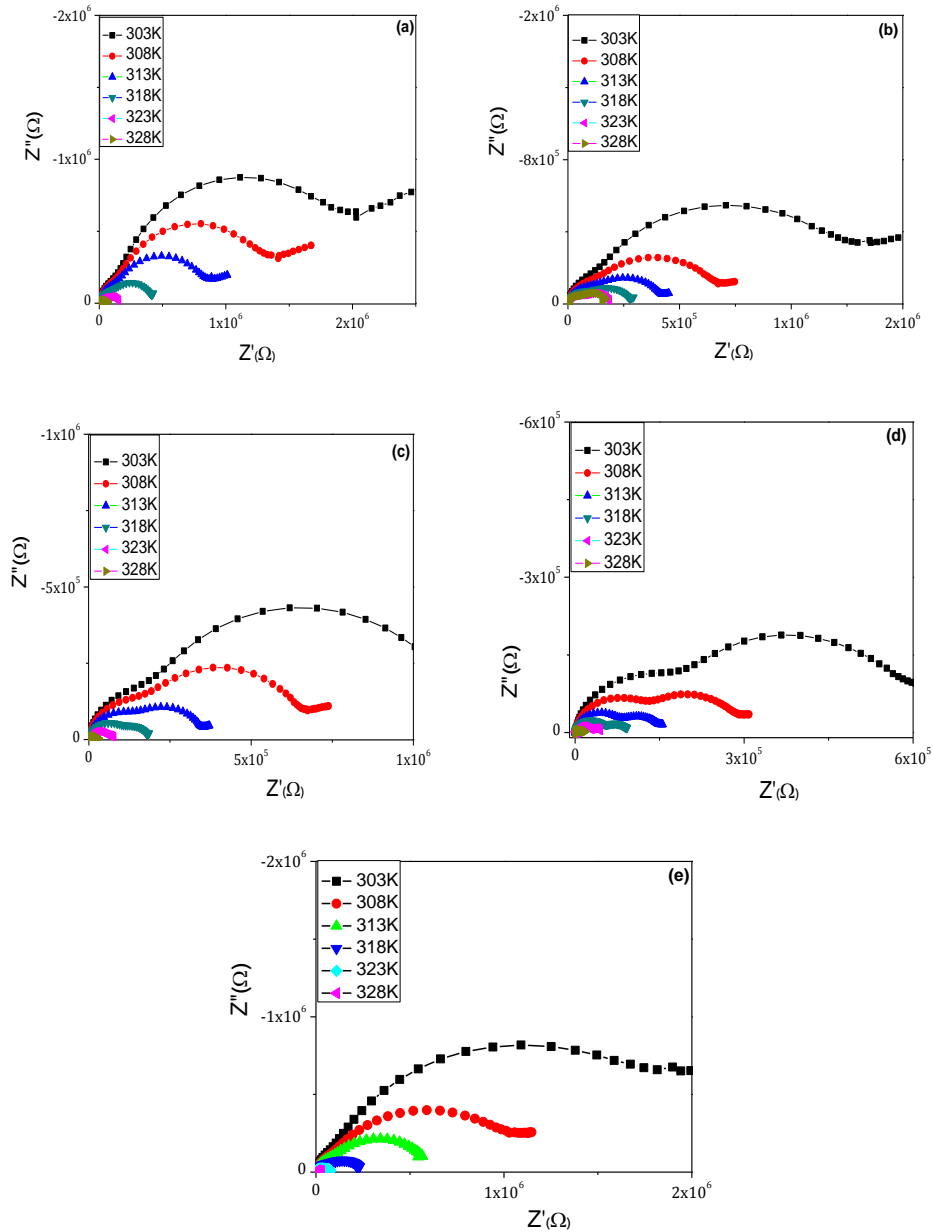


Fig. 5.7 Impedance plots of PASP series (a) PASP -5, (b) PASP -10, (c) PASP -15, (d) PASP -20 and (e) PASP -25 at different temperatures.

After studying the silver ion conducting polymer electrolytes, the effect of Al_2O_3 nano-filler (different than SiO_2) in lithium ion conducting plasticized PEO-based system is also studied. For this, PLA series i.e., PEO- LiCF_3SO_3 -PEG- Al_2O_3 system, in which

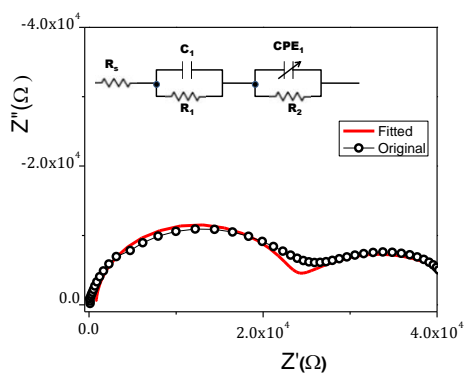


Fig. 5.8 Equivalent-circuit fitting for PASP-20 at 313K.

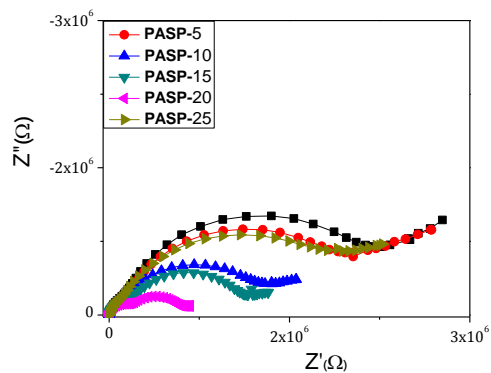


Fig. 5.9 Impedance plot of PASP series at 318K.

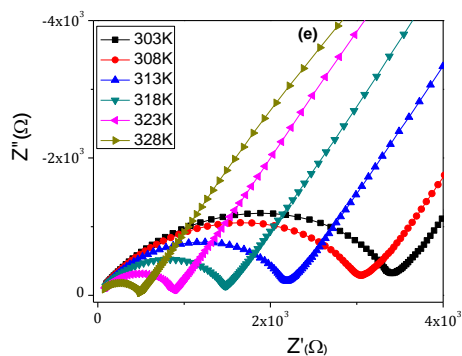
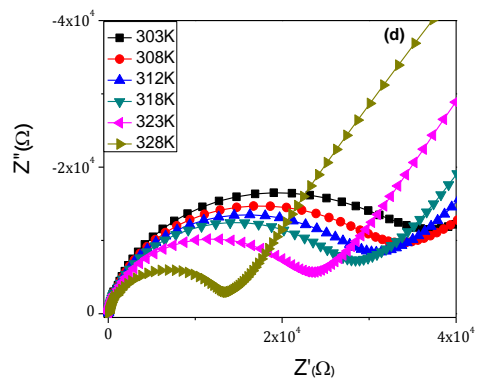
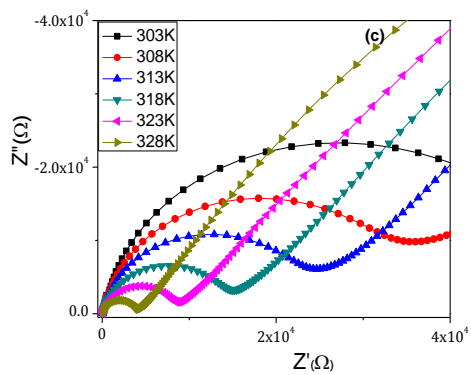
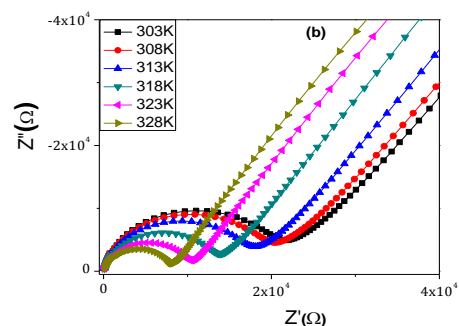
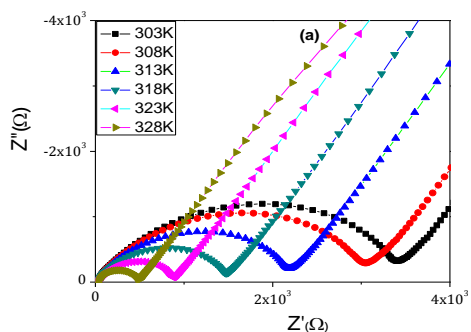


Fig. 5.10 Impedance plots of PLA series (a) PLA-1, (b) PLA-2, (c) PLA-3, (d) PLA-4 and (e) PLA-5 at different temperatures.

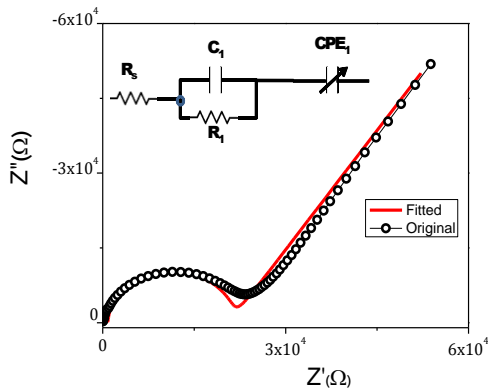


Fig. 5.11 Equivalent-circuit fitting for PLA-4 at 313K.

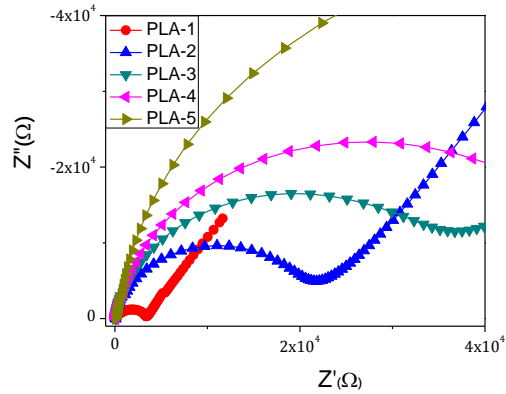


Fig. 5.12 Impedance plot of PLA series at 313K.

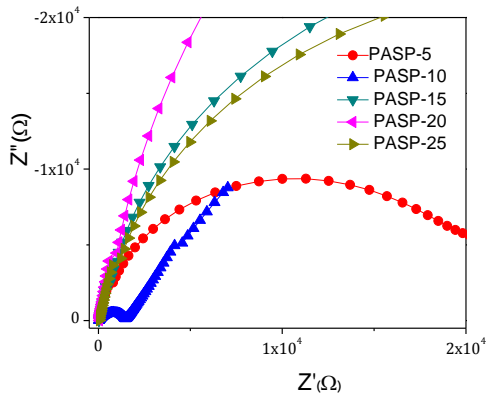
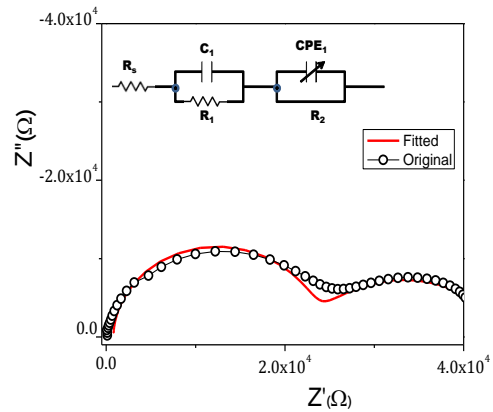


Fig. 5.13 Impedance plots of PLP series at 313 K. **Fig. 5.14** Equivalent-circuit fitting for PLP-15 at 313K.



the metal salt (AgCF_3SO_3) and nano-filler (SiO_2) have been replaced with lithium salt (LiCF_3SO_3) and nano-filler (Al_2O_3), respectively in this series the content of nano-filler has been varied. Complex impedance plots of PLA-1, PLA- 2, PLA-3, PLA-4 and PLA-5 polymer nano-composites at different temperatures are shown in Figs. 5.10 (a)-(e). The figures show a semi-circle in the high frequency range, which is related to conduction process in the bulk of the complex. This plot shows a depressed semicircular arc followed by an inclined spur at low frequencies. With the increase in temperature, the bulk resistance of the sample decrease and the conductivity thus shows a gradual enhancement. Fig. 5.11 depict equivalent- circuit (inset of Fig.) fitted impedance curve PLA-4 polymer film. Fig. 5.12 shows impedance spectra of all the samples of PLA series. All impedance plots reveals only one arc and a spike in the investigated temperature range. The presence of inclined spur is a signature of divergence from the ideal behavior [16]. As seen

from Fig. 5.12, after 1wt% of Al_2O_3 the resistance of the samples increases with the increasing Al_2O_3 content.

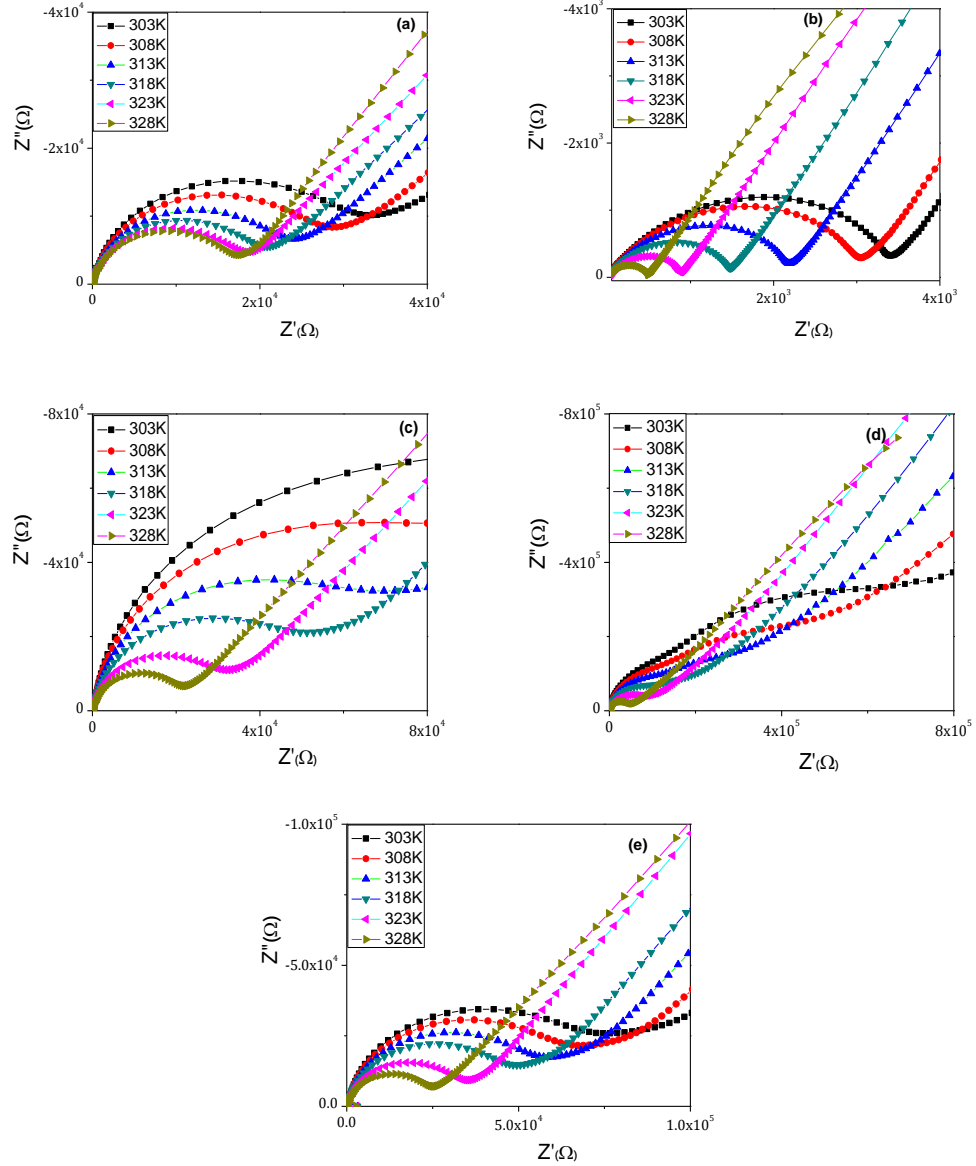


Fig.5.15 Impedance plots of PLP series (a) PLP-5, (b) PLP-10, (c) PLP-15, (d) PLP-20 and (e) PLP-25 at different temperatures. After achieving maximum conductivity in PLA series at 1wt% of nano-filler (discussed in next section), the complex impedance spectrum pattern of the plasticized nano composite polymer electrolyte system i.e., PLP series: PEO- LiCF_3SO_3 - Al_2O_3 -PEG for different PEG concentrations at 313K are plotted and shown in Fig. 5.13. Figure shows a decrease in the value resistance with increase in PEG content in this series i.e., PLP-10 sample shows lowest bulk resistance and further increase in PEG concentration leads a rise in

bulk resistance value. This decrease can be explained on the basis that plasticizer must have interrupted polymer-polymer interaction by occupying inter and intra chain, which results in a decrease in the polymer-polymer interaction and thereby decrease in the bulk resistance. Fig. 5.14 depicts the equivalent circuit fitting for PLP-15 polymer film at 313K. Complex impedance spectrum pattern of the all samples of PLP series are plotted and are shown in Figs.5.15 {(a) to (e)} at different temperatures. The impedance spectrum comprises of high-frequency semicircular arc followed by a steeply rising spike in the low frequency region. Similar to other workers [17, 18] as well as in other investigated systems here, in this series too, the bulk resistance decreases with increase in temperature.

5.3 DC Conductivity

The conductivity is the most important investigated parameter of electrolyte systems. It depends on the level of doping on concentration of the cations. The ion transport in these polymer electrolytes is based on the hopping mechanism between coordinating sites, local structural relaxation and segmental motions of the polymer chains [18, 19]. The resistance determined from the real axis intercept of the z' on the x axis is used to evaluate the conductivity from the following equation;

$$\sigma = \left(\frac{t}{A}\right) * \left(\frac{1}{R}\right) \dots\dots\dots(5.1)$$

where t is the sample thickness and A is the area of the sample and R is the resistance.

Logarithmic conductivity as a function of inverse temperature at different content of salt (AgCF_3SO_3) i.e., PA-system is plotted in Fig. 5.16(a). Interestingly, even though there is a slight curvature in some of the plots, all the polymer electrolytes showed an enhancement of the ionic conductivity when the temperature is increased. The log of conductivity vs. temperature relationship indicates that the conduction mechanism in samples is thermally assisted. Above the glass transition temperature, the amorphous region progressively increases with increase in temperature and the polymer chain acquires faster internal modes in which bond rotations produce segmental mobility. This, in turn favors the hopping of inter and/or intra chain ion movements and the conductivity of the polymer electrolytes increases. The rise in conductivity with the temperature suggests the free volume due to easy expansion of polymer [20, 21]. This increase in ionic conductivity in the present PEO- AgCF_3SO_3 based

electrolyte is temperature assisted process [22, 23].

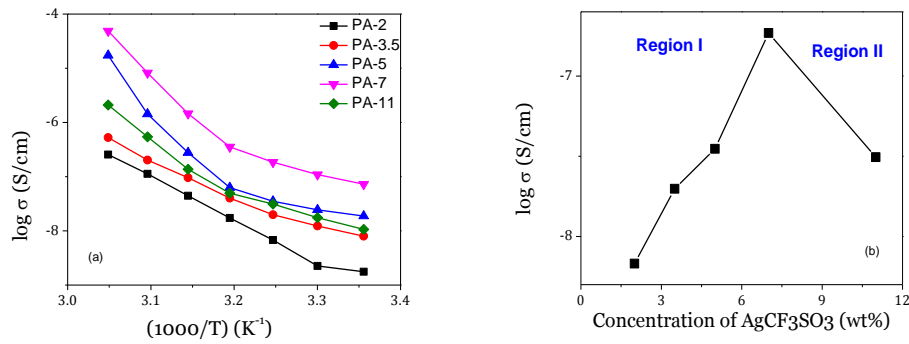


Fig.5.146 Variation of dc conductivity as a function of (a) temperature for PA system and (b) AgCF_3SO_3 salt at 313K.

The log conductivity versus different content of AgCF_3SO_3 at 313 K temperature for PA-series is plotted and shown in Fig.5.16 (b) which depicts a significant increase in ionic conductivity with addition of AgCF_3SO_3 salt. The highest conducting sample is PEO-7wt% AgCF_3SO_3 and its conductivity at room temperature is $7.2 \times 10^{-7} \text{ S}\cdot\text{cm}^{-1}$. A three order increase in magnitude of conductivity compared to pure PEO (of the order of $10^{-10} \text{ Scm}^{-1}$ at ambient temperature [24]) is observed. In addition to this, the conductivity value of the sample increases with the salt concentration and reaches an optimum value at 7 wt % of AgCF_3SO_3 in the present case and then decreases. This variation could be explained in terms of the number of free charge carriers or mobile ions. Therefore, in the region-I, the increasing trend of conductivity is due to larger number of ions of AgCF_3SO_3 salt whereas in region II, it may be due to ion re-association process [18, 19]. In FTIR spectra for sample 11wt% AgCF_3SO_3 (Fig.4.3), attributed the presence of peak at 1240 cm^{-1} to ion pairs which also supports the decrease in conductivity due to ion re-association process at higher concentration of salt. Similar behavior of conductivity with salt concentration has been reported by many workers [25-33].

Variation of logarithmic conductivity with inverse temperature with different amount of nano-filler SiO_2 in PA-system is shown in Fig. 5.17 (a). The observed increase in conductivity is attributed to increase of the fraction of free volume in the polymer electrolytes due to increase in temperature. Fig. 5.17 (b) shows the variation of conductivity with SiO_2 concentrations for PAS series at 313 K. The conductivity increases with nano-filler SiO_2 concentration up to 20 wt %. Wiczorek *et.al.* [34] and Croce *et.al.* [35] suggested that addition of

nano-filler in polymer system, results an interaction of cations with Lewis acid base type oxygen and OH surface group on alumina grains. It also provides additional sites creating favorable high conducting pathways in the vicinity of grains for the migration of ions [35-41]. However, the conductivity does not continue to rise indefinitely with increasing concentration of SiO₂. It falls after an optimum concentration of SiO₂ leading to aggregate of SiO₂ particle in the systems which impede the ionic movement by acting as insulators [19, 41]. A clear signature of this observation is seen in FTIR spectra (Fig. 4.4) in chapter 4 for PAS-25. Liu *et.al.* [42] also observed fall in conductivity at higher concentrations of nano-filler SiO₂.

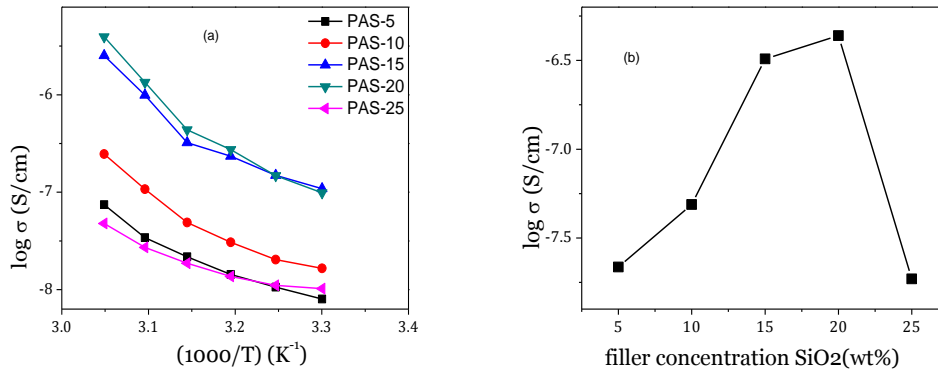


Fig. 5.157 Variation of dc conductivity as a function of (a) temperature for PAS system and (b) nano-filler SiO₂ at 303K.

The variation of temperature dependent conductivity for the plasticized PASP system i.e.; PEO: AgCF₃SO₃ (7wt%): SiO₂(20wt%): PEG is shown in Fig. 5.18(a). It is worth noticing that conductivity of PASP-25 shows initially the lowest value of conductivity but with the rise in temperature, conductivity values do not remain low and rise further with increase in temperature. It is clear from the plot [Fig. 5.18 (b)] of logarithmic conductivity versus different content of PEG at 318 K (PASP series) that the conductivity increases with up to PASP-20 (20 wt% of PEG) because the presence of plasticizer decreases the viscosity between the chains. The existence of such less viscous separate ionic pathways increase the migration of free Ag⁺ - ions through the plasticizer.

The Ag⁺-ions may have preferred to conduct through these less viscous new paths, which, consequently, enhance the mobility of the ions. As discussed in chapter 4 [40, 43, 44], the addition of plasticizer influences inter-chain and intra-chain separation between the plasticizer and polymer. However, a dilution effect predominated with further addition of the

plasticizer to the system, and consequently, the conductivity drops at PASP-25 of PEG. This may have been due to the formation of linkages between the plasticizer itself; this causes re-crystallization supported by XRD (Chapter 4). It is worth mentioning here that the overall conductivity values of the polymer nano-composite samples with PEG plasticizer (PASP-system) are lowest compared to samples without PEG (PAS-system).

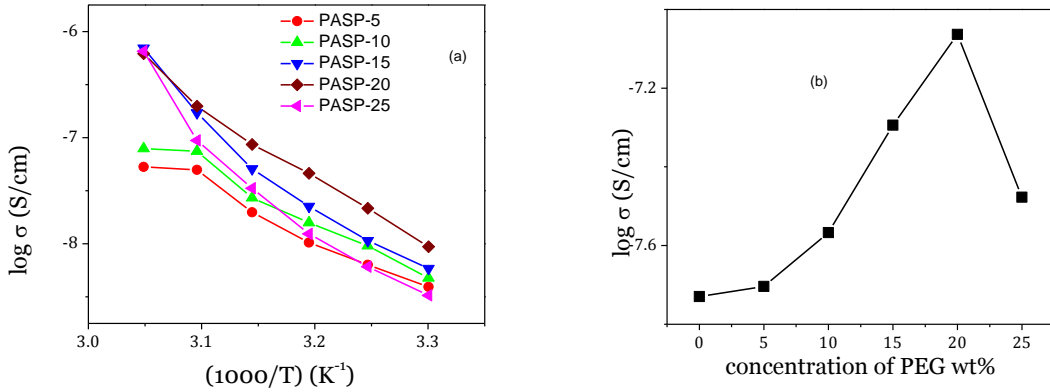


Fig.5.168 Variation of dc conductivity as a function of (a) temperature for PASP system and (b) plasticizer PEG at 318 K.

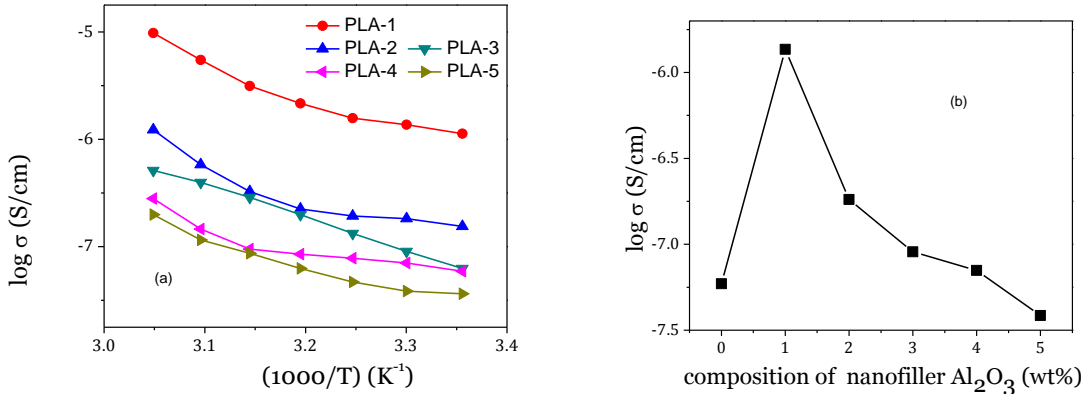


Fig.5.19 Variation of dc conductivity as a function of (a) temperature for PLA system and (b) nano-filler Al₂O₃ at 313K.

Lithium triflate is generally used in lithium ion batteries as a salt of the electrolyte. In PLA system, temperature dependence of dc conductivity is shown in Fig. 5.19 (a). The variation of conductivity with temperature follows near Arrhenius behaviour. The relationship between conductivity and Al₂O₃ concentration at room temperature is shown in Fig. 5.19(b). The conductivity increases for only PLA-1 and then drops continuously. The optimum conductivity for 1wt% of Al₂O₃ is observed to be 1.1×10^{-6} S/cm at room temperature. The introduction of nano-filler makes the system more amorphous and promotes ionic as well as segmental mobility [45, 46]. The increase in ionic conductivity is attributed to a

reduction of crystallinity or increase in amorphousness of composite polymer electrolyte. In this case, amorphous phase arises from random distribution of Al_2O_3 nano-filler. A polymer chain in amorphous is more flexible, which results in an increase in segmental motion of the polymer [47]. Above 1wt% of Al_2O_3 , the nano-filler tend to retard the ion motion by gradual cluster formation. XRD data and SEM micrographs showed Al_2O_3 the crystallites after 1 wt%. Dissanayake *et.al.* [36] reported that at higher filler concentrations, the grains get close to each other and block the pathways to reduce the conductivity.

Fig. 5.20 (a) shows the variation of ionic conductivity with temperature for PLAP series PEO: LiCF_3SO_3 : Al_2O_3 : PEG polymer electrolytes. The temperature-conductivity plots (Fig. 5.20(a)) depict Arrhenius behavior i.e.; conductivity increases linearly with temperature. Variation of conductivity with different amount of plasticizer PEG is shown in Fig. 5.20(b). Enhancement in conductivity is observed up to 10wt% of PEG and thereafter it tends to reduce. Generally, PEG increases the inter and intra-chain free volume of the system [48-50], but the addition of large amount of PEG plasticizer leads to the dilution effect which increases the cohesive energy of the polymer matrix and hinders the ionic mobility. Similar to silver based systems (PAS and PASP systems) in lithium based systems (PAL and PLA systems) too, the overall conductivity decreases for all samples with the addition of PEG compared to above discussed PLA system.

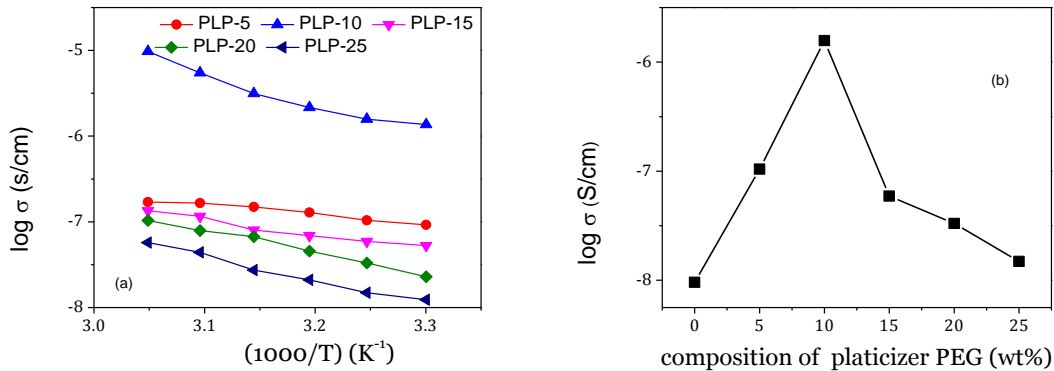


Fig.5.20 Variation of dc conductivity as a function of (a) temperature for PLP system and (b) Plasticizer PEG at 313K.

5.4 AC Conductivity

In order to get a complete picture of transport properties of the polymer composites, a proper understanding of AC conductivity is required. AC conductivity is a

complex quantity it can be expressed as,

$$\begin{aligned}\sigma^* &= \sigma' + j\sigma'' \\ &= \frac{t}{A} \left[\frac{1}{R} + j\omega C \right]\end{aligned}\quad (5.2)$$

where, t and A are the thickness and area of the sample, respectively. Thus, the impedance data has direct relevance to extract real and imaginary parts of conductivity [5].

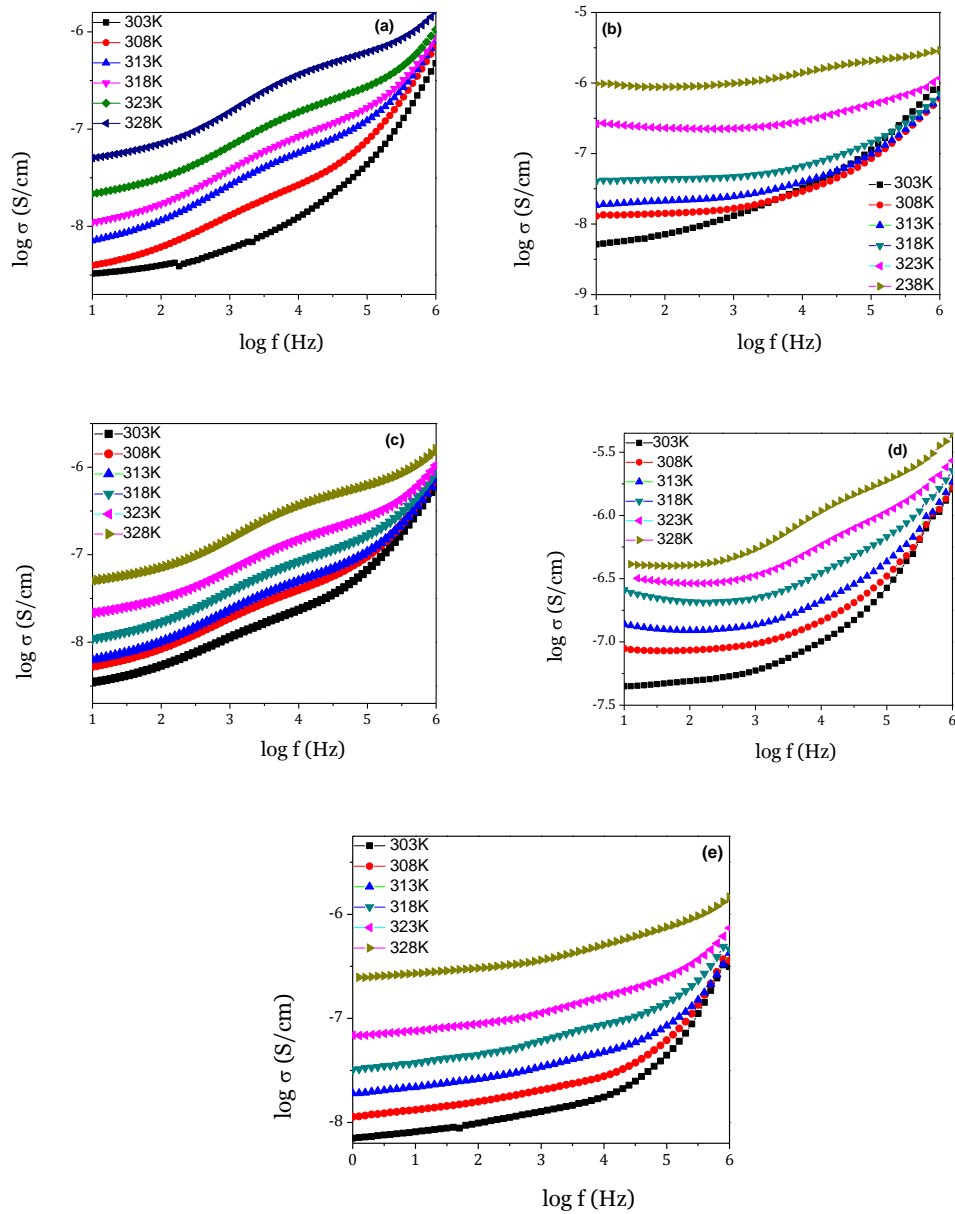


Fig.5.21 *Ac conductivity spectra for (a) PA-2, (b) PA-3.5, (c) PA-5, (d) PA-7 and (e) PA-11 polymer films at different temperatures.*

Analysis of AC conductivity is generally divided into three regions a low, mid and

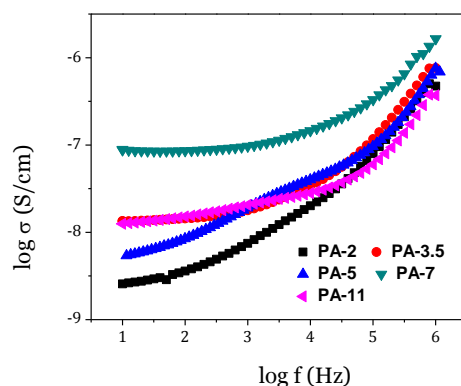


Fig.5.22 *Ac conductivity spectra for PA-series at 313K.*

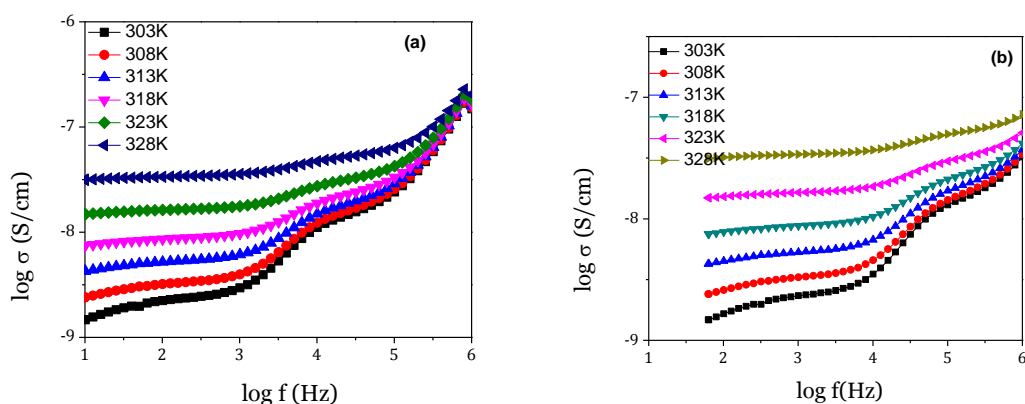


Fig.5.23 *Ac conductivity spectra for (a) PAS-20 and (b) PAS-25 polymer films at different temperatures.*

high frequency region [51]. At first, the frequency dependent conductivity spectra for various samples of polymer salt system (PA-system) PA-2, PA-3.5, PA-5, PA-7 and PA-11 at different temperatures are analyzed and shown in Figs. 5.21 (a)-(e). With the increase in frequency, conductivity is observed to increase. At low frequencies, conductivity values are low due to electrode polarization effects at the electrode-electrolyte interface [51-53]. More and more charge accumulation starts occurring at electrode and electrolyte interface when frequency is low. With the increase in frequency, mobility of charge carriers increases, Ag^+ ions is high near to relaxation time and hence conductivity increases with frequency. At higher frequencies, the observed rise in conductivity ascribes the frequency-dependence of ionic motion in accordance with Jonsher's universal power law [54] behavior which attributes the couple of forward and backward ion displacements occurring simultaneously. The conductivity is found to be increasing with the increase in temperature. As the temperature increases, the frequency at which the disper-

sion becomes prominent shifts towards higher frequency region [18, 55]. Similar behavior is also reported for other fast ionic conductors [13, 18, 51, 54].

Fig. 5.22 shows the ac conductivity versus frequency plot for all samples of PA series at 313K. It is clear that the ac conductivity $\sigma_{ac}(\omega)$ for all the samples exhibit the same characteristics of the curve with different conductivity values depending on the salt composition. Ac conductivity shows highest values for PA-7 polymer electrolyte film i.e.; the film with lowest crystallinity, least bulk resistance and highest dc conductivity.

The effect of addition of nano-filler in polymer salt matrix with optimized conductivity in PA-system is studied to see the effect of nano-filler on ac conductivity. The ac conductivity plots for the PAS-20 and PAS-25 polymer nano-composites are shown in Figs. 5.23 (a) to (b) at different temperatures. Ac conductivity spectra shows plateau at low frequencies. With the rise in temperature, ac conductivity increases and the dispersion frequency systematically shifts towards high frequency side. At the mid frequency region, the conductivity increases continuously because at that frequency, the charge carrier gets excitation energy from the electrical signal. Due to this excitation energy, the mobility of the charge carrier increases which in turn, decreases the relaxation time and thus, the conductivity increases.

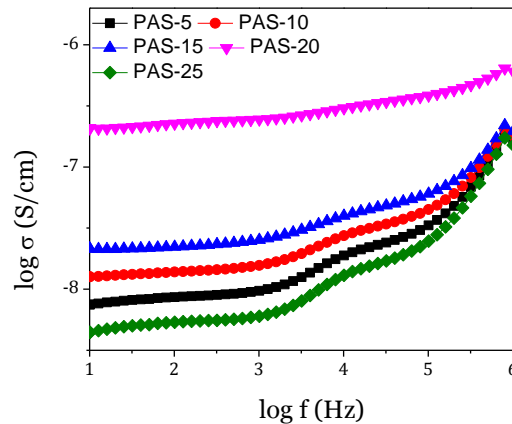


Fig. 5.24 Ac conductivity spectra of all the samples of PAS system at 313K.

The conductivity spectrum for different compositions of PAS system at 313K is shown in the Fig.5.24. Polymer film of PAS-20 is the highest conducting sample in this series. The ac conductivity plots of various samples of PASP-system at different temperatures are

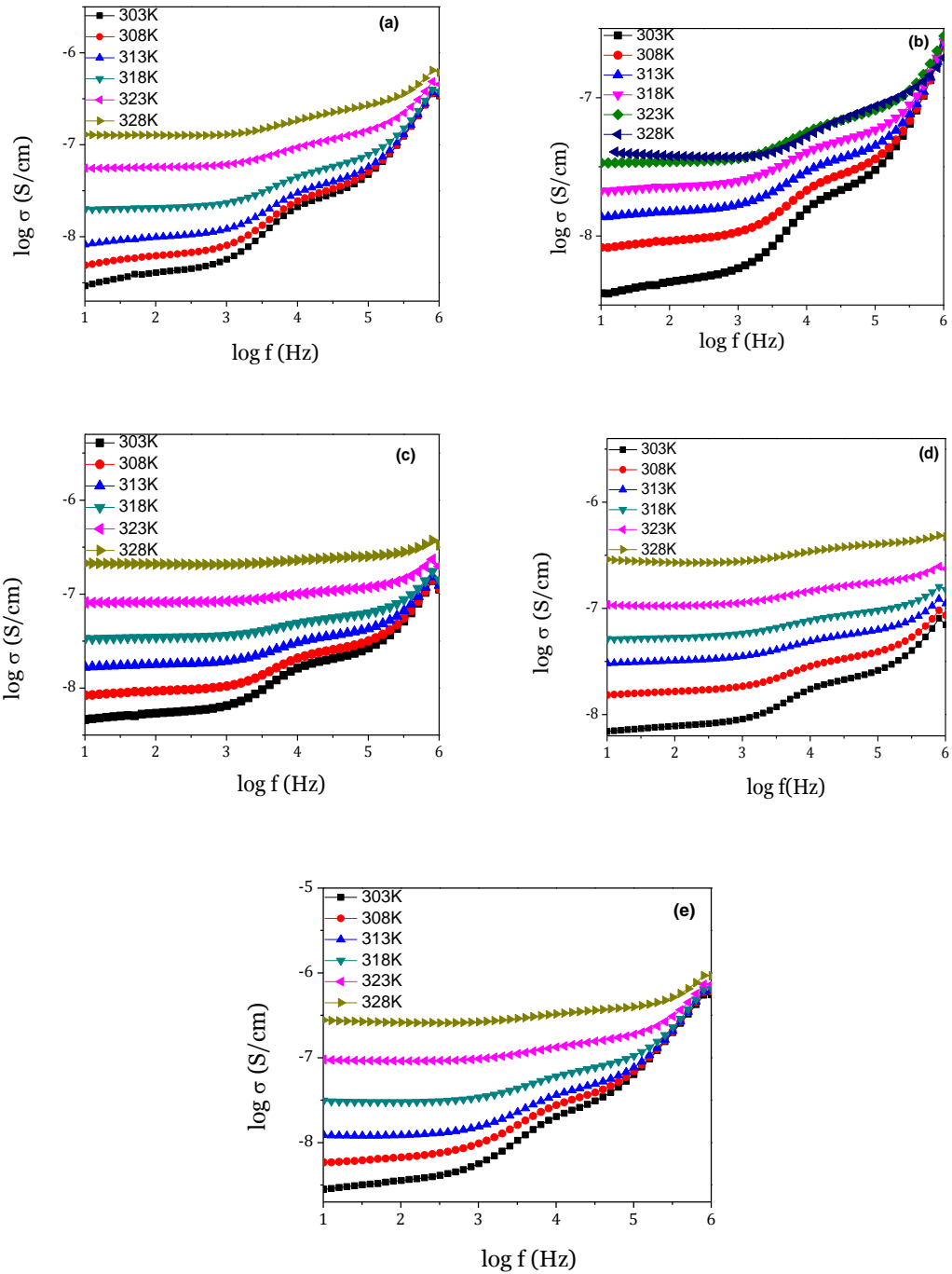


Fig.5.25 *Ac conductivity spectra for (a) PASP-5, (b) PASP-10, (c) PA-15, (d) PASP-20 and (e) PASP-25 polymer films at different temperatures.*

shown in the Figs. 5.25 (a) to (e). The ac conductivity behavior of all the other polymer samples is qualitatively similar. As the temperature rises from 303 to 328 K, the value of the electrical conductivity is enhances; a case of a typical ionic conductor [56]. The frequency-independent behavior of conductivity in the low frequency region corresponds to

the electrode-electrolyte interfacial polarization. In high frequency region, the ac conductivity spectra are not well separated and also do not show significant rise as in low frequency region. The occurrence of this type of behavior indicates the electrochemical characteristics of PEO-AgCF₃SO₃-SiO₂-PEG electrolyte system. Suthanthiraraj *et.al.* [30] suggested that this behavior owing to the occurrence of ionic conduction arising due to Ag⁺ ionic interaction and complexation phenomenon. The conductivity spectra for different compositions of PASP system at 313K temperature is shown in Fig. 5.26 which indicates that the conductivity increases and attains a maximum value at PEG- 20wt%.

The effect of nano-filler in Li-ion conducting system is shown in Figs.5.27 (a) to (e) which depicts the ac conductivity plot of various compositions of PLA-series at different temperatures. The frequency dispersion is present in all the samples at different temperatures. All the samples exhibit the same characteristic curves with different conductivity values depending on the amount of nano particle Al₂O₃. The conductivity spectra for all the samples of PLA-series are shown in Fig.5.28(a) which clearly shows that the conductivity increases with increasing nano particle filler content and a maximum conductivity is obtained for the system with Al₂O₃-1wt% sample and there after the conductivity continuously decreases with further addition of nano particles.

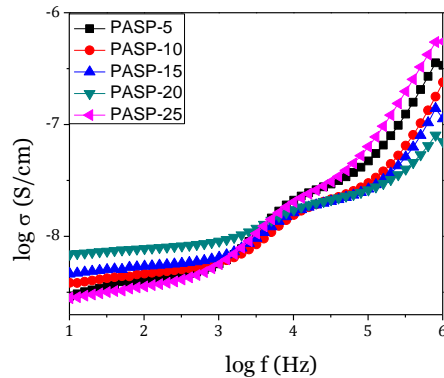


Fig.5.26 Ac conductivity spectra of all the samples for PASP system at 313K.

The conductivity spectra for all the samples of Li system plasticized with PEG are shown in Fig. 5.28 (b) which clearly show the conductivity increases up to 10wt% of PEG plasticizer content. The ac conductivity plots of the PLP-system with different PEG concentrations PLP-5, PLP-10, PLP-15 and PLP-20 at different temperatures are shown in the Fig. 5.29 (a) to (d). Here with the increase in temperature, the conductivity rises

and high frequency dispersion shifts to higher frequency region.

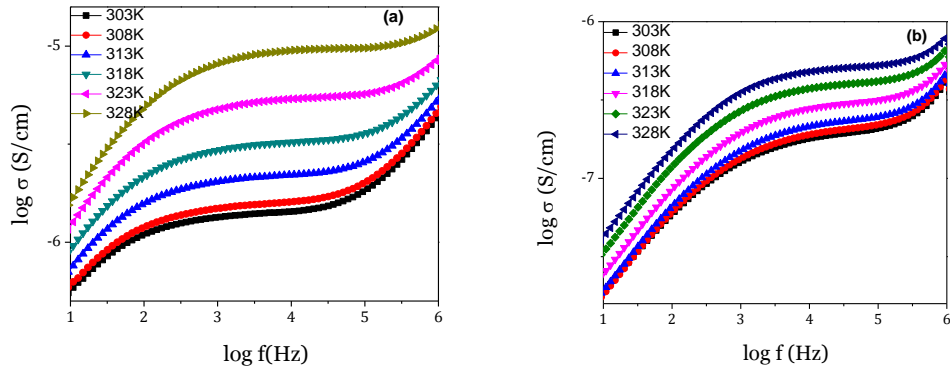


Fig.5.27 *Ac conductivity spectra for (a) PLA-1 and (b) PLA-2 polymer films at different temperatures.*

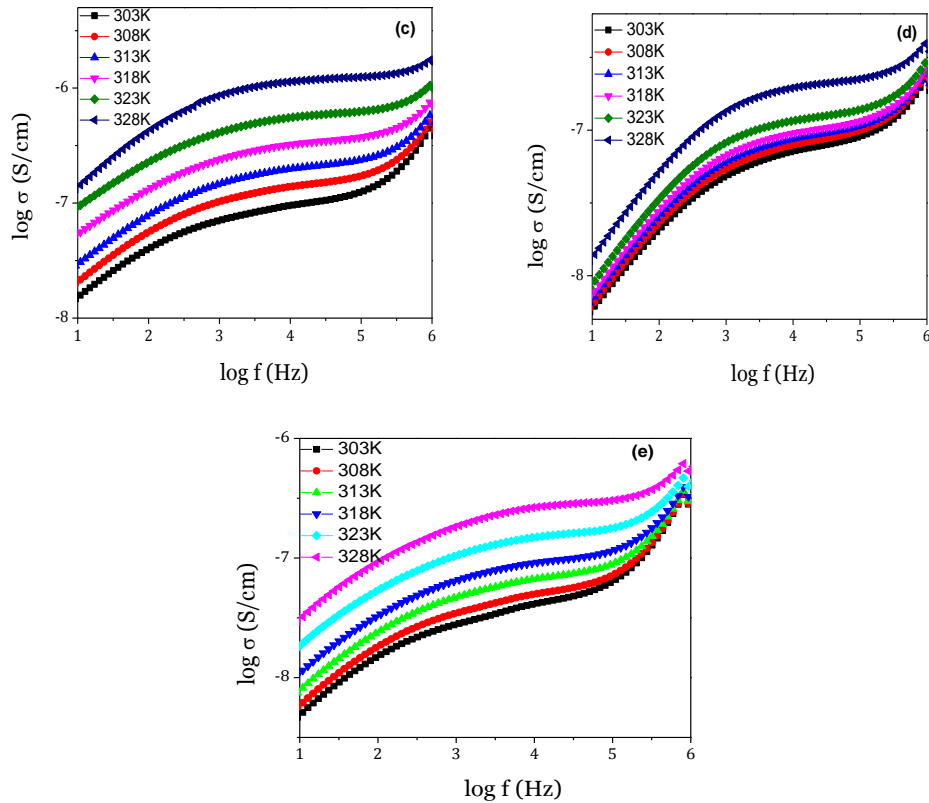


Fig.5.27 *Ac conductivity spectra for (c) PLA-3, (d) PLA-4 and (e) PLA-5 polymer films at different temperatures*

Frequency dependence of conductivity is a sum of dc conductivity due to the movement of free charges and polarization conductivity due to the movement of bound charges. With decreasing frequency, the conductivity, σ decreases and approaches the direct current conductivity σ_{dc} . The low conductivity value at low frequencies is related to the accumulation of ions due to the slow periodic reversal of the electric field.

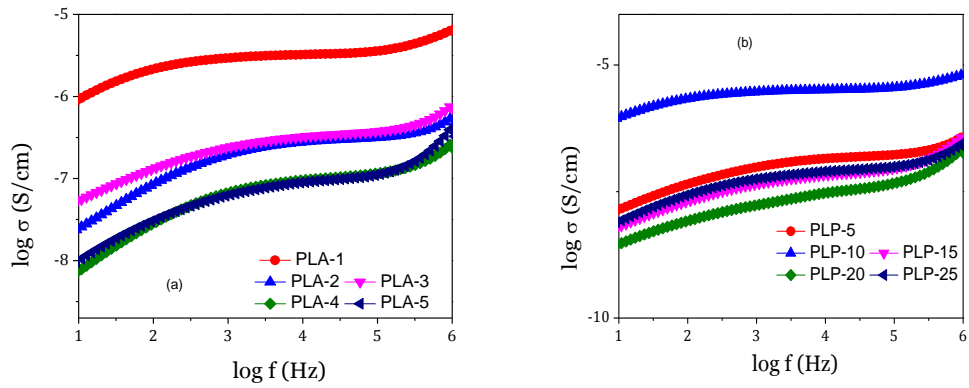


Fig.5.28 *Ac conductivity spectra of all the samples for (a) PLA and (b) PLP systems at 313K.*

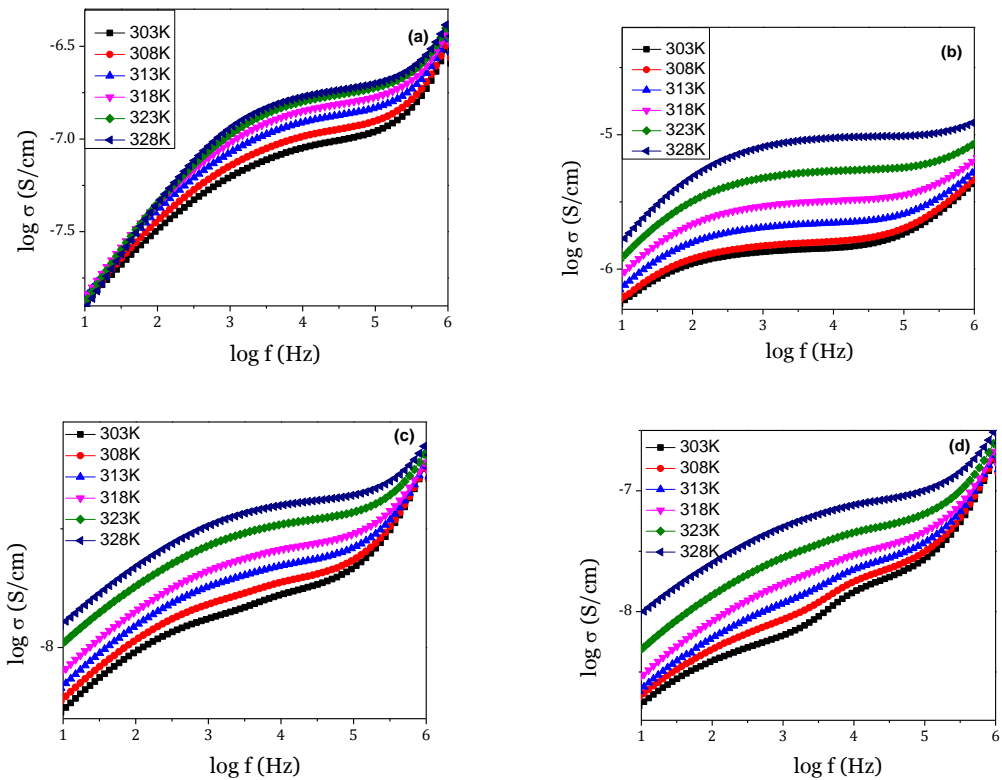


Fig.5.29 *Ac conductivity spectra for (a) PLP-5, (b) PLP-10, (c) PLP-15, and (d) PLP-20 polymer films at different temperatures.*

In all prepared systems, the power law nature $\sigma(\omega) \propto \omega^n$ is observed in the high frequency region and the conductivity sharply increases with frequency. The variation of conductivity with frequency may be expressed to the well known power law of ac behavior [54, 57-61] which indicates a non-random process, where in the ion motion is correlated given by the following equation,

$$\sigma(\omega) = \sigma_{dc} + A\omega^n \dots\dots\dots(5.4)$$

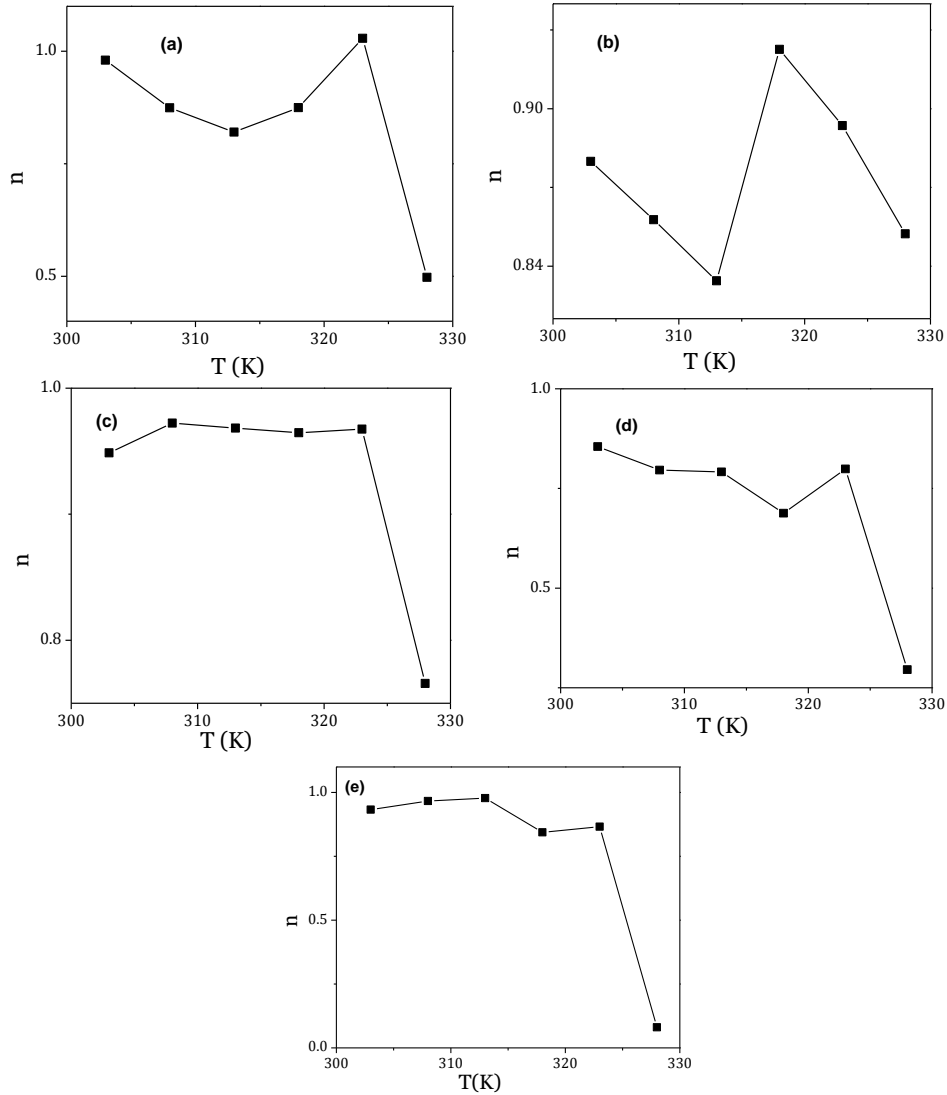


Fig.5.30 Variation of frequency exponent n with temperature for (a) PA-7, (b) PAS-15, (c) PASP-10, (d) PLA-1 and (e) PLP-5 samples. where $\sigma(\omega)$ is the conductivity at a particular frequency, σ_{dc} is the dc conductivity at zero frequency, A is a constant and n is the frequency exponent lies in the range of $0 < n < 1$. The above expression is known as the *power law of ac behavior*. Because the power law of ac behavior is observed in wide range of materials, Jonscher called it “Universal Behavior” [59, 60, 62]. The above mentioned eq. 5. 4 is accepted universally for considering the sample conductivity, frequency dependent conductivity etc.

The frequency exponent n was calculated from the slope of the plot $\log(\sigma' - \sigma_{dc})$ vs. $\log \omega$, which is a straight line. Jonscher [59] had shown that a non-zero n in the dispersive region of conductivity is due to the energy stored in the short range collective motions. The magnitude of n appears to be associated with high degree of modification.

Various different theories as mentioned in Chapter 2 have been proposed to understand the conduction mechanism in the amorphous materials.

For PS-system, the calculated values of the frequency exponent n are tabulated in Table 5.1. Its values lie in the range 0.5 to 0.9, i.e., less than 1 and are observed to decrease with temperature for all AgCF_3SO_3 concentration. The exponent is a measure of degree of interaction with the polymer environment [63]. It is observed from Fig. 5.30(a) that exponent n which decreases with increasing temperature, exhibits a minimum at a certain temperature after which it begins to increase. The reason is assigned to breaking of internal correlation between the sites and relaxing ions and relaxing species become independent of each other which results in tunneling process rather than hopping. This over-lapping large polaron tunneling (OLPT) model is found to be best suitable to explain the conduction process in the present system of samples and is well reported by many workers [64-67].

Fig. 5.30(b) shows the variation of power law exponent for the PAS-system for 15wt% SiO_2 . Here the value of frequency exponent n initially decreases with increase in temperature up to 313K and then it shows a sudden rise at 318K and decreases with further increase in temperature. For PASP-10 polymer film (Fig. 5.30(c)) system, frequency exponent n value slightly increases at 308K and then shows no variation up to 323K and drops at 328K. The variation of n with temperature suggests that the samples follow OLPT model.

The values of n decreases initially and reaches minimum at 313K for PLA system with increase in temperature and finally drops sharply at 328K as revealed from Fig.5.30 (d). Finally, the PLP system also seems to follow the OLPT model where the variation of the values of exponent n in Fig. 5.30 (e) shows the similar trend. The value of frequency independent dc conductivity (σ_{dc}), frequency exponent n and constant A for all the samples of five different series are given in Tables 5.1 (a) to (e). The values of n are clearly independent of composition. Amongst the different mechanisms, OLPT model is the best suitable for the present polymer electrolyte systems.

Table 5.1 Values of the dc conductivity, frequency dependent conductivity parameters A and n at 318K.

(a) PA system

Sample name	$\sigma_{dc} (\Omega^{-1}cm^{-1})$	$A(\Omega^{-1}cm^{-1} rad^{-n})$	n
PA-2	4.40×10^{-8}	2.04×10^{-11}	0.75
PA-3.5	4.00×10^{-8}	4.45×10^{-12}	0.88
PA-5	7.84×10^{-8}	2.86×10^{-12}	0.89
PA-7	3.54×10^{-7}	1.17×10^{-11}	0.87
PA-11	6.27×10^{-8}	1.50×10^{-12}	0.79

(b) PAS system

Sample name	$\sigma_{dc} (\Omega^{-1}cm^{-1})$	$A(\Omega^{-1}cm^{-1} rad^{-n})$	n
PAS-5	1.42×10^{-8}	8.02×10^{-13}	0.89
PAS-10	3.05×10^{-8}	7.44×10^{-13}	0.90
PAS-15	2.73×10^{-7}	6.90×10^{-13}	0.92
PAS-20	2.33×10^{-7}	2.23×10^{-10}	0.58
PAS-25	1.19×10^{-8}	8.64×10^{-13}	0.88

(c) PASP system

Sample name	$\sigma_{dc} (\Omega^{-1}cm^{-1})$	$A(\Omega^{-1}cm^{-1} rad^{-n})$	n
PASP-5	1.97×10^{-8}	1.74×10^{-13}	0.95
PASP-10	2.70×10^{-8}	6.02×10^{-14}	0.97
PASP-15	5.08×10^{-8}	1.01×10^{-13}	0.90
PASP-20	8.63×10^{-8}	1.73×10^{-12}	0.68
PASP-25	3.33×10^{-8}	2.39×10^{-13}	0.94

(d) PLA system

Sample name	$\sigma_{dc} (\Omega^{-1}cm^{-1})$	$A(\Omega^{-1}cm^{-1} rad^{-n})$	n
PLA -1	1.17×10^{-6}	6.43×10^{-10}	0.77
PLA-2	2.87×10^{-7}	7.47×10^{-14}	0.95
PLA-3	3.25×10^{-7}	1.50×10^{-13}	0.94
PLA -4	9.49×10^{-8}	1.06×10^{-13}	0.91
PLA -5	8.66×10^{-8}	1.79×10^{-13}	0.98

(d) PLP System

Sample name	$\sigma_{dc} (\Omega^{-1}cm^{-1})$	$A(\Omega^{-1}cm^{-1} rad^{-n})$	n
PLP-5	1.04×10^{-7}	2.18×10^{-13}	0.96
PLP-10	1.17×10^{-6}	6.43×10^{-10}	0.77
PLP-15	5.90×10^{-8}	4.30×10^{-7}	0.10
PLP-20	3.31×10^{-8}	1.42×10^{-8}	0.17
PLP-25	1.48×10^{-8}	4.89×10^{-8}	0.23

References :

- [1] J. E. Bauerle, *J. Phys. Chem. Solids* 30 (1969) 2657.
- [2] J. R. Macdonald (ed.), *Impedance spectroscopy emphasizing solid state materials and systems* (New York Wiley) 1987.
- [3] G. H. Sluyter, *A series of papers entitled "Impedance spectroscopy of Galvanic cell", Rec. Trav. Chim.*, 79 1092 1101 (1960).
- [4] D. R. Franceschetti, P. C. Shipe, *Solid State Ionics* 11 (1984) 285.
- [5] J.R. Macdonald, *Annals of Biomedical Engg.* 20 (1992) 289-305.
- [6] A. K. Jonscher, *Phys. Thin Films* 11 (1980) 232.
- [7] K. W. Wagner, *Ann d Physik*, 40 (1913) 817.
- [8] A.K Jonscher and J. M. Reau , *J. Mater. Sci. I*, 3 (1978) 563.
- [9] K. Singh and S. S. Bhoga. *Complex Impedance Spectroscopy Solid State ionic and its application Vol. 1 Ch2 pp.16* (2007)
- [10] U. Retter, H. Lohse, *Chapter II.5, Electrochemical Impedance Spectroscopy*, F. Scholz (ed.), *Electroanalytical Methods, 2nd ed.*, 159, @ Springer-Verlag Berlin Heidelberg (2010).
- [11] I.D. Raistrick, *Annual Rev. Mater. Sci.* 16 (1986) 343-370.
- [12] E. Barsoukov, J.R. Macdonald, *Impedance Spectroscopy: Theory, experiment, and applications*, Wiley, New York, (2005).
- [13] M.S. Jayswal, D.K.Kanchan, P. Sharma, M.Pant, *Solid State Ionics*, 186 (2011) 7-13.
- [14] M. Venkateswarlu, K.N. Reddy, B. Rambabu, N. Satyanarayana, *Solid State Ionics*, 127 (2000) 177–184.
- [15] R. Baskaran, S. Selvasekarapandian, N. Kuwata, J. Kawamura, T. Hattori, *Mater Chem Phys* 98 (2006) 55–61.
- [16] S. K. Deraman, N.S. Mohamed, and R.H.Y. Subban, *Int. J. Electrochem. Sci.*, 8 (2013) 1459 - 1468
- [17] B. Scrosati, F. Croce and L. Persi, *J. Electrochem. Soc.* 147(5) (2000) 1718.
- [18] D.K. Pradhan, R.N.P. Choudhary, B.K. Samantaray, *eXPRESS Polymer Letters Vol.2, No.9* (2008) 630–638
- [19] S. Ramesh , K. Ramesh, A. K. Arof, *Int. J. Electrochem. Sci.*, 8 (2013) 8348 - 8355
- [20] S.D. Druger, A. Nitzam, M.A. Ratner, *J chem. Phys* 79 (1983) 3133.
- [21] S.D. Druger, M.A. Ratner, A. Nitzam, *J Phys. Rev B* 31(1985) 3939.
- [22] C.S. Sunandana, P.S. Kumar, *Bull. Mater. Sci.* 27(2004)1-17.
- [23] A.S. Ayeshe, *Polymer J.* 41(2009) 616-621.
- [24] L.L. Yang, A.R. Mchie, G.C. Farrington, *J. Electrochem. Soc.* 133 (1986) 1380-1385.
- [25] S.Z.Z. Abidin, A.M.M. Ali, O.H. Hassan, M.Z.A. Yahy, *Int. J. Electrochem. Sci.*, 8 (2013) 7320 - 7326
- [26] S. Ramesh, T.F. Yuen, C.J. Shen, *Spectrochim. Acta A* 69 (2008) 670-675.
- [27] S. Rajendran, M. Sivakumar, R. Subadevi, *Mater Lett* 58, (2004)641- 649.

- [28] J.D. Jeon, S.Y. Kwak, B.W. Cho, *J Electrochem Soc.* 152A (2005) 1583
- [29] Z. Tang, J. Wang, Q. Chen, W. He, C. Shen, X. X. Mao, J. Q. Zhang, *Electrochimica Acta*, 52(24) (2007) 6638-6643.
- [30] S. A. Suthanthiraraj, R. J Kumar and B. Paul, *Ionics*, 16(2009) 145- 151.
- [31] S. Ibrahim, M. R. Johan, *Int. J. Electrochem. Sci.*, 7 (2012) 2596 - 2615
- [32] M.R. Johan, S.H. Oon, S. Ibrahim, S.M.M Yassin, Y.H. Tay, *Solid State Ionics* 196 (2011) 41
- [33] S. Ibrahim, S.M.M Yassin, R. Ahmad, M.R. Johan, *Ionics*. 17 (2011) 399
- [34] W. Wieczorek, P. Lipka, G. Zukowska, H. Wycislik, *J Phys Chem B*, 102 (1998) 6968.
- [35] F. Croce, L. Persi, F. Ronci, B. Scrosati, *Solid State Ionics*, 135 (2000) 47.
- [36] MAKL Dissanayake, PARD Jayathilaka, RAP Bokalawala, I Albinsson, B.E Mellander, *J. Power Sources*, 409 (2003) 119-121
- [37] P. Sharma, D.K. Kanchan, *Polymer Int.* (2013) DOI: 10.1002/pi.4504.
- [38] M.S. Michael, M.M.E. Jacob, S.R.S. Prabakaran, S. Radhakrishna, *Solid State Ionics* 98(1997) 167.
- [39] M.A.K. L. Dissanayake, *Ionics* 10(2004) 221-225.
- [40] T.S. Min, M.R. Johan, *Ionics*. 17 (2011) 485
- [41] M.R. Johan, L.B. Fen, *Ionics*. 16 (2010) 335.
- [42] Y. Liu, J.Y. Lee, L. Hong, *J. Power Sources*, 109 (2002) 507.
- [43] M.Kumar, S.S. Sekhon, *Ionics* 8(2002) 223-233.
- [44] G. Wypych, *Handbook of plasticizers*, ChemTec Publishing, William Andrew (2013).
- [45] B. Scrosati, F. Croce, and L. Persi, *J. Electrochem. Soc.* 147 (2000) 1718.
- [46] S. Rajendran, O. Mahendran, R.Kannan, *J. Phys. Chem. Solids* (2002) 303.
- [47] H.W. Chen, T.P. Lin, F.C. Chang, *Polymer*, 43 (2002) 5281.
- [48] L.R.A.K. Bandara, M.A.K.L. Dissanayake, and B.E. Mellander, *Electrochim. Acta*, 43, 1447 (1998).
- [49] I.E. Kelly, J.R. Owen, and B.C.H. Steele, *Electronal. Chem.*, 168 (1984) 467.
- [50] D.R. Macfarlane, J. Sun, P. Meakin, P. Fasoulopoulos, J. Hey, and M. Forsyth, *Electrochim. Acta*, 40 (1995) 2131.
- [51] S.A. Suthanthiraraj, M.K. Vadivel, *Ionics* 18(2012) 385-394.
- [52] A. Serghei, M. Tress, J. R. Sangoro, F. Kremer, *Phys. Rev. B* 80(2009)184301.
- [53] C. Cametti, I. Fratoddi, I. Venditti, M. V. Russo, *Langmuir* 27(2011)7084-7090.
- [54] A K. Jonscher, *Nature* 267 (1977) 673.
- [55] M. Pant, D.K.Kanchan, N. Gondaliya, *Mater. Chem. Phys.* 115(2009) 98-104.
- [56] A. Chandra, B. Bagchi, *J. Chemical Phys.* 112(2000)1876-1886.
- [57] R. Murugaraj, G.Govindaraj, D. George, *J. Mater. Sci.* 37(2002)5101-5106.
- [58] A.N. Papathanassiou, *J. Phys. Chem. Solids*.66(2005)1849-1850.
- [59] A. K. Jonscher, *Dielectric Relaxation in Solids*, Chelsea Dielectric Press, London, 1983.
- [60] A. K. Jonscher, *J. Mater. Sci.* 16 (1981) 2037.
- [61] S. R. Elliott, *Adv. Phys.* 36 (1987) 135.

- [62] A. K. Jonscher, *J. Phys. D: Appl. Phys.* 32(1999) R57-R70.
- [63] R. Vaish, K.B.R. Varma, *Ionics* 17(2011) 727-731.
- [64] M. Tan, Y. Koseoglu, F. Alan, E. Senturk, *J. Alloys Compounds* 509(2011) 9399–9405.
- [65] E V. Gopalan, K. A. Malini, S. Saravanan, D S. Kumar, Y. Yoshida, M. R. Anantharaman, *J. Phys. D: Appl. Phys.* 41 (2008) 185005.
- [66] D. K. Modak, U. K. Mandal, M. Sadhukhan, B. K. Chaudhuri, T. Komatsu, *J. Mater. Sci.* 36 (2001) 2539 – 2545.
- [67] M. Z. Kufian, S. R. Majid and A. K. Arof, *Ionics*, 13 (2007) 231-234.
-

CHAPTER 6

MODULS AND DIELECTRIC ANALYSIS

A *nalysis of frequency dependent electric modulus & dielectric properties, including relaxation time and dielectric constant, as well as dielectric loss factors respectively of solid polymer electrolytes are discussed in this chapter.*

6.1 Introduction

The term dielectric is broader than the term insulating material. Here the dielectric material term means the substance whose basic electrical property is the ability to be polarized and in which electrostatic field can exist. For most of the applications of dielectric materials, the vital properties are the dielectric constant ϵ' and the dielectric loss factor, (i.e., $\tan \delta$) [1].

Dielectric polarization results due to the existence of atomic and molecular forces. It appears whenever charges in a material are somewhat displaced with respect to one another under the influence of an electric field. In a capacitor, the negative charges (-ve) within the dielectric are displaced towards the positive electrode (+ve), while the positive charges shift in the opposite direction. As charges are confined in an insulator, restoring forces are activated which either do work, or cause work to be done on the system in short, energy is transferred. During charging a capacitor, the polarization effect opposing the applied field draws charges onto the electrodes, storing energy and on discharge, this energy is been released. A result of which the interaction in certain materials, which possess easily polarizable charges, will greatly influence the degree of charge which can be stored in a capacitor. The proportional increase in storage ability of a dielectric with respect to vacuum is defined as the *dielectric constant of the material* [1, 2].

6.2 Dielectric Analysis

In general, dielectric analysis of the material provides the measure of electrical characterization of polymer material where the real part of dielectric permittivity (ϵ') is proportional to the capacitance and measures the alignment of dipoles and imaginary part of dielectric permittivity (ϵ'') is proportional to the conductance and represents the energy required to align dipoles and move ions.

Therefore, in order to understand the effect of variation of silver salt concentration on the dielectric properties in PEO-AgCF₃SO₃ polymer electrolytes (PS-system), the frequency dependence real (ϵ') and imaginary (ϵ'') part of permittivity at different temperature are plotted and shown in Fig. 6.1 and 6.2 respectively. The plot of real part of

permittivity (ϵ') shows dispersion at low frequency region with a gradually decrease in mid-frequency region and finally attain a constant value at high frequency. The increase in ϵ' values at lower frequencies results mainly due to the contribution of the electrode

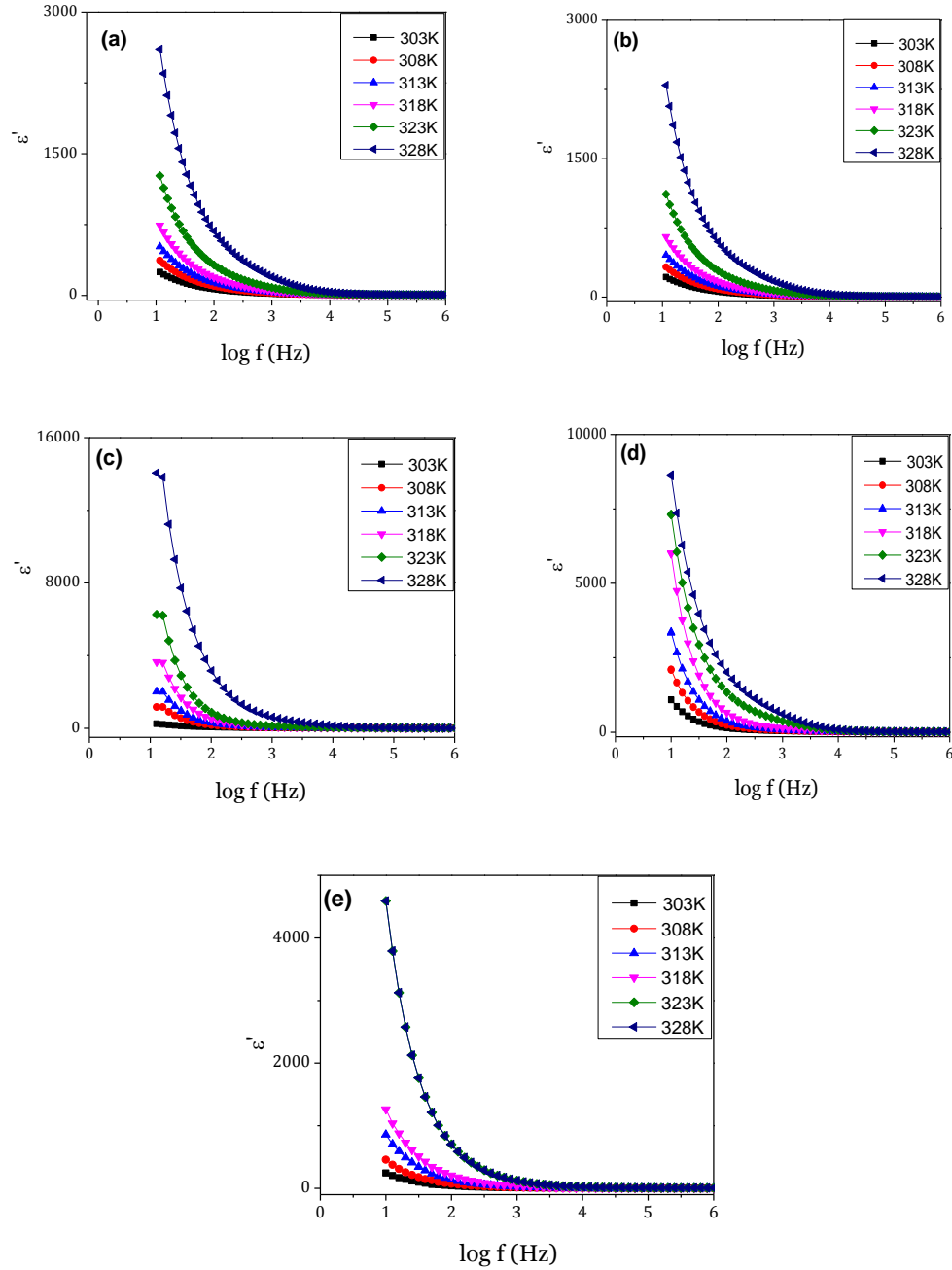


Fig. 6.1 The real part of dielectric permittivity, ϵ' plots for (a) PA-2, (b) PA-3.5, (c) PA-5, (d) PA-7 and (e) PA-11 of PA series at various temperatures.

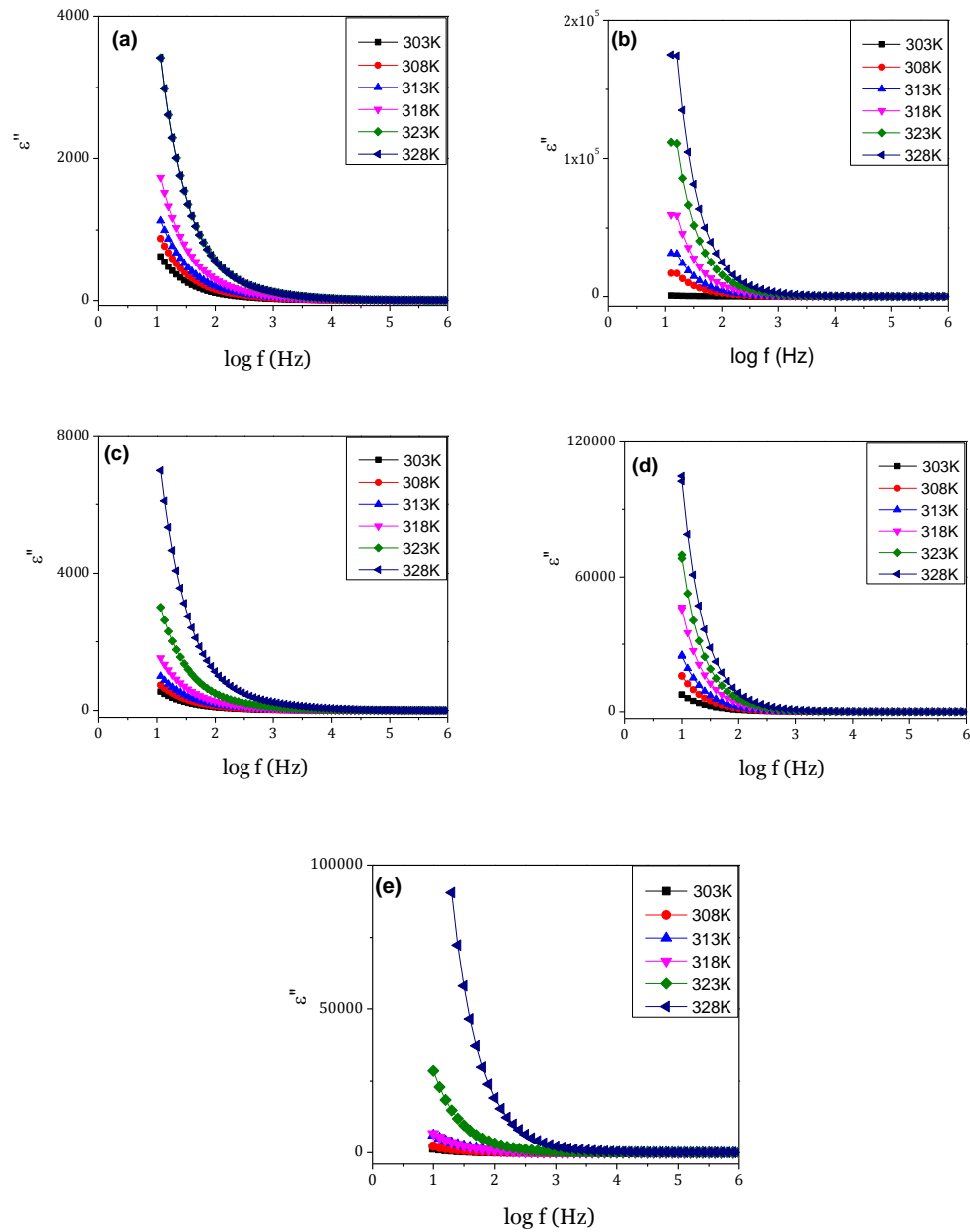


Fig. 6.2 The imaginary part of dielectric permittivity, ϵ'' plot for (a) PA-2, (b) PA-3.5, (c) PA-5, (d) PA-7 and (e) PA-11 of PA series at various temperatures.

polarization and Maxwell-Wagner interfacial polarization [3-5]. The electrode polarization phenomena occur due to formation of electric double layer capacitances by buildup of free charges at the interface between the electrolyte and the electrode [6]. This buildup of electrical polarization and drop of the electric field in the bulk are reflected by the increase in the complex dielectric function at low frequencies.

In the Maxwell-Wagner phenomena, the free charges build up during the electro-migration at the interfacing boundaries of different dielectric constants in the dielectric

material, which results in the formation of nano-capacitors in the dielectric material [7].

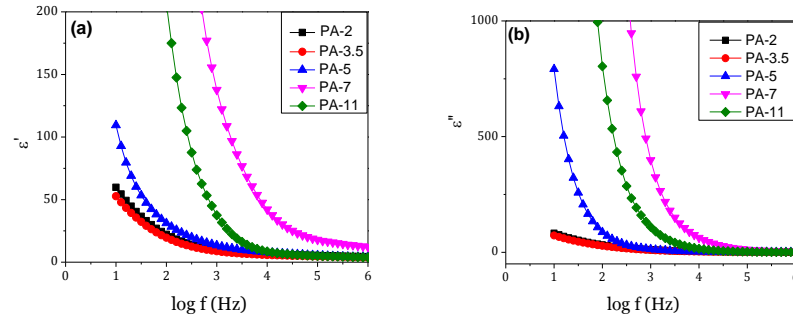


Fig.6.3 The plot of (a) real part ϵ' and (b) imaginary part ϵ'' of dielectric permittivity with different amount of AgCF_3SO_3 for PA System at 313K.

At sufficiently high frequencies, the free charges do not follow the fast changes developed in the ac field and thus only molecular polarization occurs at these frequencies [8-13]. In other words, dielectric constant decreases sharply with increase in frequency and becomes constant at high frequencies [8]. Both ϵ' and ϵ'' rise sharply at low frequencies with temperature and this rise shifts towards high frequency side and saturates [9] for all the samples of the PA-series. Figs. 6.3 (a) and (b) represent plots of real (ϵ') and imaginary (ϵ'') part of dielectric constant as a function of log frequency for different amount of AgCF_3SO_3 containing PEO polymer electrolytes.

At higher frequencies i.e.; in the range of 10^4 to 10^6 Hz, the measured dielectric constant is almost independent of the composition. The dielectric constant of the polymer film with 7wt% of AgCF_3SO_3 is observed to be highest and this sample shows maximum dispersion frequency. It is observed from figure that at low frequencies, the real (ϵ') and imaginary (ϵ'') parts of permittivity remain almost constant for PA-2wt% and PA-3.5wt%, whereas for PA-5wt% and PA-7wt% it increases and finally for PA-11wt% its value decreases. Figs. 6.7 (a) to (e) depict the frequency dependent dielectric constant plots for different concentrations of nano-filler SiO_2 in polymer salt system (PAS-system). According to Agrawal *et.al.*, [14] the decrease of ϵ' and ϵ'' with increasing frequency may be attributed to electrical relaxation or inability of dipoles to rotate rapidly leading to a lag between frequency of oscillating dipoles and that of applied field. They added that, as the frequency increases, the ionic and orientational source of polarizability decreases and finally disappear due to inertia of mobile ions to result in a nearly constant

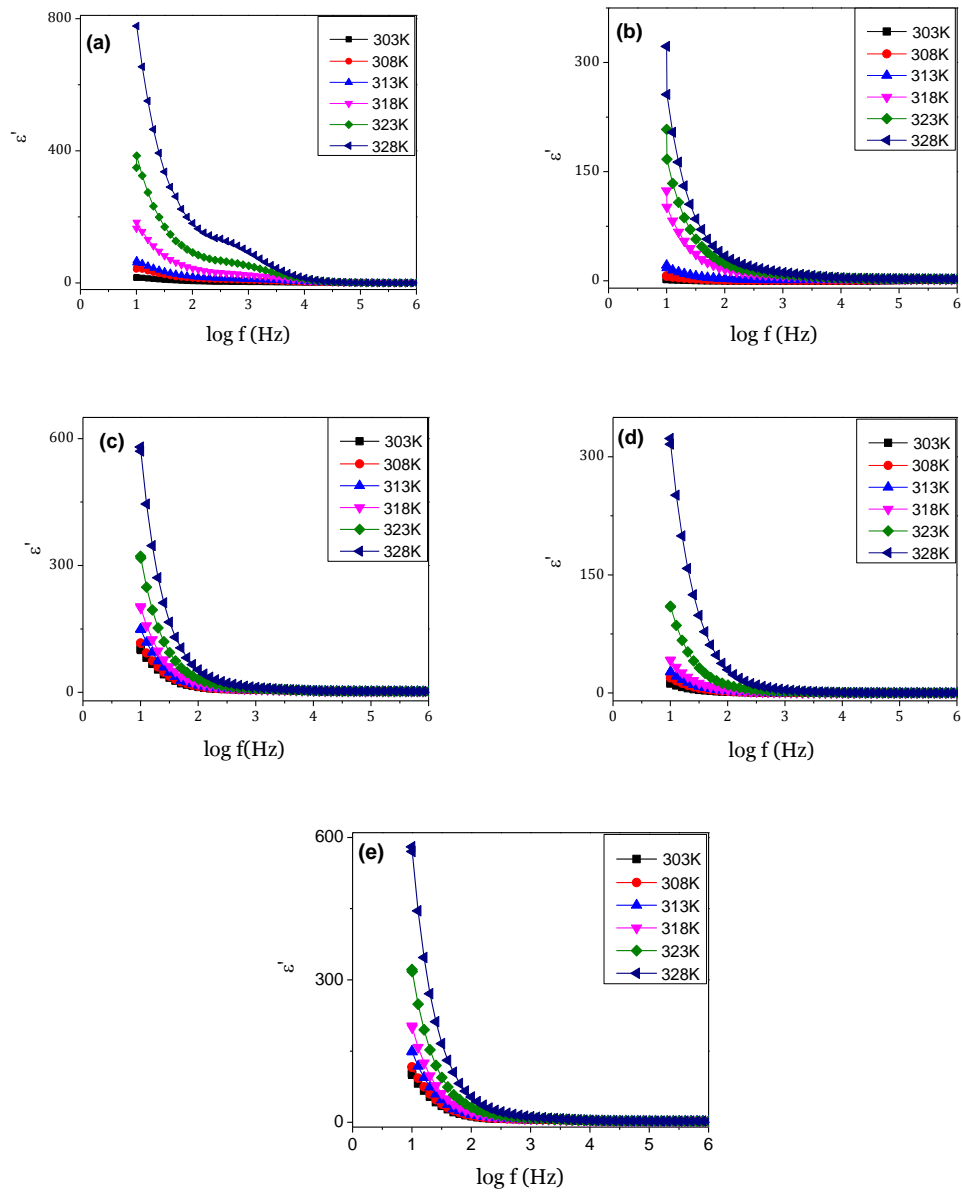


Fig.6.4 The plots of frequency dependent ϵ'' for (a) PAS-5, (b) PAS-10, (c) PAS-15, (d) PAS-20 and (e) PAS-25 of PAS series at various temperatures.

value of dielectric permittivity. Figs. 6.6(a) and (b) shows the variation of dielectric permittivity i.e.; ϵ' and ϵ'' with frequency for different SiO_2 concentration in PAS system at 313K. Non – uniform variation in the dielectric permittivity values with addition of SiO_2 are the main feature of the present system. Both ϵ' and ϵ'' values remain nearly same for PAS-5, PAS-10 and PAS-15 % of SiO_2 dispersed in PEO- AgCF_3SO_3 composite electrolyte and an increase in the values is observed only at higher concentration of SiO_2 i.e.; PAS-20wt%. This type of behavior indicates that the filler provides almost constant crys-

talline domain channels initially and then it starts segregating due to non complexation in polymer matrix. The alignment of these extra domains enhances the dielectric value of the materials. Agrawal *et.al.*,[14] discussed that dispersion at lower frequencies seems to be higher in case of composite electrolyte (PEO–SiO:NH₄SCN) compared to SPEs.

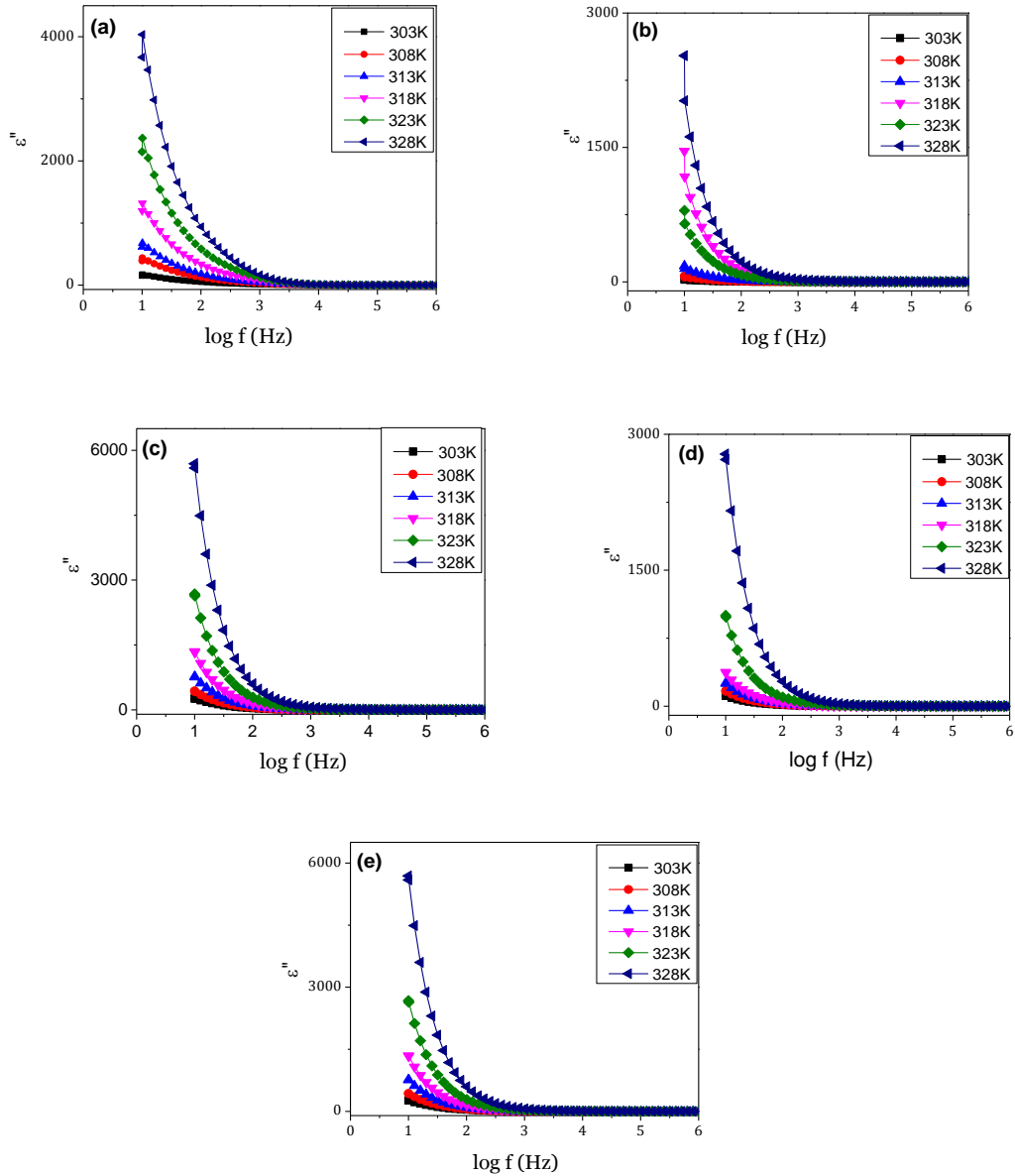


Fig.6.5 The plots of frequency dependent ϵ' for (a) PAS-5, (b) PAS-10, (c) PAS-15, (d) PAS-20 and (e) PAS-25 of PAS series at various temperatures.

The effect of plasticizer PEG in polymer nano-composites PASP-system in terms of dielectric permittivity is studied. The frequency dependent ϵ' and ϵ'' variation of all the samples of PASP-system at different temperatures are shown in Figs. 6.7 and 6.8, res-

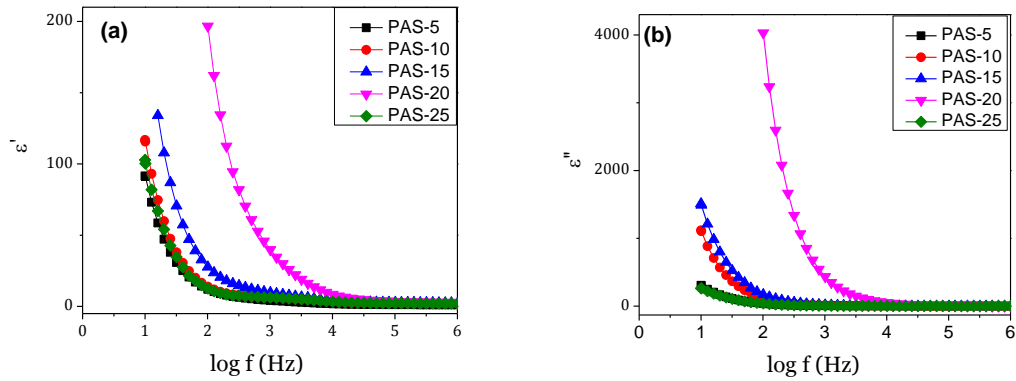


Fig. 6.6 The plot of (a) real part ϵ' and (b) imaginary part ϵ'' of dielectric of various amount of SiO_2 for PAS System at 313K

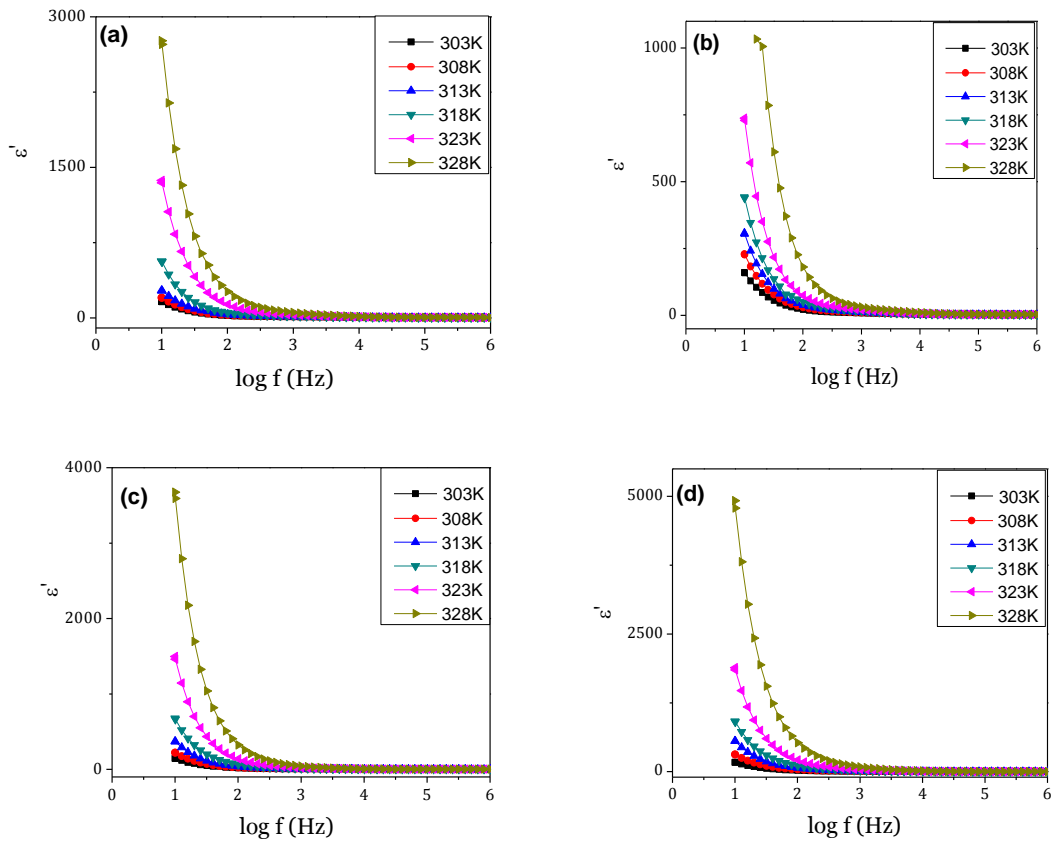


Fig. 6.7(a)-(d) The plots of real part of dielectric permittivity, ϵ' for (a) PASP-5, (b) PASP-10, (c) PASP-15 and (d) PASP-20 of PASP series at various temperatures.

pectively. A strong frequency dispersion of permittivity is observed in the low frequency region followed by a nearly frequency independent behavior. In the dielectric plots of PASP system shown in Fig. 6.9, the frequency of dispersion are not wide and well separated as observed for PAS system and are very close to each other. In this system, the as

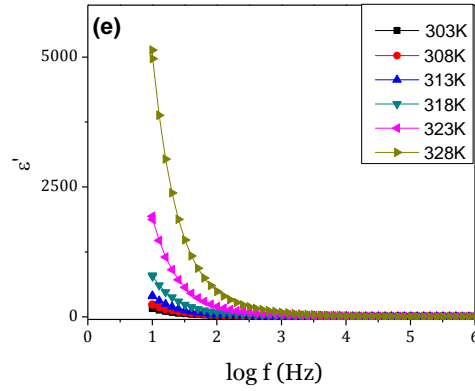


Fig. 6.7(e) The plot of ϵ' for PASP-25 at various temperatures.

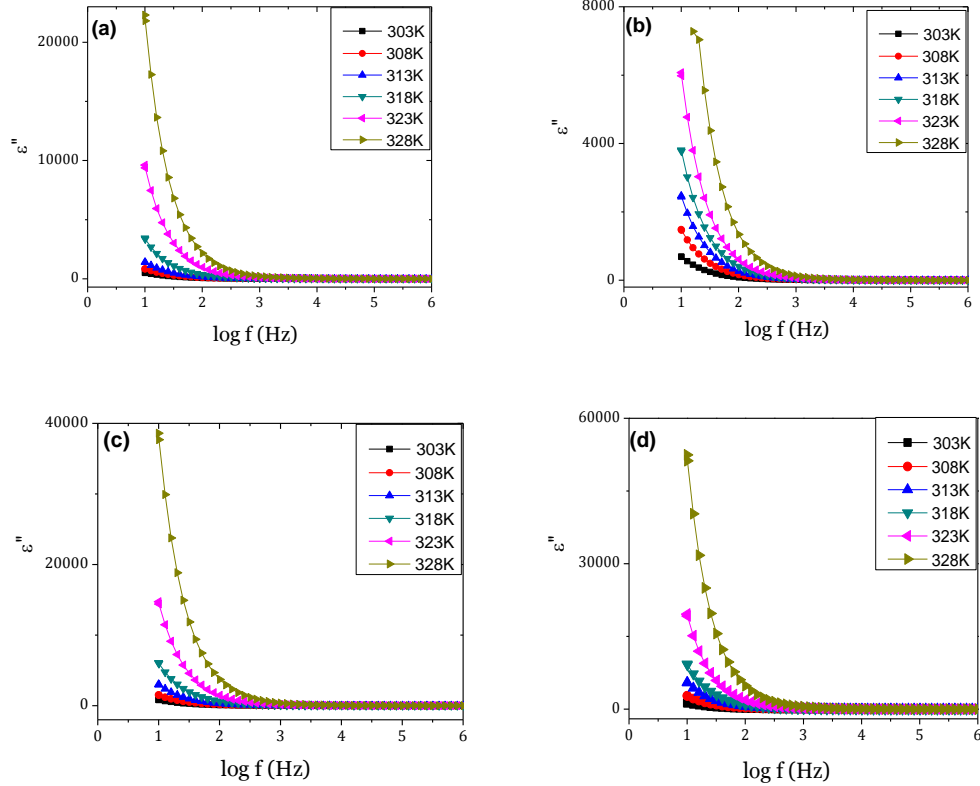


Fig.6.8 (a)-(d) The plots of ϵ'' variation as a function of frequency for (a) PASP-5, (b)PASP-10, (c) PASP-15 and (d) PASP-20 of PASP series at various temperatures.

sociation of PEG with polyethylene oxide (PEO) results in the reduction in system flexibility. S.K. Tripathi and co-researchers [15] mentioned that on addition of nanofiller Al_2O_3 to plasticized polymer electrolyte the dielectric constant and dielectric loss showed dispersion mainly near lower frequency region. R.H.Y Subban *et. al.* [16] mentioned that the variation in ϵ' and ϵ'' with angular frequency could be attributed to the formation of a

space charge region at the electrode and electrolyte interface, which is known as the non-

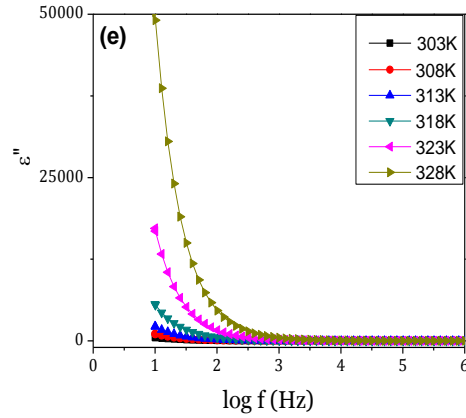


Fig.6.8 (e) Plot of ϵ'' variation as a function of frequency for PASP-25 at various temperatures.

Debye type behaviour. The compositional variations of real and imaginary parts of dielectric permittivity are shown in Figs. 6.9 (a) and (b), respectively. The highest conducting film depicts the highest dielectric constant value as well as highest losses too.

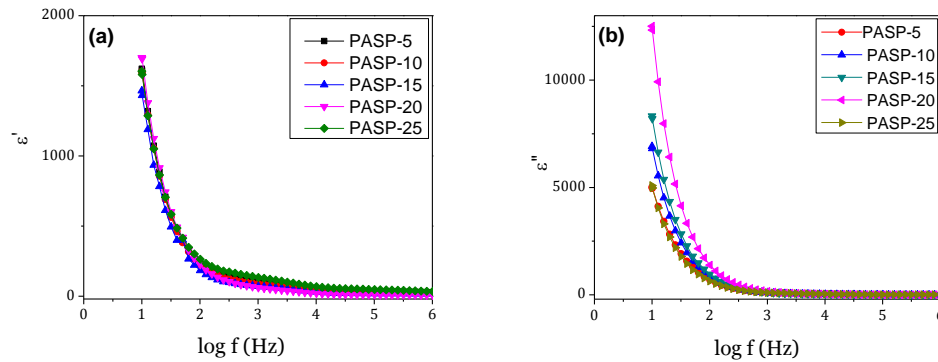


Fig. 6.9 The plots of (a) real part ϵ' and (b) imaginary part ϵ'' of dielectric permittivity for for PASP System at 313K

In Li-ion conducting series (PLA system), the variation in ϵ' and ϵ'' as a function of frequency for different polymer films at different temperatures are depicted in Figs. 6.10 (a) to (e) and Figs. 6.11 (a) to (e) respectively. According to Saroj *et.al.*, [17], the rise in ϵ' and ϵ'' values with the increase in temperature are due to progressively dissolution of crystalline phase into amorphous phase. Dielectric permittivity plots of various concentrations of Al_2O_3 in PLA-series are shown in Figs. 6.12 (a) and (b) at 313 K. A sharp rise is observed for 1wt% of Al_2O_3 but, beyond this concentration of Al_2O_3 , it decreases and becomes constant. A gradually increase in Al_2O_3 content must have prompted the cluster formation which in fact hinders the conducting channels resulting in gradually

decreases in ϵ' and ϵ'' values.

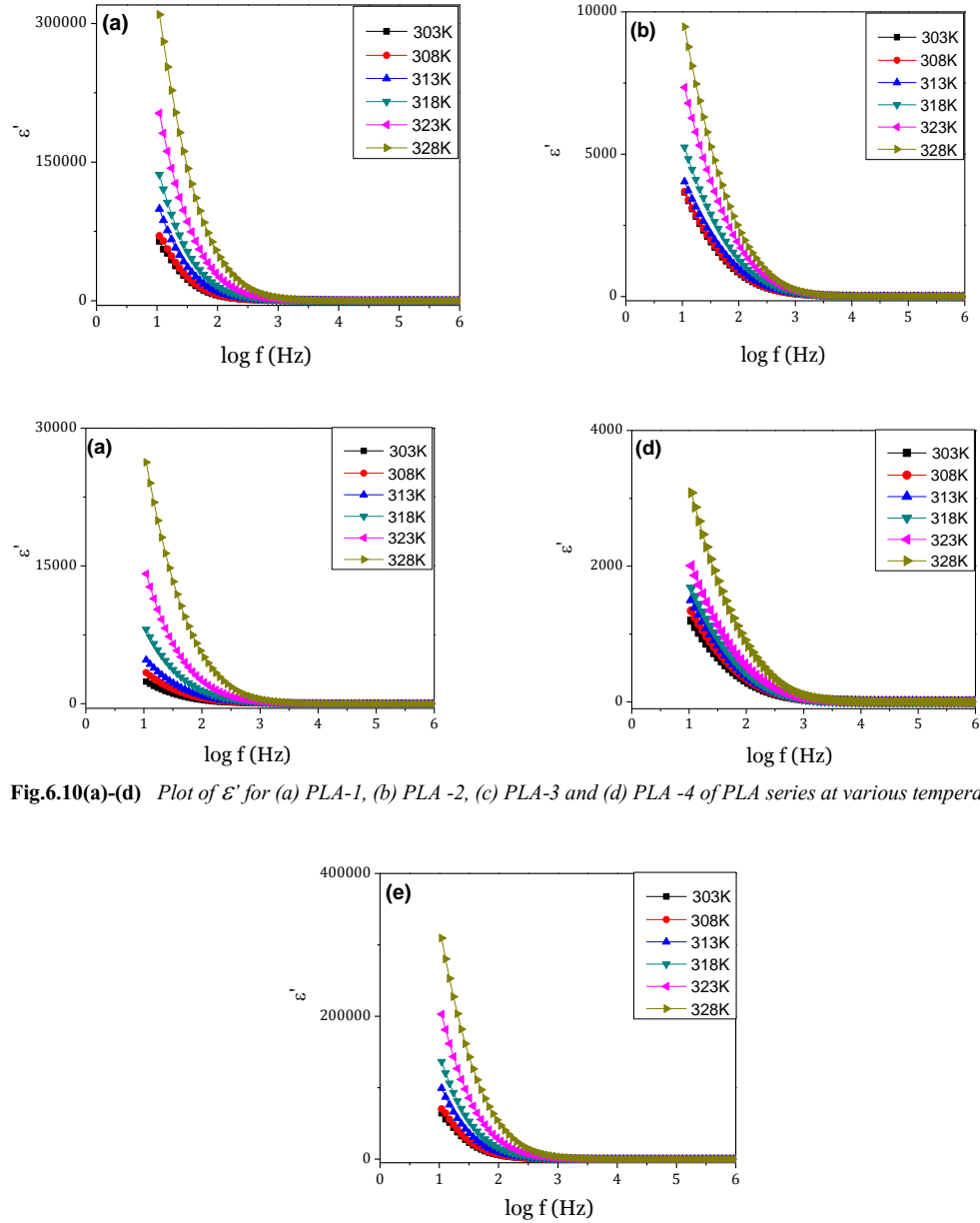


Fig.6.10(a-d) Plot of ϵ' for (a) PLA-1, (b) PLA -2, (c) PLA-3 and (d) PLA -4 of PLA series at various temperatures.

Fig.6.10 (e) Frequency dependent ϵ' variation for PLA-5 of PLA series at various temperatures.

With different PEG concentrations in lithium ion conducting nano-composite system i.e., PLP series, are shown in Figs. 6.13 and 6.14 at different temperatures. It is observed that on increasing the temperature, dielectric permittivity values increase which can also be attributed to the enhanced flexibility as well as segmental mobility of polymer chains resulting from rise in free volume due to addition of plasticizer. S. Ranjendran and coworkers [18] reported that in PMMA–LiClO₄–DMP polymer electrolytes, the rise of ϵ'

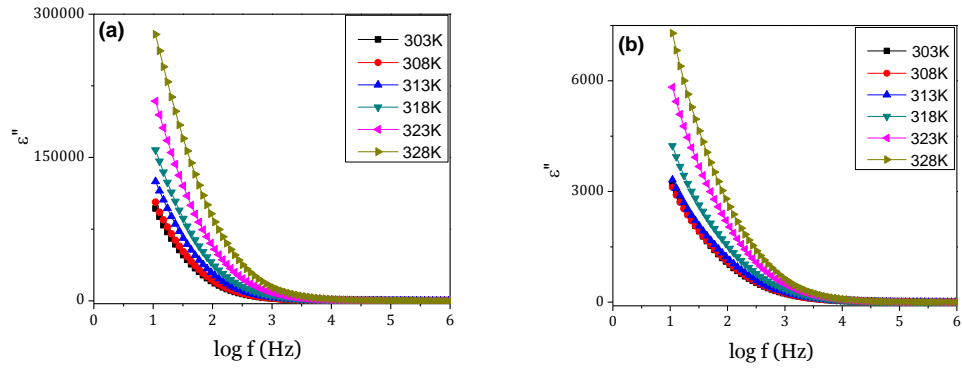


Fig. 6.81 Frequency dependent ε'' variation for (a) PLA-1 and (b) PLA-2 at various temperatures.

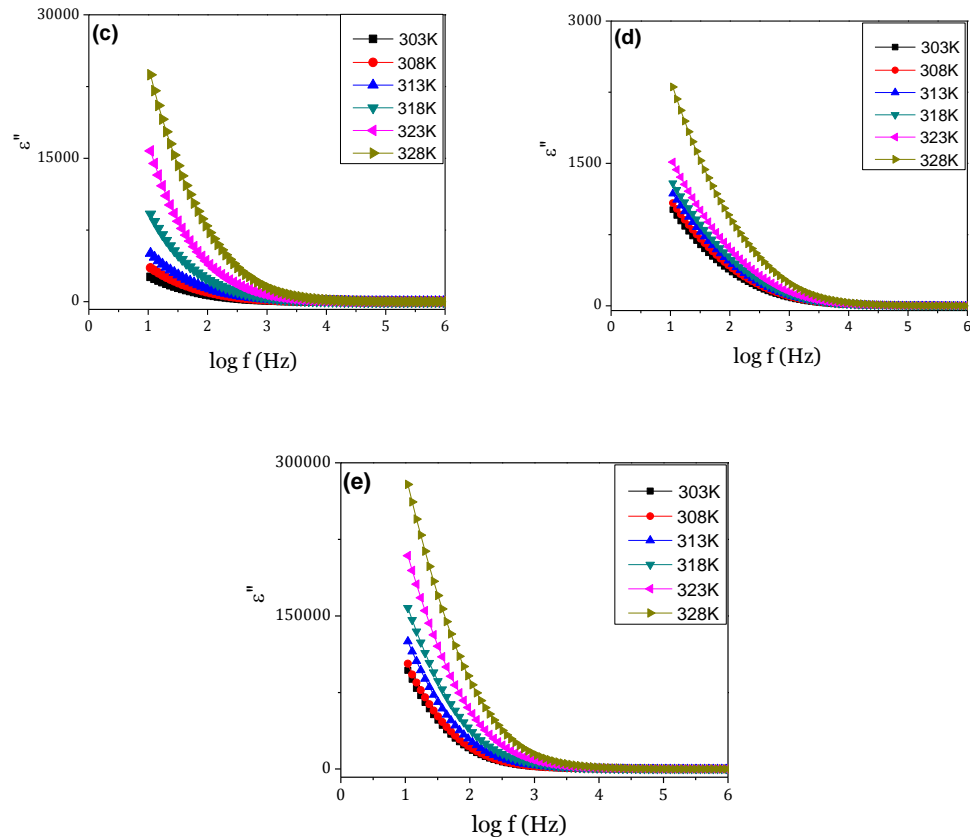


Fig. 6.11 Frequency dependent ε'' variation for (c) PLA-3, (d) PLA-4 and (e) PLA-5 of PLA series at various temperatures. and ε'' towards low frequency with increase in temperature are also due to electrode polarization effects. The decrease of ε' and ε'' with frequency is attributed to the electrical relaxation process, but at the same time the material electrode polarization cannot be ignored as the samples are ionic conductors.

The material electrode interface polarization of the composites masks the other re-

laxation process at low frequencies. There is a significant effect of plasticizer on the value of ϵ' and ϵ'' with strong low frequency dispersion. The plasticizer results in more localization of charge carriers along with mobile ions causing higher ionic conductivity. This may be the reason for higher ϵ' and ϵ'' strong low frequency dispersion [17, 18].

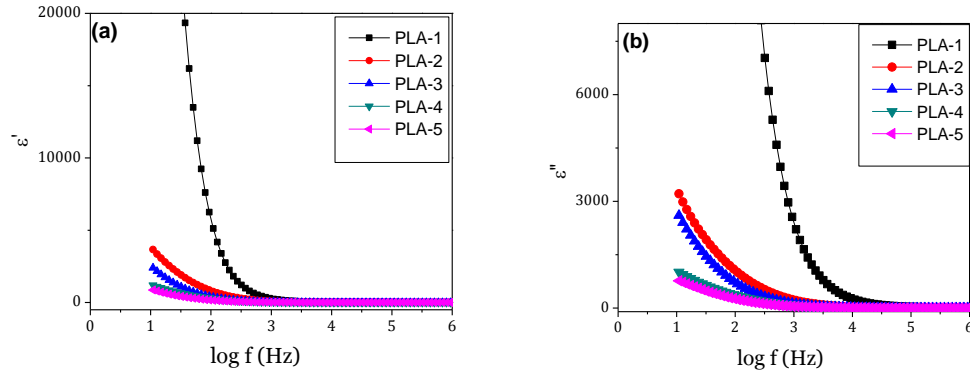


Fig. 6.12 The plot of (a) real part ϵ' and (b) imaginary part ϵ'' of dielectric permittivity for PLA System at 313K.

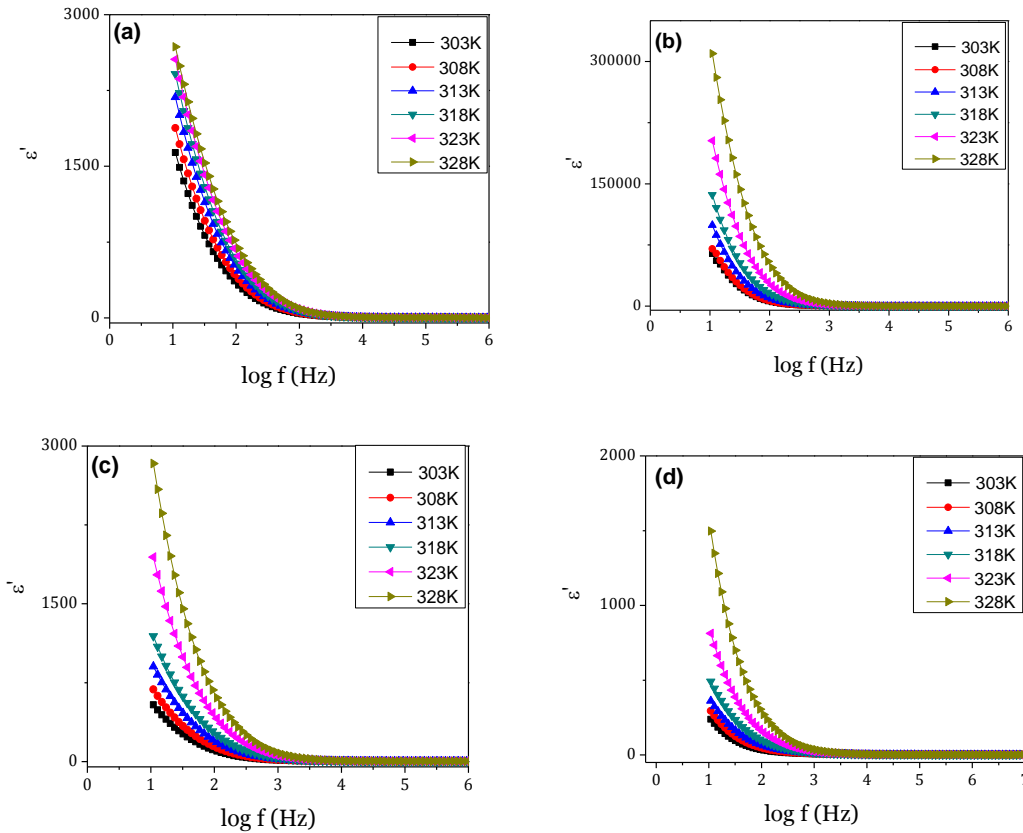


Fig. 6.13 Plot of ϵ' for (a) PLP-5, (b) PLP-10, (c) PLP-15, and (d) PLP-20 of PLP series at various temperatures.

It is observed that on increasing the temperature, dispersion frequency shifts towards higher frequency side in all the samples indicating that (i.e. above T_g) the polymer

chain becomes more flexible and increases charge carrier density with the increase in temperature. At high frequency, the data at different temperatures merges, revealing that dielectric constant ϵ' and dielectric permittivity ϵ'' are independent of temperature.

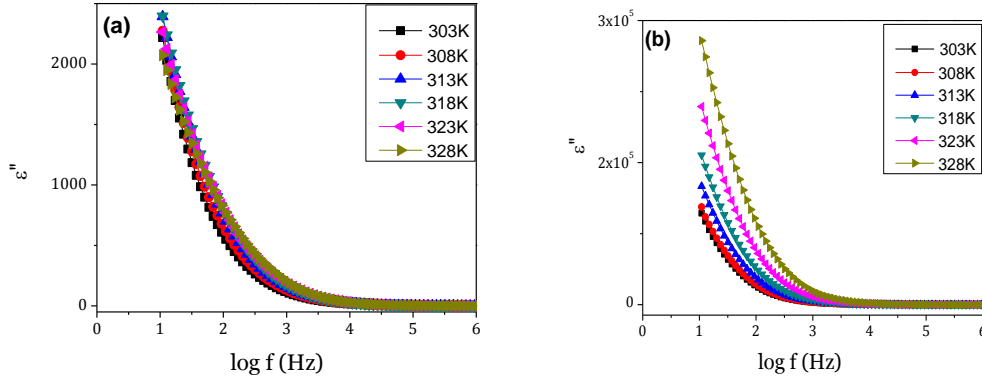


Fig. 6.14 ϵ'' variation as a function of frequency for (a) PLP-5 and (b) PLP-10 of PLP series at various temperatures.

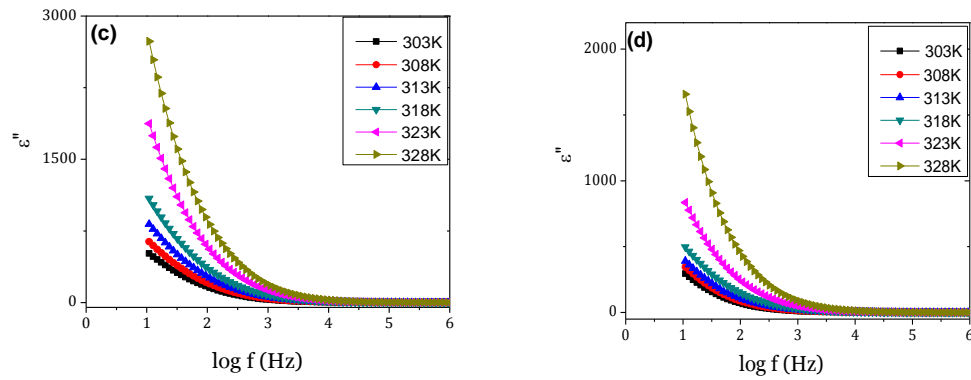


Fig. 6.14 ϵ'' variation as a function of frequency for (c) PLP-15 and (d) PLP-20 of PLP series at various temperatures.

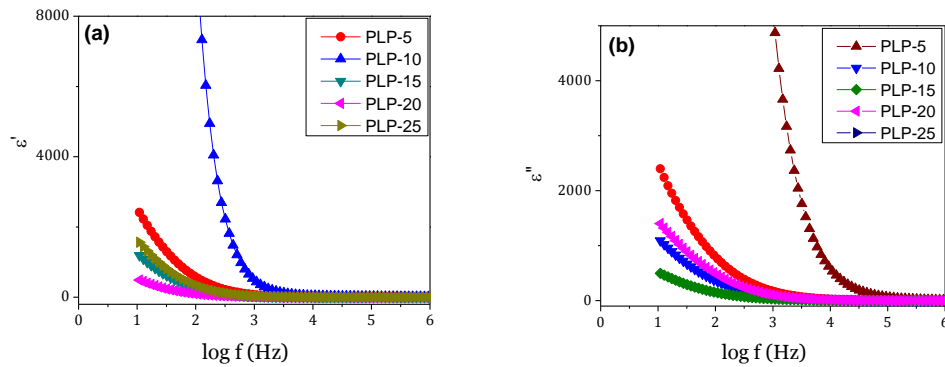


Fig.6.15 The plot of (a) real part ϵ' and (b) imaginary part ϵ'' of dielectric permittivity for PLP System at 313K

Figs.6.15 (a) and (b) show variation of dielectric permittivity i.e.; ϵ' and ϵ'' of PLP system at 303K. In this system, the dielectric constant increases with the increase in the PEG content up to 10wt% thereafter it reduces.

6.3 Modulus Analysis

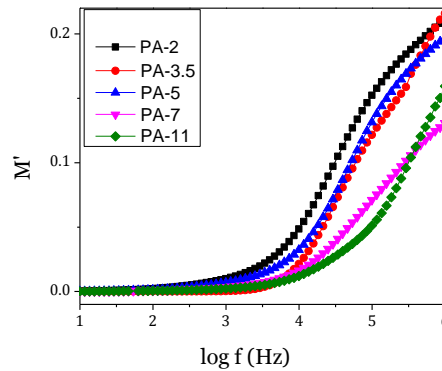


Fig. 6.16 A plot of real part M' of Modulus for PA series for different amount $AgCF_3SO_3$ at 313K.

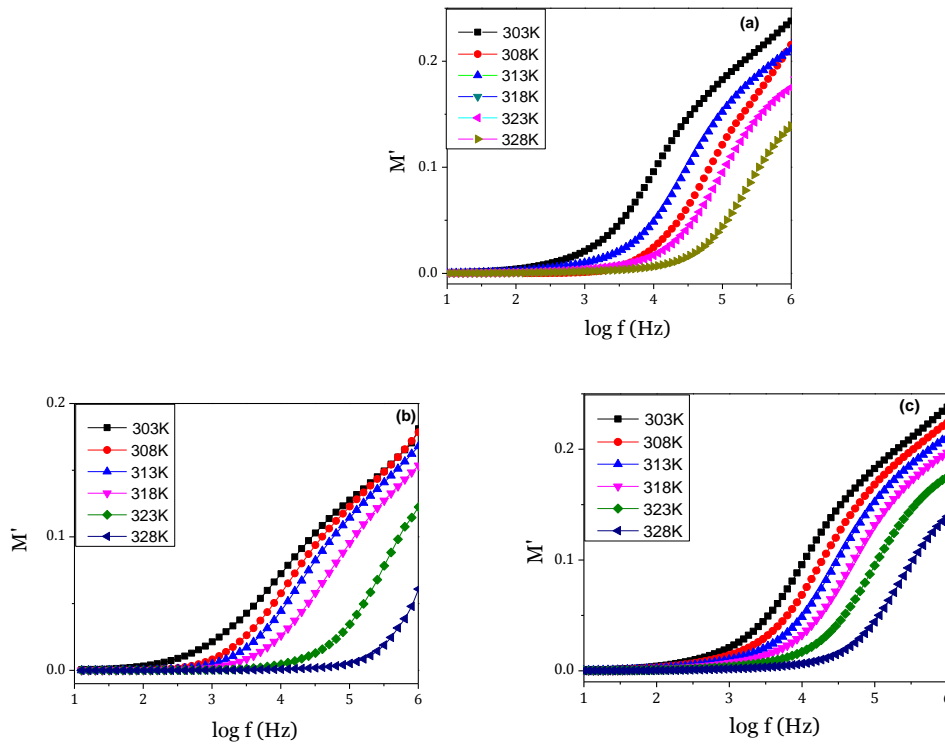


Fig.6.17 The real part M' of Modulus plots for (a) PA-2,(b) PA-3.5 and (c) PA-5 of PA series at various temperatures.

The dispersion behaviour of the conductivity in the frequency domain is more conveniently interpreted in terms of conductivity relaxation time τ , using the electrical modulus $M^* = 1/\epsilon^*$ representation [19].

Complex electric modulus M^* formalism is used frequently when the relaxation behaviour is supposed to be due to the motion of ions or electrons [19-21]. Although, initially modulus analysis employ to separate space-charge effects from the bulk conductivity, but

now the M^* representation is widely used to analyze ionic conductivities by associating a conductivity relaxation time (τ) with the ionic process [22]. The use of modulus formalism in presenting frequency dependent dielectric or conductivity data has the advantage of eliminating any spurious effect due to contacts or interfaces (Maxwell- Wagner effects) [20]. The dielectric modulus parameter also represents the bulk dielectric behaviour of the polymer electrolytes because of the elimination of polarization effect [21].

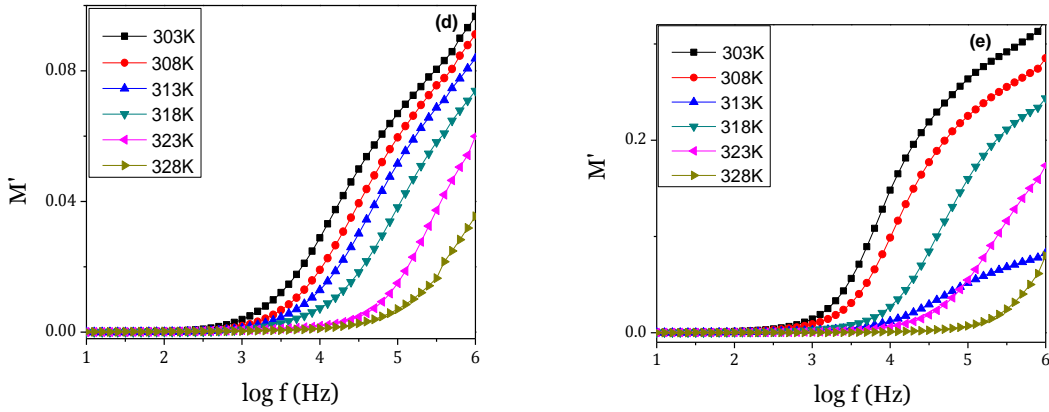


Fig.6.17 (d) & (e) M' plot for (d) PA -7 and (e) PA-11 of PA series at various temperatures.

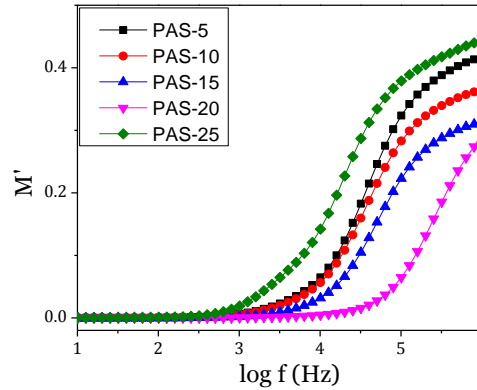


Fig.6.18 A plot of real part M' of Modulus for PAS series for different amount SiO_2 at 313K.

Figure 6.16 shows the real part of the modulus spectrum of PA system for various composition of salt AgCF_3SO_3 at 313K. The value of M' at different concentration of AgCF_3SO_3 approaches to zero, at low frequencies, which indicates that the electrode polarization make negligible contribution to M^* and lack of restoring force flow of charges under the influence of steady electric field [20]. At higher frequencies, M' attains a max

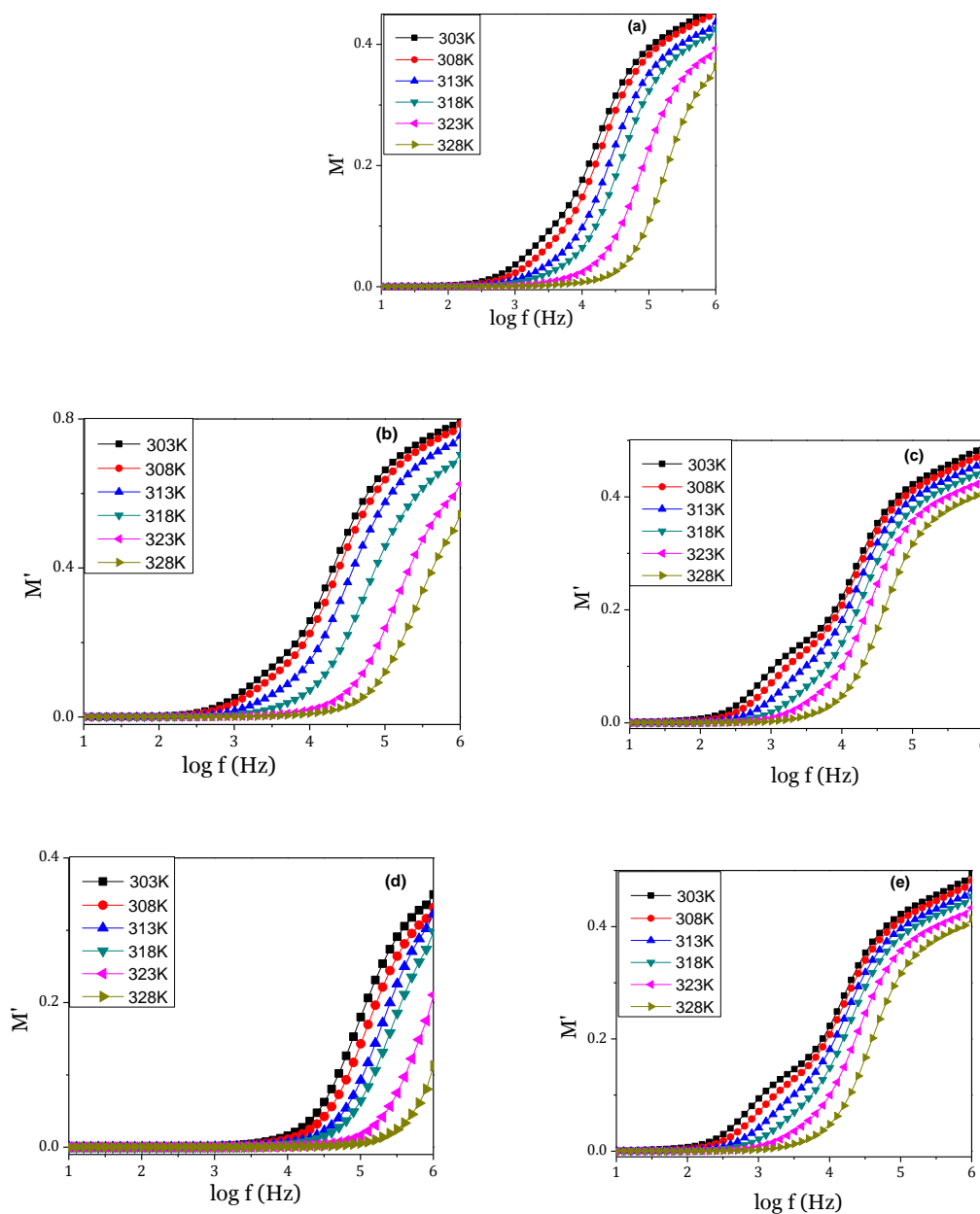


Fig. 6.19 M' plots for (a) PAS-5, (b) PAS-10, (c) PAS-15, (d) PAS-20 and (e) PAS-25 of PAS series at various temperatures. The dispersion is observed in the range from 10^3 to 10^4 Hz.

While looking into the spectra (Figs. 6.17(a) to (e)) of all the samples of this series at various temperatures, it is observed that the dispersion spreads over wide range of frequencies. And the maximum value of M' decreases with increase in temperature. This decrease in peak value indicates increase in the mobility of the polymer segment and ions with the temperature because the orientation of the charge carriers and molecular dipoles is easier at high temperature.

When, the nano-filler SiO_2 , which generally increases the amorphous level in the electrolytes [23], is added in PA system, the real part of modulus (Fig. 6.18) shows the large change in dispersion frequency i.e., 10^3 to 10^5 Hz and a shifting of dispersion towards higher frequency side with nano-filler except for 25 wt% of SiO_2 . The real part of modulus (M') of all the samples at different temperatures (Fig. 6.19) shows the shift of dispersion towards high frequency side as in the case of PA system. The peak values of M' are increased with the addition of nano-filler in PAS system which indicates the increase in conductivity of the samples.

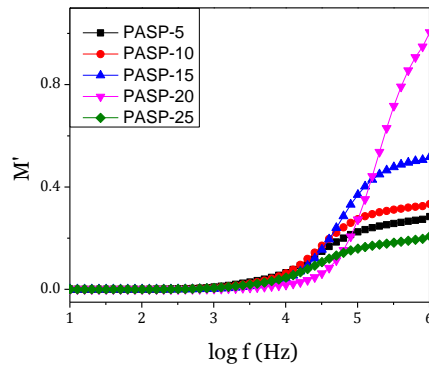


Fig. 6.20 A plot of real part M' of Modulus for PASP series for different amount PEG at 313K.

Generally, with the intension to increase the flexibility of polymer matrix low molecular weight plasticizer is added to nano-composite polymer electrolyte. As plasticizer can interrupt polymer-polymer interactions by occupying inter and intra-chain free volume [24]. This decrease in polymer-polymer interaction affects the flexibility of the polymer matrix. The plot of real part of modulus M' for the next system, where the amount of plasticizer PEG is varied and the amount of salt (AgCF_3SO_3) and nano-filler (SiO_2) are kept constant is shown in Fig. 6.20 for various PEG contents at 313K. It is observed that on increasing the PEG amount, the dispersion is confined to particular frequency (10^4 Hz). PEG instead of increasing inter- and intra chain separation, it forms long chains due to the similar structural nature of PEO and PEG. This reduces the flexibility and level of amorphous nature of the system. In addition to this, Fig. 6.20 indicates the shifts of dispersion towards higher frequency side on increasing the plasticizer content except for 25wt%. Temperature dependence of M' variation plots for different compositions of PASP-system are depicted in Fig. 6.21 (a) to (e). With the increase in temperature, the

dispersion frequency shifts towards high frequency side.

The real (M') part of all samples of PLA series in which salt AgCF_3SO_3 is been replaced by LiCF_3SO_3 and nano-filler SiO_2 by Al_2O_3 are shown in Fig. 6.22. It is obvious that at lower frequencies, M' values are very small and tend to zero, indicating the

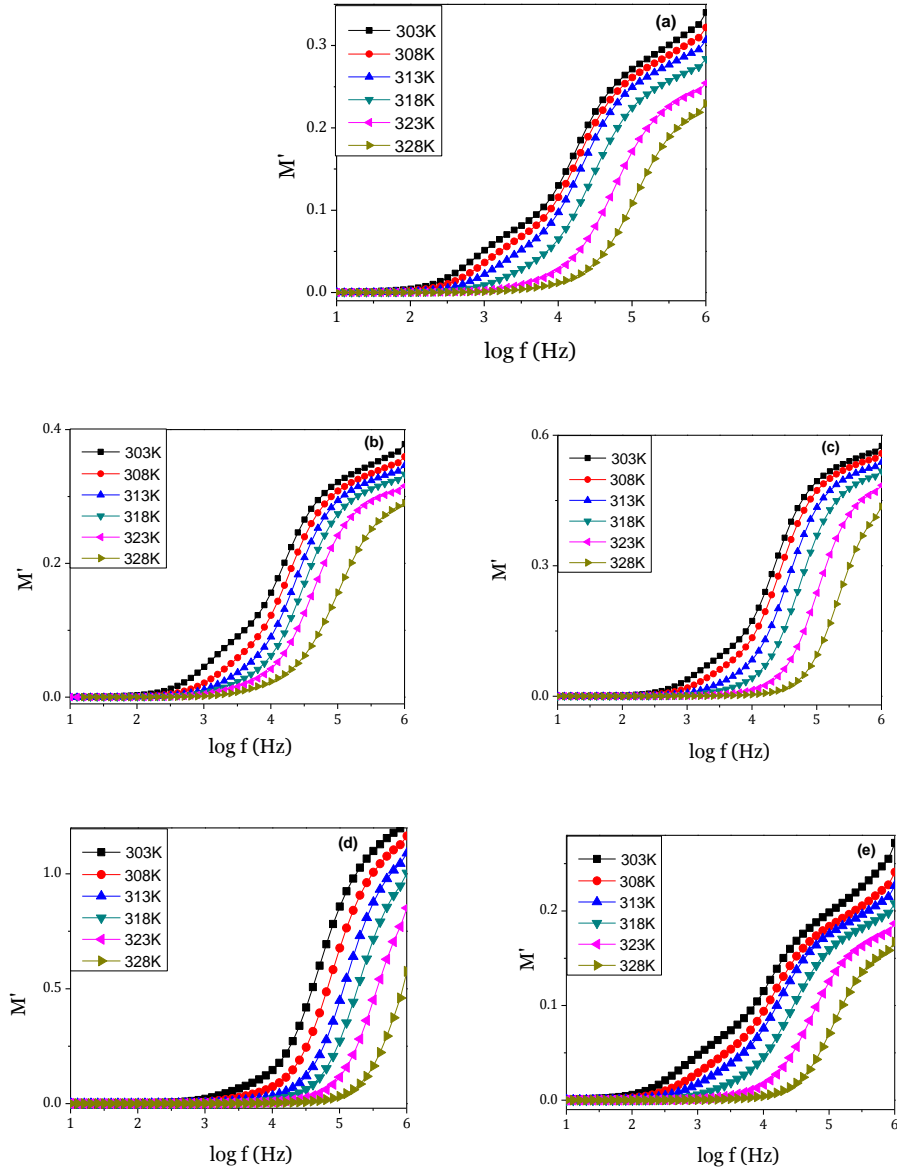


Fig. 6.21 The M' plots for (a) PASP-5, (b) PASP-10, (c) PASP-15, (d) PASP-20 & (e) PASP-25 of PASP series at different temperatures. suppression of electrode polarization [25]. The nature of the graph does not alter for LiCF_3SO_3 salt and nano-filler Al_2O_3 . The temperature dependence of real part of modulus (Fig. 6.23) at high frequency is observed, suggesting singularity of relaxation mechanism. The sample with 3wt% of Al_2O_3 shows dispersion along with shifting with increasing

temperature.

The real M' part of modulus for different amount of plasticizer PEG as a function of frequency at 313K is shown in Fig. 6.23 for PLP series. A wide range of dispersion

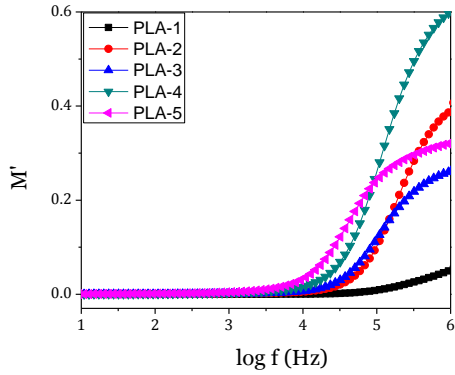


Fig. 6.22 M' plot for PLA series at 313K.

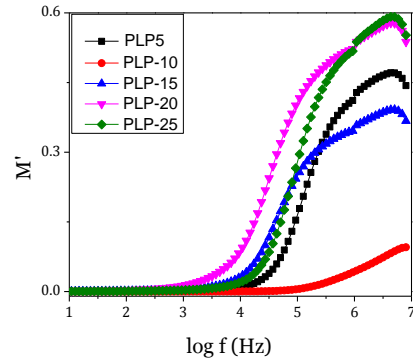


Fig. 6.23 M' plot for PLP series at 313K.

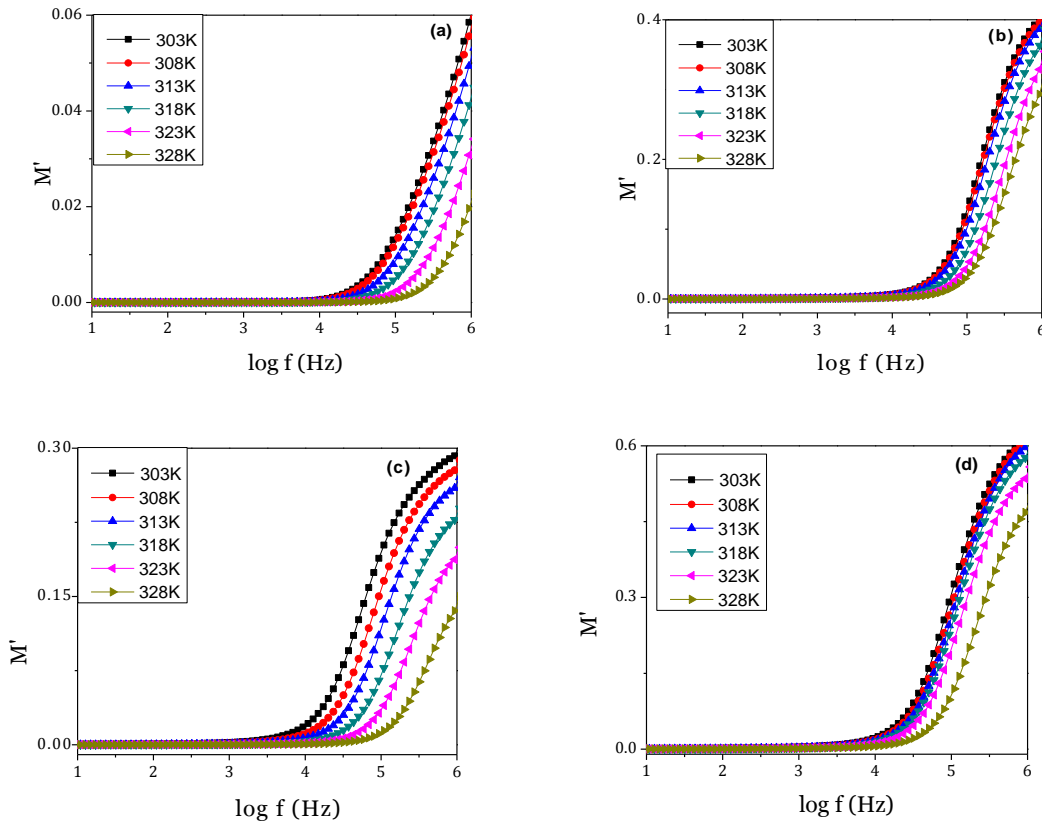


Fig. 6.24 M' plots for (a) PLA-1, (b) PLA-2, (c) PLA-3, and (d) PLA-4 of PLA series at various temperatures.

i.e., from 10^2 to 10^5 Hz along with the shifting towards higher frequency side is observed.

The real part of modulus (M') at different temperatures are shown in Figs. 6.24(a) to (e),

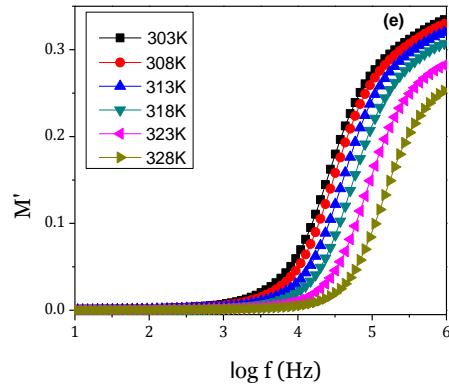


Fig. 6.24 (e) M' plot for PLA-5 of PLA series at various temperatures.

in which the spectrum shifts towards lower frequency side except for 10wt% PEG. All the plots are observed to show 'S' shaped characteristic feature which is an indication of ionic conductors [26].

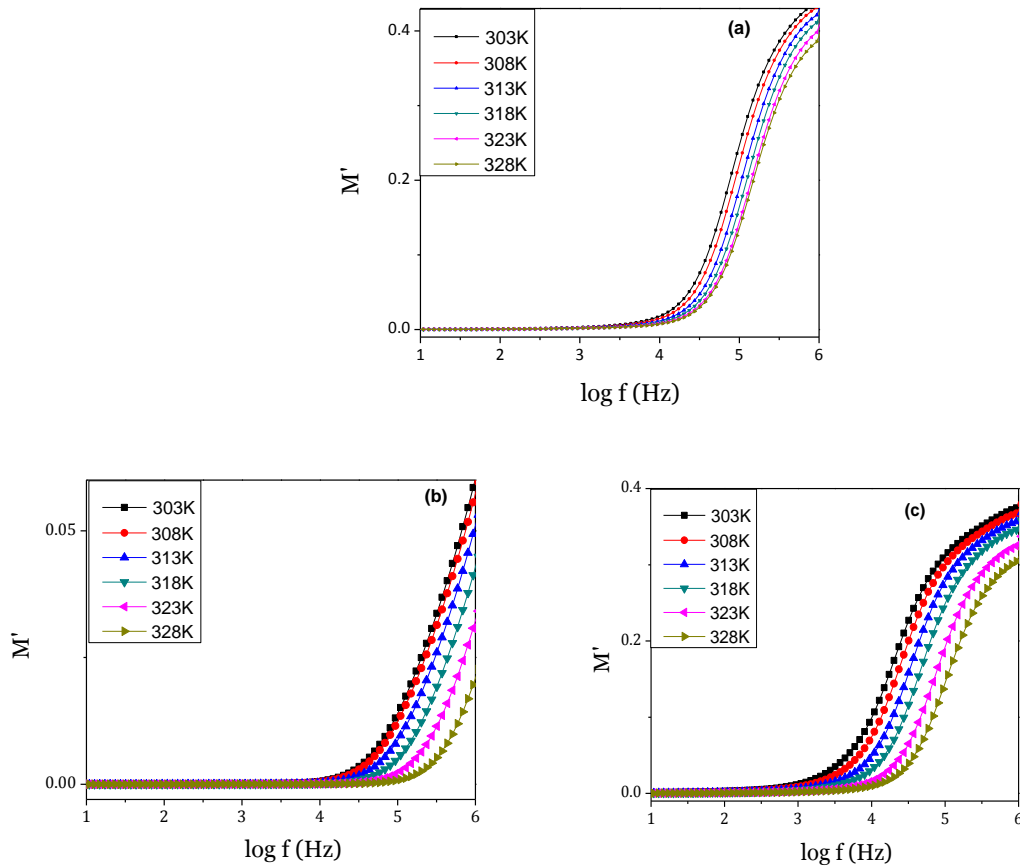


Fig. 6.25 (a)-(c) The M' spectra for (a) PLP-5, (b) PLP-10 and (c) PLP-15 of PLP series at various temperatures.

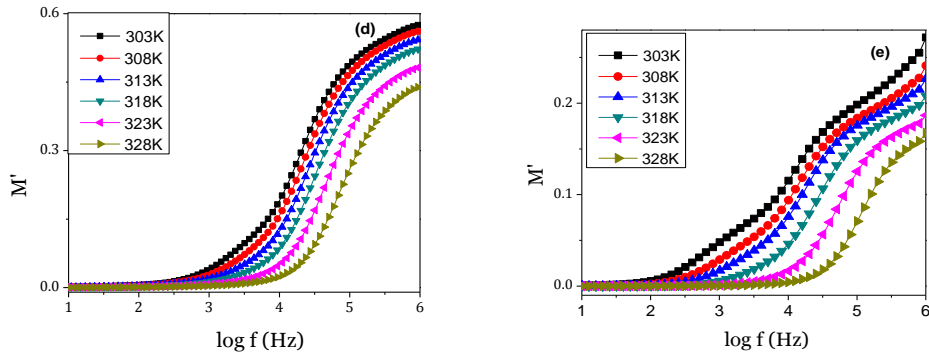


Fig. 6.25 (d) & (e) The M' spectra for (d) PLP -20 and (e) PLP-25 of PLP series at various temperatures.

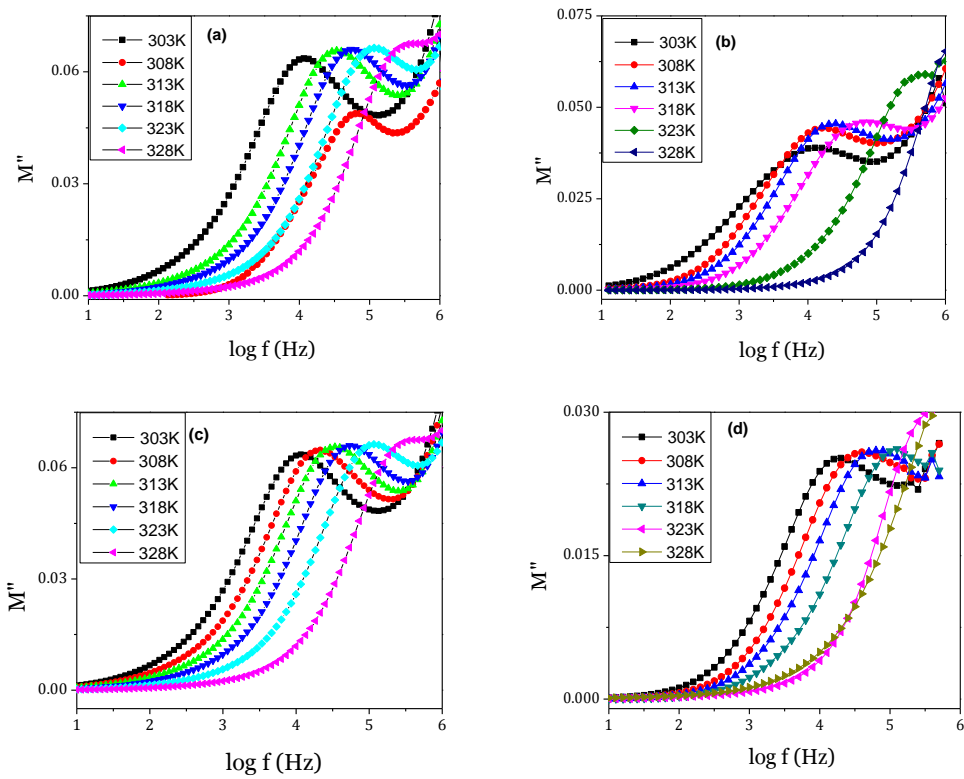


Fig. 6.26 M'' spectra for (a) PA-2, (b) PA -3.5, (c) PA-5 and (d) PA -7 of PA series at various temperatures.

Now, the variation of the imaginary part of the modulus (M'') with frequency at different temperatures for all the samples for PA series is shown in Fig. 6.26 (a) to (e). Similar to M' spectra, the M'' plots also show a long tail at low frequencies. It is also seen that M'' spectra have an asymmetry of the peak approximately centered in the dispersion region of M' . The observed long tail behavior at low frequencies is the result of the large capacitance associated with the electrodes [27, 28]. In the low frequency region which the ions can move over long distance i.e., ions can perform successful hopping from one site to

the neighboring site. On the other hand, the high frequency wing of the M'' peak suggests that the ions are spatially confined to their potential wells and can make only localized motion within the wells [29]. It is clear from above figure that the shape of the spectrum remains constant but the frequency of the modulus maximum M''_{max} shifts to higher frequency side with increase in temperature. It may also be noted that the magnitude of M'' peak with temperature is found to be constant. The constancy of the height of the modulus plot suggests the invariance of the dielectric constant and distribution of relaxation times with temperature [30, 31]. The imaginary part M'' of modulus spectra for various amount of AgCF_3SO_3 at 313 K are shown in Fig. 6.27. It is observed that with increasing the amount of AgCF_3SO_3 , the M''_{max} peak shifts towards higher frequency side i.e., relaxation time decreases till 7wt%. It means, the increasing amount of salt content

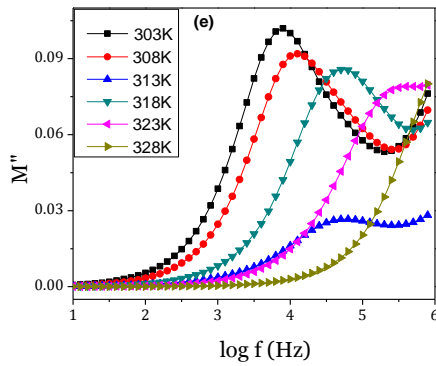


Fig. 6.26 (e) M'' spectra for PA-11 of PA series at various temperatures.

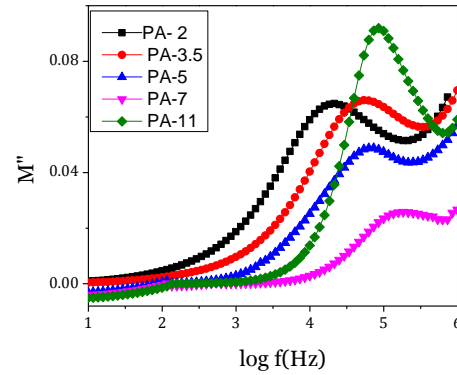


Fig. 6.27 M'' plot for PA series at 313K.

supplies the larger number of charge carriers but after 7 wt%, the process of ion association must have started and the system turning into less flexible resulting into the shifting of M''_{max} peak towards the lower frequency side.

The variation of the imaginary part of modulus, M'' with frequency at different temperatures for all sample of PAS system in which the amount of nanofiller SiO_2 is varied is shown in Fig. 6.28. The shape of the spectrum remains same as that observed in PA series but, in the present case not only the peak of M''_{max} shifts towards the higher frequency side, but an increment in the peak height is also observed along with rise in temperature. The inconstancy of the height of modulus plot is an indication the variance of dielectric constant.

The Fig. 6.29 shows the M''_{max} Peak shift towards higher frequency side with in-

creasing the amount of SiO₂ till 20wt%. The presence of SiO₂ makes the system more amorphous and increases the intra chain distances. However, the flexibility reduces due to the cluster formation after optimum value, resulting into the shifting of M''_{max} peak towards lower frequency side.

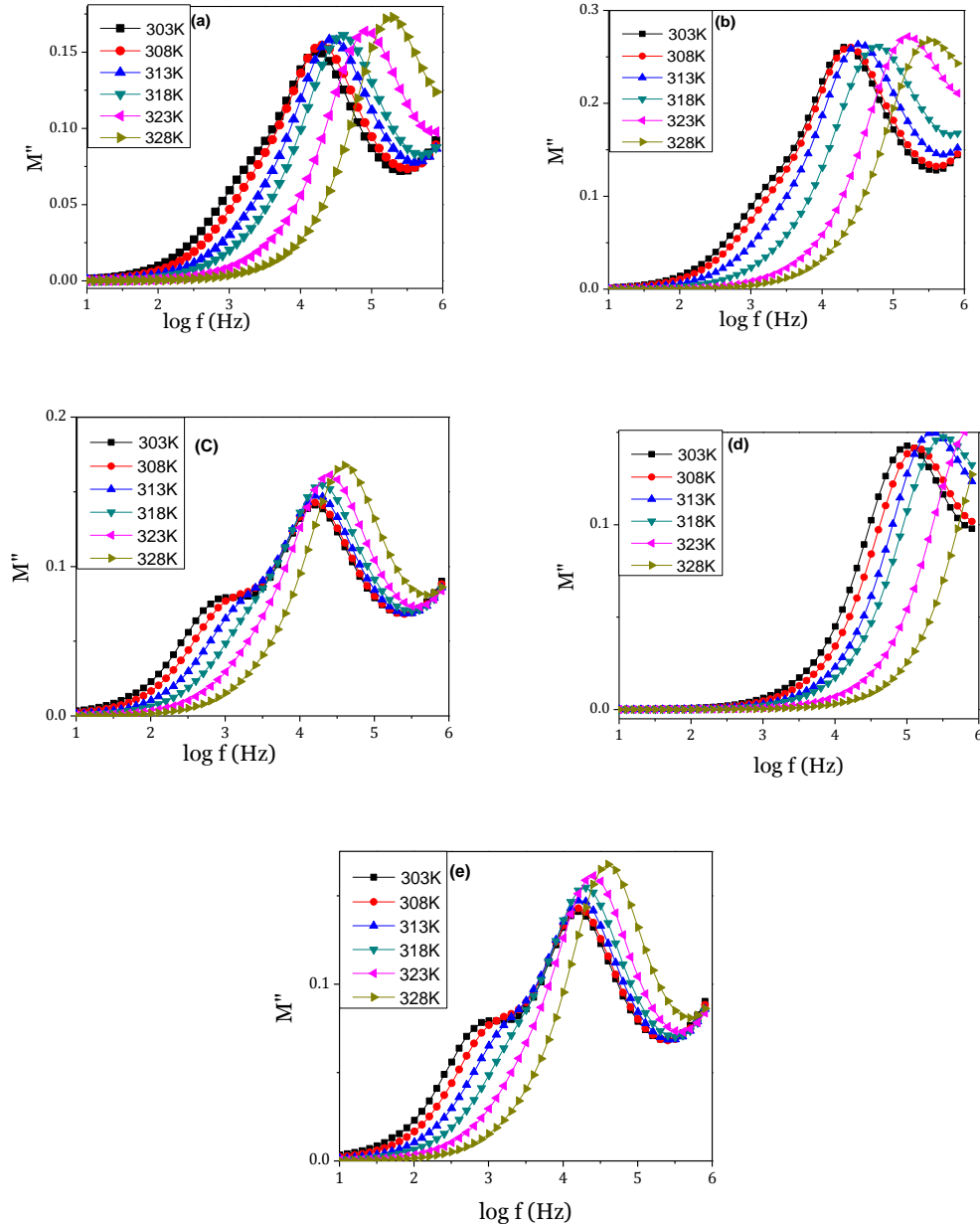


Fig. 6.28 M'' spectra (a) PAS-5, (b) PAS-10, (c) PAS-15, (d) PAS-20 and (e) PAS-25 of PAS series at different temperatures.

In the polymer nano-composite composition with highest ionic conductivity (Chapter 5), the plasticizer PEG is added. Generally, plasticization of polymer nano composites improves the ionic conductivity and the amorphous content of polymer electro

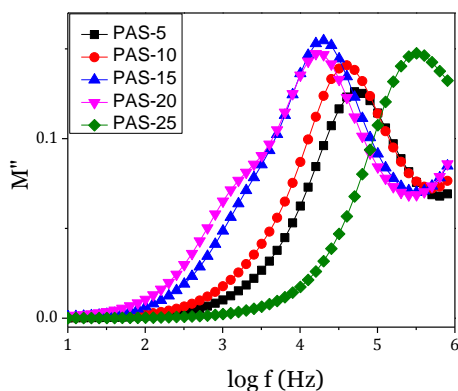


Fig. 6.29 M'' spectra for PAS series at 313K.

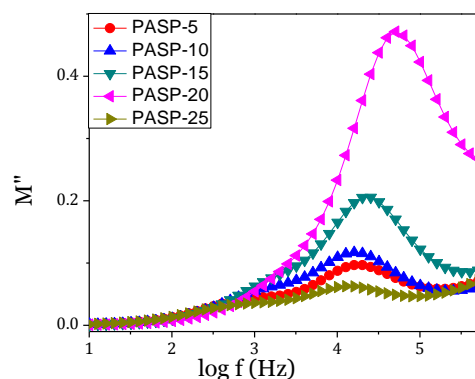


Fig. 6.30 M'' spectra for PASP series at 313K.

lytes [32]. Figs. 6.30 (a) to (e) show the plot of imaginary part of the modulus (M'') with frequency for all samples of PASP series at different temperatures. Beside, the shifting of peak values towards higher frequency side, the magnitude of the peak levels off on addition of plasticizer PEG. However, no appreciable shifting is observed on increasing the amount of PEG in the values of imaginary part of modulus in Fig. 6.31. But, for sample with 20wt% PEG, the peak intensity has shifted slightly towards higher frequency side, which is in accordance with conductivity variation.

The frequency dependent M'' plots at different temperatures for all the samples of PLA series, wherein the silver salt is replaced by lithium salt and nano-filler SiO_2 is replaced by Al_2O_3 , are shown in Figs.6.32 (a) to (e). Similar to silver and other solid electrolytes [25, 27, 28], the spectra of M'' shifts towards high frequency side with the rise in temperature. M'' spectra for various concentrations of Al_2O_3 in PLA systems at 313 K are shown in Fig. 6.33. With increasing the amount of Al_2O_3 the M''_{max} peak shifts towards lower frequency side after 1wt%. This observation clearly indicates that larger amount of the nanofiller Al_2O_3 does not support conduction mechanism because the system becomes more crystalline confirmed from XRD results.

The frequency dependent plot of imaginary part of modulus, M'' for various amounts of PEG in PLP series (Fig. 6.34) indicates the shift of peak of M''_{max} towards higher frequency side up to 10wt% PEG thereafter in opposite side. The temperature dependent M'' spectrum of different samples of PLP series are shown in Figs.6.35 (a) to (e).

The peaks of M'' are related with the translational ion dynamics and mirrors the

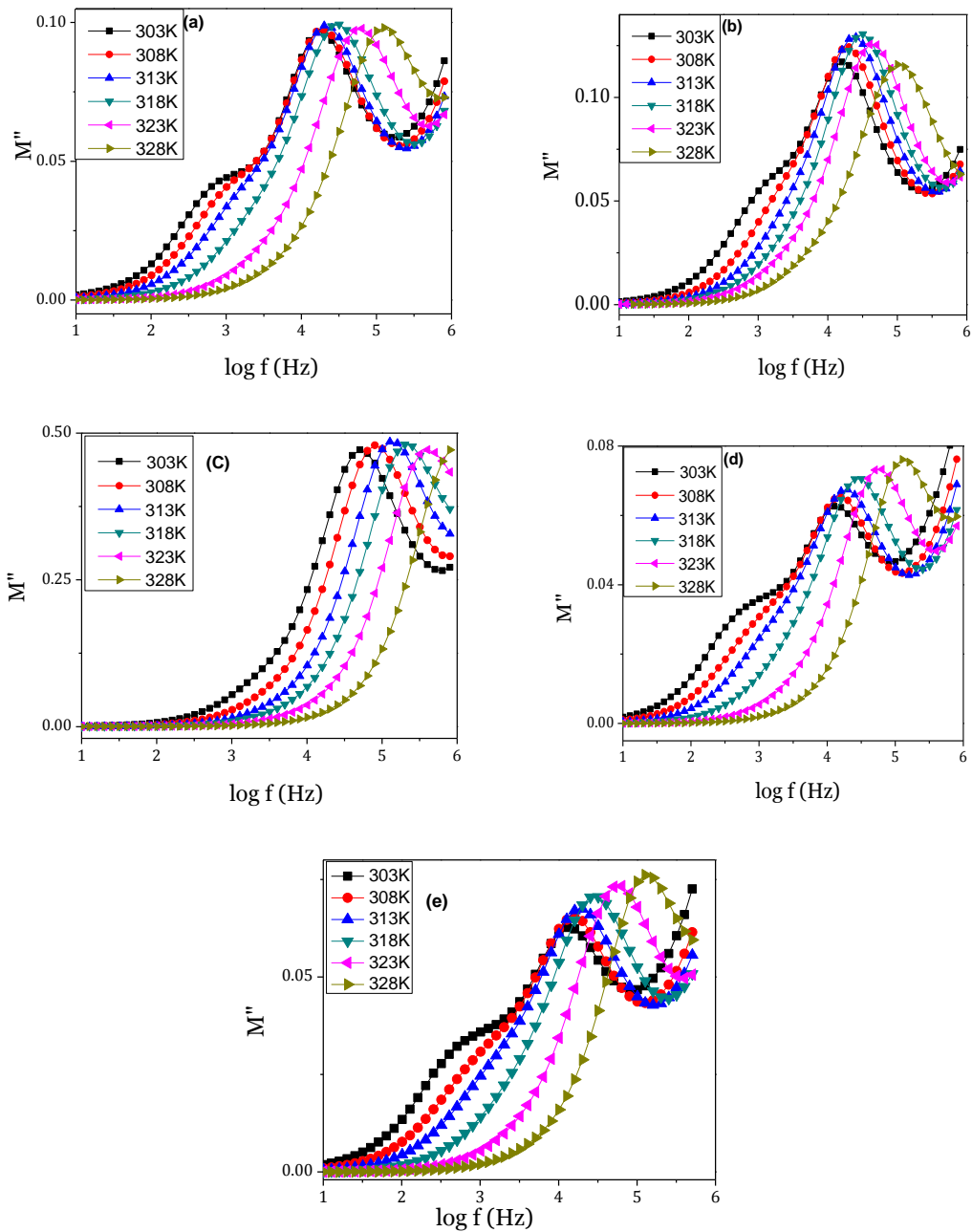


Fig. 6.31 M'' spectra for (a) PASP-5, (b) PASP-10, (c) PASP-15, (d) PASP-20 & (e) PASP-25 of PASP series at various temperatures.

conductivity relaxation of the mobile ions. It is worth noticing that the relaxation peak is owing to ‘fast segmental motion’ which is responsible for reducing the relaxation time—consequently the transport properties. It is clear from all above figures that the frequency of the modulus maximum M''_{max} shifts to higher frequency side with increase in tempera-

ture. The magnitude of M'' peak with temperature is found to be constant for samples with plasticizer.

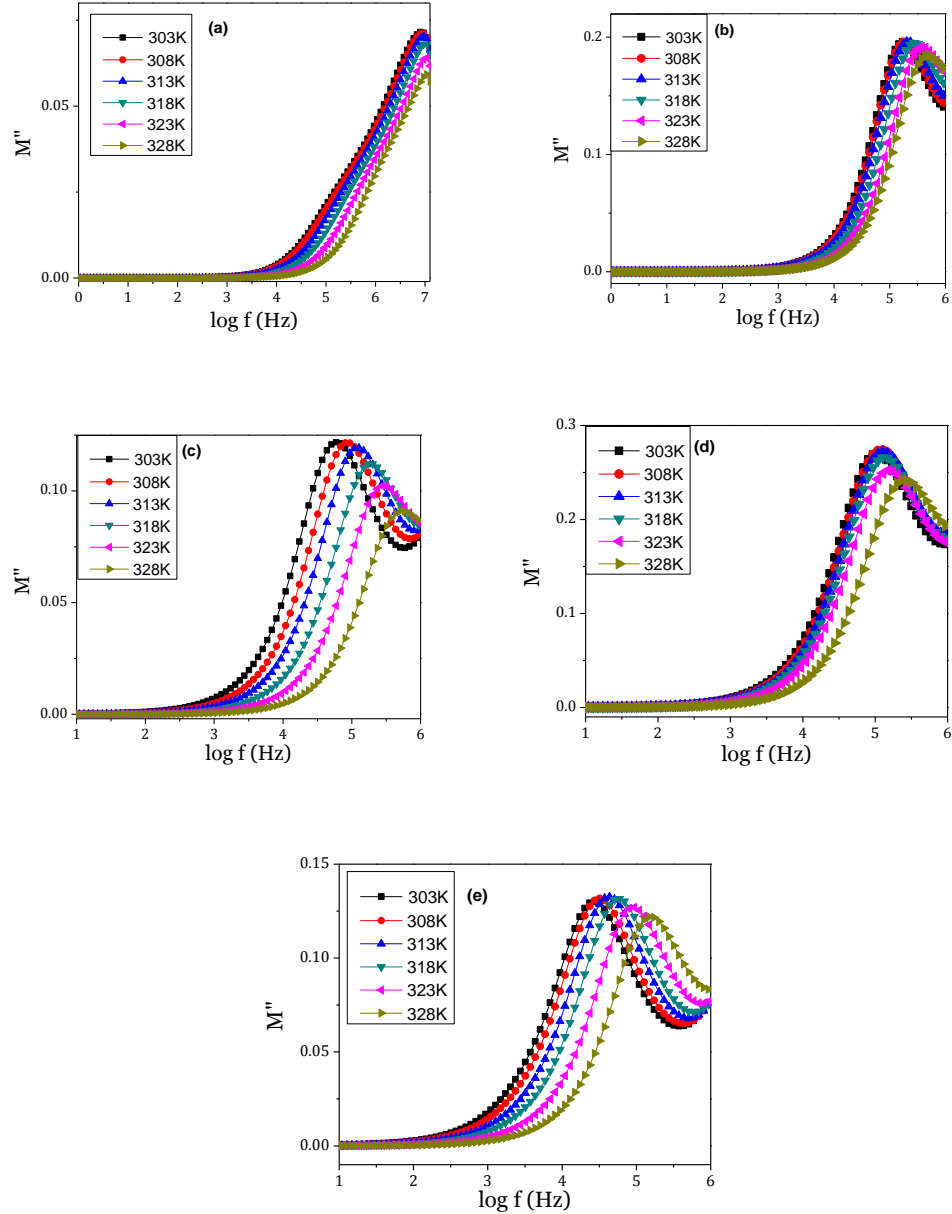


Fig. 6.32 M'' spectra for (a) PLA-1, (b) PLA -2, (c) PLA-3, (d) PLA -4 and (e) PLA-5 of PLA series at different temperatures.

The peak frequency (f_{max}) of the modulus peak (M''_{max}) is assumed to represent a characteristic frequency of the conductivity relaxation [30]. Various parameters can be determined from its data. The obtained modulus plots are non-symmetric and are in agreement with the non-exponential behaviour of the electrical function [33] which is

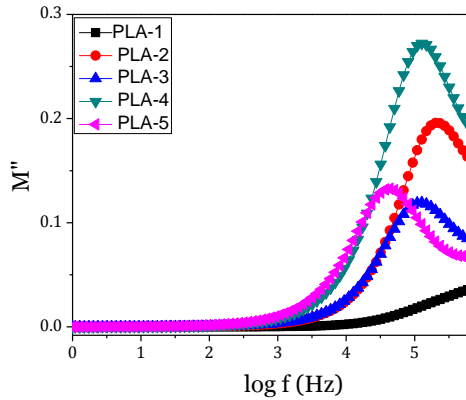


Fig. 6.33 M'' plot for PLA series at 313K..

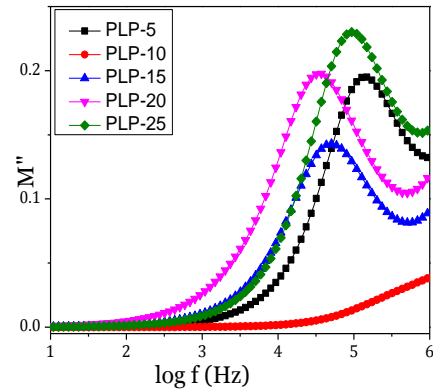


Fig. 6.34 M'' spectra for PLP series at 313K.

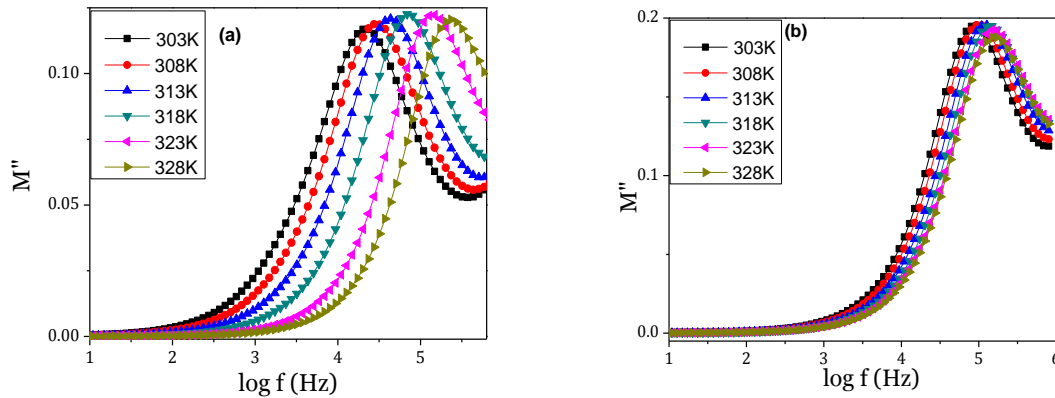


Fig.6.35 (a)&(b) M'' spectra for (a) PLP-5, (b) PLP -10 of PLA series at different temperatures.

well described by the Kohlrausch –William Watts (KWW) exponential function. This stretched exponential function was first introduced by R. Kohlrausch [34] in 1854 to describe the discharge of a capacitor. This exponent is often used as a phenomenological description of relaxation in disordered systems. But, in 1970, G. Williams and D.C. Watts used the Fourier transform of the stretched exponential to describe dielectric spectra of polymers; in this context, the stretched exponential or its Fourier transform are also called the Kohlrausch-Williams-Watts (KWW) function. [35]. Generally, the value of stretched exponent β lies between 0 and 1 has great significance, but compressed exponential function of value greater than 1 i.e. $\beta > 1$ has less practical importance, with the notable exception of $\beta = 2$, which gives the normal distribution.

In present case, the value of stretched exponent β can be evaluated by knowing the full width at half height (FWHH) of the M'' plot, where $\beta = (1.14 / \text{FWHH})$ value. The value of β , at ambient temperature for other samples are given in table 6.1, which gener-

ally lies between 0 and 1. Considering β parameter smaller than 1, some authors [39-41] have suggested that it can be correlated to a distribution of relaxation times in the materials. In the PA series, the width at half height of the modulus spectrum for the sample with 7 wt% of AgCF_3SO_3 at different temperature is close to 2.2 decades and the β results in the value of 0.50.

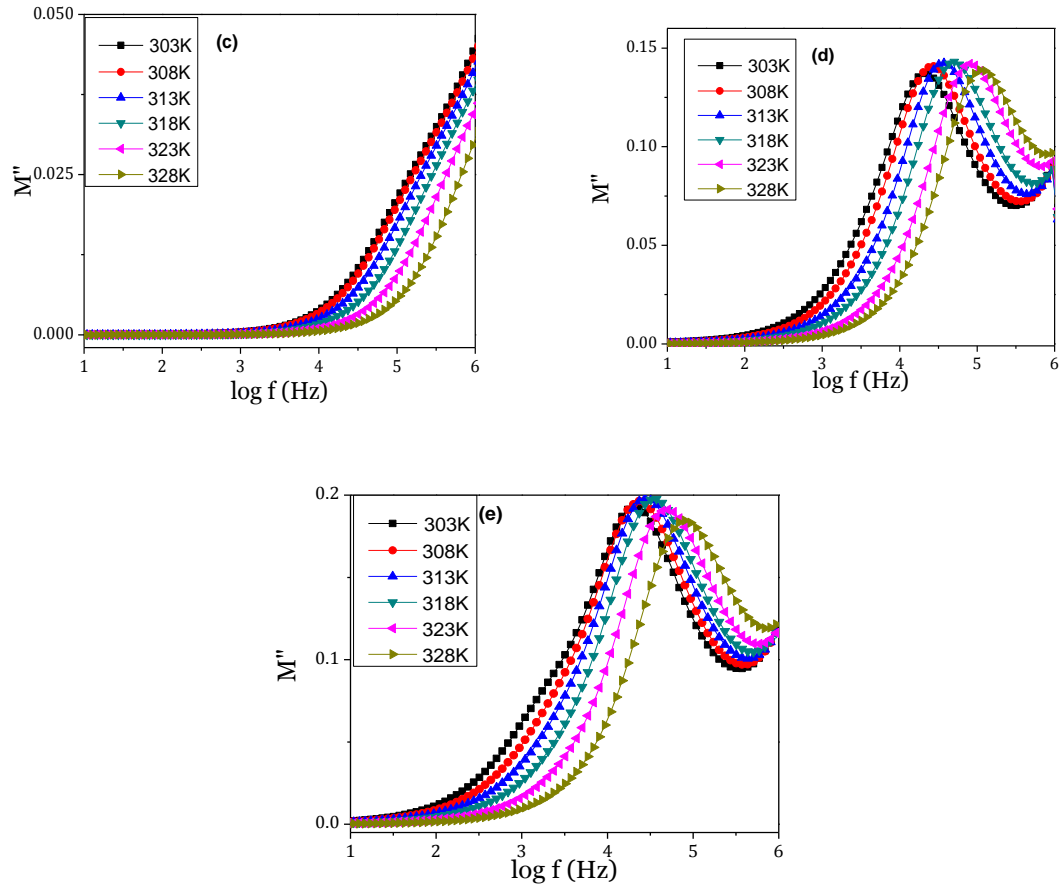


Fig. 6.35 (c)-(e) M'' spectra for (c) PLP-15, (d) PLP-20 and (e) PLP-25 of PLA series at different temperatures.

In the present investigated systems, the values of β seems to level off in the range 0.56 -0.67, which is found to be insensitive to the variation of temperature and composition. At low temperature, the relaxation occurs via isolated non interacting dipoles, becoming more and more Debye like and β values tend towards unity [42] and also there is a general tendency of β to decrease with temperature.

In the PAS series, the width at half height of the modulus spectrum at different temperatures is 2.05 decades and the β results in the value of 0.67 for 20wt% of SiO_2 and the values of β ranges from 0.47 to 0.67 for different amount of SiO_2 . While the width

at half height of the imaginary part of modulus is close to 1.5 decades in the PASP series, where the amount of PEG has been varied, and the β value of sample 5wt% of PEG is observed to be 0.76 and the value for different amount of PEG are confined between 0.6-0.7.

Table 6.1 KWW exponential function β from modulus plot of all five series

PA - SERIES		PAS - SERIES		PASP - SERIES		PLA - SERIES		PLP - SERIES	
Sample	β	Sample	β	Sample	β	Sample	β	Sample	β
PA-2	0.60	PAS-5	0.60	PASP-5	0.76	PLA-1	0.91	PLP-5	0.81
PA-3.5	0.67	PAS-10	0.54	PASP-10	0.67	PLA-2	0.76	PLP-10	0.91
PA-5	0.67	PAS-15	0.47	PASP-15	0.65	PLA-3	0.63	PLP-15	0.87
PA-7	0.6	PAS-20	0.67	PASP-20	0.76	PLA-4	0.54	PLP-20	0.84
PA-11	0.63	PAS-25	0.47	PASP-25	0.76	PLA-5	0.95	PLP-25	0.76

In a series with Lithium triflate i.e., PLA series, the modulus spectrum at different temperatures provides β values in the range of 0.5 to 0.9. On the other hand, with the addition of plasticizer PEG in PLP series, such a large distribution is not observed and the width at half height is close to 1.5 decades and the β value of the sample 25wt% of PEG is found to be 0.76.

The efforts carried out by ionic charge carriers within the polymer materials to follow the change in the direction of applied field results in the occurrence of relaxation time [30]. Relaxation time τ is obtained from the frequency corresponding to M''_{max} value and from the condition $\tau = 1/2\pi f_{max}$, where τ is the estimated relaxation time for the ionic charge carrier [42]. The shift of M''_{max} towards high frequency with increasing temperature indicates that relaxation time decreases with temperature. The variation of relaxation time with temperature for sample PA-5 is presented in Fig. 6.36 (a) and it reveals that the temperature dependence of relaxation time appears to obey Arrhenius law [43-44]. The activation energy calculated from the slope of the Arrhenius plot is 1.02 eV. The variation of relaxation time $\log \tau$ as a function of composition (AgCF_3SO_3) salt at 313 K for PA series given in Fig. 6.36(b), reveals that with the increase in conductivity, the relaxation time decreases and vice versa. The relaxation time for sample 10wt% nano-

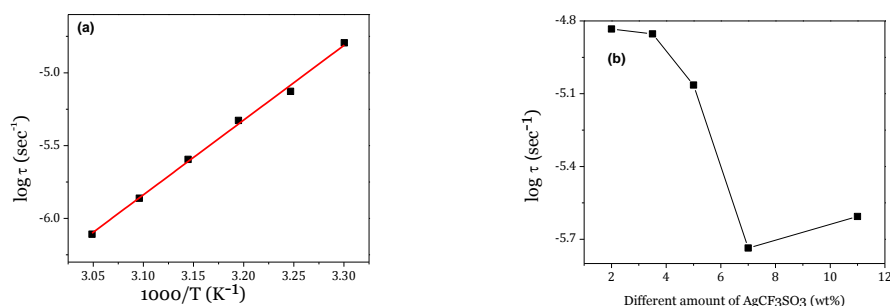


Fig. 6.36 Variation of relaxation time, τ (a) with temperature for PA-5 sample and (b) for different amount of $AgCF_3SO_3$ in PA-system at 313K.

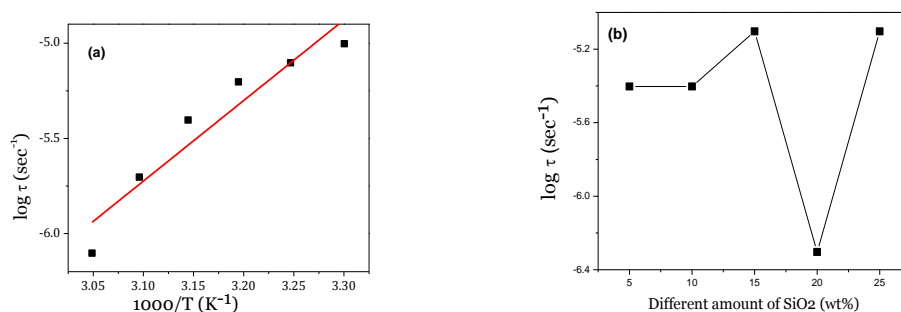


Fig. 6.37 Variation of relaxation time, τ (a) with temperature PAS-20 sample and (b) for different amount of SiO₂ PAS system at 313K

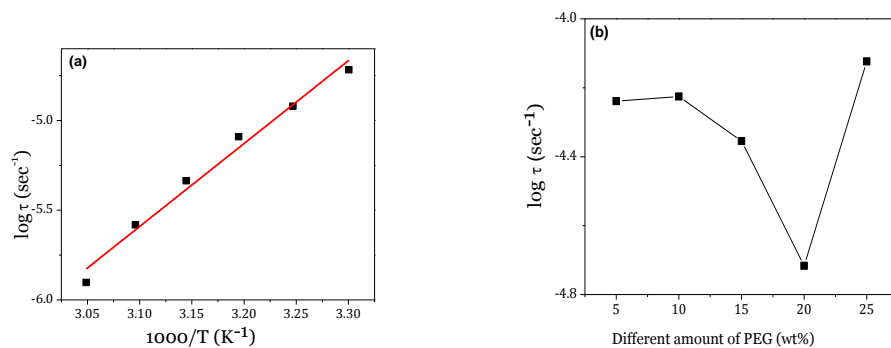


Fig. 6.38 Variation of relaxation time, τ (a) with temperature PASP-20 and (b) for different amount of PEG system at 313K.

filler SiO₂ in a PAS series shows [Fig. 6.37(a)] a thermally activated process and the activation energy obtained from the slope is observed to be 0.73 eV. It is clear that on addition of nano-filler, new conducting pathways are formed and the activation energy is decreased. The variation of relaxation time as a function of nano-filler SiO₂ at 313 K for PAS series in Fig. 6.37(b) shows the non-uniform behavior because of the generation of uneven conducting channels by nano-filler due to random dispersion.

On plasticization (PASP series), the relaxation time decreases with the tempera-

ture indicating again a thermally assisted process as shown in Fig. 6.38 (a). The activation energy obtained from the slope is 0.93 eV, which is higher than that of the sample in PAS series. With the addition of PEG, viscosity of polymer system changes and instead of decreasing, the overall effect is the increase in activation energy. The variation of relaxation time as a function of plasticizer is similar as observed for conductivity in Fig. 6.38 (b).

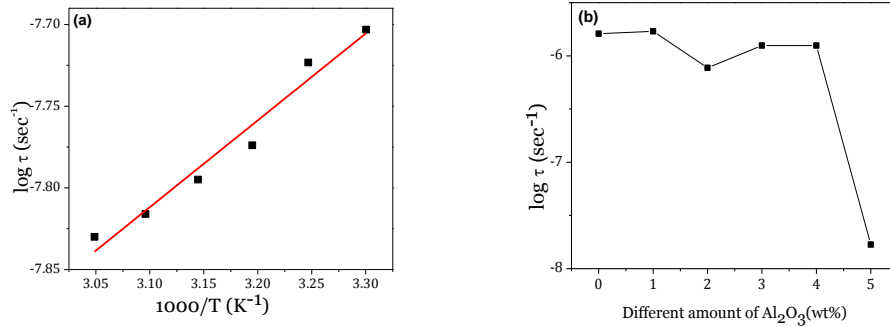


Fig. 6.39 Variation of relaxation time, τ (a) with temperature PLA-1 sample and (b) for different amount of Al₂O₃ PLA system at 313K.

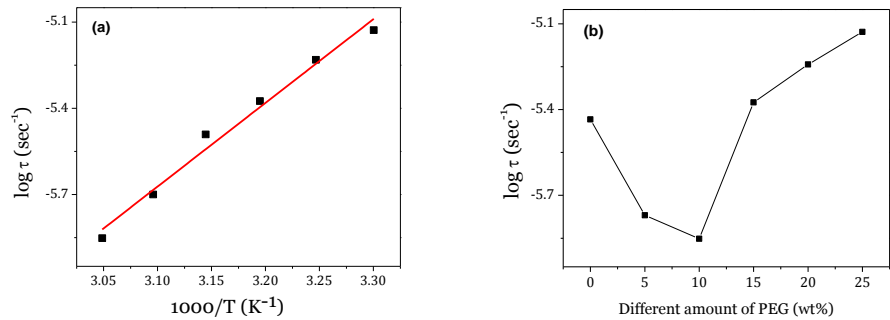


Fig. 6.40 Variation of relaxation time, τ (a) with temperature PLP-15 sample and (b) for different amount of PEG for PLP system at 313K.

In Lithium salt polymer electrolyte with 1wt% of Al₂O₃, relaxation time decreases with increase in temperature shown in Fig. 6.39(a). The activation energy in PAL system is found to be very low i.e., 0.12 eV whereas in silver based system (PAS), it is 0.73 eV ascribing that the conduction of lithium ions is faster than that of silver ion because of the smaller size of lithium ions. However, the variation of relaxation time with Al₂O₃ in PLA series [Fig. 6.39 (b)] is not similar to the variation of conductivity. The activation energy increases from 0.12 eV to 0.5 eV. In PAS and PLA series, the logarithm relaxation time and conductivity do not vary accordingly with composition. Due to the Lewis-acid base interaction between the filler surface and the CF₃SO₃⁻ anion, the nano filler (Al₂O₃) acts

as anionic acceptors and the surface area of filler grows which is responsible for increase in free volume. The drift of the motion of cations may be random in nature resulting in different relaxation times at different concentration of nano-fillers. For PA, PASP and PLP systems, the variation in relaxation time is observed to be in accordance with the variation in conductivity with the composition.

6.4 Scaling of Modulus

Universality of conductivity and dielectric relaxation processes in an ion conducting material can be established using scaling of respective spectra to show whether the processes are independent of charge concentration and/or are thermally activated. According to Sidebottom [45], for any dynamic process, by scaling, one may separate the thermodynamics from the inherent physics involved in the dynamical process which is

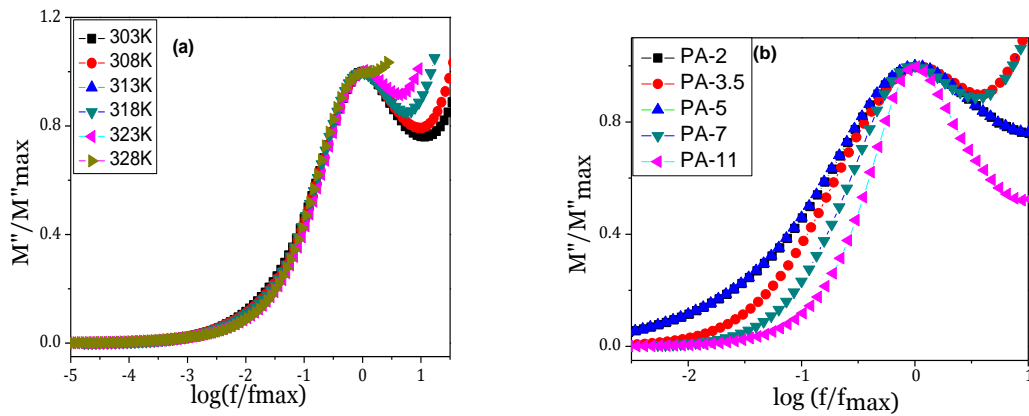


Fig. 6.41 Plot of M''/M''_{max} Vs. $\log(f/f_{max})$ (a) with temperature PA-5 sample and (b) for different amount of $AgCF_3SO_3$ in PA system at 313K.

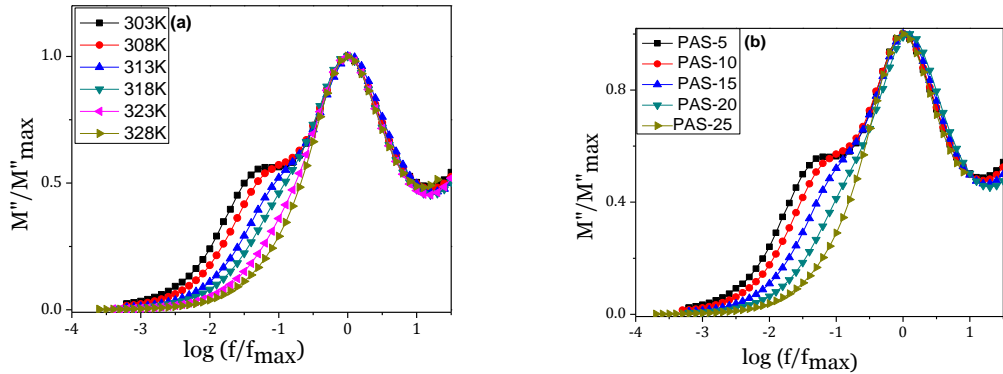


Fig. 6.42 Plot of M''/M''_{max} Vs. $\log(f/f_{max})$ (a) with temperature PAS-15 sample and (b) for different amount of SiO_2 in PAS system at 313K.

completely described by a single scaling function. To collapse all different data sets to one common curve is an indication that the process can be separated into a common physical mechanism modified only by thermodynamic scales [46].

The scaling in ac conductivity was proposed by Isard [47] for ion conducting glasses. In 1996, Sidebottom et al. [46] observed the conductivity master curve for alkali oxide glasses, polymers and doped crystals and concluded that the ion dynamic processes are independent of temperature.

In 1997, Roling et al. [48, 49] analyzed the scaling properties of the conductivity spectra of sodium borate glasses containing different amounts of sodium oxide. Subsequently, Ghosh and his coworker [50] argued that the scaling formalism of Roling *et al.* was unable to merge all of the conductivity isotherms into a single master curve for lithium tellurite glasses, even in the higher composition range. In present case Ghosh's scaling law [50] is used to scale modulus spectra in which Y-axis (imaginary part of modulus) is scaled by the peak value of M'' and X-axis (frequency axis) is scaled by the frequency corresponding to M''_{max} value.

To have further look into the relaxation mechanism of polymer electrolyte systems, the imaginary part of dielectric modulus (M''/M''_{max}) is plotted as a function of frequency $\log(f/f_{max})$ for 5wt% AgCF_3SO_3 for PA series given in Fig. 6.41(a). The superimposability of all the data points at all temperatures has been observed except a small

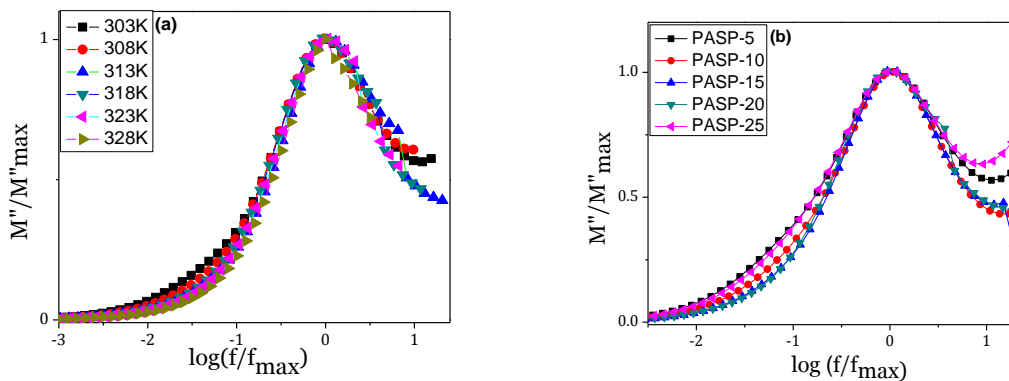


Fig. 6.43 Plot of M''/M''_{max} Vs. $\log(f/f_{max})$ (a) with temperature for PASP-15 sample and (b) for different amount of PEG in PASP system at 313K.

portion at higher frequencies which results in a time-temperature superposition (TTSP) principle. The non-merging of compositional plot on a single master curve for different

compositions of PA series at 303K shown in Fig. 6.41 (b) indicates that the microscopic dynamic process occurring at different compositions do not follow the similar relaxation mechanism. Further modification of PA system by incorporating nano-filler SiO₂ to form PAS system, the data points in the modulus plots neither coalesce for different temperatures Fig. 6.42(a) nor for different compositions of SiO₂ [Fig. 6.42(a)].

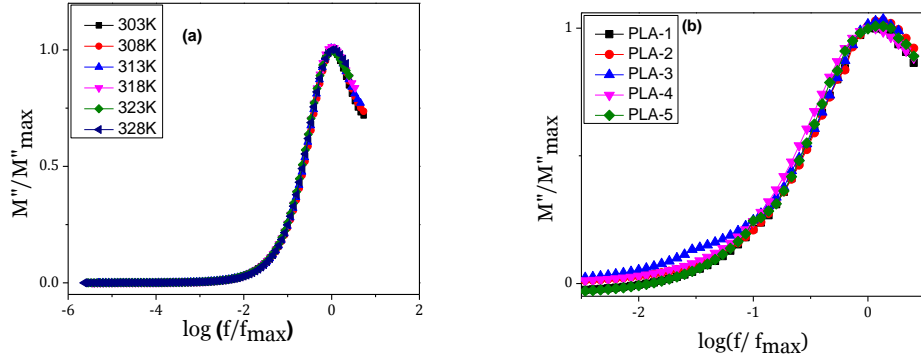


Fig. 6.44 Plot of M''/M''_{max} Vs. $\log(f/f_{max})$ (a) with temperature for PLA-2 sample and (b) for different amount of Al₂O₃ PLA system at 313K.

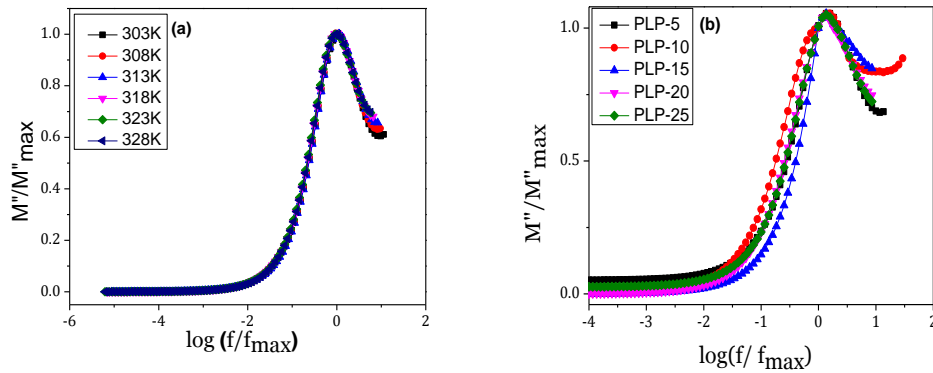


Fig. 6.45 Plot of M''/M''_{max} Vs. $\log(f/f_{max})$ (a) with temperature for PLP-5 sample and (b) for different amount of PEG in PLP system at 313K.

However, the data points for the imaginary part of dielectric modulus (M''/M''_{max}) for 15 wt% PEG in PASP system coalesced at different temperatures [Fig. 6.43(a)] but the plots do not scale with composition (PEG) at all [Fig. 6.43(b)]. In the Lithium based polymer electrolyte (PLA) system, the modulus plots at different temperatures coalesce, while for different amounts of nano-filler (Al₂O₃) at 313 K do not coalesce as shown in Fig. 6.44 (a) & 6.44 (b). The addition of plasticizer (PEG) into the nano-composite systems i.e., PLP series shown in Fig. 6.45(a), the dielectric modulus (M''/M''_{max}) coalesce at

all temperatures but not for different PEG concentrations [Fig. 6.45(b)].

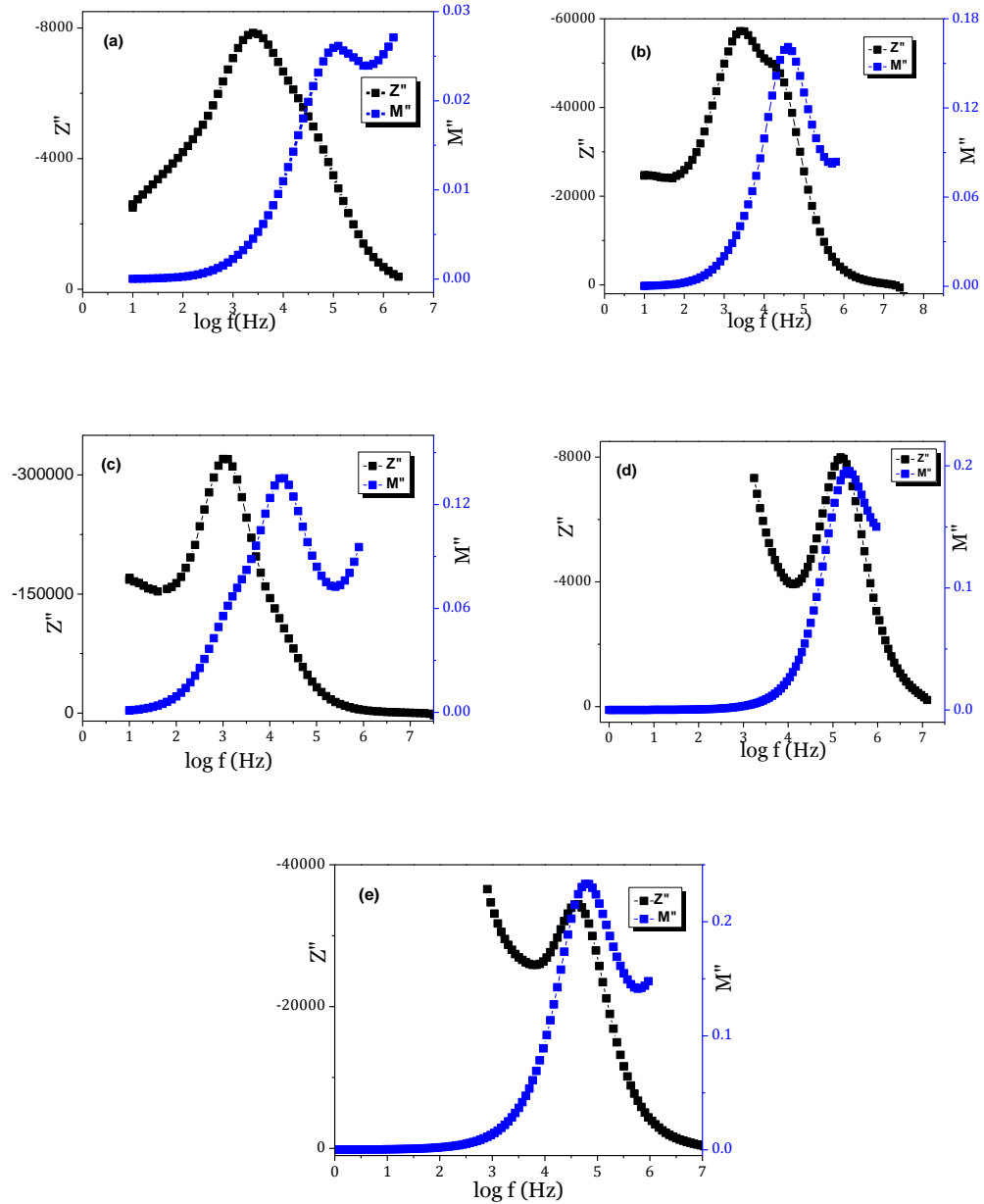


Fig. 6.46 Plot of Z'' and M'' vs $\log f$ at 318K for (a) PA-7, (b) PAS-5, (c) PASP-10, (d) PLA-3 and PLP-10 samples.

The plotting of data in terms of impedance, electric modulus and dielectric permittivity simultaneously is extremely advantageous for distinguishing the different relaxation processes occurring inside the materials. For an ideal circuit, the impedance and modulus spectroscopic plots i.e., Z'' , M'' vs $\log f$ plots are completely super imposable and is given by eqn. (as below):

$Z'' = R[\omega RC]/(1 + \omega RC)^2$ and $M'' = (C_0/C) [\omega RC]/(1 + \omega RC)^2$ Therefore, comparison of Z'' and M'' data is very useful and the Debye like peak shapes in the spectroscopic plots is thus given by the term, $[(\omega RC)/(1 + \omega RC)^2]$ in the imaginary parts of both Z'' and M'' . It can be seen that the Z'' peak is scaled by R where as the M'' peaks are scaled by (C_0/C) . But in the case of practical solid electrolytes, they need to be represented by a series array of RC elements in order to account for various layers within the materials [28]. As a result, there is usually a distribution of relaxation times, in which case the maxima in the impedance and modulus spectra no longer coincide. To understand the non-Debye behaviour of the prepared systems, impedance and modulus spectrum have been plotted. Figs. 6.46 (a) to (c) show plots of Z'' and M'' vs $\log f$ for 7wt% of AgCF_3SO_3 , 5 wt% of SiO_2 and 10 wt% of PEG for PA, PAS and PASP series respectively. It can be seen from these figures that Z''_{max} and M''_{max} do not coincide at the same frequency and a broadened modulus spectra is obtained which is an indication of the broad distribution of relaxation times. It also reveals that the Z'' spectra are broadened on the lower frequency side of the peak maximum and M'' spectra are broadened on the high frequency side. The large rise in Z'' occurring at low frequencies is caused mainly due to the electrode polarization [51]. Figs.6.46 (d) and 6.46(e) show plot of Z'' and M'' vs $\log f$ at 313K of 2wt% of Al_2O_3 for PLA series and 25wt% of PEG in PLP series. Here also, the peaks of Z''_{max} and M''_{max} do not coincide at the same frequency and the broadening is not as large as for silver salt system indicating narrow distribution of relaxation time in lithium system.

References:

- [1] E.J. Murphy, S.O. Morgan, *Bell Syst. Tech. J.* 16(1937) 493 -512.
- [2] L. L. Hench, J. K. West, *Principles of Electronic Ceramics*, John Wiley & Sons, New York, 1990.
- [3] V. Raghvan, *Material Science & Engineering - A First Course*, Prentice- Hall, New Delhi, 1998.
- [4] A. K. Thakur, D. K. Pradhan, B. K. Samantaray, R. N. P. Choudhary, *J. Power Sources*, 159 (2006) 272–276.
- [5] D. K. Pradhan, R. N. P. Choudhary, B. K. Samantaray, *eXPRESS Polym Lett.*, 2 (2008) 630–638.
- [6] R. J. Sengwa, S. Choudhary, S. Sankhla, *Express Polym. Letts.*, 2 (2008) 800–809.
- [7] R. J. Klein, S. Zhang, S. Dou, B. H. Jones, R. H. Colby, J. Runt, *J. Chem. Phys.* 124 (2006) 144903(8pp).
- [8] A. Kyritsis, P. Pissis, *Macromolecular Symposia* 119 (1997) 15–24.
- [9] F. Kremer, A. Schonhalls, *Broadband dielectric Spectroscopy*, Springer 2003.
- [10] N. Shinyashiki, R. J. Sengwa, S. Tsubotani, H. Nakamura, S. Sudo, S. Yagihara, *J. Phys.Chem. A.*, 110 (2006) 4953–4957.
- [11] L. Nunez, S. G. Barreiro, C. A. G. Fernandez, M. R. Nunez, *Polymer*, 45 (2004) 1167.
- [12] J. Soumen, W.H. Zhong, *J. Mater. Sci.* 43 (2008) 4607-4617.
- [13] R. Mishra, K. J. Rao, *Solid State Ionics*, 106 (1998) 113-127.
- [14] S. L. Agrawal, M. Singh, M. Tripathi, M. M. Dwivedi, K. Pandey, *J Mater Sci*, 44 (2009) 6060–6068.
- [15] S. K. Tripathi, A. Gupta, A. Jain, M. Kumari, *Indian J. Pure Appl. Phys.* 51 (2013) 358-361.
- [16] R. H.Y Subban , A. K. Arof , *New Mat J Electrocham Systems*, 6 (2003) 197-203.
- [17] A.L. Saroj, R.K. Sigh, *J. Phys. Chem. Solids* 73(2012) 162-168.
- [18] S. Ranjendran, O. Mahendran, R. Kannan, *J. Phys. Chem. Solids* 63 (2002) 303-307.
- [19] P. B. Macedo, C. T. Moynihan, R. Bose, *Phys. Chem. Glasses*, 13 (1972) 171-179.
- [20] I.M. Hodge, M.D. Ingram, A. R. West, *J. Electroannal. Chem.* 74(1976) 125-143.
- [21] G. Williams, D. K. Thomas. "*Phenomenological and molecular theories of dielectric and electrical relaxation of materials.*" *Novocontrol Applications Note—Dielectrics* (1998).
- [22] M. Deka, A. Kumar, *J Solid State Electrochem.* 17(2013) 977–986.
- [23] N.S.T. Do, D. M. Schaetzl, B. Dey, A.C. Seabaugh, S. K. F. Shirey, *J. Phys. Chem. C* 116 (2012) 21216–21223.
- [24] M. Forsyth, P. Meakin, D.R. MacFarlane, A.J. Hill, *Electrochim. Acta* 40(1995)2349-2351.
- [25] G.M. Tsangaris, G.C. Psarras, N. Kouloumbi, *J. Mater. Sci.* 33(1998) 2027-2037.
- [26] D. L. Sidebottom, P. F. Green, R. K. Brow, *Phys. Rev.B* 56(1997) 170-177.
- [27] A.Karnakar, A.Ghosh, *Current Appl. Lett.* 12(2012) 539-543.
- [28] M. Pant, D.K. Kanchan, N.Gondaliya, *Mater. Chem. Phys.* 115(2009) 98-104.
- [29] M.P. Dasaria, K. Sambasiva Rao, P. Murali Krishna and G. Gopala Krishna, *Acta Physica Polonica A* 119 (2011) 387-394.

- [30] Y. Feldman, A. Puzenko, Y. Ryabov, *Chem. Phys.*, 284 (2002) 139-168.
- [31] J.M. Reau, S. Rossignol, B. Tanguy, J.M. Rojo, P. Herrero, R.M. Rojas, J. Sanz, *Solid State Ionics* 74(1994) 65.
- [32] M. Kumar, S.S. Sekhon, *Ionics* 8(2002) 223-233.
- [33] C. T. Moynihan, L. P. Boesch, N. L. Laberge, *Phys. Chem. Glasses*, 14, (1973) 122-125.
- [34] R. Kohlrausch, *Prog. Ann. Phys. Chem.* 91(1854) 179.
- [35] G. Williams, D. C. Watts, *Transactions of the Faraday Society*, 66 (1970) 80–85.
- [36] S. Ramesh, Chai MF, *Mater Sci Eng B*, 139(2007) 240-245.
- [37] J. M. Bobe, J. M. Reau, J. Senegas, M. Poulain, *Solid State Ionics*, 82 (1995) 39-52.
- [38] J. M. Reau, S. Rossignol, B. Tanguy, J. M. Rojo, P. Herrero, R. M. Rojas, J. Sanz, *Solid State Ionics*, 74 (1994) 65.
- [39] R. Kohlrausch, *Annalen der Physik*, 167 (1), (1854) 56–82.
- [40] G. Williams, D. C. Watts, *Transactions of the Faraday Society*, 66 (1970) 80–85.
- [41] C. Lin, H. G. K. Sundar, C. A. Angel, *Solid State Ionics*. 442 (1986) 18-19.
- [42] H. Naili, N. Zouari, T. Mhiri, A. Daoud, *J. Mol. Struct.*, 519 (2000) 143.
- [43] A.K. Jonscher, *Phys. State Solidi* , 32 (1975) 665.
- [44] H. K. Patel, S. W. Martin, *Phys. Rev.*, B 45 (1992) 10292.
- [45] D. L. Sidebottom, *Phys. Rev. Lett.* 82 (1999) 3653-3656.
- [46] D. L. Sidebottom, P. F. Green, R. K. Brow, *J. Non-Cryst. Solids*, 203 (1996) 300-305.
- [47] J. O. Isard, *J. Non-Cryst. Solids*, 4 (1970) 357.
- [48] B. Roling, A. Happe, K. Funke, M. D. Ingram, *Phys. Rev. Lett.*, 78 (1997) 2160-2163
- [49] B. Roling, *Solid State Ionics*, 105 (1998) 185.
- [50] A. Ghosh, A. Pan, *Phys. Rev. Lett.*, 84 (2000) 218.
- [51] P. Smith, *Dielectric behavior and structure*, Mc Graw Hill, New York, 1995.
-

CHAPTER 7

CONCLUSION

***T**his chapter summarizes all the experimental results observed in the present investigation of polymer nano-composite electrolytes.*

In the present investigation, a systematic study on PEO-based polymer electrolytes has been done. For this, in order to find the optimized PEO-silver salt concentration, the AgCF_3SO_3 amount has been varied in PEO polymer. Thereafter, the amount of nano-filler SiO_2 is varied to examine the transport mechanism of this nano-composite polymer electrolyte. Finally, it was plasticized with PEG to further enhance the transport mechanism to PEO- AgCF_3SO_3 - SiO_2 polymer electrolyte system. To augment further the silver electrolyte, silver salt as well as nano-filler SiO_2 have been replaced by lithium salt LiCF_3SO_3 and Al_2O_3 respectively. Characterization of all the samples is performed using FTIR, XRD, DSC, SEM and transport measurements. Effect of nanofiller without/with plasticization on conduction and relaxation mechanism in PEO based polymer electrolytes has been studied.

The change in molecular vibrational spectra due to the interaction of host polymer with salt, nanofiller and plasticizer in the system has been analyzed by FTIR. The characteristic vibrational peaks of PEO at 841, 940, 1057 and 1093 cm^{-1} and a broad band in the wave number range 2700-3000 cm^{-1} are present in all the prepared samples. In addition to this, the presences of the new peaks at 636 and 1028 cm^{-1} confirms the complexation of AgCF_3SO_3 and host polymer PEO. Addition of nano-filler SiO_2 reduces the overall intensity of the system, along with the broadening of C-H stretching band and appearance of new peak around 1736 cm^{-1} at higher SiO_2 content. Plasticization reduces the amorphousity as compared to nano-system. In the Li^+ -ion conducting system (PLA-system), LiCF_3SO_3 and plasticizer PEG make a good complexation with PEO which is confirmed by the appearance of IR peaks of $\delta_{\text{as}}(\text{CF}_3)$, $\delta_{\text{s}}(\text{SO}_3)$ and SO_3 at 526, 636 and 1033 cm^{-1} respectively. Plasticization of polymer nano-composites also indicates an overall increase in intensity of IR spectra as compared to without plasticizer.

DSC studies provide valuable information about the variation in glass transition temperature T_g and melting temperature T_m of the prepared polymer electrolytes. In the silver salt systems highest conducting samples show lowest T_g value and lowest T_m value in their respective series. While plasticization of polymer electrolytes made the system stiffer. Similarly, in Lithium salt systems i.e., PLA and PLP series, the T_g values are observed to be lower than the systems with plasticizer PEG indicating reduction in flexibili-

ty due to addition of plasticizer in .

XRD results show a significant reduction in the intensity of sharp peak of PEO even at higher concentration of salt which indicates the dominance of amorphous phase. But by the addition of nanofiller SiO_2 , the diffraction pattern are observed to shift towards lower angle side with small broadening with decreased intensity, expect $x= 25$ wt% of SiO_2 . An increase in peak intensity is observed on plasticization with PEG compared to that of the PAS series. The addition of nanofiller disturbs the crystalline regions and lead to an increase in the amorphous phase of the system. Whereas, upon plasticization, a significant structural reorganization takes place, leading to an increase in peak intensity as compared to that of the system with nanofiller.

SEM micrographs show the formation of spherulites and reduction in the size of spherulites on addition of salt AgCF_3SO_3 upto 7wt% (PA-7) is observed. Addition of nanofiller in both the system i.e. PAS and PLA improves the uniformity, smoothness and homogeneity of the surface. But on plasticization (PASP and PLP series), surface roughness is the main feature.

The ionic transference number (t_i) of polymer films confirms the conduction mechanism principally due to the transport of ions and the highest conducting sample in their respective represent the highest transference number (in the range of 0.8-0.9 in different systems).

In PEO polymer electrolytes, the addition of PEG plasticizer does not significantly improve the electrical properties in silver ion as well as in lithium conducting systems.

Temperature dependence of dc conductivity follows Arrhenius theory. All the samples with the highest transport number show the highest ionic conductivity. These samples show a power law variation at high frequencies. Dispersion in ac conductivity spectra obeys Jonscher's power law and the frequency exponent n are found to be smaller than 1.

The real part of dielectric permittivity, ϵ' decreases with the increase in frequency and saturates at higher frequencies whereas the dielectric loss, ϵ'' also varies inversely with frequency. The frequency and temperature dependent dielectric studies confirm the ion migration and polarization effects.

The modulus plots confirm the non-Debye behavior and suggest the distribution of relaxation time in the conduction process. Non exponential decay function from modulus spectra provides β values are close to 0.5-0.9 and independent of temperature and composition.

The variation of relaxation time τ with composition is in consonance with the variation in conductivity for PA, PASP and PLP systems, whereas for PAS and PLA systems it is not. Conduction mechanism of the system is mainly affected by the addition of nanofiller not plasticizer PEG.

Coalescing of the data points in the scaling of modulus spectra of PA, PASP, PLA and PLP systems at different temperatures substantiate the fact that relaxation process is temperature independent, while the modulus spectra at different compositions do not merge on master curve which indicates that the relaxation mechanism is composition dependent.

In summary, PEO-based systems make a good polymer composite. All prepared polymer composites show a rise in conductivity on addition of salt, nanofiller and plasticizer. Addition of nanofiller to PA electrolyte system (polymer-salt system) enhances the electrical properties. But the plasticization of PAS system increases the crystalline phase of the system due to similar structure of PEO and PEG. However, lithium ion conducting systems (PLA and PLP) showed higher rise in conductivity as compared to silver ion conducting systems. Hence, lithium ion conducting systems can be used as a good electrolyte.

----- THE END-----

LIST OF PUBLICATIONS

Publications in Journal:

1. Conductivity and dielectric behavior of AgCF₃SO₃ doped PEO polymer films
N. Gondaliya, D. K. Kanchan, P. Sharma, M.S. Jayswal, M. Pant
*Integrated Ferroelectrics (Taylor & Francis)*119 (2010) 1-12.
2. Structural and conductivity studies of poly (ethylene oxide)-silver triflate polymer electrolyte system
N. Gondaliya, D. K. Kanchan, P. Sharma and P. Joge
Materials Sciences and Applications (USA) 2 (2011) 1639-1643.
3. Effect of silicone dioxide and poly(ethylene glycol) on the conductivity and relaxation dynamics of poly(ethylene oxide)-silver triflate solid polymer electrolyte
N. Gondaliya, D. K. Kanchan, P. Sharma and P. Joge
Journal of Applied Polymer Science 125 (2012) 1513-1520.
4. Dielectric and electric properties of plasticized PEO-AgCF₃SO₃-SiO₂ nano-composite polymer electrolyte system
N. Gondaliya, D. K. Kanchan, P. Sharma, Manish S. Jayswal
*Polymer Composites (Wiley)*33 (2012) 2195-2200.
5. Modulus and Dielectric Study of PEO: LiCF₃SO₃: PEG: Al₂O₃ Nano Composite Polymer Electrolytes
N. Gondaliya, D. K. Kanchan, P. Sharma
National Journal of Applied Sciences and Engineering, 1 (2012) 18-24.
6. Effect of a plasticizer on a solid polymer electrolyte
N. Gondaliya, D.K.Kanchan, P. Sharma,
Society of Plastics Engineers, (2013) DOI 10.2417/spepro.004646

Paper presented in Conferences:

1. Conductivity studies in Silver Based Poly (Ethylene Oxide) PEO Solid Electrolyte
N. Gondaliya, D. K. Kanchan, M. Pant, P. Sharma, M. Jayswal
54th DAE Solid State Physics Symposium (2009) 901-902.
2. Conductivity and dielectric behavior of AgCF₃SO₃ doped PEO polymer Electrolyte
N. Gondaliya, D.K. Kanchan, M. Pant, P. Sharma, M. Jayswal
International conference on Electroceramics, Delhi University, Delhi, 13-17 Dec. 2009.
3. Study of Relaxation Dynamics in PEO: AgCF₃SO₃ Solid Polymer Electrolytes
N. Gondaliya, D.K. Kanchan, P. Sharma, M. Pant, Manish S. Jayswal
3rd International Symposium on Materials Chemistry, BARC, Mumbai, 7-11 Dec. 2010, Proceedings of DAE-BRNS, pp.151-152
4. Dielectric and Conductivity in Silver-Poly (Ethylene Oxide) Solid Polymer Electrolytes Dispersed With SiO₂ Nanoparticles
N. Gondaliya, D. K. Kanchan, P. Sharma, M. Pant, M. Jayswal
AIP Conf. Proc. 1313 (2010) 112-114.
5. Conductivity Studies on PEO-AgCF₃SO₃ Electrolyte System with Nano-Porous Fillers
N. Gondaliya, D. K. Kanchan, P. Sharma, M. Pant, M. Jayswal
AIP Conf. Proc. 1313 (2010) 177-179.
6. Dielectric and conductivity in PEO-AgCF₃SO₃-Al₂O₃-PEG plasticized nano-composite polymer electrolyte.
N. Gondaliya, D.K. Kanchan, P.Sharma, M. Pant, M.S. Jayswal, P.Joge
14th International Conference of International Academy of Physical Sciences (CONIAPS-XIV), SVNIT, Gujarat, 22-24 Dec. 2011
7. Effect of plasticizer in PEO-AgCF₃SO₃-SiO₂ nano composite polymer electrolyte.
N. Gondaliya, D.K. Kanchan, P. Sharma, M. Pant, Manish S. Jayswal, P. Joge
14th International Conference of International Academy of Physical Sciences (CONIAPS-XIV), SVNIT, Gujarat, 22-24 Dec. 2011
8. Conductivity Studies on Plasticized (PEG) PEO-AgCF₃SO₃-SiO₂ Nano Composite Polymer Electrolytes.

- N. Gondaliya**, D.K. Kanchan, P. Sharma, M. Pant, M. S. Jayswal, P. Joge
National Conference on Recent Trend in Material Science, JUIT, Solan, H.P. 8-10 October, 2011
9. FTIR Studies of SiO₂ Doped PEO-AgCF₃SO₃ Composite Polymer Electrolyte.
N. Gondaliya, D.K. Kanchan, P. Sharma, M. S. Jayswal, P. Joge
9th National Conference on Solid State Ionics (NCSSI-9), JIIT, Noida U.P., 15-17 Dec. 2011
 10. Effect of plasticizer on PEO-AgCF₃SO₃-SiO₂ nano composite polymer electrolytes
N. Gondaliya, D.K. Kanchan, P. Sharma, M. Pant, M. S. Jayswal
National conference on Physics for Tomorrow, St.Xavier's college, Gujarat, 3-4 March 2011
 11. Effect of Al₂O₃ on Conductivity of PEO Based Nano Composite Polymer Electrolyte.
N. Gondaliya, D.K. Kanchan, P. Sharma, M. Pant, P. Joge
17th National Symposium on Solid State track Detectors and their Applications, MSU Baroda, Gujarat, 17-19 Oct 2011
 12. Effect of Al₂O₃ and PEG on relaxation time in PEO-LiCF₃SO₃ polymer electrolytes
N. Gondaliya, D. K. Kanchan, P. Sharma, Manish S. Jayswal, P. Joge
AIP Conf. Proc. 1447 (2012) 247-248.
 13. Effect of Al₂O₃ on Conductivity of PEO based Nano Composite Polymer Electrolytes
N. Gondaliya, D. K. Kanchan, P. Sharma,
Narosa Publishing House Pvt. Ltd., (2012) ISBN 978-81-8487-259-0.

Publications in Journal as co-author:

1. Transport properties and relaxation studies in BaO substituted Ag₂O-V₂O₅-TeO₂ glass system
M. Pant, D.K.Kanchan, **N. Gondaliya**
Materials Chemistry and Physics, 115(2009) 98-104.
2. Effect of ethylene carbonate concentration on structural and electrical properties of PEO-PMMA polymer blends
P. Sharma, D.K.Kanchan, **N. Gondaliya**
Ionics(Springer), (2012) DOI 10.1007/s11581-013-0851-z.
3. Effect of Nano-Filler on Structural and Ionic Transport Properties of Plasticized Polymer Electrolyte
P. Sharma, D. K. Kanchan, **N. Gondaliya**
Open Journal of Organic Polymer Materials(USA), 2 (2012) 38-44.
4. Conductivity Studies in blended plasticized PEO-PMMA nano-composite electrolyte system
P. Sharma, D.K.Kanchan, **N. Gondaliya**, M.S. Jayswal, P. Joge,
Narosa Publishing House Pvt. Ltd., (2012) ISBN 978-81-8487-259-0.
5. Dielectric Properties of PVA-PEO polymer blend films
P. Joge, D. K. Kanchan, **N. Gondaliya**, P. Sharma,
Narosa Publishing House Pvt. Ltd., (2012) ISBN 978-81-8487-259-0.
6. Conductivity relaxation in Ag⁺- ion conducting PEO-PMMA-PEG polymer blends,
P. Sharma, D.K.Kanchan, **N. Gondaliya**, M. Pant, M.S. Jayswal
Ionics (Springer), 19 (2013) 301-307.
7. Conductivity Studies on filler free and filler doped PVA-PEO based blend polymer electrolytes
P. Joge, D. K. Kanchan, P. Sharma, **N. Gondaliya**
Advanced Materials Research, 665 (2013) 227-232.
8. Influence of nano filler on conductivity in PEO-PMMA-AgNO₃ polymer blend
P. Sharma, D.K.Kanchan, **N. Gondaliya**, M.S. Jayswal
Indian J Pure and Applied Physics, 51 (2013) 346-349.
9. Structural and electrical properties of plasticized polymer blend electrolytes
P. Sharma, D.K. Kanchan **N. Gondaliya**,
National Journal of Applied Sciences and Engineering 1(2012)32-40.
10. Relaxation process in PbI₂-Ag₂O-V₂O₅-B₂O₃ system: Dielectric, AC conductivity and modulus studies
M.S. Jayswal, D.K.Kanchan, P. Sharma, **N. Gondaliya**
Materials Science and Engineering: B (Elsevier)178 (2013) 775-784.

Publications in Proceedings as co-author:

1. Conductivity studies in irradiated and unirradiated AgI-Ag₂O-V₂O₅-TeO₂ super ionic glass system: a comparative study
P. Sharma, D. K. Kanchan, M. Pant, **N. Gondaliya**, K. P. Singh
18th National Symposium on Radiation Physics (NSRP), MLSU, Udaipur, Rajasthan 19-21 Nov. 2009.
2. Frequency Dependent Conductivity of PbI₂ Doped Silver Boro-Vanadate Super Ionic Glass System
Manish S. Jayswal, D.K. Kanchan, P. Sharma, M. Pant, **N. Gondaliya**
AIP Conf. Proc. 1313 (2010) 233-235.
3. Characterization studies of plasticized PEO-PMMA nano-composite polymer electrolyte system
P. Sharma, D.K.Kanchan, **N. Gondaliya**, M. Pant, M.S. Jayswal, P. Joge,
AIP Conf. Proc. 1447 (2012) 241-242.
4. Relaxation Dynamics in PAAM: AgNO₃: EC Solid Polymer Electrolytes
P. Sharma, D.K. Kanchan, M. Pant, **N. Gondaliya**, M. S. Jayswal
3rd International Symposium on Materials Chemistry, BARC, Mumbai, 7-11Dec.(2010)
5. Effect of Swift Heavy Ion Irradiation on Conductivity and Relaxation Time in PVA-PEO-EC-LiCF₃SO₃ Blends
P. Joge, D.K. Kanchan, P. Sharma, M. Jayswal, **N. Gondaliya**, D.K. Awasthi
AIP Conf. Proc. 1512 (2013) 502-503.
6. Effect of EC & LiCF₃SO₃ on Conductivity and Relaxation in PVA-PEO Blends
P. Joge, D. K. Kanchan, P. Sharma, **N. Gondaliya**
AIP Conf. Proc. 1512 (2013) 506-507.

Papers presented in conferences/symposiums:

7. Conductivity and Modulus Studies on PbI₂ doped silver boro vanadate super ionic glass system
Manish S. Jayswal, D.K. Kanchan, P. Sharma, M. Pant, **N. Gondaliya**
8th National Conference on Solid State Ionics (NCSSI), Sagar University, Sagar, M.P. 7-9 Dec. 2009.
8. Conductivity studies in PVA-AgNO₃ polymer electrolyte
P. Sharma, D.K. Kanchan, P. Joge, **N. Gondaliya**, M. Pant
54th DAE Solid State Physics Symposium, MSU Baroda, Gujarat, 14-18 Dec. 2009
9. Effect of AgI on the conduction mechanism of silver vanadate super ionic glasses
P. Sharma, D.K. Kanchan, M. Pant, Manish S. Jayswal, **N. Gondaliya**
International conference on Electroceramics, Delhi University, Delhi, 13-17 Dec. 2009
10. Electrical conductivity and relaxation studies of silver based barium Vanado-tellurite glasses
M. Pant, D.K. Kanchan, P. Sharma, Manish Jayswal, **N. Gondaliya**
National Conference on Advances on Materials & Devices for Renewable EnergySources, Jaipur Engineering College, Kukas, Rajasthan, February 2010
11. Effect of Modifier on the Structural and Transport Studies of Ag₂O Based Barium Vanado-Tellurite Glasses
M. Pant, D.K. Kanchan, P. Sharma, Manish S. Jayswal, **N. Gondaliya**
National Conference on Recent Trends in Exotic Materials,
Sharda University, Greater Noida, U.P., 26-28 Aug. 2010
12. Influence of mixed iodide salts on the conductivity behavior in Ag₂O - V₂O₅ - B₂O₃ Superionic glass system
P. Sharma, D.K. Kanchan, M. Pant, Manish S. Jayswal, **N. Gondaliya**
National Conference on Recent Trends in Exotic Materials,
Sharda University, Greater Noida, U.P., 26-28 Aug. 2010
13. Relaxation Studies in PbI₂ Doped Silver-Vanado-Borate Super-Ionic Glass System
P. Sharma, D.K. Kanchan, **N. Gondaliya**, M. Pant, Manish S. Jayswal Dielectric
National Conference on Recent Trends in Exotic Materials,
Sharda University, Greater Noida, U.P., 26-28 Aug. 2010
14. Impedance and Dielectric studies of Silver Oxide Based Quaternary Glass System
M. Pant, D.K. Kanchan, P. Sharma, **N. Gondaliya**, Manish S. Jayswal

- 5th Asian Conference on Electrochemical Power Sources, ACEPS-5, National University of Singapore, Singapore, 17-19 Sep. 2010
15. Dynamics in PAAM: AgNO₃: EC Solid Polymer Electrolytes
P. Sharma, D.K. Kanchan, M. Pant, **N. Gondaliya**, Manish S. Jayswal
Relaxation 3rd International Symposium on Materials Chemistry, BARC, Mumbai, 7-11 Dec. 2010 Proceedings of DAE-BRNS, pp.513
 16. Effect of Plasticizer Concentration on the Conductivity in PAAM: AgNO₃ Solid Polymer
P. Sharma, D.K. Kanchan, **N. Gondaliya**, P. Joge
55th DAE Solid State Physics Symposium, Manipal University, Manipal, Karnataka, 26-30 Dec. 2010, AIP Conf. Proc. 1349, (2011) pp. 933-934
 17. Study of Relaxation Dynamics in Mixed Iodide Doped Silver-Vanado-Borate Superionic Glass System.
P. Sharma, D.K. Kanchan, **N. Gondaliya**, P. Joge
55th DAE Solid State Physics Symposium, Manipal University, Manipal, Karnataka, 26-30 Dec. 2010, AIP Conf. Proc. 1349, (2011) pp. 551-552
 18. Conductivity Studies in PVA-PEO-PEG Blended Polymer Films Complexed with Silver Salt
P. Joge, D.K. Kanchan, P. Sharma, **N. Gondaliya**
55th DAE Solid State Physics Symposium, Manipal University, Manipal, Karnataka, 26-30 Dec. 2010, AIP Conf. Proc. 1349, (2011) pp. 1053-1054
 19. Electrical conduction studies on a newly plasticized PAAM:AgNO₃ nano-composite polymer electrolyte system
P. Sharma, D.K. Kanchan, **N. Gondaliya**, M. Pant, Manish S. Jayswal
National conference on Physics for Tomorrow, St.Xavier's college, Gujarat, 3-4 March 2011
 20. Conductivity and IR studies on PVA-PEO blends.
P. Joge, D.K. Kanchan, P. Sharma, **N. Gondaliya**
National conference on Physics for Tomorrow, St.Xavier's college, Gujarat, 3-4 March 2011
 21. Conductivity Studies in PEO-PMMA-AgNO₃ Plasticized Polymer Blends
P. Sharma, D.K. Kanchan, **N. Gondaliya**, M. Pant, M. S. Jayswal, P. Joge
National Conference on Recent Trend in Material Science, JUIT, Solan, H.P. 8-10 October, 2011
 22. Vibrational and conductivity Studies on PVA-PEO Blends
P. Joge, D.K. Kanchan, P. Sharma, **N. Gondaliya**
National Conference on Recent Trend in Material Science, JUIT, Solan, H.P. 8-10 October, 2011
 23. Dielectric Properties of PVA-PEO Polymer Blend Films.
P. Joge, D.K. Kanchan, **N. Gondaliya**, P. Sharma
17th National Symposium on Solid State track Detectors and their Applications, MSU Baroda, Gujarat, 17-19 Oct 2011
 24. Conductivity studies on Plasticized Blend of PEO-PMMA Nano-Composite Electrolyte System.
P. Sharma, D.K. Kanchan, **N. Gondaliya**, M. Pant, Manish S. Jayswal, P. Joge
17th National Symposium on Solid State track Detectors and their Applications, MSU Baroda, Gujarat, 17-19 Oct 2011
 25. Dielectric Studies in PbI₂-Ag₂O-V₂O₅-B₂O₃ Solid Electrolytes
Manish S. Jayswal, D.K. Kanchan, M. Pant, P. Sharma, **N. Gondaliya**
9th National Conference on Solid State Ionics (NCSSI-9), JIIT, Noida U.P., 15-17 Dec 2011
 26. Electrical Conductivity Studies in PEO-PMMA-AgNO₃ Polymer Blend With Nano Filler Al₂O₃
P. Sharma, D.K. Kanchan, **N. Gondaliya**, M. Pant, M.S. Jayswal, P. Joge
9th National Conference on Solid State Ionics (NCSSI-9), JIIT, Noida U.P., 15-17 Dec 2011
 27. Effect Of Nano-Filler On Electrical Properties of PVA-PEO Blend Polymer Electrolyte
P. Joge, D.K. Kanchan, P. Sharma, **N. Gondaliya**
9th National Conference On Solid State Ionics (NCSSI-9), JIIT, Noida U.P., 15-17 Dec 2011
 28. Characterization of Plasticized PEO-PMMA Nano-Composite Polymer Electrolyte System
P. Sharma, D.K. Kanchan, **N. Gondaliya**, M. Pant, M. S. Jayswal, P. Joge.
56th DAE SSPS -2011, SRM University, Tamilnadu, 19-23 Dec 2011
 29. Effect of PEO on conduction mechanism in PVA-PEO blends
P. Joge, D.K. Kanchan, P. Sharma, **N. Gondaliya**

- 14th International Conference of International Academy of Physical Sciences (CONIAPS-XIV), SVNIT, Gujarat, 22-24 Dec. 2011*
- 30.** Ionic transport studies in PbI₂ doped silver-vanado-borate super ionic glass system.
Manish S. Jayswal, D.K. Kanchan, P. Sharma, **N. Gondaliya**, M. Pant
14th International Conference of International Academy of Physical Sciences (CONIAPS-XIV), SVNIT, Gujarat, 22-24 Dec. 2011
- 31.** Relaxation Dynamics of PVA-PEO Polymer Blend Electrolyte Films
P. Joge, D.K. Kanchan, P. Sharma, **N. Gondaliya**
National Symposium on Advances In Materials Science And Technology (AMST-2012), Gujarat University, 3-4 Feb. 2012
- 32.** Conductivity studies on filler free and filler doped PVA-PEO based blend polymer electrolytes
P. Joge, D.K. Kanchan, P. Sharma, **N. Gondaliya**
3rd National Conference on Condensed Matter and Materials Physics CMMP-2012, Sardar Patel University, Gujarat, 3-5 March 2012
-